SYNTHESIS, CHARACTERISATION AND BIOLOGICAL ACTIVITY OF 2-(METHYLTHIOMETHYL)ANILINES, 2-(METHYLTHIO)ANILINES, THEIR SCHIFF-BASE DERIVATIVES AND METAL(II) (CO, NI, CU) COMPLEXES

A thesis submitted in fulfillment of the requirements

for the degree of

Doctor of Philosophy

In

Chemistry

By

TEMITOPE ELIZABETH OLALEKAN

DEPARTMENT OF CHEMISTRY

RHODES UNIVERSITY

GRAHAMSTOWN 6140, SOUTH AFRICA

AUGUST 2012

ABSTRACT

A series of 31 sulfur-nitrogen donor ligands and 64 metal(II) complexes have been investigated. The thiomethylated aniline ligands 2–(methylthiomethyl)aniline **2MT** and 2–(methylthio)aniline **2MA** were synthesized with their substituted derivatives (-Me, -MeO, -Cl, -Br, $-NO_2$) to serve as chelating agents. These ligands behave as bidentate ligands with SN donor group with Co(II), Ni(II) and Cu(II). The Co(II) and Ni(II) complexes have the ML_2Cl_2 molecular formula while the Cu(II) complexes formed with $MLCl_2$ stoichiometry where L is the bidentate ligand.

The ligands and their metal(II) complexes have been characterized by elemental analysis and with spectroscopic techniques. The trend observed in the NMR spectra and IR frequencies of the thiomethylated compounds shows there is a significant difference between the 2MT and 2MA series as a result of sulfur lone pairs extending the conjugation of the aromatic ring in the case of the latter. The effect of the position and electronic nature of ring substituent on the NMR shifts of the amine protons is discussed. The 6- and 5-membered chelate complexes formed by the 2MT and 2MA ligands respectively do not show significant diversity in their spectroscopic properties.

From the elemental analysis for the Co(II) and Ni(II) complexes, their compositions reveal 1:2 M:L stoichiometry with 2 chlorine atoms from the respective metal salts. In addition, the spectroscopic data are largely indicative of tetragonally distorted structures for these solid complexes. The X-ray crystallography data reveal the Cu(II) complexes exist as square pyramidal dimers and with long Cu–Cl equitorial bonds fit into the tetragonally distorted octahedral structure. The electrolytic nature of Co(II) and Cu(II) complexes in DMF were found to be similar, they behave as non electrolytes in contrast to Ni(II) complexes which are 1:1 electrolytes. The electronic spectra of these metal(II) complexes were found to be different for both their solid forms and in solutions of DMF and DMSO and this has been discussed.

The thiomethylated aniline ligands possess the amine and thioether groups which are present in many known biologically active compounds, hence the biological activity of the ligands and their metal complexes were tested against three strains of bacteria and one fungus. The methoxy-substituted derivatives were found to possess better inhibitory activity and this was similarly reflected in the metal(II) complexes. The activity of the complexes can be said to be in the order, Cu(II) > Co(II) > Ni(II).

The Schiff-base derivatives were prepared from the ligands and *para*-methoxysalicylaldehyde and their Cu(II) complexes were synthesized in order to determine their biological activity. The Schiff-base ligands were found to be less active than their parent ligands. The Cu(II) complexes are not soluble in water, DMSO or DMF, as a result and could not be evaluated for their biological activity.

Based on the good results from the antimicrobial evaluation, the antiplasmodial activity of some of the Co(II), Ni(II) and Cu(II) complexes of the thiomethylated ligands against *Plasmodium falciparum* (FCR-3) was determined. At 50 μM concentration level, the Cu(II) complexes show activity equal or better than the prophylactic chloroquine. The Cu(II) complexes with the methoxy-substituted demonstrated exceptional activity but their Co(II) and Ni(II) analogues did not show any activity.

The cytotoxicity of the active Cu(II) complexes at 50 μM concentration was determined against the breast cancer cell line (MDA-MB-231). The compounds destroyed the cancer cell in the range of 28–40%, thus showing their preferred activity against the parasitic cell instead of the cancer cell. The selectivity demonstrated by these compounds have shown them to be potential antimalarial agents and this could be further investigated.

ACKNOWLEDGEMENTS

My appreciation goes to Prof. Gareth Watkins who supervised this research study and to Dr. Denzil Beukes who co-supervised it. I thank you for your scholarly and financial participation, encouragements and understanding during the course of the work. God bless you richly.

I acknowledge Dr. A. Edkins at the Biomedical and Biotechnology Research Unit at Rhodes University who conducted the cytotoxicity assay and Ms Tembisa Jauka for her assistance in the antimicrobial studies. In the same vein, my acknowledgement goes to Dr. van Zyl at the Department of Pharmacy and Pharmacology at University of Witwatersrand for carrying out the antiplasmodial screening.

My thanks go to Dr. Eric Hosten and Dr. Bernardus van Brecht of the Department of Chemical Science, Nelson Mandela Metropolitan University Port Elizabeth, South Africa for their assistance towards obtaining the solid reflectance spectra and X-ray crystallography data of the complexes respectively.

I thank Dr. Tshentu at the Inorganic Unit of Department of Chemistry for his academic contributions. My appreciation also goes to the technical team at the Rhodes University for their contributions towards the success of this research.

My appreciation goes to my colleagues and friends who have in one way or the other been helpful to me during this research program. The list includes Dr. Sobola Abdullahi, Afolayan Anthonia, Tatenda, Maynard, Mr. Okewole, Adeniyi Ogunlaja, Gaelle Ngnie, Racheal Odiri and Vanessa Komlan amongst many others.

My appreciation goes to my mother, sisters and brothers for their moral support and encouragements from far away. May God be with you and keep you.

I appreciate Oluremi my dear husband for believing in me, for his rare support, encouragements and patience. Thank you so much.

I express my immense gratitude to the Organization for Women in Science for the Developing World (OWSDW) Italy for granting me the fellowship and for financial support through the course of my study. My profound gratitude also goes to Rhodes University for the bursary award and waiver of fees.

Finally, I thank God my father for opening the door that no one could open for me to study for this doctorate program and for keeping me through it. Thank you Lord.

TABLE OF CONTENTS

CHAPTER 2

EXPERIMENTAL SECTION

CHAPTER 3

DISCUSSION

CHAPTER 4

BIOLOGICAL ACTIVITY OF COMPOUNDS

LIST OF TABLES *page no.*

LIST OF FIGURES *page no.*

LIST OF SCHEMES *page no.*

LIST OF ABBREVIATIONS

2MA	2–(Methylthio)aniline
2MT	2–(Methylthiomethyl)aniline
$CHCl_3$	Chloroform
CHNS	Carbon Hydrogen Nitrogen
COSY	Correlation spectroscopy
CQ	Chloroquine
CQDP	Chloroquine diphosphate
DCM	Dichloromethane
DDT	Dichlorodiphenyltrichlroethane
DHFR	Dihydrofolate reductase
DHPS	Dihydropteroate synthase
DMF	Dimethylformamide
DMSO	Dimethylsulphoxide
DNA	Deoxyribonuclei acid
Eadd	1,12-bis(2-hydroxy-3-ethylbenzyl)-1,5,8,12-tetraazadodecane]
ENBPI	Ethylenediamine-N,N′-bis[propyl(2-hydroxy-(R)-benzylimino)]
FQ	Ferroquine
HCQ	Hydroxychloroquine
ITN	Insecticide Treated Nets
LLIN	Long lasting insecticidal nets
MIC	Minimum inhibitory concentration
NN	Nitrogen-Nitrogen
ONO	Oxygen-Nitrogen-Oxygen
PCR	Polymerase chain reaction
pMS	*para*-methoxysalicylaldehyde-2-(methylthiomethyl)aniline
pMS-2MA	*p*ara-methoxysalicylaldehyde-2-(methylthio)aniline
R	Substituent
SN	Sulphur-Nitrogen

INTRODUCTION AND LITERATURE REVIEW

1.1 INTRODUCTION AND RATIONALE

This research study is based on synthesis of arylamine-thioether ligands and their substituted derivatives to serve as chelating agents to complex with metal(II) ions. The derived ligands and metal complexes are to be characterized with elemental analysis, by spectroscopic means and structurally with X-ray crystallography where suitable single crystals could be grown. These compounds are to be tested for their biological activity as antimicrobial agents, antiplasmodial and anticancer agents.

The arylamine-thioether or thiomethylated ligands are derived from two unsubstituted compounds; 2–(methylthiomethyl)aniline **2MT** and 2–(methylthio)aniline **2MA** to form two series of ligands. The ligands chosen are to act as bidentate sulphur-nitrogen donors and they differ in the presence of an alkyl group in the former which prevents direct thioether attachment to the ring as in the case of 2MA. The resulting change in physicochemical properties and biological activity imposed on these sets of ligands is to be reported. In addition, six- and five-member chelates are expected to form on complexation of these ligands with metal ions and the consequent difference in properties of these complexes are to be studied.

The substituents (**R**) chosen are the methyl, methoxy, bromo, chloro and nitro groups and these are substituted on the benzene ring in a position *ortho* and *para* to the amino group on the ring (**Fig. 1.1**).

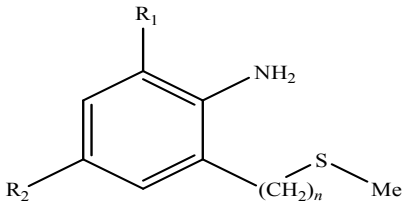

$R_1 = H$ $R_2 = R$ *para* $n = 0$ 2MA *series*
$R_1 = R$ $R_2 = H$ *ortho* $n = 1$ 2MT *series*

Fig. 1 .1 The *ortho* and *para* substituted 2MA and 2MT series

This was done so that any resulting trend in physicochemical property and biological activity of these compounds due to change in electronic nature and position of ring substituent could be studied. The names and structures of these ligands are listed in **Tables 1.1** and **1.2** respectively with abbreviated names given to denote the position of the substituent relative to the aryl amino group.

The common donor groups that are usually present in ligands used in pharmaceutical synthesis are shown in **Fig. 1.2**. As can be observed with this list, possession of N or S donor atom is common to 75% of these groups and those combining the N and S donor atoms are not common. The choice of the 2MT- and 2MA-based compounds is based on exploring their potential bioactivity due to the presence of both N (NH_2) and S (thioether) moieties in each molecule.

The hard-borderline and soft nature of N and S respectively permits them to form strong chelates with the borderline Co(II) and Ni(II) and borderline-soft Cu(II) in accordance to "Hard acid and soft base theory".[1]

Metal ions from Mn(II) to Zn(II) were considered so as to be able to study the characteristics of the derived complexes in relation to their positions across the period table. In addition, these metal ions are of biological relevance in living organisms, hence their complexes with the ligands of study were to be tested for their biological activity.

Mn(II) is essential in malic enzyme, isocitrate dehydrogenase and pyruvate decarboxylase. Fe(II) in haemoglobin, Co(II) is associated with low symmetry sites in enzymes, its complexes can carry molecular oxygen and Co(III) is the central ion in cobalamin and cobamides. Cu(I) and Cu(II) with cuproproteins also transport molecular oxygen and act as good catalysts in related oxidation-reduction processes and Zn(II) is essential to several metalloenzymes such as carboxypeptidase A.[2]

Table 1.1 Names and structures of 2–(methylthiomethyl)anilines

Entry	Abbreviation	R	IUPAC name	Structure
1	2MT	H	2–(methylthiomethyl)aniline	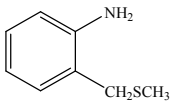
2	2–Me–2MT	Me	2–methyl–6–((methylthio)methyl)aniline	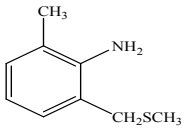
3	4–Me–2MT	Me	4–methyl–2–((methylthio)methyl)aniline	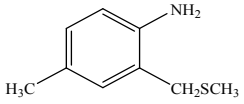
4	2–MeO–2MT	MeO	2–methoxy–6–((methylthio)methyl)aniline	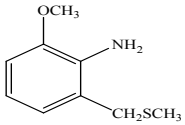
5	4–MeO–2MT	MeO	4–methoxy–2–((methylthio)methyl)aniline	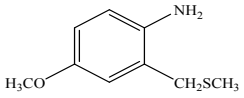
6	2–Cl–2MT	Cl	2–chloro–6–((methylthio)methyl)aniline	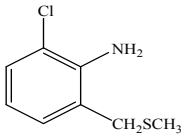
7	4–Cl–2MT	Cl	4–chloro–2–((methylthio)methyl)aniline	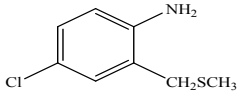
8	2–Br–2MT	Br	2–bromo–6–((methylthio)methyl)aniline	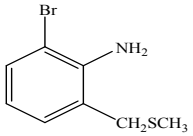
9	4–Br–2MT	Br	4–bromo–2–((methylthio)methyl)aniline	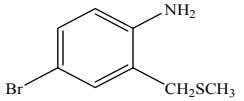
10	2–NO_2–2MT	NO_2	2–(methylthiomethyl)–6–nitroaniline	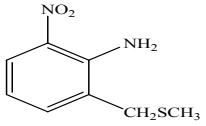
11	4–NO_2–2MT	NO_2	4–nitro–2–((methylthio)methyl)aniline	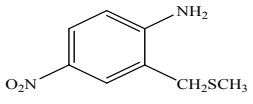

Table 1.2 Names and structures of 2–(methylthio)anilines

Entry	Abbreviation	R	IUPAC name	Structure
1	2MA	H	2–(methylthio)aniline	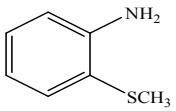
2	2–Me–2MA	Me	2–methyl–6–(methylthio) aniline	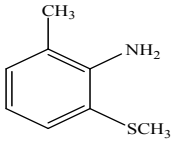
3	4–Me–2MA	Me	4–methyl–2–(methylthio) aniline	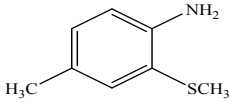
4	2–MeO–2MA	MeO	2–methoxy–6–(methylthio) aniline	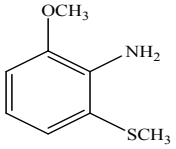
5	4–MeO–2MA	MeO	4–methoxy–2–(methylthio) aniline	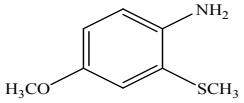
6	2–Br–2MA	Cl	2–bromo–6–(methylthio) aniline	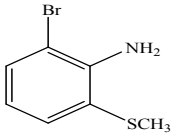
7	4–Br–2MA	Cl	4–bromo–2–(methylthio) aniline	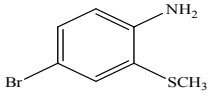
8	2–Cl–2MA	Br	2–chloro–6–(methylthio) aniline	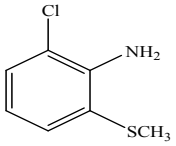
9	4–Cl–2MA	Br	4–chloro–2–(methylthio) aniline	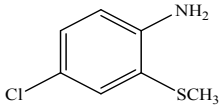

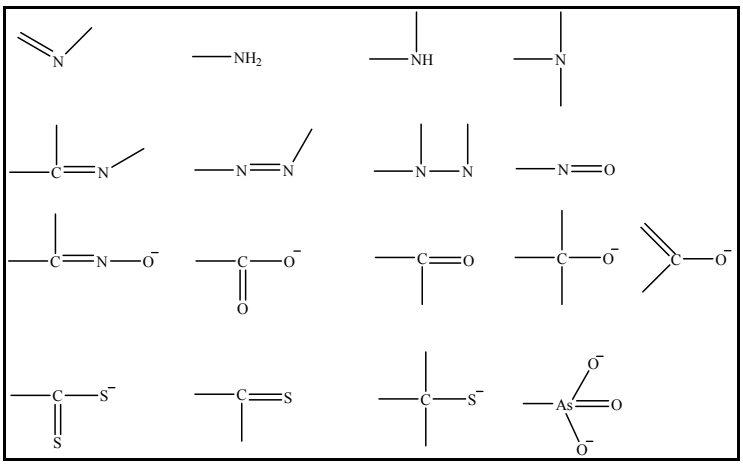

Fig. 1.2 Donor groups commonly used in modern pharmaceuticals

Many of these ligands have been previously prepared (reviewed later in Section **1.2.2**) and some of them characterized by NMR spectroscopy and mass fragmentation pattern. However no systematic or detailed characterization encompassing the CHNS analysis and the various spectroscopic techniques is yet to be reported for any of these ligands. The biological activity of 2MT and 2MA ligands has not been previously reported, although some research has been conducted on the 2–aminobenzothiazoles, the precursor to 2MA. In the same vein, no biological evaluation of their metal(II) complexes have been reported. These issues are addressed in this research.

In the course of practical investigations in the laboratory, only the Co(II), Ni(II) and Cu(II) complexes could be synthesized. The Mn(II), Fe(II) and Zn(II) complexes did not form under similar reaction conditions employed for other metal(II) complexes; the individual reactants precipitated out of solution.

As a result of antibacterial activity shown by some ligands and their Cu(II) complexes especially, the corresponding Schiff-bases were derived in a condensation reaction with *para*-methoxysalicaldehyde. The choice of this aldehyde is based on its antimicrobial and antioxidant property. Cu(II) complexes of the Schiff-base ligands were also synthesized so the effect of chelation could enhance their biological activity. The names and formula of the Schiff-base ligands are listed in **Table 1.3.**

In this research study, 20 thiomethylated ligands were synthesized and their Co(II), Ni(II) and Cu(II) complexes (53) were isolated. 11 Schiff-base ligands were derived from the parent thiomethylated ligands with their corresponding 11 Cu(II) complexes; a total of 95 compounds were synthesized.

Table 1.3 Names and structures of pMS–derived Schiff base ligands

Entry	Abbreviation	IUPAC name	Structure
1	pMS–2MT	2-((E)-(2-(methylthio)methyl) phenylimino)methyl)-5-methoxyphenol	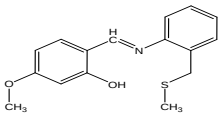
2	pMS–4Me2MT	2-((E)-(4-methyl-2-((methylthio)methyl) phenylimino)methyl)-5-methoxyphenol	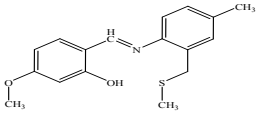
3	pMS–4MeO2MT	2-((E)-(4-methoxy-2-((methylthio)methyl) phenylimino)methyl)-5-methoxyphenol	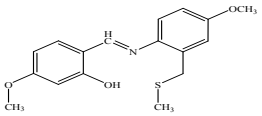
4	pMS–4Cl2MT	2-((E)-(4-chloro-2-((methylthio)methyl) phenylimino)methyl)-5-methoxyphenol	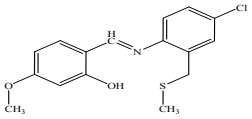
5	pMS–4Br2MT	2-((E)-(4-bromo-2-((methylthio)methyl) phenylimino)methyl)-5-methoxyphenol	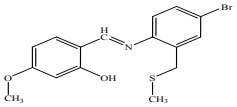
6	pMS–4$NO_2$2MT	2-((E)-(2-((methylthio)methyl)-4-nitrophenylimino)methyl)-5-methoxyphenol	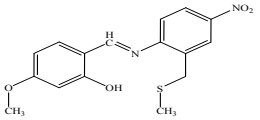
7	pMS–2MA	2-((E)-(2-(methylthio)phenylimino)methyl)-5-methoxyphenol	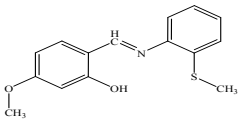
8	pMS–4Me2MA	2-((E)-(4-methyl-2-((methylthio) phenylimino)methyl)-5-methoxyphenol	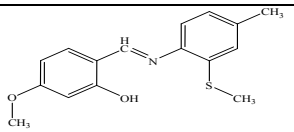
9	pMS–4MeO2MA	2-((E)-(4-methoxy-2-((methylthio) phenylimino)methyl)-5-methoxyphenol	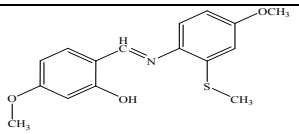
10	pMS–4Cl2MA	2-((E)-(4-chloro-2-((methylthio) phenylimino)methyl)-5-methoxyphenol	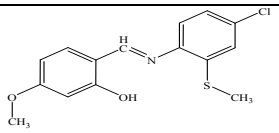
11	pMS–4Br2MA	2-((E)-(4-bromo-2-((methylthio)methyl) phenylimino)methyl)-5-methoxyphenol	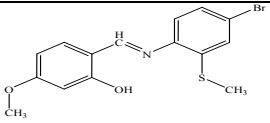

1.2 SN AND NN DONOR LIGANDS AND THEIR METAL(II) COMPLEXES

1.2.1 Applications of thiomethylated anilines

Thiomethylated anilines belong to a class of sulfur-nitrogen (SN) and/or nitrogen-nitrogen (NN) donor groups. They are useful intermediates in production of many organic compounds which are themselves precursors of certain reactions. By reduction with Raney nickel,[3] they can be used to generate ortho-methylated anilines – which are useful intermediates in production of dyes, rubber, herbicides,[4] as well as in electro-optical and many other industrial processes. They find application in preparation of sulfoxides[5] which are desulfurized to generate methylated anilines[6] and as starting materials[7] for deriving aminobenzaldehydes which are also useful precursors to many important heterocyclics. By coupling 2–(methylthioaniline) with another suitable aromatic polymer, suitable chelating resin[8] has been derived for use in preconcentration of metal ions such as Cd, Hg, Ni, Co, Cu and Zn for analytical purposes.

Their applications are summarized in the **Scheme 1.1** below.

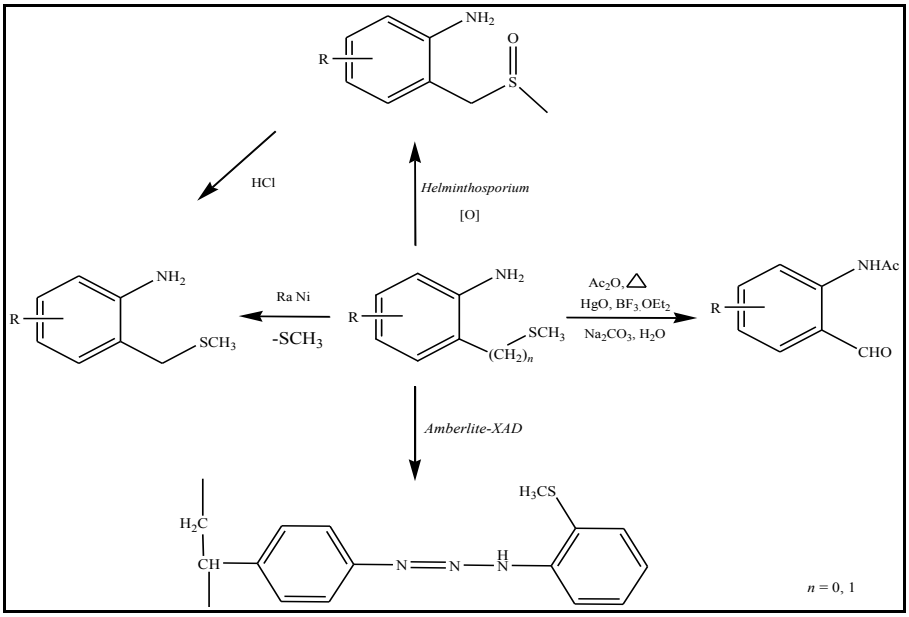

Scheme 1.1 Applications of thiomethylated anilines

1.2.2 Review on synthesis of 2MT and 2MA ligands

Many 2–(methylthiomethyl)anilines with electron-withdrawing and –donating substituents at different positions on the phenyl ring have been reported (that is, R = H, *o*-Me, *p*-Me, *o*-MeO, *p*-MeO, *o*-Cl, *p*-Cl, *o*-NO_2, *p*-NO_2). The synthetic routes to these compounds have employed various starting materials and reaction conditions. The common starting reagents include appropriate aniline or *N*-chloroaniline with dimethyl sulfide[3,6,9-13] or dimethyl sulfoxide-trifluoroacetic anhydride.[14]

More recently, 2–(methylthiomethyl)aniline (2MT) was derived from nitration of benzyl chloride derived from benzyl alcohol and subsequent reduction to the amine.[5] The reaction conditions employed in these syntheses have varied from low temperature within[3,13] or without[14] an inert gas environment to high temperature/reflux[6] condition. It is noteworthy that each of these different methods resulted in similar comparable products.

The mechanism[3,11] of the reaction as illustrated in **Scheme 1.2** generally involves the mono-*N*-chlorination (with a suitable halogenating agent such as *t*-BuoCl, *N*-chlorosuccinimide, chlorine) of the starting aniline to the corresponding *N*-chloroderivative, which is reacted with disubstituted sulfide (dimethyl sulfide, dimethyl sulfoxide-trifluoroacetic anhydride) to produce the azasulfonium salt. Abstraction of alpha proton of the azasulphonium salt by a base gives the azasulphonium ion intermediate, which undergoes an intramolecular Sommelet-Hauser (2, 3-sigmatropic)[15-17] rearrangement type with exclusive attack on the aromatic ring ortho to the amino function to give the sulfinylimine, accompanied by hydrogen transfer and rearomatization to give the ortho-substituted-thiomethylated aniline.

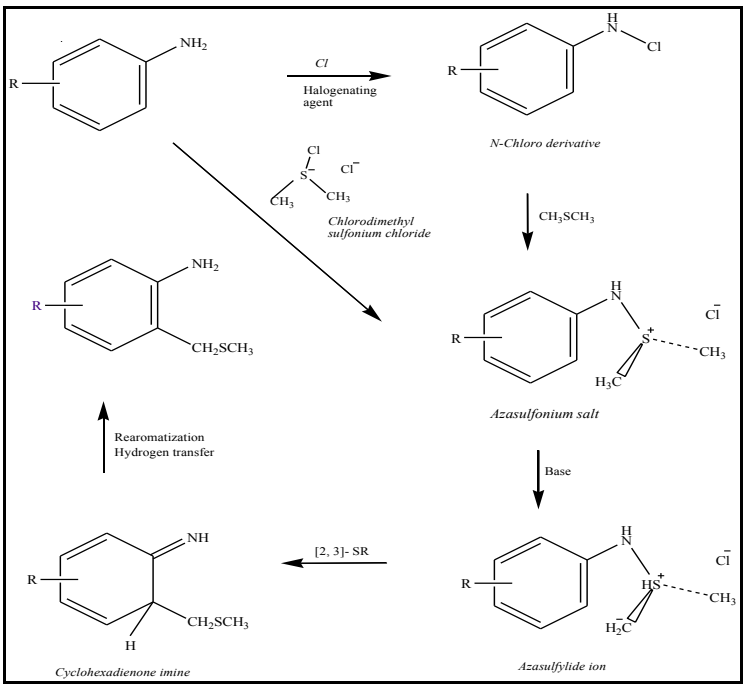

Scheme 1.2 The mechanism of formation for 2–(methylthiomethyl)anilines

2–(Methylthio)aniline (2MA) has been reported. The common procedure[18-20] involves the methylation of 2-aminothiophenol into 2-(methylthio)aniline by methyl iodide in dry ethanol at low temperature in a basic medium, though a similar product was derived at higher reflux temperature. [21] It has also been synthesized by copper-catalyzed amination of arylhalide with sodium azide in an inert and water free environment.[22] A mixture of 2– and 4–(methylthio)aniline was derived from the reaction of phenyl azide with sulphides in the presence of both trifluoroacetic acid and trifluoromethanesulphonic acid.[23]

The overview of some of these synthesis procedures is given in **Scheme 1.3**.

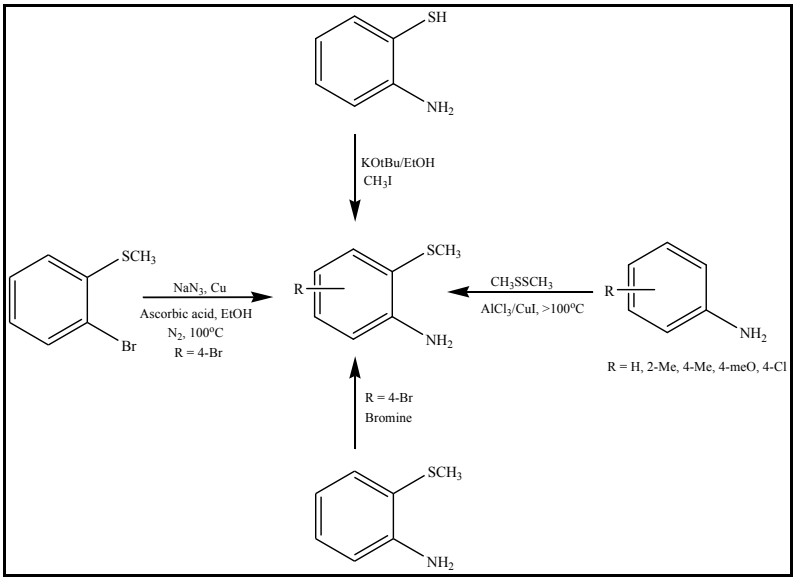

Scheme 1.3 Synthesis of 2MA by and some substituted-2MA ligands

Substituted 2–(methylthio)anilines were synthesized from the reaction of corresponding anilines with aliphatic disulfides in the presence of Lewis acid catalysts, particularly aluminum chloride and copper iodide at high temperatures of >100^{o}C; mixtures of ortho- and para- substituted methylthiolated products resulted.[24] The 4–bromo derivative has been synthesized by direct addition of bromine to 2–(methylthio)aniline, the reaction being monitored by gas chromatography.[25]

Substituted–2– and 4–(phenylthio)anilines were prepared by direct thiolation of an arene C–H bond using FeF_3/I_2 as catalyst.[26] A two-pot synthetic route can also be used to generate substituted 2–(methylthio)anilines. By alkaline hydrolysis of the appropriate 2–aminobenzothiazoles at a high temperature and subsequent methylation with methyl iodide, the crude substituted 2–(methylthio)anilines were derived.[27]

Variously substituted 2–aminobenzothiazoles were synthesized from reactions of appropriate anilines with potassium thiocyanate in the presence of bromine in acetic acid.[28-32] Similar products were also derived when ammonium thiocyanate was used.[33-35] Concentrated sulphuric acid in place of bromine was used to generate 6–methyl–2–aminobenzothiazole.[36-37]

1.2.3 Review on metal complexes of 2MT, 2MA and NN donor ligands

Co(II), Ni(II) and Cu(II) complexes of the substituted 2MT ligands (R = H, *o*-Me, *o*–Cl and *p*–Cl) have been previously reported by Kratzl *et al*.[38] The Cu(II) complexes were prepared by combining the appropriate metal salt in ethanol with the desired aniline derivative in the same solvent in a 1:2 mass ratio. Co(II) and Ni(II) complexes were prepared using similar mass reacting ratio, however both solutions were heated to boiling before they were mixed together and the solid complexes formed on cooling the mixture. The formulae of complexes formed are $CuLCl_2$, NiL_2Cl_2 and CoL_2Cl_2 (L is the series of 2MT ligands) respectively.

Complexes of Co(II), Ni(II) and Cu(II) with 2MA have been reported[39-41] with general formula CoL_2Cl_2, NiL_2Cl_2 and $CuLCl_2$ respectively, where L is 2MA and acts as a bidentate ligand. Dunski and Crawford[39] derived the metal complexes by dropwise addition of ethanol solution of appropriate metal chloride to 2MA in ethanol at room temperature. However on heating both reactants to reflux, CuL_2Cl_2 was obtained.

Some complexes of the stoichiometry $PdCl_2(NH_2\text{-}SMe)_2$ and $[Pt(NH_2\text{-}SMe)_2][PtCl_4]$ were also derived[40] with 2MA, the *S*–demethylation of the ligand is reported to occur when these complexes are heated in dimethylformamide yielding the thiolo-bridged complexes $M_2Cl_2(NH_2\text{-}S)_2$. The analogous nickel complex was not demethylated under similar conditions however.

1.2.4 Spectral and magnetic properties of 2MT, 2MA, related compounds and complexes

Functional groups associated with primary amine in 2MA ligands have been assigned their infrared and Raman shifts. Generally the N–H asymmetric and symmetric stretches, NH_2 scissor bend and C–N stretch were assigned[19,23,39] infrared frequencies in the ranges 3470 – 3424, 3365 – 3325, 1600 – 1610 and 1300 – 1310 cm^{-1} respectively. In the modeling studies[42] of 2MA, Raman shifts of 3345, 1683 and 1305 cm^{-1} were assigned to the N–H asymmetric stretching, NH_2 bending and C–N stretching modes respectively.

The infrared absorptions of the metal(II) complexes are characterized by the amine N–H stretches which are shifted to lower wavenumber on coordination compared to the parent ligand. As expected, coordination normally leads to a shift of the N–H stretching vibration to lower frequencies;[40] the range of shifts reported usually between 150 and 300 cm^{-1} for the metal complexes. The NH_2 bend and C–N stretch likewise undergo shifts to lower frequencies by 10 – 30 cm^{-1}.

In the complexes of 2MT and related ligands with Co(II), Ni(II) and Cu(II), the NH_2 asymmetric and symmetric stretches were red shifted by 150–200 cm^{-1} in the coordination compounds.[38,41,43,44] The N–H infrared frequencies of 2MA complexes reported[39] were shifted to a much lower frequency (by 150–270 cm^{-1}) compared to those of 2MT complexes. The magnetic moments for these complexes are 4.79, 3.11 and 1.77 B.M. for Co, Ni and Cu complexes respectively.[39]

Aniline as a ligand belongs to a class of N donor group and two moles of it can be used in coordination to a metal ion. Infrared studies of aniline and its complexes with Mn(II), Co(II), Ni(II), Cu(II), Zn(II), Cu(II), Pd(II) and Pt(II) halides were made using 15-N[45,46] and 2-D[47] labelling. Different vibrations in the compound were assigned on the basis of observed shifts in frequency of each group on deuteration; NH_2 stretching and scissoring vibrations were assigned 3440 – 3481, 3360–3395 and 1618 cm^{-1} respectively, and C–N stretch 1271–1278 cm^{-1}.

In the aniline complexes, a decrease of 100 – 200 cm^{-1} occurred for asymmetric and symmetric NH_2 stretches and a lower frequency shift of 40 – 70 cm^{-1} for C–N was observed; this is expected with the decrease in C=N double bond character. Absorptions in the region 370 – 450 cm^{-1} were suggested to due to metal to nitrogen stretch and in the series of metal(II) complexes studied,[45] their frequencies decreased in the order Pt > Pd > Cu > Co > Mn > Zn > Cd. The trend was ascribed to be partly due to differences in absorption profile attributed to coupling between NH, vibrations in amino groups having different relative conformations in the different complexes. These conformations appear to be determined by the over-all configuration (planar square, tetrahedral or octahedral) and by the size of the halogen atoms. Metal to chlorine stretches in these complexes in the range 295–334 cm^{-1} were assigned on the basis of their absence in the spectra of the corresponding bromide and iodide complexes. Two bands were observed for tetrahedral complexes due to the asymmetric and symmetric stretching vibrations.[45]
In another study[48] of infrared spectra of octahedral and tetrahedral aniline complexes with Co(II), Ni(II), Cu(II) and Zn(II), metal to nitrogen and metal to halogen stretching frequencies were assigned on the basis of the band shifts which occur on 15–N labelling and metal ion and halogen substitution; bands in the region 170–320 cm^{-1} and 350–450 cm^{-1} to M–Cl and M–N bands respectively. Lower frequency shift of these bands was observed in the complexes on moving from lower to higher coordination number.

Metal to ligand bands in *cis*- and *trans*-$[Pt(An)_2X_2]$ (X = Cl, Br, I) were assigned[49] by 15–N labelling and varying the halogen. The stretching frequency for Pt – N is 374 cm^{-1} in both *cis*- and *trans*- complexes while bands at 330, 230 and 170 cm^{-1} were assigned ν(Pt – X) for X = Cl, Br and I respectively.

In the complexes of 2MA with Ru, Ni, Pd and Pt reported, the M–Cl bands in the infrared region are found to be dependent on the structure of the compounds. Two M–Cl bands in Ru(II) complex, RuL_2Cl_2,[19] were assigned 310 cm^{-1} and 320 cm^{-1} indicating the chlorine atoms are *cis* to each other.[50] In a study[51] of low frequency infrared spectra of NiL_2Cl_2 (L, bidentate), $[PdL_2]Cl_2$ (L, bidentate) and PtL_2Cl_2 (L, monodentate), where L is 2MA, a M–Cl band was observed at 345 cm^{-1} for the nickel complex; which could indicate an octahedral nickel complex with *trans* chlorine atoms for the nickel complex. The earlier work of Livingstone on other Ni(II) complexes supported this.[52] No M–Cl band was observed in the region 270–360 cm^{-1} expected for Pd–Cl, supporting the presence of ionic chlorides. It was suggested the complex PtL_2Cl_2 may have a *cis* structure due to two M–Cl bands observed at 336 cm^{-1} (symmetric) and 325 cm^{-1} (asymmetric), the weak symmetric band not infrared active in the *trans* isomer.

Complexes of nickel(II) with N donor ligands such as aniline, pyridine, quinoline and dipyridine were isolated and found to exhibit diverse geometries with the colour of the complexes changing as the ligands are replaced. For $NiCl_2(aniline)_2$,[53] when aniline was replaced with ligands of stronger field such as pyridine[54], quinoline[55] and dipyridine,[56] the colour of the complexes were blue or yellow. These complexes exhibited varying geometries as octahedral, tetrahedral or square planar depending on their coordination number of the ligands. Their magnetic moments were found to be typical of octahedral (μ = 3.20–3.41 B.M.), tetrahedral (μ = 3.54 B.M.) and diamagnetic square planar complexes. The nickel complex of the type $Ni(NNS)_2$ has moment 3.42 B.M. which is above the range 2.9-3.3 B.M. generally accepted as typical of octahedral Ni(II). However, it falls within the range 3.3-3.5 B.M. found for many tetragonal Ni (II) complexes.[57]

The solid reflectance spectra[38] of Co(II) complexes of 2MT show three bands in the ranges 480–500, 540 and 560–590 nm while the electronic spectra in DMF show two bands at 600–610 and 660–670 nm (log ε about 2.5). A change in configuration from octahedral to tetrahedral was implied with these large shifts in wavelengths and with change in colour from pink to dark blue on dissolution in DMF. The magnetic moments of Co(II) complexes of 2MT studied are between 5.24 and 5.28 B.M.[38]

In the electronic spectra of Ni(II) complexes of 2MT ligands,[38] an octahedral structure was assigned due to three bands observed in their solid reflectance spectra at 410–420, 650–660 and 725–740 nm which were shifted to 420, 620 and 685–700 nm respectively in solution spectra with DMF. It was suggested the shift to higher energy could be as a result of replacement of Cl with DMF as the latter is higher in spectrochemical series. The magnetic moments for these complexes are in the range 3.04-3.20 B.M.[38]

For the copper(II) complexes of 2MT, 2Me–2MT, 2Cl–2MT and 4Cl–2MT already reported, distorted octahedral or tetragonal structures were suggested. Their absorption spectra were found to be almost identical to those of $Cu(ClO_4)_2$ in DMF,[58] displaying only one absorption maximum in the near UV region. Magnetic moments were measured between 1.86 and 1.95 B.M.[58]

1.3 SCHIFF BASE LIGANDS AND COMPLEXES

Schiff-base was first synthesized by Hugo Schiff.[59] Schiff-bases are derived from condensation reaction between a primary amine ($-NH_2$) and a carbonyl (-C=O from a ketone or an aldehyde group). The resulting imine functionality is the hallmark for Schiff-bases products. Water is also eliminated alongside in the condensation reaction (**Fig. 1.3**). The formation of a Schiff base is a reversible reaction and generally takes place under acid or base catalysis or upon heating.

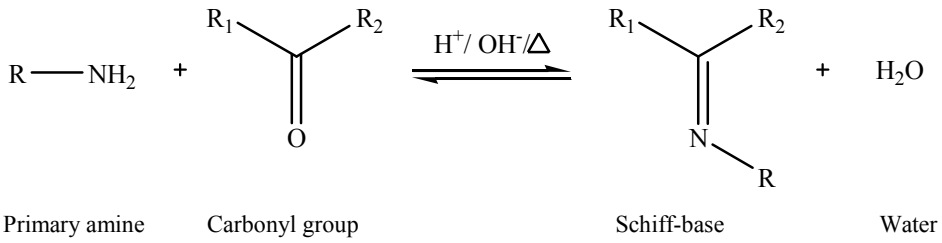

Fig. 1.3 Condensation reaction for the formation of Schiff-bases

Schiff bases of aliphatic aldehydes are relatively unstable and readily polymerizable[60,61] while those of aromatic aldehydes having effective conjugation are more stable.[62]Aldehydes react faster than ketones in formation of Schiff-bases as the reaction centres of aldehydes are sterically less hindered than that of ketones.[63]

Schiff bases are better coordinating ligands when they bear a functional group, usually the hydroxyl, sufficiently near the site of condensation in such a way that a five- or six-membered chelate can be formed with a metal ion.

1.3.1 Spectroscopic properties of Schiff bases

Schiff-base ligands have been characterized by infrared, nuclear magnetic resonance and ultraviolet/visible spectroscopic methods. The $\nu_{C=N}$ (as well as ν_{C-O} for those with hydroxyl group) stretching frequency is the main typical feature used for the characterization of Schiff-bases and chemical shifts of the azomethine proton (HC=N) are usually investigated in the NMR study.

The $\nu_{C=N}$ frequency of Schiff-bases generally occurs in the region 1680-1603 cm^{-1} when H, alkyl or phenyl groups are bonded to carbon and nitrogen atoms.[64] The position of this vibrational frequency is affected by the physical state of the compound, the nature of the substituent, conjugation with either carbon or nitrogen or both, and hydrogen bonding.

For Schiff bases of the type Ar–CH=N–R (where Ar is an un-substituted phenyl group), two different ranges were reported[65,66] for $\nu_{C=N}$ frequency; 1650-1638 $cm^{-1}$and 1650-1645 cm^{-1} respectively.

With substitution of a nitro or halogen group on the phenyl ring, a range of 1657-1631cm^{-1} was observed.[65] A frequency region of 1631–1613 cm^{-1} were found for the compounds of the type Ar–CH=N–Ar.[67] The presence of an OH group at the 2-position of the phenyl ring effects a red shift, with a frequency shift of about 8 cm^{-1} using *N*-benzylideneaniline as a reference. In these compounds, the phenolic C–O stretching vibration occurs between 1288 and 1265 cm^{-1}.

The C=N stretching frequency is generally shifted to lower energies upon coordination to metal ions through both O and N atoms. Kovacic[68] assigned the $\nu_{C=N}$ frequency in some substituted salicyl-aldiminatocopper(II) complexes in both the solid state and in solution. In nujol mull, it was found at 1603–1616 cm^{-1}, while in dichloromethane the band is shifted to 1601–1612 cm^{-1}. In the Cu(II) complexes, the phenolic C–O appears in the region 1310–1330 cm^{-1}, as compared to 1265–1288 cm^{-1} in the free ligands.

Absorption due to the free O–H stretching vibration is not always observed in the infrared spectra of Schiff-bases derived from 2-hydroxybenzaldehyde and aniline.[68] This has been attributed to the formation of intra-molecular hydrogen bonding resulting in a stable six-membered chelate, as seen below (**Fig. 1.4**). Instead, a broad, weak band having some fine structures is found in the region from 3100–2700 cm^{-1},

most of the fine structure is due to the C–H modes. However, Baker and Shulgin[69] as well as Kovacic[68] have assigned a weak band near 2730 cm^{-1} to the internally hydrogen bonded O–H stretching vibration.

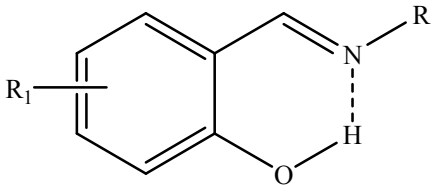

Fig. 1.4 Hydrogen bonding in salicyaldimines

UV/Visible spectra of some Schiff-bases have been reported. The Schiff-base ligands synthesized by Abdu-Elzaher[70] exhibited three peaks at about 270 nm, 330 nm, and 372 nm and were characterized as follows: the first two peaks were attributed to benzene $\pi \rightarrow \pi^*$ and imino $\pi \rightarrow \pi^*$ transitions while 372 nm was assigned to $n \rightarrow \pi^*$ transition. Zhoa *et al.*[71] has also assigned the band at 334 nm to the azomethine chromophore $\pi \rightarrow \pi^*$ transition while the bands at higher energies (212 and 281 nm) were regarded as associated with the benzene $\pi \rightarrow \pi^*$. However, Ramesh and Maheswara[72] assigned $\pi \rightarrow \pi^*$ and $n \rightarrow \pi^*$ of the imine bond to the bands at 295–249 nm and 330–346 nm respectively. On the other hand, the azomethine chromophore $\pi \rightarrow \pi^*$ or $n \rightarrow \pi^*$ transition always undergoes either a red or blue shift in the complexes, depending on the nature of the Schiff base and the metal ion. This is usually used as an indication of the involvement of imino nitrogen in coordination to metal ion. The bands assigned to benzene $\pi \rightarrow \pi^*$ transitions are always only slightly affected.[72]

1.3.2 Application of Schiff bases

Schiff-bases have useful applications as antibacterial[73-78] and antifungal agents.[79-80] Schiff base products obtained from aminopyridines and *o*-hydroxyaromatic aldehydes have been demonstrated to serve as analytical agent for metal analyses,[81-83] hence encouraging investigations of the corresponding metal complexes.

Schiff bases are often used as ligands in coordination chemistry to form metal complexes owing to their metal binding ability.[82,84-86] Schiff bases are able to stabilize many different metals in various oxidation states, controlling the performance of metals in a large variety of useful applications in biological, clinical, analytical and industrial in addition to their important roles in catalysis and organic synthesis.[87]

Not only have they played a seminal role in the development of modern coordination chemistry, but they can also be found at key points in the development of inorganic biochemistry.[88]

A considerable number of Schiff-base complexes have potential biological interest, being used as successful models of biological compounds.[89-90] Schiff base complexes incorporating phenolic group as chelating moieties in the ligand are considered as models for executing important biological reactions and mimic the catalytic activities of metalloenzymes.[91]

Macrocyclic derivatives of these Schiff bases have many fundamental biological functions, such as photosynthesis and transport of oxygen in mammalian and other respiratory system.[92-93] Schiff base ligands containing various donor atoms (like N, O, S) show broad biological activity and are of special interest because of the variety of ways in which they are bonded to metal ions.

It is known that the existence of metal ions bonded to biologically active compounds may enhance their activities.[87,94-95] In recent years, because of new interesting applications found in the field of pesticides and medicine, the metal complexes with tridentate O, N, N types of alternative structures have attracted the attention of chemists. Various metal complexes with bi- and tridentate Schiff-bases containing nitrogen and oxygen donor atoms play important role in biological system and represent interesting models for metalloenzymes, which efficiently catalyze the reduction of dinitrogen and dioxygen.[96]

Schiff-base formation in the biological environment is widely found in the chemistry of pyridoxal phosphate (PLP), a derivative of pyridoxine otherwise known as vitamin B_6. The role of this coenzyme is significant for living matter as far as the metabolism of amino acids is concerned.[97] In PLP-dependent enzymes, the coenzyme binds to the protein through the formation of an imine with the E- amino group of a lysine residue.[98] Stereochemical investigations[99] carried out with the aid of molecular models showed that Schiff-bases formed between methyl-glyoxal and the amino group of the lysine side chains of proteins can bend back towards the N atom of peptide groups in such a way that a charge transfer can occur between these groups and the oxygen atoms of the Schiff bases.

Salicylaldiminato Schiff-bases have been used in DNA cleavage due to their intramolecular charge transfer.[100,101] Schiff bases are involved as intermediates in the processes of non-enzymatic glycosylations.

1.3.3 Copper complexes of Schiff-bases

Copper complexes containing Schiff-base ligands are of great interest since they exhibit biological activities such as antitumor and anti-*Candida*.[102] Some copper complexes have been found to inhibit cellular proteasome and cause inhibition of cancer cell growth.[103]

The Cu(II) complexes of Schiff-bases are also important in catalysis and act as models in bioinorganic system because of charge symmetry and the possible fine-tuning of the electronic properties by different substitutions. This can create active sites with potential regioselective molecular recognition, as suggested by the head-to-tail arrangements of the molecules found in the crystal structures.[104-105]

Cu(II) complex with the Schiff base derived from 5-nitro-salicylaldehyde and ethylenediamine suggests coordination through azomethine N atom and phenolic oxygen after deprotonation.[104-105] The copper complex offered a large variety of molecular structures and electronic properties as well as the possibility of enhancing, or 'switching on' the nonlinear optical properties of the organic ligands through complexation to a metal center.[106]

Cu(II) complex with Schiff-base (salicylaldehyde-amino ethanol) and phenanthroline base has a suggested square pyramidal geometry.[107] The Schiff base coordinates in tridentate manner through ONO system, while heterocyclic base in bidentate manner through N-N system.[107] The complex exhibits visible light-induced cleavage of double standard DNA and thus is of current importance for therapeutic applications.[108-109] The photo excited electronic state of the complex initiates a series of chemical reactions that lead to the oxidative cleavage of the nucleic acid. The compound exhibits red-light-induced photo cleavage of DNA and has found clinical applications in the emerging field of photodynamic therapy (PDT) of various cancers[110- 111] and hepatotoxicity.

The brown colored Cu(II) complex with a Schiff base derived from 4-aminoantipyrine and 2-hydroxy-1-naphthaldehyde has been characterized.[112] The ligand is monobasic and tridentate in nature forms the complex through azomethine nitrogen, antipyrine ring oxygen, phenolic oxygen after deprotonation and acetate ion forming square planar geometry. The complex exhibits wide applications in biological system and industrial uses, especially in catalysis and dying.

Cu(II) complexes with two flexible Schiff bases, bis-[(N, N'-3,5-di-tert-butylsalicylidene)-4,4'-diaminodiphenyl] ether and bis-[(N,N'-3-tert-butyl-5-methylsalicylidene) 4, 4'-diaminodiphenyl] ether

were prepared in high yields and their structures were determined by X-ray single-crystal diffraction.[113] Infrared spectrum of the complexes shows coordination through azomethine nitrogen atom and deprotonated phenolic oxygen atom. The X-ray structure shows clearly that complex is a double helical structure. The neutral helix contains two Cu(II) ions and two deprotonated ligands with the Cu....Cu separation, that is shorter than other analogous Schiff base dinuclear Cu(II) complexes.[114] Each copper center is bonded to two salicyladimine units to attain pseudo-tetrahedral coordination geometry. The complexes have attracted much attention because of the fundamental role of helicity in biology and the potential applications in the fields of asymmetric catalysis and non-linear optical materials.[115] A new macrocyclic ligand was synthesized by reaction of 2, 6-diaminopyridine and 1,7-bis(2-formylphenyl)-1,4,7-trioxaheptane and its Cu(II) complex synthesized by template effect is binuclear. The comparative electrochemical study shows that the complex exhibited a quasi-irreversible reduction process in DMSO solution.[116]

A comprehensive review on the biological activity of Schiff bases and their metal complexes has been written by Arulmurugan *et al*.[117]

1.4 ANTIBIOTIC SUSCEPTIBILITY TESTING (AST)

1.4.1 General introduction

The history of antimicrobials began in 1877 with the observations of Pasteur and Joubert, who discovered that one type of bacteria could prevent the growth of another. They did not know at that time that the reason one bacterium failed to grow was that the other bacterium was producing an antibiotic. Antimicrobial therapy is the treatment of infectious disease using, typically, chemotherapeutic agents that either kill microbes or otherwise interfere with microbial growth.

In general, antimicrobial drugs can be classified[118] into two categories; the first comprises of those obtained from natural sources such as beta-lactam antibiotics (*e.g.* penicillins, cephalosporins) and protein synthesis inhibitors (*e.g*. aminoglycosides, tetracyclines, chloramphenicol). The second category includes the synthetic antibiotics such as the sulphonamides, cotrimoxazole, antivirals, antifungals, antimalarials, anticancer drugs *etc.*

1.4.2 Modes (mechanism) of action

It is always desirable to know the mode of action of an agent and five modes of antimicrobial action have been identified[119] viz.

(i) Inhibition of cell wall synthesis

(ii) Disruption of cell membrane function

(iii) Inhibition of protein synthesis

(iv) Inhibition of nucleic acid synthesis (i.e., inhibition of replication of genetic material or transcription).

(v) Action as antimetabolites

For an antibiotic to affect the growth of a microbial cell it must (i) enter the cell and reach the site of action, (ii) bind to a target molecule involved in an essential cell process, (iii) markedly inhibit this process. An antibiotic can be bactericidal or bacteriostatic. A bactericidal effect occurs when the antibiotic interaction results in an irreversible disruption or binding whereas a bacteriostatic effect involves lower affinity binding and as such is reversible when the antibiotic is removed from the environment.[119]

1.4.3 Classification of organisms based on activity

The result of the activity of antimicrobial agents has led into the classification of microorganisms into categories of susceptibility. The Kirby-Bauer method[120] and its modifications recognize three categories of susceptibility as susceptible, intermediate susceptible and resistant.

An organism is said to be "susceptible" to a drug when the infection caused by it is likely to respond to treatment with this drug at the recommended dosage.

“Intermediate susceptibility” covers two situations. It is applicable to strains that are "moderately susceptible" to an antibiotic that can be used for treatment at a higher dosage because of its low toxicity or because the antibiotic is concentrated at the focus of infection. The term also applies to those strains that are susceptible to a more toxic antibiotic that cannot be used at a higher dosage. In this situation the intermediate category serves as a buffer zone between susceptible and resistant.

The term "resistant" implies that the organism is expected not to respond to a given drug, irrespective of the dosage and the location of the infection.[121]

Bacteria demonstrate two kinds of resistance to antibiotics, namely intrinsic and acquired resistance. Intrinsic resistance means that the species was resistant to an antibiotic even before its introduction. Acquired resistance means that the species was originally susceptible to an antibiotic, but later became resistant. Bacteria can acquire antibiotic resistance either by mutation or through exchange of genetic material among same or closely related species. The sudden acquisition of resistance to antibiotics poses difficulties in treating infections. Resistance to several different antibiotics at the same time is even more significant problem. It is because of the acquired resistance that bacterial isolates must be subjected to antibiotic susceptibility testing.

1.4.4 Antibiotic susceptibility testing methods[122]

1. Quantitative Methods
2. Qualitative Methods
3. Automated Susceptibility Tests
4. Newer Non-Automated Susceptibility Tests
5. Molecular Techniques

1. Quantitative methods: In these tests, the minimum amount of antibiotic that inhibits the visible growth of an isolate or minimum inhibitory concentration (MIC) is determined. Bacterial isolate is subjected to various dilutions of antibiotics. The highest dilution of antibiotic that has inhibited the growth of bacteria is considered as MIC. These tests can be performed on broth or agar. These are classified as:

1. Broth dilution methods
    a. Macrobroth dilution MIC tests
    b. Microbroth dilution MIC tests
2. Agar dilution methods

Macrobroth dilution tests: A serial two-fold dilution of antibiotic are made in test tubes from 0 to maximum concentration that is achieved *in vitro* without toxic effect on patient. The inoculum density of bacterial isolate to be tested is standardized with 0.5 McFarland turbidity standard. The suspension should have a final inoculum of 5 X 10^5 CFU/mL. 1mL of bacterial suspension is added to rows of antibiotic solution and incubated at 37^{o}C overnight. The lowest concentration of antibiotic that completely inhibits visual growth of bacteria (no turbidity) is recorded as MIC.[122]

Microbroth dilution tests: A polystyrene tray containing 80 wells is filled with small volumes of serial two-fold dilutions of different antibiotics. The inoculum suspension and standardization is done according to McFarland standard. The bacterial inoculum is then inoculated into the wells and incubated at 37^{o}C overnight. MIC is determined as in macrobroth dilution test.

Agar dilution method: A serial two-fold dilution of the antibiotic is prepared in Mueller-Hinton agar. The bacterial inoculum is standardized according to McFarland standard. Using a micropipette a measured small volume (usually 1–10 mL) is inoculated on the surface of agar and incubated at 37^{o}C overnight. The lowest concentration of antibiotic that inhibits visible growth on surface of agar is taken as MIC.

2. Qualitative Methods: These tests categorize a bacterial isolate as sensitive, intermediate or resistant to a particular antibiotic. This is the disk diffusion susceptibility test.

Disk diffusion test: In this method the standardized bacterial isolate is spread on an agar plate and then paper disc containing specific concentration of antibiotics are placed and incubated at 37^{o}C overnight. If the organism is susceptible to the antibiotic, it does not grow around the disk thus forming a zone of inhibition. Strains resistant to an antibiotic grow up to the margin of disk. The diameter of zone of inhibition[123] must be measured and result read from the Kirby-Bauer chart as sensitive, intermediate or resistant.

3. Automated Susceptibility Methods: Determination of bacterial growth in wells containing antimicrobial agent are performed in short period of time using computer-assisted instruments. Various techniques include turbidimetric detection, flourimetric detection and Video Image processing.

Newer Non-Automated Susceptibility Tests include the alamarBlue® assay which incorporates an oxidation-reduction indicator that both fluoresces and changes color in response to chemical reduction of growth medium resulting from microorganisms and mammalian cell growth.[123] Etest® is a predefined, stable gradient of 15 antibiotic concentrations on a plastic strip which makes use of innovative dry chemistry technology and is used to determine the on-scale minimum inhibitory concentration (MIC) of antibiotics, antifungal agents and anti-mycobacterial agents.[124] The Spiral Gradient Endpoint (SGE) test provides highly sensitive and repeatable MIC determinations by the agar dilution method. A gradient of antimicrobial concentrations is produced in the agar by deposition of a stock solution with a spiral plater.[125]

4. Molecular Techniques involve the detection of gene coding for resistance to one or several drugs by techniques such as polymerase chain reaction (PCR) and deoxyribonucleic acid (DNA) hybridization.[122]

Important features of quality assurance in antibiotic susceptibility testing are listed below[126]

- Use antibiotic discs of 6 mm diameter
- Use correct content of antimicrobial agent per disc
- Stock the supply of antimicrobial discs at -20^{o}C
- Use Mueller-Hinton medium for antibiotic sensitivity determination
- Use appropriate control cultures
- Use standard methodology for the test
- Use coded strains from time to time for internal quality control
- Keep the antibiotic discs at room temperature for one hour before use
- Incubate the sensitivity plates for 16-18 hours before reporting
- Incubate the sensitivity plates at 35^{o}C/37^{o}C as appropriate
- Space the antibiotic discs properly to avoid overlapping of inhibition zone
- Use inoculum size that produces near confluent growth
- Ensure an even contact of the antibiotic disc with the inoculated medium
- Measure the zone sizes precisely using a ruler
- Interpret the zone sizes by referring to standard charts.

1.5 ANTIMALARIAL AGENTS

1.5.1 Malaria disease

Malaria is an infectious disease transmitted by the bite of an infected female mosquito of the *Anopheles* genus. The malaria causative agent, transmitted by the mosquito vector, is a unicellular eukaryote (*i.e.* protist) belonging to the *Apicomplexa* phylum and named *Plasmodium spp*. It is an obligate intracellular parasite. Five species *Plasmodium spp*. are infectious to humans: *P. falciparum*, *P. vivax*, *P. ovale*, *P. malariae*, and *P. knowlesi*. *P. falciparum* is responsible for most of the deaths from malaria. Malaria is present in most inter-tropical countries, and is the cause of an estimated one in every five childhood deaths (20%) in Africa. It is calculated that an Africa child has on average 1.6 to 5.4 episodes of malaria fever each year and a child there dies from malaria every 30 s.[127] Malaria is a major public health problem which puts 3.3 billion people at risk and affects almost half a billion people worldwide, resulting in around 1–3 million deaths each year,[128] with a recent encouraging decrease to under 1 million casualties in recent years.[127]

1.5.2 Advances in antimalarial agents

As a result of its continuing danger to public health, various approaches have been used in order to eliminate or reduce significantly the menace of malaria. These include the use of insecticides, vaccines and chemotherapy.[129]

Insecticides (e.g. DDT) which act as poisons to mosquito can be sprayed in a given area (indoor residual spraying (IRS)) or coated on materials such as bed nets (insecticide treated nets (ITN) and long lasting insecticidal nets (LLIN)). The indiscriminative use of massive insecticide sprayings, however, has led to the resurgence of insect resistance. The ITN and LLIN approaches have been effective and could lower transmission by 90% and child mortality by 10% if used by all. However, a recent study has shown mosquito are developing resistance to insecticides, even the newest long lasting compounds (*i.e*. the LLIN approach), in short period of time.[130]

Several pathways and protein targets are currently assessed as potential targets for vaccines and are on clinical trial[131] and a recent and promising study has been led and published on a phase 3 clinical trial for over more than 15 000 patients in seven African countries.[132]

Chemotherapy is an approach that involves the use of chemical agents. So far, malaria control has relied heavily on a restricted number of chemically related drugs belonging to either the quinoline or the antifolate groups. Quinoline-based antimalarials include quinine, chloroquine, *etc*. It is generally believed that they target the catabolism of the host's haemoglobin by the parasite which take place in the acidic food vacuole,[133,134] specifically inhibiting haemozoin formation.[135]

Until the mid 20th century, chloroquine (CQ) (**Fig. 1.5**) was the most efficient molecule to efficiently treat malaria but the parasite has developed a global resistance to the molecule.

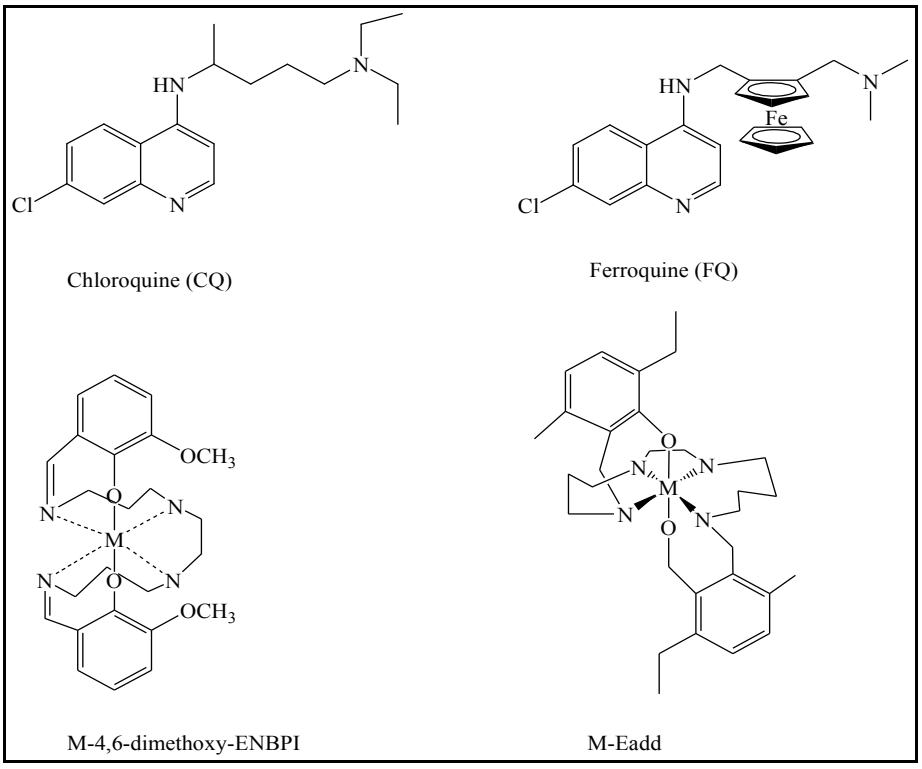

Fig. 1.5 Antimalarial drugs and potential metal-based antimalarial drugs

Other types of antimalarial drugs are the antifolates, which interfere with folate metabolism, a pathway essential to malaria parasite survival. This class of drugs includes effective causal prophylactic and

therapeutic agents, some of which act synergistically when used in combination with one another. The most commonly used antifolate combinations are pyrimethamine, chloroquanide or dapsone as a dihydrofolate reductase (DHFR) inhibitor combined with sulfalene or sulfadoxine as a dihydropteroate synthase (DHPS) inhibitor.[136] The antifolates have been proven to be susceptible to resistance by the malaria parasite. Resistance is caused by point mutations in DHFR and DHPS, the two key enzymes in the folate biosynthetic pathway that are targeted by the antifolates.[137] There are numerous marketed monotherapies from this class. Drug combinations of proguanil and atovaquone (malarone) are also available.[138]

In search of new and more effective organic drugs that can prevent the parasite resistance, a significant contribution in the field of antimalarial chemotherapy has been identified as the active component, artemisinin. Artemisinin-based combination therapies are considered the most efficient treatment to cure malaria patients.[127] Difficulties in the formation of artemisinin led to discovery of its water soluble counterparts, dihydroartemisinin and artesunate.[139] These compounds are believed to be activated by the iron-rich environment inside the parasite.[140] Generation of such a reactive chemical entity produces several chemical transformations.[141-143] Although extremely efficient to treat malaria patients, artemisinin is currently threatened by the emergence of resistant parasite in south east Asia.[144,145]

1.5.3 Antimalarial drug resistance

Antimalarial drug resistance has been defined as the ability of a parasite to survive and/or multiply despite the administration and absorption of a drug given in doses equal to or higher than those usually recommended but within tolerance of the subject. The drug in question must gain access to the parasite or the infected red blood cell for the duration of the time necessary for its normal action. Resistance can become firmly established within a parasite population, existing for long periods of time. The first type of resistance to be acknowledged was to chloroquine in Thailand in 1957.

The parasite has generated a detoxification mechanism in which the haematin (harmful to *Plasmodium* in high concentrations by causing lipid peroxidation) forms a highly insoluble, microcrystalline substance present in the food vacuole called haemozoin.[146] Several mechanisms have been proposed for the formation of haemozoin.[147-149] The hypothesis that haematin is the target of some antimalarials originated from early studies showing that chloroquine forms a complex with haematin.[150] Since then haem,

haematin and haemozoin have been drug targets for antimalarials. Artemisinin forms radical adducts with haem that act against the parasite.[151]

Haematin is believed to be the main target of the quinoline-based drugs and there has been evidence that these drugs act by preventing the detoxification of haematin. The mechanism of action by which these drugs are able to avoid the formation of haemozoin has been the subject of various debates and hypotheses.[152-154] Given that haemozoin formation is unaltered in drug resistance; it remains an excellent target for new drugs. Recent advances in understanding of these drugs' interactions with both haematin and haemozoin have been made.[155]

1.5.4 Metal-based antimalarial agents

Metals may also be used to enhance the efficacy of organic drugs and rational design of metal–based therapeutic agents has increased after the important discovery of Cis–platin, a successful Pt-based anticancer drug.[156,157] Use of metals in medicine has advantages in giving more effective syntheses of stable transition metal complexes with variable and predictable structures. Ligand properties can be selected to tune the overall properties of the medicinal product and this provides more knowledge of the biological effects of metals in the organism in order to enhance efficient biological targeting. These parameters have helped in the development of new drugs for major medical human problems including cancer along with bacterial, viral and parasitic infections such as malaria.[158]

Metal complexes with amodiaquine and primaquine were reported in 1987 by Wash *et al*.,[159] however the activity of these drugs was not increased by complexation. Analogues of metal-chloroquine complexes were designed; Sanchez-Delgado *et al*[160] modified the chloroquine template by incorporating a transition metal into the molecular structure, the rhodium complexes of the derived compound showed enhancement by 4.5 fold compared to the standard drug chloroquine diphosphate (CQDP). This propelled the group to move further exploring with Ru(II) and chloroquine (CQ), a new molecular design was used by varying the ancillary ligands and the overall charge of the complexes. The potency of all complexes of Ru-CQ was higher.[161] For greater efficacy, gold complexes were isolated which showed an activity 5-10-fold greater than chloroquine.[162] Encouraged by this enhancement of activity, a new series of gold-CQ complexes were developed with different changes including variations of the phosphine ligand, in the counteranion and the oxidation state of gold and the use of other biological important ligands.[163]

However, no clear structure-activity correlations could be established for this series of compounds. Iridium-CQ complexes have also been evaluated, displaying moderate activity.[164] Pt-CQ derivatives have been synthesized and tested on malaria by various research groups, the compounds showed higher activity than free ligands.[165]

As analogues of ferrocene complexes have shown potentials as drugs with medical applications,[166] many complexes have been prepared based on ferrocene-conjugate analogues of known antimalarial drugs.[167-171] No enhancement was noted except in the case of ciprofloxacin,[169-171] with more than 20 times activity in CQ-resistant strains. These compounds showed only moderate antimalarial activities in 8 parasite strains, which implies that the presence of the ferrocenyl moiety in these structures does not significantly change their biological activity in malaria.[172] Low or decreased activity was shown by chloroquine diphosphate associated with ferrocene carboxylic acid *via* a salt bridge suggesting an antagonistic effect between both parts,[173] and when ferrocene is condensed on the quinoline ring or on the endocyclic nitrogen,[174] or attachment of ferrocenyl group to the terminal nitrogen associated with a modulation of the lateral chain length.[175] The bisquinolines-derivatives however were active against CQ-resistant strain.[176] The ferrocenyl bisquinoline showed activity on CQ-resistant strain (D2d) but was less active on the CQ-susceptible strain (HB3).[177]

Ferroquine FQ (**Fig. 1.5**)[178,179] was formed by introduction of the ferrocenyl moiety into the lateral side chain of chloroquine. Ferroquine in different formulations as base, ditartrate or dihydrochloride salts[173] has been found to be active against both CQ-resistant and CQ-susceptible parasites. The antimalarial activity against CQ-resistant parasites is partly facilitated by the location of the ferrocene moiety inside the lateral chain.[175] As it possesses planar chirality, ferroquine has enantiomers; the activities of the pure enantiomers and the racemate have been compared. Both enantiomers and racemate were found to be equally active *in vitro* against the CQ-susceptible and CQ-resistant *P. falciparum* strains HB3 and Dd2. When tested *in vivo* against *P. vinckei*, both enantiomers were slightly less active than the racemic mixture which could be suggestive of synergistic effect between the enantiomers. Similar results were obtained for the different enantiomers and the racemate from the *in vitro* cytotoxicity studies in the L5178Y cell proliferative assay.[180]

Ferroquine has shown a higher efficacy than chloroquine; curative doses for chloroquine for CQ-susceptible *P. vinckei* is 70 mg Kg^{-1} per day and 400 mg Kg^{-1} per day for the CQ-resistant clone while that for ferroquine is 10 mg Kg^{-1} per day for all strains tested, irrespective of the route of administration.[181,182]

In order to produce drugs with better activity and improved property, modifications were made to ferroquine by modifying the tertiary and secondary amines. Changes in tertiary amines showed 2-10 fold improved activity more than CQ and of same activity with FQ.[175] FQ derivatives mimicking hydroxychloroquine (HCQ) were prepared, which structurally differ from FQ in the presence of side chains on the tertiary amines and in the possession of OH group, designed to reduce the cytotoxicity effects as compared to FQ. These compounds showed increase activity compared to CQ but lower activity than FQ.[183] Changes in the secondary amines resulted in an analogue with higher antimalarial activity than that of CQ and comparable to that of ferroquine. These studies showed that the remarkable activity of FQ depends on the position of the ferrocenic nucleus in the side chain and that the *in vitro* antimalarial activity is not disturbed by slight modifications in the lateral basic side chain.[184]

More analogues of ferroquine with thiosemicarbazones were prepared.[185] From comparison of the activity of a series of analogues synthesized by the combination of FQ with thiosemicarbazones (those without the ferrocenic moiety and those without the 4-aminoquinoline moiety), the authors concluded that the aminoquinoline moiety which allows transport of the compounds to parasite food vacuole seems to be the major contributor to antimalarial activity of FQ while the ferrocene moiety within the lateral chain is responsible for maintaining a strong antimalarial activity on CQ-resistant *P. falciparum*.

Trioxaquinines[186] contain two moieties covalently linked together; 1,2,4-trioxane (as in artemisinin) and 4-aminoquinoline (as in CQ). They were produced based on the concept of hybrid molecules with a dual mode of action. These molecules have shown considerable activity against the CQ-resistant strains of *P. falciparum*.[187,188] One of the trioxaquines, PA1103/SAR116242 has been selected as a drug candidate.[189] These hybrid compounds might be considered a possible response to the recently growing resistance of various parasites to artemisinin.[190,191]

Another approach towards development of antimalarial compounds is the use of chelating ligands with metal ions. Ligands such as ethylenediamine-N,N′-bis[propyl(2-hydroxy-(R)-benzylimino)] (ENBPI)[192,193] and [1,12-bis(2-hydroxy-3-ethylbenzyl)-1,5,8,12-tetraazadodecane] (Eadd)[194] (**Fig. 1.5**) have formed stable complexes with Al(III), Fe(III), Ga(III) and In(III) and these compounds were modified by variation of the substituents on the aromatic rings and the hydrocarbon backbone independently. All the complexes except those of In(III) showed activity against CQ-susceptible (HB3) and CQ-resistant (FCR-3 and Indo-1) strains of *P. falciparum.* The 4,6-dimethoxy-ENBPI Fe(III) proved to be the most potent of the series, inhibiting both CQ-susceptible and CQ-resistant parasites. The selective biological activity of this compound has been explained taking into account the spatial

orientation of the peripheral regions of the aromatic moieties including the methoxy functionalities, rather than just the central metal core. The antimalarial activity of these compounds has been observed to correlate well with their ability to inhibit formation of β-haematin *in vitro*, likely *via* the formation of specific drug/haem propionate salt.[192,193]

As a result of the encouraging results of the metal-based drugs, a large number of metal complexes with Cu,[195,196] Pd,[197] Mn, Co[198] centers have been reported recently. From the biological studies of these compounds, they do not exceed the activity of gold-chloroquine complexes, ferroquine and ruthenium-chloroquine complexes.

Metal complexes of trimethoprim, chloroquine and pyrimethamine with Mn(II), Co(II), Cu(II) and Pt(II) were synthesized[199,200] and tested for *in vitro* activity against *P. falciparum* K1 CQ-resistant strain. Their cytotoxicity was determined using L-6 cells. The Pt(II) complex of chloroquine showed most potency (IC_{50} 0.15595 μM, cytotoxicity 77.35 μM), however all the complexes show less activity compared to CQ. The effect of Cu(II) complexation on the antimalarial activity of a class of naphthoquinone ligands was reported.[195] The copper complexes show enhanced activities against *P. falciparum* 3D7 strain when compared with their parent ligands, the most potent possesses the meta substitution of the methyl group in the arylazo ring with antimalarial activity ED_{50} (μg/mL) 3.5 and selectivity index of 2.45. The most potent of the series has the most positive redox potential (+0.38 V) indicating that facile reduction to the cuprous species with subsequent activation of intracellular oxygen may be one of the likely mechanisms of their antimalarial activities.[195]

1.5.5 Mechanism of action

Though the mechanism of action of these metal-CQ complexes is not fully understood, two potential targets of action are proposed based on the accepted mechanisms of action for chloroquine: the inhibition of haemozoin formation and DNA interaction. CQ is believed to act by concentrating on the parasite food vacuole and preventing the crystallization of toxic haem into haemozoin, leading to membrane damage and parasite death.[201] It is well established that chloroquine forms complexes with haematin in solution and is an inhibitor of β-haematin formation.[201-203] From the interaction studies[204-206] of some metal-CQ complexes with haematin by spectrophotometric titration and experiments carried out by Sanchez *et al* to measure the abilities of metal-CQ derivatives to inhibit the formation of β-haematin at the lipid-water interface, it was concluded that the main mechanism of action of the complex metal-CQ is the inhibition

of formation of β-haematin. Trials in these targets (specifically at the lipid-water interface) are excellent predictors of the *in vitro* biological activity.

The mechanism of action of ferroquine has been suggested to be similar to that of CQ, by concentrating on the parasite food vacuole and preventing the crystallization of toxic haem into haemozoin. The target of action has also been linked to increase of partition coefficients which influence the lipophilicity and consequent biological behavior of ferroquine. Ferroquine is a stronger inhibitor of β-haematin formation as indicated by its IC_{50} value of 0.8 compared to IC_{50} value of 1.9 for chloroquine.[207] The better antimalarial activity of ferroquine has been attributed to the presence of intramolecular hydrogen bonding in its lateral side chain[208,209] which was confirmed by synthesizing an analogue (FQ–Me) in which the aniline hydrogen atom is replaced with methyl group with a resulting decrease in activity.[210] The ferrocene moiety in ferroquine is able to generate small amounts of hydroxyl radicals from H_2O_2 *via* a Fenton-like reaction, which is capable of inducing severe damage to the parasite food vacuole membranes before a detoxification mechanism in the parasite can be effective. This redox property of ferroquine has been suggested to attribute to its better antimalarial activity than CQ.[211,212] The inhibitory activity of ferroquine against CQ-resistant strains could be as a result of reduced affinity for transporter linked to CQ-resistance (PfCRT).

1.6 The spectral and magnetic properties of Cobalt(II), Nickel(II) and Copper(II)

Cobalt(II), Nickel(II) and Copper(II) have similar features characteristic of transition metal ions such as ability to form coloured complexes and exhibit various geometrical structures, however, their spectral properties and hence magnetic properties are different due to differences in their outer *d* electrons. The crystal field splitting of the *d* orbital of a metal ion in high symmetries including tetrahedral and octahedral is shown in **Fig. 1.6**.

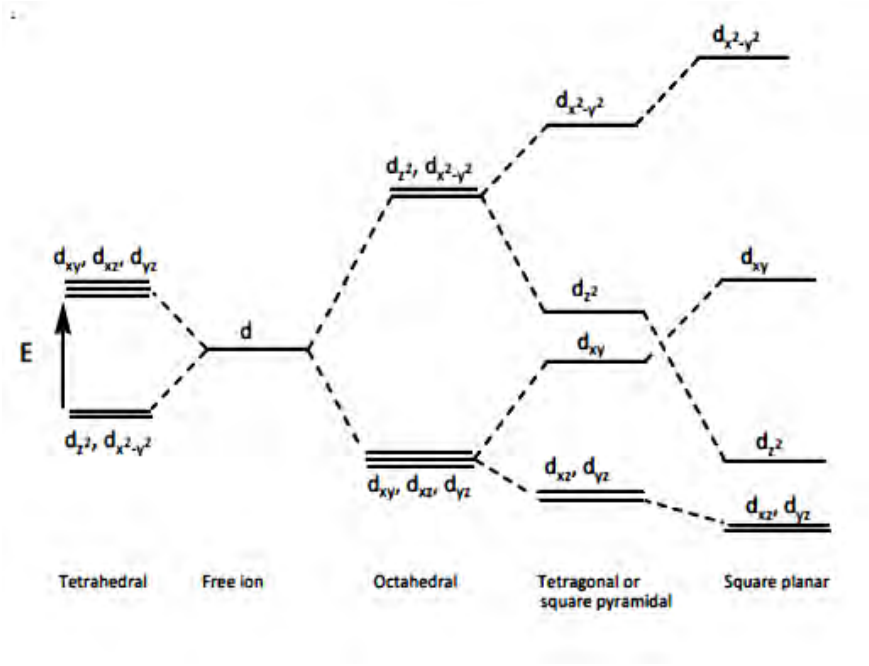

Fig. 1.6 Crystal field splitting of the *d* orbitals of a central ion in complexes of various geometries

1.6.1 Cobalt(II)

The Cobalt(II) ion has a $3d^7$ configuration and it complexes with ligands to form majorly tetrahedral or octahedral complexes (**Fig. 1.7**) majorly with orange-pink or blue-violet colors respectively. Cobalt(II) forms more tetrahedral complexes than any other transition metal ion, likely as a result of small difference in the crystal field stabilization energies between its octahedral and tetrahedral complexes when compared with that for other d^n configurations).[213]

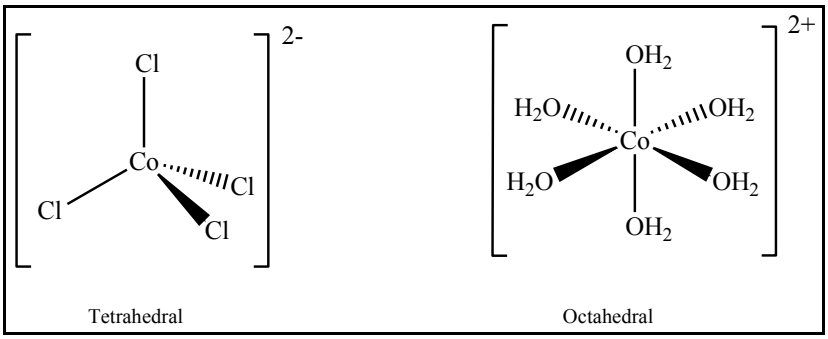

Fig. 1.7 Typical Co(II) complexes in tetrahedral and octahedral geometries

In the octahedral field Co(II) has a ground term $^4T_{1g}$. Octahedral complexes are usually high spin. Low spin complexes are few because only ligands with very strong fields can cause spin pairing of Co(II) ion (Dq > 15 000 cm^{-1}).[214] Tanabe and Sugano[215] have made a complete energy level diagram for octahedral Co(II) complexes. Three transitions are expected for high spin octahedral Co(II) complexes. The lowest energy band is a transition corresponding to $^4T_{1g} \rightarrow {}^4T_{2g}$. The highest energy transition occurs in the visible near 20 000 cm^{-1} (500 nm) and has been assigned to $^4T_{1g} \rightarrow {}^4T_{1g}(P)$.The second band due to $^4T_{1g} \rightarrow {}^4A_{2g}$ transition is not often observed; the transition involves a two-electron process for strong fields hence its intensity is much weaker compared to the other two transitions.[216] The visible band frequently has a shoulder or a fine structure to it – which has sometimes been attributed to the $^4T_{1g} \rightarrow {}^4A_{2g}$ transition but may alternatively arise as a result of spin orbit coupling,[217,218] vibrational broadening, low symmetry components to the ligand field[219] or transitions to doublet states.[217]

The ground term $^4T_{1g}$ for high spin octahedral Co(II) complexes is orbitally degenerate and provides an orbital contribution to the magnetic moments. The room temperature moments are found to be in excess of the spin only values, in the range 4.7–5.2 B.M. The moments vary considerably with temperature.[216]

Low spin octahedral Co(II) complexes have the ^2E_g ground term, their magnetic moments are expected to be in the range 1.70 – 1.85 B.M. and to be independent of temperature change.[216]

Tetrahedral Co(II) complexes are high spin with ground term $^4A_2$. Three transitions are similarly expected; the lowest energy band due to $^4A_2 \rightarrow {}^4T_1(F)$ transition is not often observed as it is weak because the transition is forbidden for electric dipole absorption in pure tetrahedral symmetry. More so it lies in the infrared region in the range 3000–5000 cm^{-1} (3330–2000 nm) where it is frequently overlapped by vibrational bands. The energy of this transition is usually taken as the Dq. Transitions due to $^4A_2 \rightarrow {}^4T_1(F)$ ($\varepsilon = 10–10^2\ M^{-1}\ cm^{-1}$) and $^4A_2 \rightarrow {}^4T_1(P)$ ($\varepsilon = 10^2–2x10^3\ M^{-1}\ cm^{-1}$) lie in the near infrared and visible regions respectively.[216] The high intensities of these bands differentiate them from those of octahedral absorptions and one can conveniently distinguish between the two stereochemistries on this basis. These intense absorptions of tetrahedral Co(II) complexes make them appear blue. The bandwidths are usually wide ranging between 1500 and 2000 cm^{-1} (6660 and 5000 nm). Both bands show fine structure with multiple absorption bands. These features have been attributed to spin orbit coupling,[217,218] low symmetry components of the crystal field[219] and transition to the doublet states.[217]

The most complete calculation of the energy levels with respect to the ligand field Coulombic (*Dq*), spin orbit (λ) and electron correlation parameters (Racah B and C) for both octahedral and tetrahedral Co(II) has been made by Liehr.[220]

In the complexes of lower symmetry than tetrahedral, the second band is usually broadened and the lower symmetry components are more pronounced. In CoA_2B_2 complexes of C_2v symmetry the $^4A_{2g} \rightarrow {}^4T_1(F)$ band should be split into three transitions viz. $^4A_{2g} \rightarrow {}^4B_2$, $^4A_{2g} \rightarrow {}^4A_2$ and $^4A_{2g} \rightarrow {}^4B_1$ and the $^4A_{2g} \rightarrow {}^4T_1(P)$ band should be similarly split. Such splittings are observed[221] in many complexes of Co(II) with nitrogen and phosphorus donor, the bands occurring at 8000–10200 cm^{-1}, ~7000 cm^{-1} and ~6000 cm^{-1} (1250–980, ~1428 and ~1667 nm).

The magnetic moments for tetrahedral Co(II) complexes are usually found within the range 4.4–4.8 B.M. Unlike in octahedral complexes, the tetrahedral moments are independent of temperature.[216]

Square planar complexes of Co(II) are not common. They commonly show a weak band in the 8000–10000 cm^{-1} (1250–1000 nm) range. With z^2 orbital above those of xz, yz and xy, transitions from $(xz, yz)^4 (xy)^2$ to z^2 are expected in the near infrared. In complexes with bidentate ligands of the type $Co(LL)_2$, xy is the highest orbital and the low lying three orbitals are xz, yz and $x^2–y^2$. These four orbitals are close in energy and their relative order will generally depend on the type of ligand system being considered.[222]

The few complexes with this geometry have magnetic moments in the range 2.1–2.8 B.M. indicating one unpaired electron.[216]

1.6.2 Nickel(II)

Majority of Nickel(II) complexes have coordination numbers of four, five and six. Complexes with coordination of three, seven and eight are quite rare. Six-coordinate complexes are generally high-spin, unless one or more ligands are at a larger distance. Five-coordinate complexes can be either high-spin or low-spin. Four-coordinate complexes are high-spin in a tetrahedral or pseudotetrahedral environment and low-spin in square planar geometry.[223]

The electronic structure of Ni(II) complexes has been investigated using optical spectroscopic (optical absorption, MCD) and magnetic (magnetization, magnetic susceptibilities, EPR, NMR) techniques and several reviews have already been published.[224-228]

For Ni(II) complexes both triplet (high-spin) and singlet (low-spin) states are known as the ground state, depending on the relative value of the interelectronic repulsion and crystal field stabilization energy – which in turn depend on the covalency of the metal-ligand bonds, the nature of the ligands and the stereochemistry of the complex. When the interelectronic repulsion P overcomes the crystal field stabilization energy Δ, a low-spin state occurs; conversely when $\Delta > P$, a high-spin occurs. In intermediate situations where both $\Delta \approx P$ the ground state depends on external conditions such as pressure or temperature giving rise to spin equilibria.

Venanzi[229] has shown that for ethylenediamine complexes of Ni(II) 15–30 kcals crystal field energy is gained on going from a tetrahedral to an octahedral complex. A similar energy difference is expected also in complexes of Ni(II) with other ligands based on the calculated crystal field stabilization energies for tetrahedral and octahedral complexes.[230] This could explain why most paramagnetic Ni(II) complexes have a tendency to form octahedral structures as compared to tetrahedral configuration. Tetrahedral paramagnetic Ni(II) complexes will be formed only when the ligands are of weak field and cannot cause spin-pairing of electrons to give rise to square planar configuration, and when the steric requirements of the ligands enforces a (distorted) tetrahedral arrangement of the atoms.

In almost all its six-coordinate complexes, Ni(II) has an octahedral stereochemistry. Octahedral Ni(II) complexes are usually blue or green, a typical example is bright green $Ni(H_2O)_6$. The replacement of H_2O by ligands of higher donor strength, such as NH_3 or en, shifts the absorption spectra to higher frequencies and the colour of the corresponding six-coordinate complexes $[Ni(NH_3)_6]^{2+}$ and $[Ni(en)_3]^{2+}$ becomes blue. They have a spin triplet $^3A_{2g}$ as the ground term and three main spin-allowed bands are usually observed in octahedral Ni(II) complexes.

These transitions have been assigned in O_h symmetry to $^3A_{2g} \rightarrow {}^3T_{2g}$, $^3A_{2g} \rightarrow {}^3T_{1g}(F)$ and $^3A_{2g} \rightarrow {}^3T_{1g}(P)$. Less intense spin-forbidden transitions attributable to ^1D (^1E_g) and ^1G (^1T_g) states can also be observed. The first band due to transition to $^3T_{2g}$ is usually in the range 5000–12000 cm^{-1} (2000–833 nm). The $^3A_{2g} \rightarrow {}^3T_{1g}(F)$ band is in the range 12000–19000 cm^{-1} (833–526 nm) and has often been found to show a shoulder or appear as a doublet especially when Dq/B is near unity.[214] This doublet structure has been

ascribed to a gaining of intensity of the $^3A_{2g} \rightarrow {}^1E_g$ transition through configurational interaction with the $^3T_{1g}$ (F) level.[231,232] Spin-orbit coupling will mix some triplet character into the ^1E_g term, thus lifting the spin selection rule slightly; the resultant small absorption band then distorts the main band.[233,234]

The third transition to $^3A_{2g} \rightarrow {}^3T_{1g}(P)$ ranges between 20000–29000 cm^{-1} (500–345 nm). Transitions to spin singlet levels are in the region 11 000–15 000 cm^{-1} (909–666 nm) for $^3A_{2g} \rightarrow {}^1E_g$ and in the range 17000–22000 cm^{-1} (588–455 nm) for $^3A_{2g} \rightarrow {}^1T_{1g}$.The energy level diagram for octahedral Ni(II) complexes inclusive of spin-orbit coupling has been presented by Liehr and Ballhausen.[233]

In complexes of the type NiA_4B_2, NiA_2B_2 and $NiAB_2$ (where A is monodentate, bidentate and tetradentate respectively and B is monodentate) where ligands of different field strengths are present, the symmetry is lowered to D_{4h} by tetragonal distortion. The lowest energy band is usually affected by the lower symmetry and is observed to split. The splitting of the energy levels increases the number of observable transitions. Six spin-allowed transitions may be anticipated and in practice at least five are observed, some spin-forbidden bands may also appear. Spin-allowed transitions are in order of increasing energy $^3B_{1g} \rightarrow {}^3B_{2g} < {}^3B_{1g} \rightarrow {}^3E_g < {}^3B_{1g} \rightarrow {}^3E_g < {}^3B_{1g} \rightarrow {}^3A_{2g} < {}^3B_{1g} \rightarrow {}^3E_g < {}^3B_{1g} \rightarrow {}^3A_{2g}$. The transitions to the doubly degenerate ^3E_g levels are usually the most intense features with molar coefficient values close to 10. The highest energy bands are more intense.[235]

The structures of five-coordinated complexes are square pyramidal (C_{4v} symmetry) or trigonal bipyramidal (D_{3h} symmetry). Nickel(II) complexes in these configurations are not common and do occur only when particular steric requirements and donor power of the ligand stabilize these geometries. The electronic ground state of nickel(II) complexes in these geometries can either be a spin singlet (low-spin configuration, diamagnetic) or spin triplet (high-spin configuration). Five-coordinate Ni(II) complexes with polydentate (polyamines, salicyaldimines, polyarsines and polyphosphines)[226,236] and monodentate ($[Ni(CN)_5^{3-}]$, $[Ni(OAsMe)_5]^{2+}$) ligands have been prepared and characterized. The square pyramidal complexes $[Ni(CN)_5^{3-}]$ and $[Ni(OAsMe)_5]^{2+}$ are low-spin and high-spin respectively, and $[NiBr(Me_6tren)]^+$ and $[NiBr(np_3)]^+$ are trigonal bipyramidal high-spin and low-spin complexes, respectively. In general, low-spin complexes are formed by donor atoms with low electronegativity, such as C, P, As and S, whereas high-spin complexes are formed by highly electronegative donors like O and N.[237]

Square pyramidal complexes possess an orbitally non-degenerate ground level, $^3B_1$. Transitions observed are $^3B_1 \rightarrow {}^3E$ occurring in the near IR region in the range 4000–9000 cm^{-1} (2500–1110 nm, $\varepsilon \approx 10$–20 M^{-1} cm^{-1}), $^3B_1 \rightarrow {}^3E$ at 12000–18000 cm^{-1} (833–555 nm, $\varepsilon \approx 10$–20 M^{-1} cm^{-1}) with a shoulder on the low frequency side due to $^3B_1 \rightarrow {}^3B_2$ transitions, $^3B_1 \rightarrow {}^3A_2(P)$ occurring at 17000–25000 cm^{-1} (588–400 nm) as a weak band and $^3B_1 \rightarrow {}^3E(P)$ which is the most intense band in the range 19 000–29 000 cm^{-1} (526–345 nm, $\varepsilon \approx 100$–800 M^{-1} cm^{-1}).[228]

The electronic spectra[228] of trigonal bipyramidal high-spin Ni(II) complexes are characterized by four bands:

$^3E' \rightarrow {}^3E''$	5000–8000 cm^{-1} (2000–1250 nm, $\varepsilon \approx 10$–30 M^{-1} cm^{-1})
$^3E' \rightarrow {}^3A_1'' + {}^3A''_2$	8000–14 000 cm^{-1} (1250–714 nm, $\varepsilon \approx 10$–20 M^{-1} cm^{-1})
$^3E' \rightarrow {}^3A'_2$	17 000–22 000 cm^{-1} (588–455 nm, $\varepsilon \approx 20$–30 M^{-1} cm^{-1})
$^3E' \rightarrow {}^3E'' + {}^3A'_2(P)$	22500–26200 cm^{-1} (444–382 nm, $\varepsilon \approx 50$–200)

For four-coordinate Ni(II) complexes the commonest geometry is square planar. The planar configuration is stabilized by strong nickel–ligand covalent bonding (both σ- and π-bonding). Ligands with higher donor strength favour square planar structures whereas those with weaker donor strength prefer the tetrahedral configuration. The tetrahedral configuration is only favoured as compared to the planar one by the spin pairing energy and by the minimization of electrostatic repulsion energy. The bulkiness of the substituents on donor atoms may also prevent a planar structure due to steric hindrance and a distorted tetrahedral structure may become preferred.[227]

The electronic ground state of a square planar complex is $^1A_{2g}$. The spectra of square planar Ni(II) complexes frequently consist[238] of a strong band in the region 18 000–25 000 cm^{-1} (555–400 nm, $\varepsilon \approx 50$–500 M^{-1} cm^{-1}) with a second band in the range 23 000–30 000 cm^{-1}. These bands are assigned to the transitions $^1A_{1g} \rightarrow {}^1A_{2g}$ and $^1A_{1g} \rightarrow {}^1B_{1g}$ respectively. Another weaker band sometimes observed in the 11 000–15 000 cm^{-1} region is probably a spin forbidden transition. The major difference between the spectra of square complexes and those of octahedral or tetrahedral complexes is the absence of any band below 10 000 cm^{-1} – which confirms that the energy gap between d_{x2-y2} and d_{xy} is larger than this value and accordingly the complexes are planar. Detailed discussion of the structure and bonding in square Ni(II) complexes has been given by Gray.[239]

The electronic spectra of tetrahedral Ni(II) complexes are characterized by 3 spin-allowed transitions. The tetrahedral crystal field splitting is about half that in an octahedral field, as a result the absorption bands in tetrahedral complexes have lower energies and are shifted towards the infrared as compared to octahedral bands. The tetrahedral bands are more intense (by a factor of about ten times) because of the absence of a centre of symmetry in these complexes. The lowest energy band, $^3T_1 \rightarrow {}^3T_2$ in the region 4000–7000 cm^{-1} (2500–1428 nm, $\varepsilon \approx 10$–$50\ M^{-1}\ cm^{-1}$) is not often observed. The second band in the near infrared in the range 7000–11 000 cm^{-1} ($\varepsilon \approx 100$–$200\ M^{-1}\ cm^{-1}$) is assigned to $^3T_1 \rightarrow {}^3A_2$ transition. The highest energy transition $^3T_1 \rightarrow {}^3T_1(P)$ shows a very broad band in the region 15 000–20 000 cm^{-1} (666–500nm, $\varepsilon \approx 10$–$50\ M^{-1}\ cm^{-1}$) with weaker bands on either side of it being assigned to spin-forbidden bands.[240]

Jahn-teller effect will be operative in this configuration though the distortion of the tetrahedron is not expected to be large.[240]

Review articles on the theory of magnetic susceptibility of Ni(II) complexes have been written [241-245] and the authors showed regular octahedral complexes of Ni(II) are always paramagnetic. The experimental magnetic moments lie usually within the range 2.9–3.3 BM. The larger values are generally observed due to orbital contribution derived from the mixing of low-lying excited states into the ground state or as a result of orbital contribution directly from orbitally degenerate ground state. The magnetic moments usually observed at room temperature for Ni(II) complexes are found in **Table 1.4**.

In NiA_6 complexes with O_h symmetry, the ground state $^3A_{2g}$ and the next excited state $^3T_{2g}$ are well separated in energy by >7000 cm^{-1} (<1428 nm), the magnetic moment does not vary largely with temperature and anisotropic effects are also of little significance unless at very low temperatures (<4 K). At temperatures below 4 K the differences in thermal populations of the ground state levels due to zero field splitting become important and larger anisotropies are observed.[242]

Table 1.4 Typical values of the effective magnetic moment at room temperature of nickel(II) complexes in various geometries[228]

Coordination	μ_{eff} (BM)
Octahedral	2.9–3.3
Trigonal bipyramidal	3.2–3.8
Square pyramidal	3.2–3.4
Tetrahedral	3.2–4.1
Square planar	Diamagnetic

For Ni(II) complexes with tetrahedral and trigonal bipyramidal geometries, the ground states are orbitally degenerate while those of octahedral and square pyramidal structures are non-degenerate. Largest values are observed for tetrahedral and trigonal bipyramidal complexes whose ground states are orbitally degenerate. Large orbital contributions are also expected from square pyramidal complexes which have an excited state *E* lying near to the ground state. Magnetic moments cannot be used to distinguish between tetrahedral and five-coordinate complexes.[223]

Owing to the degenerate nature of the ground state for trigonal bipyramidal complexes, the computed magnetic moments are larger than those of the square pyramidal complexes. Large variation of magnetic moments with temperature is shown by complexes with trigonal bipyramidal geometry or close to it.

Square planar complexes of Ni(II) are usually diamagnetic since there are no unpaired electrons. The magnetic moments in Ni(II) tetrahedral structures are considerably higher than the spin only value through orbital contribution. The experimental moments are within the range 3.2–4.1 BM and are dependent upon temperature. Spin-orbit coupling splits the ground term $^3T_1$ term into three states of multiplicity 0, 3, 5 with the 0 state lying lower. At low temperatures only the 0 state is populated and μ becomes zero, giving a large temperature dependence of the magnetic moments.

1.6.3 Copper(II)

Copper is an important trace element for plants and animals and is involved in mixed ligand complex formation in a number of biological processes. Copper(II) has a $3d^9$ configuration. The usual

coordination numbers adopted by copper(II) are 4, 5 and most commonly 6. Regular octahedral is rare because of uneven occupancy of the highest energy *d* orbital giving rise to a distortion of the ligand octahedral array – commonly referred to as the Jahn-Teller effect.

Jahn-Teller distortion of symmetrical structures results from partially filled electronic energy levels.[246] Different repulsions are experienced by the ligands around the metal ion, the most being experienced by ligands close to or along the plane of the *d* orbital occupied by the lone electrons. Hence the ligands closest are repelled away more than the others resulting in distortion (tetragonal in octahedral structures) from the regular symmetry. That is, if there is degeneracy because one *d* orbital is filled with a pair of electrons while another of equal energy is only half filled, then by a change of geometry which resolves this degeneracy, a more stable state can be obtained. Copper(II) complexes are anomalously stable because they tend to have an irregular octahedral arrangement of ligands, with four at the corners of a square lying close to the copper(II) ion, and the other two on the perpendicular axis less close.[247] This distortion leads to an elongation of two bonds giving four short bonds and two longer ones. More rarely, the distortion can result in two short bonds and four long ones. The former distortion in the limit results in a square planar arrangement of the ligands about the copper ion.

In an octahedral field, Cu^{2+} has a ^2D ground term and one transition corresponding to ^2E_g to $^2T_{2g}$ is expected. However as a result of Jahn-teller distortion[246] which is greater in a $3d^9$ than in a d^1 ion, octahedral Cu(II) complexes generally show spectra with broad bands resulting from several overlapping bands, and the energy of the system is favourably lowered.

For the tetrahedral copper(II) complexes, the orbital splitting is inverted and the ^2E becomes the ground term. One transition ^2E to $^2T_2$ is also expected primarily in the red or near infrared between 8000 and 9000 cm^{-1} (1250–1110 nm), which is at a lower energy than the corresponding octahedral complexes ($\Delta_t = 4/9\Delta_o$).[248]

Square planar complexes of Cu(II) usually display more than one transition showing no absorption less than 10 000 cm^{-1} (1000 nm).[249]

The spin only magnetic moment for copper(II) ion would be 1.73 B.M., but due to spin orbit coupling higher values are often observed. The ionic or weak covalently bonded copper(II) complexes have moments in the range 1.9–2.2 B.M. compared to 1.72–1.82 B.M. for those having strong covalent

bonds;[250-252] abnormally low magnetic moments are observed due to partial coupling of unpaired electrons between neighboring copper atoms (antiferromagnetism).

1.7 AIMS AND OBJECTIVES

In summary, the aims and objectives of this research study are as follow:

- Synthesis of thiomethylated ligands which are 2–(methylthiomethyl)aniline and 2–(methylthio)aniline and their substituted derivatives with -Me, -MeO, -Cl, -Br and -NO_2 at the *ortho* and *para* positions to the amino group.

- Synthesis of the Co(II), Ni(II) and Cu(II) complexes of the above-mentioned ligands.

- Synthesis of the Schiff bases derived from the thiomethylated ligands and their copper(II) complexes

- Characterization of the ligands, Schiff bases and their corresponding metal(II) complexes with elemental analysis, IR/Raman, UV, NMR spectroscopy, conductivity measurements and single-crystal X-ray diffraction as appropriate.

- Study of the difference in properties of the two types of ligands as a result of direct sulfur attachment to the aromatic ring in one case. These properties are

    - NMR shifts of the proton groups
    - IR frequency absorptions.

- Study of the difference in properties of the five- and six-membered metal(II) chelates formed by the 2–(methylthio)aniline and 2–(methylthiomethyl)aniline ligands respectively. These properties include
    - colour of complexes
    - IR frequency absorptions
    - UV absorptions

- Geometry/structure of complexes.

- Study of the difference in properties of ligands and metal(II) complexes as a result of the effect of electron donating/withdrawing nature of the attached substituent groups on the aromatic ring.

- Study of the difference in properties of ligands and metal(II) complexes as a result of the position of substituent (relative to the amino group) on the aromatic ring.

- Biological study of the ligands and their metal(II) complexes
  - Antimicrobial activity against chosen strains of bacteria (*Bacillus subtilis*, *Staphylococcus aureus*, *Escherichia coli*) and fungus (*Candida albicans*)
  - Antiplasmodial activity against *P. falciparum* (FCR-3)
  - Cytotoxicity assay using breast cancer cell line (MDA-MB-231).

REFERENCES

1. R. G. Pearson, *J. Am. Chem. Soc.,* 1963, **85**, 3533.
2. D. R. Williams, *Chemical Reviews*, 1972, **72**, 203.
3. P. G. Gassman and G. D. Gruetzmacher, *J. Am. Chem. Soc.*, 1974, **96** , 5487.
4. J. Whysner, L. Vera and G. M. Williams, *Pharmaco Ther.*, 1996, **71**, 107.
5. H. L. Holland, F. M. Brown, A. Kerridge and C. D. Turner, *J. Mol. Cat. B: Enzymatic*, 1999, **6**, 463.
6. J. P. Chupp, T. M. Balthazor, M. J. Miller and M. J. Pozzo, *J. Org. Chem*., 1984, **49**, 4711.
7. P. G. Gasman, H. R. Drewes, *J. Am. Chem. Soc.*, 1974, **96**, 3002.
8. Y. Guo, B. Din, Y. Liu, X. Chang, S. Mengb and M. Tian, *Analytica Chimica Acta* 2004 **504**, 319.
9. P. Claus and W. Vycudilik, *Tetrahedron Letters*, 1968, **32**, 3607.
10. P. Claus and W. Vycudilik, *Monastshefte fur Chemie*. 1970, **101**, 396.
11. P. G. Gassman and G. Gruetzmacher, *J. Am. Chem. Soc.*, 1973, **95,** 588.
12. P. G. Gassman, T. J. Van Bergen, and G. D. Gruetzmacher, *J. Am. Chem. Soc.*, 1973, **95**, 6508.
13. P. G. Gassman, G. D. Gruetzmacher, and T. J. Van Bergen, *J. Am. Chem. Soc.*, 1974, **96**, 5512.
14. Y. Hiraki, M. Kamiya, R. Tanikaga, N. Ono and A. Kaji, *Bull. Chem. Soc. Japan*, 1977, **50**, 447.
15. M. Sommelet, *C. R. Acad. Sci.*, 1937, **205**, 56.
16. C. R. Hauser, S. W. Kantor, and W. R. Brasen, *J. Am. Chem. Soc.*, 1953, **75**, 2660.
17. G. C. Jones and C. R. Hauser, *J. Org. Chem*., 1962, **27**, 3572.
18. S. E. Livingstone, *J. Chem. Soc. (Res.)*, 1956, 437.
19. M. Maji., M. Chatterjee, S. K. Chattopadhyay and S. Ghosh, *Acta Chemica Scandinavica*, 1999, **53**, 253.
20. S. Sarkar, P. K. Dhara, M. Nethaji and P. Chattopadhyay, *J. Coord. Chem.*, 2009, **62**, 817.
21. S. E. Livingstone, *Royal Society of Chemistry*, 1956. DOI10.1039/JR9560000437.
22. S. Messaoudi, J. Brion and M. Alami, *Adv. Synth. Catal.*, 2010, **352**, 1677.
23. H. Takeuchi, S. Hirayama, M. Mitani and K. Koyama, *J. Chem. Soc. Perkin Trans. 1*, 1986, 2277.
24. P. F. Ranken and B. G. McKinnie, *J. Org. Chem.*, 1989, **54***,* 2985.
25. K. Oyaizu, F. Mitsuhashi and E. Tsuchida, *Macromol. Chem. Phys*., 2002, **203**, 1328.
26. X. Fang, R. Tang, X. Zhang and J. Li, *Synthesis*, 2011, **7**, 1099.
27. B. A. Dreikorn, G. P. Jourdan, H. R. Hall, J. B. Deeter, and N. Jones, *J. Agric. Food Chem*., 1990, **38**, 549.
28. C. G. Stuckwisch*, J. Am. Chem*. Soc., 1949, **71**, 3417.

29. M. Matsui, Y. Marui, M. Kushida, K. Funabiki, H. Muramatsu, K. Shibata, K. Hirota, M. Hosoda and K. Tai, *Dyes and Pigments*, 1998, **38**, 57.
30. G. Trapani, M. Franco, A. Latrofa, A. Reho and G. Liso, *Eur. J. Pharm. Sci.*, 2001, **14**, 209.
31. D. Shashank, T. Vishawanth, Md. Arif Pasha , V. Balasubramaniam, A. Nagendra, P. Perumal and R. Suthakaran, *International Journal of ChemTech Research*, 2009, **1**, 224.
32. J. K. Malik, Dr. F. V. Manvi1, Dr B.K. Nanjwade and S. Singhet, *Drug Invention Today*, 2009, **1**, 32.
33. N. B. Patel and S. N. Agravat, *Chemistry of Heterocyclic Compounds*, 2009, **45**, 11.
34. P.Venkatesh and S.N. Pandeya, *International Journal of ChemTech Research*, 2009, **1**, 1354.
35. N. B. Patel, S. N. Agravat and F. M. Shaikh, *Med. Chem. Res*., 2011, **20**, 1033.
36. C. F. H. Allen and J. VanAllan, *Organic Syntheses Coll*., 1955, **3**, 76.
37. C. F. H. Allen and J. VanAllan, *Organic Syntheses Coll*., 1942, **22**, 16.
38. K. Kratzl, H. Fostel and R. Sobczak , *Monatshefte fuer Chemie*, 1972, **103**, 677.
39. N. Dunski and T. H. Crawford, *J. Inorg. Nucl. Chem.*, 1969, **31**, 2073.
40. L. F. Lindoy, S. E. Livingstone and T. N. Lockyer, *Aust. J. Chem*., 1967, **20**, 471.
41. L. F. Lindoy and S. E. Livingstone, *Inorg. Chem.*, 1968, **7**, 1149.
42. V. Krishnakumar and V. Balachandran, *Spectrochimica Acta Part A*, 2005, **61**, 1811.
43. P. Hohenberg and W. Kohn, *Phys Rev B*, 1964, **136**, 864.
44. C. H. Misra, S. S. Parmar and S. N. Shukla, *Canad. J. Chem*., 1967, **45**, 2459.
45. M. A. J. Jungbauer and Columba Curran, *Spectrochim. Acta*, 1965, **21**, 641.
46. J. C. Evans, *Spectrochim. Acta,* 1960, **16**, 428.
47. M. Tsuboi, *Spectrochim. Acta*, 1960, **16**, 505.
48. J. A. Lee-Thorp, J. E. Ruede and D. A. Thornton, *J. Mol. Str.*, 1978, **50**, 65.
49. T. P. E. Auf der Heyde, G. A. Foulds, D. A. Thornton and G. M. Watkins, *J. Mol. Str.*, 1981, **77**, 19.
50. M. J. Root, B. P. Sullivan, T. J. Meyer and E. Deutsch, *Inorg. Chem*., 1985, **24**, 2731.
51. M. Ikram and D. B. Powell, *Spectrochim. Acta*, 1971, **27A**, 1845.
52. S. E. Livingstone; *Quart. Rev.,* 1966, **19**, 386.
53. I. S. Ahuja, D. H. Brown, R. H. Nuttall and D. W. A. Sharp, *J. Inorg. Nucl. Chem*., 1965, **27**, 1105.
54. J. R. Allan, D. H. Brown, R. H. Nuttall and D. W. A. Sharp, *J. Inorg. Nucl. Chem*., 1965, **27**, 1529.
55. D. M. L. Goodgame and M. Goodgame, *J. Chem. Soc*., 1963, 207.

56. R. H. Lee, E. Griswold and J. Kleinberg, *Inorg. Chem*., 1964, **3**, 1278.
57. N. S. Gill*, J. Inorg. Nucl. Chem*., 1961, **18**, 88.
58. A. B. P. Lever, *Inorg Chem*., 1965, **4**, 763.
59. H. Schiff, *Justus Liebigs Ann. Chem*., 1864, **131**, 2.
60. J. Hine and C.Y. Yeh, *J. Am. Chem. Soc.*, 1967, **89**, 2669.
61. K.N. Campbell, A.H. Sommers, and B.K. Campbell, *J. Am. Chem. Soc.*, 1944, **66**, 82.
62. C.M. Brewster, *J. Am. Chem. Soc.*, 1924, **46**, 2463.
63. R.J. Fessenden and J.S. Fessenden, *Organic Chemistry,* Pt. 2. 5th Ed. 1995: Tokyo Kagaku Dozin Co., Ltd. 680, 6.
64. S. Patai and Editor, *The Chemistry of the carbon-Nitrogen Double Bond (Chemistry of Functional Groups)*, 1970, Wiley-Interscience, 794.
65. J. Fabian and M. Legrand, *Bull. Soc. Chim. Fr.*, 1956, 1461.
66. F.H. Suydam, *Anal. Chem.*, 1963, **35**, 193.
67. L. E. Clougherty, J.A. Sousa, and G.M. Wymn, *J. Org. Chem.*, 1957, **22**, 462.
68. J. E. Kovacic, *Spectrochim. Acta*, 1967, **23A**, 183.
69. A. W. Baker and A.T. Shulgin, *J. Am. Chem. Soc.*, 1959, **81**, 1523.
70. M. M. Abd-Elzaher*, J. Chin. Chem. Soc.*, 2001, **48**, 153.
71. Y. Zhou, X. Ye, F. Xin and X. Xin, *Trans. Met. Chem.*, 1999, **24**, 118.
72. R. Ramesh and S. Maheswaran, *J. Inorg. Biochem.,* 2003, **96**, 457.
73. C. G. Saxena and S. V. Shrivastava, *J. Ind. Chem. Soc.*, 1987, **64**, 685.
74. C. N. Bhardwaj and V. R. Singh, *Indian J. Chem.*, 1994, **33A**, 423.
75. S. P. Ranga, S. Sharma, V. Chowdhary, M. Parihar and ZR. K. Mehtar, *J. Curr. Bio. Sci.*, 1998, **5**, 98.
76. Chohan and H. Zahid, *Met-based Drugs*, 1999, **6**, 187.
77. Chohan and H. Zahid, *Met-based Drugs*, 1999, **6**, 75.
78. Chohan, H. Zahid and S. Kausar, J. Chem. Soc. Pak., 2001, **23**, 163.
79. B. Dash, P. K. Mahapatra, D. Panda and J. M. Patnaik, *J. Indian Chem Soc*., 1984, **61**, 1061.
80. N. R. Rao, P. V. Rao, G. V. Reddy and M. C. Ganorkar, *Indian J. Chem.*, 1987, **26A**, 887.
81. S. Yamada and K. Yamanouchi, *Bull. Chem. Soc. Jap.*, 1969, **42**, 2562.
82. G. A. Kolawole, *J. Coord. Chem.*, 1987, **16**, 67.
83. Z. Cimerman, N. Galic and B. Bosner, *Anal. Chim. Acta*, 1997, **343**, 145.
84. L. Sacconi, P. L. Orioli, P. Paoletti and M. Ciampolini, *Proc. Chem. Soc.*, London, 1962, 255.
85. Z. H. Chohan and S. Mushtaq, *Pak. J. Pharm. Sci.*, 2000, **13**, 21.

86. S. Yamada and K. Yamanouchi, *Bull. Chem. Soc. Jap.*, 1969, **42**, 2562.
87. G. G. Mohamed, *Spectrochim. Acta A*, 2006, **64**, 188.
88. A. Kilic, E. Tas, B. Deverec and I. Yilmaz, *Polyhedron* 2007, **26**, 4009.
89. A. Prakash, B. K. Singh, N. Bhojak and D. Adhikari , *Spectrochim. Acta A*, 2010, **76**, 356.
90. R. C. Mourya, J. Chourasia and P. Sharma, *Ind. J Chem.*, 2007, **46A**, 1594.
91. A. A. Khandar, S. A. Hosseini-Yazdi, S. A. Zarei and U. M. Rabie, *Inorg. Chim. Acta*, 2005, **358**, 3211.
92. P. K. Coughlin and S. J. Lippard, *J Am. Chem. Soc.*, 1984, **106**, 2328.
93. Y. P. Cai, C. Y. Su, A. W. Xu, B. S. Kang, Y. X. Tong , H. Q. Liu and S. Jie, *Polyhedron*, 2001, **20**, 657.
94. L. Shi, W. J. Mao, Y. Yang and H. L. Zhu, *J Coord. Chem.,* 2009, **62**, 3471.
95. M. A. Phaniband and S. D. Dhumwad, *Trans. Met. Chem*., 2007, **32**, 1117.
96. V. T. Kasumov, S. Ozalp-Yaman and E. Tas, *Spectrochim. Acta A*, 2005, **62**, 716.
97. A. Salva, J. Donoso, J. Frau, and F. Munoz, *J. Mol. Struct.: Theochem.*, 2002, **577**, 229.
98. D. Dolphin, R. Poulson, and O. Avramovic, *Coenzymes and Cofactors, Vol. 1: Vitamin B6.Pyridoxal Phosphate. Chemical, Biochemical, and Medical Aspects, Pt. B*. 1986: John Wiley & Son, 792.
99. P. Otto, J. Ladik, K. Laki and A. Szent-Gyorgyi, *Proc. Natl. Acad. Sci.,* U. S. A., 1978, **75**, 3548.
100. H. Y. Shrivastava, M. Kanthimathi, and B. U. Nair, *Biochem. Bio. Phys. Res. Commun.*, 1999, **265**, 311.
101. N. Raman, J. D. Raja and A. Sakthivel, *J. Chem. Sci.*, 2007, **119**, 303.
102. D. K. Saha, U. Sandbhor, K. Shirisha, S. Paddye, D. Deobagkar, C. E. Ansond and A. K. Powell, *Bioorg. Med. Chem. Lett.,* 2004, **14**, 3027.
103. D. Chen, C. Q. Z Cui, H. J. Yang and Q. P. Dou, *Cancer Res.,* 2006, **66**, 10425.
104. L. Rigamanti, F. Demartin, A. Forni, S. Righetto and A. Pasini, *Inorg. Chem.*, 2006, **45**, 10976.
105. A. Huber, L. Muller, H. Elias, R. Klement and M. Valko, *Eur. J Inorg. Chem.*, 2005, **8**, 1459.
106. J. P Costes, J. F. Lamere, C. Lepetit, P. G. Lacroix, F. Dahan and K. Nakatani, *Inorg. Chem.*, 2005, **44**, 1973.
107. S. Dhar, M. Nethaji and R. Chakravarty, *Inorg. Chem.*, 2006, **45**, 11043.
108. H. T. Chifotides and K. R. Durbar, *Acc. Chem. Res.*, 2005, **38**, 146.
109. K. Karidi, A. Garoufis, A. Tsipis and J. Reedijk, *Dalton Trans.*, 2005, **7**, 1176.
110. M. J. Clarke, *Coord. Chem. Rev.*, 2003, **236**, 209.
111. B. W. Henderson, *Cancer Res.*, 2000, **60**, 525.

112. M. I. Raafat, M. K. Abdulla and H. F. Rizk, *Spectrochim. Acta A*, 2005, **62**, 621.

113. Z. Chu and W. Huang, *J Mol. Struct.*, 2007, **837**, 15.

114. P. E. Kruger, N. Martin and M. Nieuwenhuyzen, *J,Chem. Soc.,Dalton Trans*., 2001, **13**,1966.

115. J. Hamacek, M. Borkovec and C. Piguet, *Dalton Trans.,* 2006, **12**, 1473.

116. S. Ilhan, H. Temel, I. Yilmaz and M. Sekerci, *Polyhedron*, 2007, **26**, 2795.

117. S. Arulmurugan, H. P. Kavitha and B. R. Venkatraman, *Rasayan J. Chem.*, 2010, **3**, 385.

118. D. L. Saussy Jr., J. A. Liacos, P. E. Irving, M. J. Gobel, and B. W. Sherman., *J. Med. Chem*., 2002, **45**, 2229.

119. http://www.mansfield.ohio-state.edu/~sabedon/black13.htm. Date accessed: 08/05/2012.

120. A. W. Bauer, W. M. M. Kirby, J. C. Sherris and M. Turck, *Am. J. Clin. Pathol.* 1966, **36**, 493.

121. *Blood Safety and Clinical Technology: Guidelines on Standard Operating Procedure,* http://www.searo.who.int/en/Section10/Section17/Section53/Section482_1788.htm, *World Health Organization*. Date accessed: 09/10/2011.

122. P. N. Sridhar Rao *Antibiotic Susceptibility Testing,* www.microrao.com. Date accessed: 05/15/2012.

123. M. V Lancaster and R. D. Fields, *Antibiotic and cytotoxic drug susceptibility assays using resazurin and poising Agents*, U.S. Patent No. 5,501,959, 1996.

124. http://www.biomerieux-diagnostics.com/servlet/srt/bio/clinical-diagnostics/dynPage?doc=CNL_CLN_PRD_G_PRD_CLN_22. Date accessed: 1/5/2013.

125. http://www.pharmaceuticalonline.com/doc.mvc/Spiral-Gradient-Endpoint-Test-0001. Date accessed: 1/5/2013.

126. *Clinical Laboratory Standards Institute. 2006. Performance standards for antimicrobial disk susceptibility tests; Approved standard*—9th ed. CLSI document M2-A9. 26:1. Clinical Laboratory Standards Institute, Wayne, PA.

127. http:/www.who.int/malaria/world_malaria_report_2010/worldmalariareport2010.pdf. Date accessed: 07/06/2012.

128. R. G. A, Feachem, A. A. Phillips, J. Hwang, C. Cotter, B. Wielgosz, B. M. Greenwood, O. Sabot, M. H. Rodriguez, R. R. Abeyansighe, T. A. Ghebreyesus and R. W. Snow, *Lancet*, 2010, **376**, 566.

129. K. R. Dronamraju and P. Arese, *Malaria: genetic and Evolutionary Aspects (Emerging Infectious Diseases of the 21st Century)*, Springer, New York, 2010.

130. J. F. Trape, A. Tall, N. Diagne, O. Ndiath, A. B. Ly. J. Faye, F. Dieye-Ba, C. Roucher, C. Bouganali, A. Badiane, F. D. Sarr, C. Mazenot, A. Touré-Baldé, D. Raoult, P. Druilhe, O. Mercereau-Puijalon, C. Rogier and C. Sokhna, *Lancet Infect. Dis*., 2011, **11**, 925.

131. S. B. Sirima, S. Cousens and P. Druilhe, *N. Engl. J. Med*., 2011, **365**, 1062.

132. A. Leach, J. Vekemans, M. Lievens, O. Ofori-Anyanam, C. Cahill, S. Owusu-Agyei, S. Abdulla, E. Macete, P. Njuguna, B. Savarese, C. Loucq and W. R. Ballou, The Clinical Trials Partnership Committee, *Malar. J*., 2011, **10**, 224.

133. M. Foley and L. Tilley, *Pharmacol. Ther.,* 1998, **79**, 55.

134. L. Tilley, P. Loria and M. Foley, *Antimalar. Chemother.,* 2001, **47**, 87.

135. J. Ziegler, R. Linck and D. W. Wright, *Curr. Med. Chem.,* 2001, **8**, 171.

136. C. Seoung-Ryoung, P. Mukherjeea and M. A. Avery, *Curr. Med. Chem.,* 2008, **15**, 161.

137. A. Dieckmann and A. Jung, *Parasitology,* 1986, **93**, 275.

138. C. H. Sibley, J. E. Hyde, P. F. G. Sims, C. V. Plowe, J. G. Kublin, E. K. Mberu, A. F. Cowman, P. A. Winstanley, W. M. Watkins and A. M. Nzila, *Trends Parasitol.,* 2001, **17**, 582.

139. M. Avery, M. Alvim-Gaston, J. Vroman, B. Wu, A. Ager, W. Peters, B. Robinson and W. Charman, *J. Med. Chem.,* 2002, **45**, 4321.

140. G. J. Posner, *Pharm. Pharmacol.,* 1997, **49**, 55.

141. B. Meunier and A. Robert, *Acc. Chem. Res.,* 2010, **43**, 1444.

142. G. Posner, C. Oh, D. Wang, L. Gerena, W. Milhous, S. Meshnick and W. Asawamahasakda, *J. Med. Chem.,* 1994, **37**, 1256.

143. G. Posner, J. Cumming, P. Ploypradith and C. Oh, *J. Am. Chem. Soc.,* 1995, **117**, 5885.

144. H. Noedl, Y. Se, K. Schaecher, B. L. Smith, D. Socheat and M. M. Fukuda, *N. Engl. J. Med*., 2008, **359**, 2619.

145. A. M. Dondorp, F. Nosten, P. Yi, D. Das, A. P. Phyo, J. Tarning, K. M. Lwin, F. Ariey, W. Hanpithakpong, S. J. Lee, P. Ringwald, K. Silamut, M. Imwong, K. Chotivanich, P. Lim, T. Herdman, S. S. An, S. Yeung, P. Singhasivanon, N. P. Day, N. Lindegardh, D. Socheat and N. J. White, *N. Engl. J. Med*., 2009, **361**, 455.

146. S. H. Abdalla and G. Pasvol, *Malaria: A Hematological Perspective* (Tropical Medicine: Science and Practice, Vol. 4), Imperial College Press, London, 2004.

147. M. Pisciotta and D. Sullivan, *Parasitol. Int.,* 2008, **57**, 89

148. A. N. Hoang, K. K. Ncokazi, K. A. de Villiers, D. W. Wright and T. J. Egan, *Dalton Trans.,* 2010*,* **39**, 1235

149. A. N. Hoang, R. D. Sandlin, A. Omar, T. J. Egan and D. W. Wright, *Biochemistry,* 2010, **49**, 10107.
150. S. N. Cohen, O. P. Kenneth and Y. K. Lemone, *Nature,* 1964, **202**, 805.
151. A. Robert, Y. Coppel and B. Meunier, *Chem. Commun.,* 2002, 414.
152. D. J. Sullivan, I. Y. Gluzman, D. G. Russell and D. E. Goldberg, *Proc. Natl. Acad. Sci.*, U. S. A., 1996, **93**, 11865
153. S. R. Vippagunta, A. Dorn, H. Matile, A. K. Bhattacharjee, J. M. Karle, W. Y. Ellis, R. G. Ridley and J. L. Vennerstrom, *J. Med. Chem.,* 1999, **42**, 4630.
154. T. J. Egan, R. Hunter, C. H. Kaschula, H. M. Marques, A. Misplon and J. C. Walden, *J. Med. Chem.,* 2000, **43**, 283.
155. T. J. Egan, *Drug Des. Rev.,* 2004, **1**, 93.
156. B. Rosenberg, L. Van Camp and T. Krigas, *Nature*, 1965, **205**, 698.
157. B. Rosenberg, L. Van Camp, J. E. Trosko and V. H. Mansour, *Nature*, 1969, **222**, 385.
158. E. Alessio, *Bioinorganic Medicinal Chemistry*, Wiley–CH Verlag & Co., Germany, 2011.
159. N. Wash, H. B. Singh, A. Gajanana and A. N. Raichowdhary, *Inorg. Chim. Acta,* 1987, **135**, 133.
160. R. A. Sánchez-Delgado, M. Navarro, H. Pérez and J. A. Urbina, *J. Med. Chem.,* 1996, **39**, 1095.
161. C. S. K. Rajapakse, A. Martínez, B. Naoulou, A. A. Jarzecki, L. Suárez, C. Deregnaucourt, V. Sinou, J. Schrevel, E. Musi, G. Ambrosini, G. K. Schwartz and R. A. Sánchez-Delgado, *Inorg. Chem.,* 2009, **48**, 1122.
162. R. A. Sánchez-Delgado, M. Navarro and H. Pérez, *J. Med. Chem.,* 1997, **40**, 1937.
163. M. Navarro, F. Vásquez, R. A. Sánchez-Delgado, H. Pérez, V. Sinou and J. Schrével, *J. Med. Chem.,* 2004, **47**, 5204.
164. M. Navarro, S. Pekerar and H. A. Pérez, *Polyhedron,* 2007, **26**, 2420.
165. N. Bellotti de Souza, A. M. L. Carmo, D. C. Lagatta, M. J. M. Alves, A. P. S. Fontes, E. S. Coimbra, A. D. da Silva and C. Abramo, *Biomed. Pharmacother.,* 2011, **65**, 313.
166. D. R. van Staveren and N. Metzler-Nolte, *Chem. Rev.,* 2004, **104**, 5931.
167. C. Biot, L. Delhaes, L. A. Maciejewski, M. Mortuaire, D. Camus, D. Dive and J. S. Brocard, *Eur. J. Med. Chem.,* 2000, **35**, 707.
168. J. Guillon, S. Moreau, S. Mouray, V. Sinou, I. Forfar, S. B. Fabre, V. Desplat, P. Millet, D. Parzy, C. Jarry and P. Grellier, *Bioorg. Med. Chem.,* 2008, **16**, 9133.
169. A. Saleh, J. Friesen, S. Baumesteir, U. Gross and W. Bohne, *Antimicrob. Agents Chemother.,* 2007, **51**, 1217.

170. R. W. Winter, J.X. Kelly, M. J. Smilkstein, R. Dodean, D. Hinrichs and M. K. Riscoe, *Exp. Parasitol.,* 2008, **118**, 487.

171. F. Dubar, R. Wintjens, E. S. Martins-Duarte, R. C. Vommaro, W. de Souza, D. Dive, C. Pierrot, B. Pradines, A. Wohlkonig, J. Khalife and C. Biot, *Med. Chem. Commun.,* 2011, **2**, 430.

172. J. Quirante, F. Dubar, A. González, C. Lopez, M. Cascante, R. Cortés, I. Forfar, B. Pradines and C. Biot, *J. Organomet. Chem.,* 2011, **696**, 1011.

173. O. Domarle, G. Blampain, H. Agnaniet, T. Nzadiyabi, J. Lebibi, J. Brocard, L. Maciejewski, C. Biot, A. J. Georges and P. Millet, *Antimicrob. Agents Chemother.*, 1998, **42**, 540.

174. C. Biot, L. Delhaes, H. Abessolo, O. Domarle, L. A. Maciejewski, M. Mortuaire and P. Delcourt, *J. Organomet. Chem.*, 1999, **589**, 59.

175. C. Biot, W. Daher, C. M. Ndiaye, P. Melnyk, B. Pradines, N. Chavain, A. Pellet, L. Fraisse, L. Pelinski, C. Jarry, J. Brocard, J. Khalife, I. Forfar-Bares and D. Dive, *J. Med. Chem.*, 2006, **49**, 4707.

176. K. Raynes, *Int. J. Parasitol.*, 1999, **29**, 367.

177. C. Biot, J. Dessolin, I. Ricard and D. Dive, *J. Organomet. Chem.,* 2004, **689**, 4678.

178. C. Biot, G. Glorian, L. A. Maciejewski and J. S. Brocard, *J. Med. Chem.*, 1997, **40**, 3715.

179. M. Henry, S. Briolant, A. Fontaine, J. Mosnier, E. Baret, R. Amalvict, T. Fusaı, L. Fraisse, C. Rogier and B. Pradines, *Antimicrob. Agents Chemother.*, 2008, **52**, 2755.

180. L. Fraisse and D. Ter-Minassian, International application PCT/FR2006/000842, (2006).

181. L. Delhaes, H. Abessolo, C. Biot, P. Deloron, J. Karbwang, M. Mortuaire and L. A. Maciejewski, *Parasitol. Res.,* 2001, **87**, 239.

182. A. Yayon, Z. I. Cabantchik and H. Ginsburg, Proc. *Natl. Acad. Sci.* U. S. A., 1985, **82**, 2784.

183. C. Biot, W. Daher, N. Chavain, T. Fandeur, J. Khalife, D. Dive and E. De Clercq, *J. Med. Chem.,* 2006, **49**, 2845.

184. C. Biot, W. Castro, C. Y. Bottéd and M. Navarro, *Dalton Trans.*, 2012, **41**, 6335.

185. C. Biot, B. Pradines, M. H. Sergeant, J. Gut, P. J. Rosenthal and K. Chibale, *Bioorg. Med. Chem. Lett.*, 2007, **17**, 6434.

186. F. Bellot, F. Coslédan, L. Vendier, J. Brocard, B. Meunier and A. Robert, *J. Med. Chem.,* 2010, **53***,* 4103.

187. O. Dechy-Cabaret, F. Benoit-Vical, A. Robert and B. Meunier, *ChemBioChem,* 2000, **4**, 281.

188. A. Robert, O. Dechy-Cabaret, J. Cazelles and B. Meunier, *Acc. Chem. Res.,* 2002, **35**, 167.

189. F. Cosledan, L. Fraisse, A. Pellet, F. Guillou, B. Mordmuller, P. G. Kremsner, A. Moreno, D. Mazier, J. P. Maffrand and B. Meunier, *Proc. Natl. Acad. Sci. U. S. A.,* 2008, **105**, 17579.

190. A. M. Dondorp, F. Nosten, P. Yi, D. Das, A. P. Phyo, J. Tarning, K. M. Lwin, F. Ariey, W. Hanpithakpong, S. J. Lee, P. Ringwald, K. Silamut, M. Imwong, K. Chotivanich, P. Lim, T. Herdman, S. S. An, S. Yeung, P. Singhasivanon, N. P. J. Day, N. Lindegardh, D. Socheat and N. J. White, *N. Engl. J. Med.*, 2009, **361**, 455.

191. S. M. Taylor, J. J. Juliano and S. R. Meshnick, *N. Engl. J. Med.*, 2009, **361**, 1807.

192. D. E. Goldberg, V. Sharma, A. Oksman, I. Y. Gluzman, T. E. Wellems and D. Piwnica-Worms, *J. Biol. Chem.*, 1997, **272**, 6567.

193. J. Ziegler, T. Schuerle, L. Pasierb, C. Kelly, A. Elamin, K. A. Cole and D. Wrigth, *Inorg. Chem.*, 2000, **39**, 3731.

194. S. E. Harpstrite, A. A. Beatty, S. D. Collins, A. Oksman, D. E. Goldberg and V. Sharma, *Inorg. Chem.*, 2003, **42**, 2294.

195. N. H. Gokhale, K. Shirisha, S. B. Padhye, S. L. Croft, H. D. Kendrick and V. Mckee, *Bioorg. Med. Chem. Lett.*, 2006, **16**, 430.

196. A. C. Tella and J. A. Obaleye, *Eur. J. Chem.*, 2009, **6**, S311.

197. P. Chellan, N. Shunmoogam-Gounden, D. T. Hendricks, J. Gut, P. J. Rosenthal, C. Lategan, P. J. Smith, K. Chibale and G. S. Smith, *Eur. J. Inorg. Chem.*, 2010, **22**, 3520.

198. P. A. Ajibade and G. A. Kolawole, *Transition Met. Chem.,* 2008, **33**, 493.

199. S. R. Krungkrai and Y. Yutharvong, *Trans. R. Soc. Trop. Med. Hyg.*, 1987, **81**, 710.

200. A. Robert and B. Meunier, *Chem. Eur. J.* 1998, **7**, 1287.

201. A. Dorn, S. R. Vippagunta, H. Matile, C. Jacquet, J. L. Vennerstrom and R. G. Ridley, *Biochem. Pharmacol.*, 1998, **55**, 727

202. T. J. Egan, E. Hempelmann and W. W. Mavuso, *J. Inorg. Biochem.*, 1999, **73**, 101.

203. T. J. Egan, R. Hunter, C. H. Kaschula, H. M. Marques, A. Misplon and J. C. Walden, *J. Med. Chem.,* 2000, **43**, 283.

204. A. Martínez, C. S. K. Rajapakse, B. Naoulou, Y. Kopkalli, L. Davenport and R. A. Sánchez-Delgado, *J. Biol. Inorg. Chem.*, 2008, **13**, 703.

205. A. Martínez, C. S. K. Rajapakse, D. Jalloh, C. Dautriche and R. A. Sánchez-Delgado, *J. Biol. Inorg. Chem.,* 2009, **14**, 863.

206. M. Navarro, W. Castro, A. Martínez and R. A. Sánchez-Delgado, *J. Inorg. Biochem.*, 2011, **105**, 276.

207. C. Biot, D. Taramelli, I. Forfar-Bares, L. Maciejewski, M. Boyce, G. Nowogrocki, J. S. Brocard, N. Basilico, P. Olliaro and E. J. Egan, *Mol. Pharmaceutics*, 2005, **2**, 185.

208. F. Dubar, J. Khalife, D. Dive and C. Biot, *Molecules*, 2008, **13**, 2900.

209. F. Dubar, T. J. Egan, B. Pradines, D. Kuter, K. K. Ncokazi, D. Forge, P. Jean-Francois, C. Pierrot, H. Kalamou, J. Khalife, E. Buisine, C. Rogier, H. Vezin, I. Forfar, C. Slomianny, X. Trivelli, S. Kapishnikov, L. Leiserowitz, D. Dive and C. Biot, *ACS Chem. Biol.*, 2011, **6**, 275.

210. C. Biot, N. Chavain, F. Dubar, B. Pradines, J. Brocard, I. Forfar and D. Dive, *J. Organomet. Chem.,* 2009, **694**, 845.

211. N. Chavain, H. Vezin, D. Dive, N. Touati, J. F. Paul, E. Buisine and C. Biot, *Mol. Pharmaceutics,* 2008, **5**, 710.

212. F. Dubar, S. Bohic, C. Slomianny, J. C. Morin, P. Thomas, H. Kalamou, Y. Guérardel, P. Cloetens, J. Khalife and C. Biot, *Chem. Commun.,* 2012, **48**, 910.

213. A. B. Blake and F. A. Cotton, *Inorg. Chem*., 1964, **3**, 5.

214. C. J. Ballahausen, *Introduction to Ligand Field Theory,* McGraw-Hill, 1962, 255.

215. Y. Tanabe and S. Sugano, *J. Phys. Soc. Japan,* 1954, **9,** 753, 766.

216. D. Nicholls in *Comprehensive Inorganic Chemistry* 1st ed., Vol. 3 (ed. J. C. Bailar, H. J. Emeleus, Ronald Nyholm and A. F. Trotman-Dickenson), Pergamon Press, 1973, 1080.

217. H. A. Weakliem, *J. Chem. Phys.* 1962, **36,** 2117.

218. F. A. Cotton and G. Wilkinson, *Advanced Inorganic Chemistry,* 2nd edition, Interscience, 1966.

219. J. Ferguson, *J. Chem. Phys.* 1963, **39**, 116.

220. A. D. Liehr, *J. Phys. Chem.* 1963, **67**, 1314.

221. A. B. P. Lever and S. M. Nelson, *J. Chem. Soc. (A)* 1966, 859.

222. A. B. P. Lever, *Inorganic Electronic Spectroscopy*, 2nd Ed. Elsevier, 1984, 503.

223. L. Sacconi, F. Mani and A. Bencini in *Comprehensive Coordination Chemistry: The synthesis, reactions, properties and applications of coordination compounds*, ed. Geoffrey Wilkinson, R. D. Gillard and J. A. McCleverty, Pergamon, Oxford, 1987, Vol. 5, 2, 45 - Late transition elements.

224. L. Sacconi, *Transition Met. Chem*., 1968, **4**, 199.

225. R. Morassi, I. Bertini and L. Sacconi, *Coord. Chem. Rev.,* 1973, **11**, 343.

226. P. L. Orioli, *Coord. Chem. Rev.,* 1971, **6**, 285.

227. E. Uhlig, *Coord. Chem. Rev.,* 1973, **10**, 227.

228. M. Ciampolini, *Inorg. Chem.,* 1966, **5**, 35.

229. L. M. Venanzi, *Chemistry of the Co-ordinate compounds,* a symposium sponsored by the Italian national Research Council, the International Union of Pure and Applied Chemistry and the Italian Chemical Society Rome, 15–21 September, 1957.

230. F. Basolo and R. G. Pearson, *Mechanisms of inorganic reactions: a study of metal complexes in solution*, John Wiley and Sons, Inc., USA, 1958, 17.

231. C. K. Jorgensen, *Acta Chem. Scand.,* 1955, **9**, 1362.
232. O. G. Holmes and D. S. McClure, *J. Chem. Phys.,* 1957, **26**, 1686.
233. A. D. Liehr and C. J. Ballhausen, *Ann. Phys.*, 1959, **6**, 134.
234. A. D. Liehr and C. J. Ballhausen, *Mol. Phys*. 1959, **2**, 123.
235. A. B. P. Lever, G. London and P. J. McCarthy, *Can. J. Chem.,* 1977, **55**, 3172.
236. R. Morassi, I. Bertini and L. Sacconi, *Coord. Chem. Rev.,* 1973, **11**, 343.
237. L. Sacconi, *Coord. Chem. Rev.,* 1972, **8**, 351.
238. A. B. P. Lever, *Inorganic Electronic Spectroscopy,* Elsevier, 1984, 535.
239. H. B. Gray, *Transition Metal Chemistry* (R. S. Carlin, ed.), 1965, Vol. 1, 239.
240. M. Gerloch, L. R. Hanton and M. R. Manning, *Inorg. Chim. Acta*, 1981, 205.
241. B. N. Figgis, *Prog. Inorg. Chem.*, 1964, **6**, 37.
242. R. L. Carlin and A. J. Van Duyneveldt, *Magnetic Properties of Transition Metal Compounds,* Springer-Verlag, New York, 1977.
243. S. Mitra, *Prog. Inorg. Chem.,* 1977, **22**, 309.
244. S. Mitra, *Trans. Met. Chem.,* 1972, **7**, 183.
245. C. J. O'Connor *Prog. Inorg. Chem.,* 1982, **22**, 203.
246. H. A. Jahn and E. Teller, *Proc. Roy. Soc. A,* 1937, **161**, 220.
247. L. E. Orgel and J. D. Dunitz, *Nature,* 1957, **179**, 462.
248. *Comprehensive Inorganic Chemistry* 1st ed. Vol. 3, ed. J. C. Bailar, H. J. Emeleus, Ronald Nyholm, A. F. Trotman-Dickenson, Pergamon, New York ,1973, 41.
249. F. A. Cotton and G. Wilkinson, *Advanced Inorganic Chemistry* 4th ed., 1981, 500.
250. M. Kato, H. B. Jonassen and J. C. Fanning, *Chem. Rev.,* 1964, **64**, 99.
251. B. N. Figgis and J. Lewis, *Progress in Inorganic Chemistry,* 1964, **6**, 210.
252. M. Gerloch, *J. Chem. Soc. A*, 1968, 2023.

EXPERIMENTAL SECTION

2.1 MATERIALS

All reagents used to synthesize the 2–(methylthiomethyl)anilines, 2–(methylthio)anilines, the Schiff-bases of their para–substituted derivatives and the metal(II) complexes were analytical grade purchased from Sigma-Aldrich and Merck, South Africa. The solvents were used as obtained except in a few cases where they were dried and distilled under nitrogen before use following standard procedures.[1]

2.2 SYNTHESIS

2.2.1 Synthesis of the 2MT and 2MA ligands

2.2.1.1 2-(Methylthiomethyl)aniline ligands

The general procedure employed for the synthesis of 2-(methylthiomethyl)aniline (R = H) and the other substituted derivatives followed that of Chupp *et al*.[2]

Synthesis of 2-(methylthiomethyl)aniline: Aniline (1.00 g, 10.7 mmol) and dimethyl sulfide (1.1 mL, 15.00 mmol) in dichloromethane (28 mL) were vigorously stirred at room temperature. *N*-chlorosuccinimide (2.04 g, 15.0 mmol) was added in small portions. The mixture was stirred for 10 min; triethylamine (2.1 mL, 15.0 mmol) was added and the mixture was heated at reflux for 12 h. The organic

layer was extracted with 10% NaOH (25 mL) and dried over anhydrous magnesium sulfate. Solvent was removed *in vacuo* to give red-brown oily crude (6.11 g). Purification of the crude was carried out by column chromatography on silica gel 60 (0.040–0.063 mm) using hexane: ether (4:1 vol/vol) as the eluent, fractions were collected in test tubes in 30 mL portions and R_f value of each fraction was determined on TLC plate (Silica gel 60 F_{254}). Fractions with similar R_f values were combined, dried *in vacuo* to remove the solvent and the NMR spectra obtained to identify the desired product. The first fraction gave 2MT as pure light yellow oil (80% yield).

Other substituted 2–(methylthiomethyl)aniline ligands (R = 2–Me, 4–Me, 2–MeO, 4–MeO, 2–Cl, 4–Cl, 2–Br, 4–Br, 2–NO_2, 4–NO_2) were similarly prepared (**Scheme 2.1**). The ligands are soluble in common polar and non-polar organic solvents except 4NO_2–2MT which is insoluble in EtOH and MeOH. Their physical and analytical data including their microanalyses and percentage yield (pure) are recorded in **Table 2.1** under Section 2.4.1.

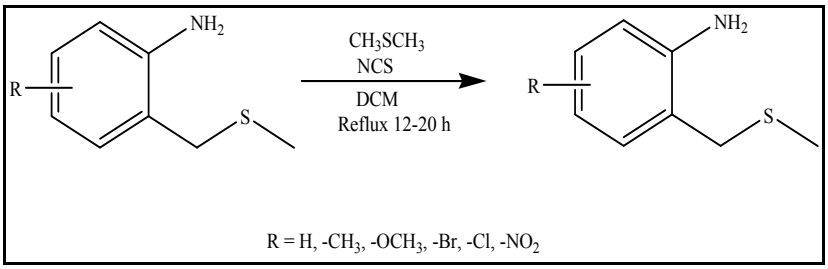

Scheme 2.1 Synthesis of substituted 2–(methylthiomethyl)anilines

2.2.1.2 2-(Methylthio)aniline ligands

2–(Methylthio)aniline was previously prepared by methylation of 2–aminothiophenol at low temperature.[3]

2–aminothiophenol (0.50 g, 4.00 mmol) in dry ethanol (10 mL) was cooled to 0^oC while stirring. Potassium *tert*–butoxide (0.45 g, 4.00 mmol) was added in portions over for 15 min, and the mixture was further stirred for 45 min. Iodomethane (0.58g, 4.10 mmol) was added slowly over 15 min and the reaction mixture was allowed to warm up to room temperature and was stirred for 45 min. The resulting

mixture was filtered and the filtrate obtained was evaporated to dryness, DCM (25 mL) was added to this residue and the solution filtered. The filtrate was evaporated under reduced pressure to obtain the crude product. Column purification of this crude carried out on silica gel using hexane/ether (5:1 vol/vol) as eluent yielded pure 2–(methylthio)aniline (0.16 g, 63%).

The substituted 2–(methylthio)anilines however were prepared employing two steps (**Scheme 2.2**). The first step[4-8] of the reaction involves the conversion of the appropriate substituted anilines to the corresponding 2–aminobenzothiazoles. In the second stage,[9] the substituted 2–aminobenzothiazoles were hydrolyzed and methylated to yield the desired crude 2–(methylthio)anilines. Column purification of the crude was carried out on silica gel using hexane/ether (6:1 vol/vol) as eluent to afford the pure compounds.

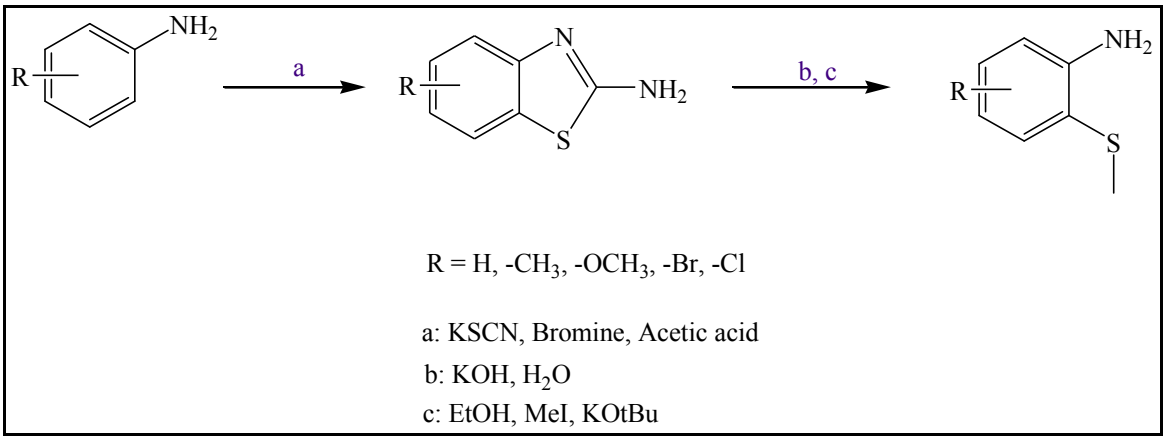

Scheme 2.2 Two–pot synthesis of substituted 2–(methylthio)anilines

Step 1 *p*-Anisidine (1.00 g, 8.10 mmol) and potassium thiocyanate (3.16 g, 32.50 mmol) in glacial acetic acid (16 mL) were rapidly stirred and bromine liquid (1.30 g, 8.10 mmol) was added dropwise. The mixture was stirred for 10 h keeping the temperature below 35^{o}C, during which a precipitate was formed. This mixture was filtered and residue washed with water. The combined filtrate was neutralized to pH 7 with aqueous ammonia solution during which a shiny brown precipitate formed, and was filtered, dried and weighed to be 2.00 g of 6–methoxy–2–aminobenzothiazole.

Step 2 6–Methoxy–2–aminobenzothiazole (0.54 g, 3.00 mmol) was slowly added to potassium hydroxide (1.54 g, 27.40 mmol) dissolved in 2 mL water. The mixture was slowly heated to 135^{o}C

allowing the water to evaporate. The temperature was then increased to 165^{o}C and held there for 2 h. The reaction mixture was allowed to cool to room temperature and quenched with 2 mL of water. The mixture was filtered to remove the unreacted 2–aminobenzothiazole. The filtrate was collected and the water removed under vacuum. Iodomethane (0.19 mL, 3.00 mmol) and 4 mL ethanol were each added to the residue and the slurry was stirred for 16 h after which ethanol was removed *in vacuo*. The residue was dissolved in water, neutralized to pH 7 with concentrated HCl and the product extracted with dichloromethane. Removal of the solvent under pressure yielded crude 4–methoxy–6–(methylthio)aniline which was purified to yield pure product (0.26 g, 9%).

Other substituted 2–(methylthio)anilines were similarly prepared with the exception of the nitro-substituted derivatives which could not be synthesized because their 2–aminobenzothiazole precursors yielded unknown products after hydrolysis and methylation processes of *step 2* above. The synthesized ligands are soluble in common polar and non-polar organic solvents. **Table 2.2** (Section 2.4.1) contains the physical and analytical data of the successfully synthesized ligands.

2.2.2 Synthesis of Schiff–bases derived from the thiomethylated ligands

pMS–2MT was prepared as described: 2MT (0.28 g, 1.86 mmol) and *p*-methoxysalicylaldehyde (0.31 g, 2.05 mmol) in 2 mL EtOH and 2 mL DCM were refluxed for 6 h. The solvent was reduced and a yellow product precipitated which was obtained by filtration, washed with ethanol, air dried and weighed as 0.37 g (69%).

A similar procedure was employed for the synthesis of other pMS–2MT and pMS–2MA Schiff–bases. In a few cases, an oily product resulted from the reaction. On purification by column chromatography on silica gel using hexane/ether (6:1 vol/vol) as eluent, the pure solid product was obtained. All the Schiff-base ligands are soluble in DCM, $CHCl_3$, DMSO and DMF but not in MeOH or EtOH. Suitable single crystals were grown from DCM/EtOH mixture. The analytical data including the yields for the Schiff–bases are recorded in **Table 2.3** (Section 2.4.1).

2.2.3 Synthesis of metal(II) complexes of the thiomethylated ligands

The general synthesis procedure employed the use of corresponding metal(II) chlorides and the ligands, both in ethanol or ethanol/dichloromethane mixture to afford Co(II) and Ni(II) complexes which formed in a 2:1 ligand:metal ratio respectively. The Cu(II) complexes were derived in 1:1 stoichiometry, however, $Cu(4Br–2MA)_2$ formed in 2:1 ligand: metal ratio.

The products were neither affected by the order of addition (ligand to metal or metal to ligand) nor by the reaction temperature (ambient synthesis or reflux).

Attempts were made to synthesize the corresponding complexes of Mn(II), Fe(II) and Zn(II) with 2MT ligand under similar reaction conditions but were not successful.

2.2.3.1 Cobalt(II) complexes

Co2MT was prepared by adding 0.06 g (0.38 mmol) 2MT in 2 mL ethanol to 0.04 g (0.15 mmol) $CoCl_2{\cdot}6H_2O$ in 2mL ethanol, stirred at room temperature for 4 h to ensure complete reaction. Light pink precipitate obtained was filtered, washed with ethanol and ethyl-acetate, dried under vacuum and weighed to be 0.13 g (79%).

Co2MA was prepared by adding ethanol solution of $CoCl_2{\cdot}6H_2O$ (0.27 g, 1.10 mmol) to 2–(methylthio)aniline (0.40 g, 2.90 mmol) in ethyl-acetate (2 mL), stirred at room temperature for 4 h to ensure complete reaction. Dark purple precipitate obtained was filtered, washed with ethanol and ethyl-acetate, air dried and weighed to be 0.08g (17%).

2.2.3.2 Nickel(II) complexes

To $NiCl_2{\cdot}6H_2O$ (0.04 g, 0.15 mmol) in ethanol (2 mL) was added an ethanol (2 mL) solution of 2MT (0.06 g, 0.38 mmol). This mixture was stirred at room temperature for 4 h to yield a green solid which was filtered, washed with ethanol and ethyl-acetate, dried under vacuum and weighed to afford 0.14 g Ni2MT in 85% yield.

To 2–(methylthio)aniline (0.10 g, 0.70 mmol) in ethylacetate (2 mL) was added ethanol (2 mL) solution of $NiCl_2{\cdot}6H_2O$ (0.07 g, 0.30 mmol) and the mixture was stirred at room temperature for 4 h. Green solid formed and was obtained by filtration, washed with ethanol and ethylacetate, air dried and weighed to give 0.09 g Ni2MA in 81% yield.

2.2.3.3 Copper(II) complexes

$CuCl_2{\cdot}2H_2O$ (0.04 g, 0.21 mmol) in 2 mL ethanol was stirred at room temperature and 2MT (0.03 g, 0.21 mmol in 2mL ethanol was added. Green precipitate was immediately formed and the mixture was further stirred for 2 h to ensure complete reaction. Cu2MT was obtained after filtering, washing with ethanol and drying and weighed 0.05 g (91%).

2–(methylthio)aniline (0.11 g, 0.80 mmol) in ethanol was stirred at room temperature and ethanol solution of $CuCl_2{\cdot}2H_2O$ (0.14 g, 0.80 mmol) was added. The mixture was further stirred for 2 h. The dark green Cu2MA solid obtained after filtering, washing with ethanol and drying was weighed as 0.19 g (88%).

Similar procedures were employed to synthesize the Co(II), Ni(II) and Cu(II) complexes of other substituted 2MT and 2MA ligands (**Scheme 2.3**). However, the synthesis of some metal(II) complexes were not successful following the above procedures. Complexes of $2NO_2$–2MT) could not be synthesized as repeated synthesis of $2NO_2$–2MT ligand failed to produce a pure product after several attempts. Co(II) and Ni(II) complexes of 2Cl–2MA and 2Br–2MA were not obtained as the individual reactants precipitated out of the reaction mixture.

All the cobalt(II), nickel(II) and copper(II) complexes were found to be stable in air, retaining their physical and chemical properties. Co(II) complexes of both 2MT and 2MA ligands are completely soluble in organic solvents such as EtOH, MeOH, CH_3CN, THF, DMF and DMSO. Ni(II) complexes are also soluble in EtOH, MeOH, CH_3CN, DMF and DMSO. The Cu(II) complexes are only completely soluble in DMF and DMSO. The analytical data of the metal(II) complexes are recorded in **Tables 2.4–2.5** for Co(II), **Tables 2.6–2.7** for Ni(II) and **Tables 2.8–2.9** for Cu(II).

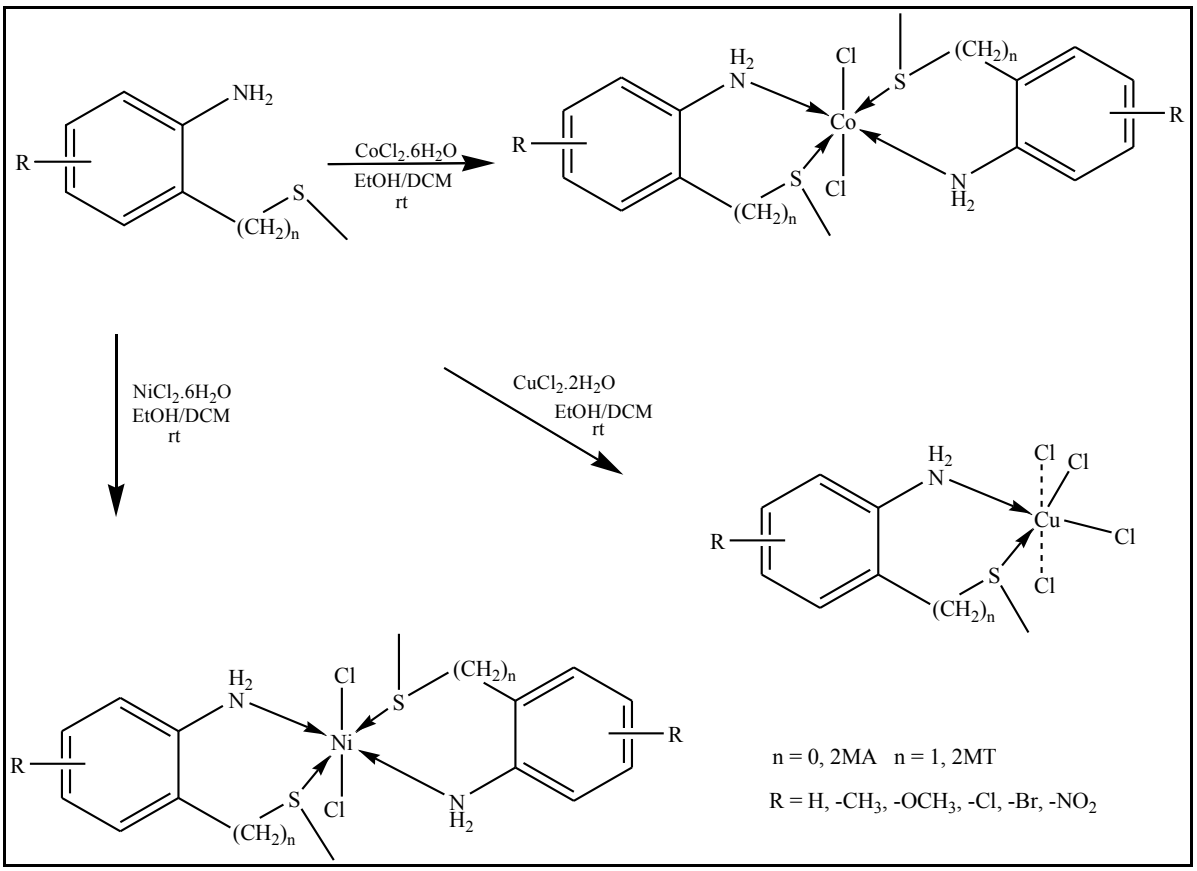

Scheme 2.3 Synthesis of metal complexes of 2MT and 2MA ligands

2.2.4 Synthesis of Cu(II) complexes of Schiff–bases

Cu(pMS–2MT) was prepared as described: The schiff–base pMS–2MT (0.06 g, 0.21 mmol) was dissolved in DCM/EtOH (2 mL/2 mL) mixture and a few drops of triethylamine was added to convert the ligand into the ionic form by proton abstraction. The solution was further stirred for 15 min maintaining the temperature at 30°C. $CuCl_2{\cdot}2H_2O$ (0.02 g, 0.10 mmol) in ethanol was added in drops and the mixture was refluxed for 1 h during which a dark grey precipitate formed. The reaction mixture was allowed to warm to room temperature and filtered. The precipitate was washed with ethanol and air-dried, the precipitate was weighed to be 0.07 g (%). Other copper(II) complexes of the schiff–bases were similarly prepared as seen in **Scheme 2.4**. They are soluble in DCM and $CHCl_3$ only. Their physical and analytical data are presented in **Table 2.10**. A single crystal suitable for X–ray crystallography was grown from chloroform/ethanol mixture.

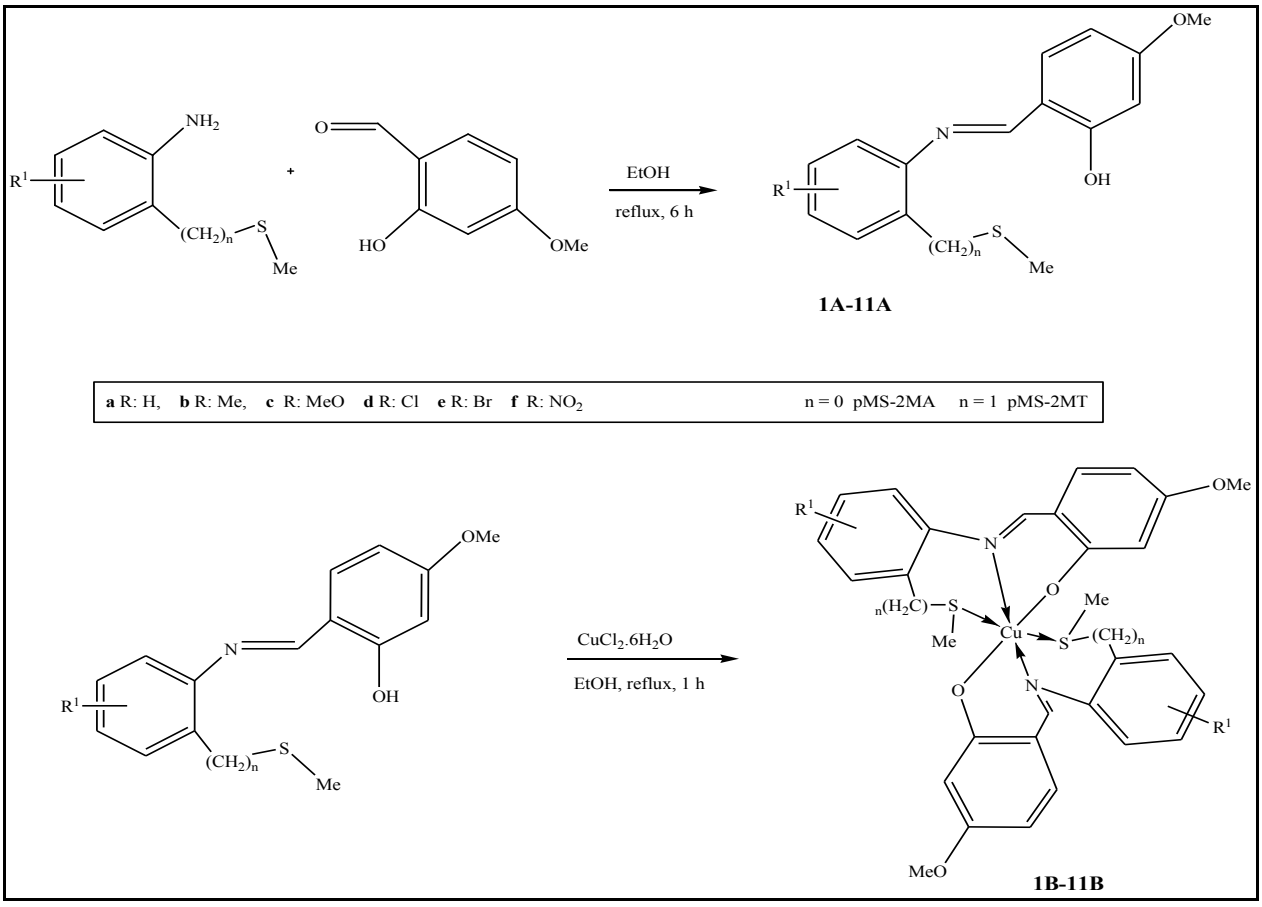

Scheme 2.4 Synthesis routes for Schiff-bases and Cu(II) complexes

2.3 PHYSICAL MEASUREMENTS

2.3.1 CHNS analysis

Elemental analysis (CHNS) was carried out by Mr. Francis Chindeka in this department on Elementar Analysensysteme varioMICRO V1.6.2 GmbH.

2.3.2 Melting point

The melting points of the solid samples were measured using Galenkemp melting point apparatus.

2.3.3 NMR

One– and two–dimensional NMR (^{1}H, ^{13}C, DEPT135, COSY, HMBC and HSQC) spectra were obtained in $CDCl_3$ relative to the residual proton in the solvent on Bruker Avance 400 MHz NMR spectrometer.

2.3.4 IR

The mid-infrared spectra (4000 – 400 cm^{-1}) were determined as solids on PerkinElmer Spectrum 100 ATR-FTIR spectrometer. Far-infrared spectra (700 – 30 cm^{-1}) were obtained in nujol mulls held between polyethylene discs and recorded on Perkin Elmer Spectrum 400 FTIR/FIR spectrometer.

2.3.5 Raman

The Raman spectra were obtained as solids on Bruker Vertex 70 Fourier spectrometer, equipped with RAM II FT-Raman module with Ge detector and Nd: YAG laser under the excitation of 1064 nm and power of 4. Each sample was collected after 20 scans.

2.3.6 Single crystal X–ray diffraction

Crystallography data were collected at -73 K using a Bruker KAPPA APEX II diffractometer with a 4-circle goniometer and sensitive CCD detector. The instrument is equipped with a graphite monochromator and used a Molybdenum fine focus sealed x-ray tube as source of x-ray (Mo-*K*α radiation, λ = 0.71073 Å) and an Oxford Cryostream 700 system for sample temperature control. Bruker APEX2 software was used for instrument control. The structures of the compounds were solved using SHELXL–97 software

package.[10-12] Numerical absorption corrections were done. All non hydrogen atoms were refined anisotropically. The positions and temperature parameters of the hydrogen atoms were fixed to the adjacent atoms. Crystallography data were run at the Nelson Mandela Metropolitan University, Port Elizabeth, South Africa by Dr. van Brecht.

2.3.7 Conductivity measurements

Conductivity measurements of complexes solution in dimethyl formide at 10^{-3} M under room temperature were taken using AZ® 86555 p^H/mV/Cond./TDS/Temp machine.

2.3.8 Electronic spectra

Electronic spectra (250–1100 nm) were obtained in solution using dimethylsulfoxide as solvent for the thiomethylated ligands and their metal complexes, and dichloromethane for the Schiff-bases and their Cu(II) complexes and were run on PerkinElmer Lambda 25 UV/VIS Spectrometer.

2.3.9 Diffuse reflectance spectra

Solid reflectance study of the metal complexes was carried out using Shimadzu UV-3100 UV-VIS-NIR Spectrometer with a MPC-3100 multipurpose large sample compartment at the Nelson Mandela Metropolitan University, Port Elizabeth, South Africa with the assistance of Dr. Eric Hosten.

2.4 RESULTS OF ANALYSIS

In this section are written the results for each experimental work carried out in the course of research. The tables presented contain the ligands and complexes, these are arranged starting from the unsubstituted ligands (or their complexes) to the ones with electron-donating substituents (–Me, –MeO) and those with withdrawing groups (–Cl, –Br, $–NO_2$).

2.4.1 Physical and analytical data

This sub-section contains the data collected on some of the physical properties of the thiomethylated ligands with their metal(II) complexes as well as those of the Schiff-bases derived from them. The tables also contain the analytical information and percentage yields for all the compounds successfully synthesized.

Table 2.1 Physical and analytical data for 2–(methylthiomethyl)anilines

Entry	Ligand	Mol. wt.	M. Pt (°C)	%Found (Calculated)				Yield %
				C	H	N	S	
1	2MT	153.24	oil	62.87 (62.70)	7.08 (7.23)	9.27 (9.14)	19.61 (20.92)	80
2	2Me–2MT	167.27	oil	62.05 (64.62)	7.83 (8.07)	8.13 (8.37)	17.85 (19.17)	57
3	4Me–2MT	167.27	65-68	63.12 (64.62)	7.87 (7.83)	8.09 (8.37)	18.11 (19.17)	69
4	2MeO–2MT	183.27	oil	58.41 (58.98)	7.36 (7.15)	7.53 (7.64)	16.96 (17.50)	97
5	4MeO–2MT	183.27	oil	57.97 (58.98)	7.92 (7.15)	7.51 (7.64)	17.32 (17.50)	26
6	2Cl–2MT	187.69	oil	50.97 (51.19)	5.68 (5.37)	7.26 (7.46)	16.05 (17.08)	33
7	4Cl–2MT	187.69	69-72	51.84 (51.19)	5.51 (5.37)	7.38 (7.46)	16.49 (17.08)	78
8	2Br–2MT	232.14	oil	41.62 (41.39)	4.26 (4.34)	6.10 (6.03)	13.57 (13.81)	60
9	4Br–2MT	232.14	68-71	41.25 (41.39)	4.22 (4.34)	5.89 (6.03)	13.42 (13.81)	62
10	$2NO_2$–2MT	198.24	70-72	47.02 (47.39)	5.25 (5.22)	13.18 (13.82)	15.09 (15.82)	51
11	$4NO_2$–2MT	198.24	70-73	47.58 (47.39)	5.30 (5.22)	13.74 (13.82)	16.01 (15.82)	33

Table 2.2 Physical and analytical data for 2–(methylthio)anilines

Entry	Ligand	Mol. wt.	M. Pt (°C)	%Found (Calculated)				Yield %
				C	H	N	S	
12	2MA	139.22	oil	58.90 (60.39)	6.72 (6.52)	9.57 (10.06)	22.03 (23.03)	16
13	2Me–2MA	153.25	oil	62.03 (62.70)	7.99 (7.24)	9.01 (9.14)	20.91 (20.92)	24
14	4Me–2MA	153.25	oil	61.97 (62.70)	7.44 (7.24)	9.02 (9.14)	20.64 (20.92)	9
15	2MeO–2MA	169.24	68-72	56.10 (56.77)	6.87 (6.55)	8.21 (8.28)	19.00 (18.95)	11
16	4MeO–2MA	169.24	oil	56.62 (56.77)	6.70 (6.55)	8.06 (8.28)	18.34 (18.95)	9
17	2Cl–2MA	173.66	oil	48.80 (48.41)	4.81 (4.64)	8.02 (8.07)	18.39 (18.46)	29
18	4Cl–2MA	173.66	oil	48.60 (48.41)	5.23 (4.64)	7.96 (8.07)	18.29 (18.46)	8
19	2Br–2MA	218.11	oil	39.54 (38.55)	3.71 (3.70)	6.36 (6.42)	14.76 (14.70)	22
20	4Br–2MA	218.11	oil	39.96 (38.55)	3.93 (3.70)	6.46 (6.42)	17.27 (14.70)	10

Table 2.3 Physical and analytical data for pMS–2MT and pMS–2MA Schiff-base ligands

Entry	Ligand	Mol. wt.	Colour	M. Pt (^{o}C)	%Found (Calculated)				Yield %
					C	H	N	S	
21	pMS-2MT	287.38	Yellow	68-69	66.59 (66.87)	6.17 (5.96)	4.89 (4.87)	11.00 (11.16)	80
22	pMS–4Me2MT	301.40	Yellow	72-73	68.18 (67.74)	7.19 (6.35)	4.59 (4.65)	10.57 (10.64)	75
23	pMS–4MeO2MT	317.40	Pale yellow	72-73	64.20 (64.33)	6.58 (6.03)	4.42 (4.41)	10.06 (10.10)	53
24	pMS–4Cl2MT	321.82	Yellow	72-73	59.72 (59.71)	5.18 (5.01)	4.35 (4.35)	9.63 (9.96)	55
25	pMS–4Br2MT	366.27	Yellow	74-75	52.43 (52.47)	4.37 (4.40)	3.85 (3.82)	8.89 (8.75)	74
26	pMS–4$NO_2$2MT	332.37	Orange	75-76	57.71 (57.82)	5.17 (4.85)	8.29 (8.43)	9.47 (9.65)	55
27	pMS-2MA	273.35	Brown	68-69	65.80 (65.91)	5.24 (5.53)	5.13 (5.12)	11.42 (11.73)	94
28	pMS–4Me2MA	287.38	Yellow	72-73	67.07 (66.87)	5.88 (5.96)	4.94 (4.87)	11.21 (11.16)	85
29	pMS–4MeO2MA	303.38	Yellow	80-81	63.38 (63.34)	6.06 (5.65)	4.66 (4.62)	10.72 (10.57)	36
30	pMS–4Cl2MA	307.80	Yellow	90-91	57.94 (58.53)	4.95 (4.58)	4.49 (4.55)	9.85 (10.42)	88
31	pMS–4Br2MA	352.25	Yellow	94-95	51.99 (51.15)	3.97 (4.01)	4.03 (3.98)	9.37 (9.10)	89

Table 2.4 Physical and analytical data for Co(II) complexes of 2–(methylthiomethyl)anilines

Entry	Complexes	Mol. wt.	Colour	M. Pt (°C)	%Found (Calculated)				Yield %
					C	H	N	S	
1A	$[Co(2MT)_2Cl_2]$	436.33	Pink	130-132	43.92 (44.04)	5.42 (5.08)	6.08 (6.42)	14.61 (14.70)	79
2A	$[Co(2Me–2MT)_2Cl_2]$	464.38	Pale blue	140-142	46.24 (46.55)	5.82 (5.64)	5.89 (6.03)	13.46 (13.81)	24
3A	$[Co(4Me–2MT)_2Cl_2$	464.38	Pink	155-157	46.99 (46.55)	6.05 (5.64)	5.98 (6.03)	13.67 (13.81)	95
4A	$[Co(2MeO–2MT)_2Cl_2$	496.38	Pink	106-108	43.41 (43.55)	5.72 (5.28)	5.57 (5.64)	12.73 (12.92)	57
5A	$[Co(4MeO–2MT)_2Cl_2].H_2O$	496.38	Dark purple	130-133	42.34 (42.03)	4.79 (5.49)	5.50 (5.45)	11.32 (12.47)	50
6A	$[Co(2Cl–2MT)_2Cl_2]$	505.22	Pink	215-217	37.91 (38.04)	4.12 (3.99)	5.44 (5.54)	12.23 (12.69)	63
7A	$[Co(4Cl–2MT)_2Cl_2]$	505.22	Pink	178-180	38.33 (38.04)	4.02 (3.99)	5.51 (5.54)	12.36 (12.69)	46
8A	$[Co(2Br–2MT)_2Cl_2]$	594.12	Pink	180-182	32.74 (32.35)	3.42 (3.39)	4.73 (4.72)	10.37 (10.79)	42
9A	$[Co(4Br–2MT)_2Cl_2]$	594.12	Pink	176-178	32.97 (32.35)	3.37 (3.39)	4.78 (4.72)	10.38 (10.79)	55
11A	$[Co(4NO_2–2MT)_2Cl_2]$	526.32	Yellow	> 200	36.64 (36.51)	3.82 (3.83)	10.65 (10.64)	12.18 (12.18)	55

Table 2.5 Analytical data for Co(II) complexes of 2–(methylthio)anilines

Entry	Complexes	Mol. wt.	Colour	M. Pt (°C)	%Found (Calculated)				Yield %
					C	H	N	S	
12A	$[Co(2MA)_2Cl_2]$	408.27	Grey purple	>200	40.23 (41.19)	4.40 (4.44)	6.63 (6.86)	14.96 (15.71)	17
13A	$[Co(2Me–2MA)_2Cl_2]$	436.33	Blue	>200	43.91 (44.04)	5.00 (5.08)	6.31 (6.42)	14.54 (14.70)	65
14A	$[Co(4Me–2MA)_2Cl_2]$	436.33	Pink	>200	43.48 (44.04)	5.32 (5.08)	6.22 (6.42)	13.40 (14.70)	43
15A	$[Co(2MeO–2MA)_2Cl_2].2H_2O$	468.38	Purple black	>200	38.10 (38.26)	4.67 (4.82)	5.42 (5.58)	12.07 (12.77)	9
16A	$[Co(4MeO–2MA)_2Cl_2]$	468.38	Purple	>200	41.36 (41.03)	5.03 (4.73)	5.83 (5.98)	13.04 (13.69)	74
18A	$[Co(4Cl–2MA)_2Cl_2]$	477.16	Pink	160-162	34.91 (35.24)	3.33 (3.38)	5.76 (5.87)	13.33 (13.44)	28
20A	$[Co(4Br–2MA)_2Cl_2]$	566.07	Pink	150-152	31.80 (29.70)	3.37 (2.85)	4.99 (4.95)	13.80 (11.33)	51

Table 2.6 Physical and analytical data for Ni(II) complexes of 2–(methylthiomethyl)anilines

Entry	Complexes	Mol. wt.	Colour	M. Pt [a] (°C)	%Found (Calculated)				Yield %
					C	H	N	S	
1B	$[Ni(2MT)_2Cl_2]$	436.09	Green	200-205	44.02 (44.07)	5.31 (5.08)	6.45 (6.42)	14.15 (14.71)	85
2B	$[Ni(2Me–2MT)_2Cl_2]$	464.14	Green	220-224	46.35 (46.58)	5.89 (5.65)	5.95 (6.04)	13.21 (13.82)	80
3B	$[Ni(4Me–2MT)_2Cl_2]$	464.14	Green	212-218	46.82 (46.58)	5.85 (5.65)	5.95 (6.04)	13.53 (13.82)	86
4B	$[Ni(2MeO–2MT)_2Cl_2]$	496.14	Green	220-226	43.57 (43.57)	5.70 (5.28)	5.61 (5.65)	12.79 (12.93)	74
5B	$[Ni(4MeO–2MT)_2Cl_2].2H_2O$	496.14	Pale green	220-228	41.50 (40.62)	5.82 (5.68)	5.11 (5.26)	10.30 (12.05)	45
6B	$[Ni(2Cl–2MT)_2Cl_2]$	504.98	Light green	210-208	36.59 (38.06)	4.18 (3.99)	4.96 (5.55)	11.17 (12.70)	78
7B	$[Ni(4Cl–2MT)_2Cl_2]$	504.98	Green	220-230	37.64 (38.06)	4.01 (3.99)	5.36 (5.55)	12.09 (12.70)	80
8B	$[Ni(2Br–2MT)_2Cl_2]$	593.88	Light green	210-220	33.13 (32.36)	3.57 (3.39)	4.61 (4.72)	9.75 (10.80)	86
9B	$[Ni(4Br–2MT)_2Cl_2]$	593.88	Green	230-236	31.71 (32.36)	3.21 (3.39)	4.58 (4.72)	9.11 (10.80)	89
11B	$[Ni(4NO_2–2MT)_2Cl_2]$	526.08	Green yellow	204-210	36.56 (36.53)	3.95 (3.83)	10.49 (10.65)	11.66 (12.19)	87

a Decomposition took place for all the Ni(II) complexes

Table 2.7 Physical and analytical data for Ni(II) complexes of 2–(methylthio)anilines

Entry	Complexes	Mol. wt.	Colour	M. Pt [a] (°C)	%Found (Calculated) C	H	N	S	Yield %
12B	$[Ni(2MA)_2Cl_2]$	408.04	Pale green	>200	40.60 (39.47)	4.88 (4.73)	6.53 (6.58)	15.07 (15.05)	81
13B	$[Ni(2Me–2MA)_2Cl_2].2H_2O$	436.09	Green	>200	40.81 (40.70)	5.83 (5.55)	5.91 (5.93)	13.43 (13.58)	70
14B	$[Ni(4Me–2MA)_2Cl_2]$	436.09	Green	>200	44.11 (44.07)	5.32 (5.08)	6.32 (6.42)	14.33 (14.71)	76
15B	$[Ni(2MeO–2MA)_2Cl_2]$	468.09	Green	>200	41.81 (41.05)	4.98 (4.74)	6.05 (5.98)	13.65 (13.70)	58
16B	$[Ni(4MeO–2MA)_2Cl_2]$	468.09	Light blue	>200	41.57 (41.05)	4.87 (4.74)	6.01 (5.98)	13.31 (13.70)	85
18B	$[Ni(4Cl–2MA)_2Cl_2]$	476.93	Light green	>200	35.97 (35.26)	3.41 (3.38)	5.68 (5.87)	13.00 (13.45)	41
20B	$[Ni(4Br–2MA)_2Cl_2]$	566.07	Pale green	>200	31.78 (29.72)	3.04 (2.85)	5.06 (4.95)	12.91 (11.33)	76

a Decomposition took place for all the Ni(II) complexes

Table 2.8 Physical and analytical data for Cu(II) complexes of 2–(methylthiomethyl)anilines

Entry	Complexes	Mol. wt.	Colour	M. Pt (^{0}C)	%Found (Calculated)				Yield %
					C	H	N	S	
1C	$[Cu(2MT)Cl_2]$	287.70	Green	153-155	33.30 (33.40)	3.97 (3.85)	4.86 (4.87)	10.93 (11.15)	91
2C	$[Cu(2Me–2MT)Cl_2]$	301.72	Dark brown	150-152	36.11 (35.83)	4.13 (4.34)	4.67 (4.64)	10.00 (10.63)	83
3C	$[Cu(4Me–2MT)Cl_2]$	301.72	Brown	158-160	36.19 (35.83)	4.09 (4.34)	4.56 (4.64)	10.45 (10.63)	89
4C	$[Cu(2MeO–2MT)Cl_2]$	317.72	Dark Brown	134-135	33.70 (34.02)	3.89 (4.12)	4.37 (4.41)	9.37 (10.09)	76
5C	$[Cu(4MeO–2MT)Cl_2]$	317.72	Brown	147-149	34.09 (34.02)	4.19 (4.12)	4.30 (4.41)	9.58 (10.09)	89
6C	$[Cu(2Cl–2MT)Cl_2]$	322.14	Green	146-147	29.54 (29.83)	2.87 (3.13)	4.32 (4.35)	9.73 (9.95)	69
7C	$[Cu(4Cl–2MT)Cl_2]$	322.14	Green	158-160	30.10 (29.83)	2.86 (3.13)	4.31 (4.35)	9.90 (9.95)	75
8C	$[Cu(2Br–2MT)Cl_2]$	366.59	Red brown	148-150	26.70 (26.21)	2.52 (2.75)	3.83 (3.82)	8.27 (8.75)	53
9C	$[Cu(4Br–2MT)Cl_2]$	366.59	Green	170-172	26.35 (26.21)	2.41 (2.75)	3.86 (3.82)	8.38 (8.75)	79
10C	$[Cu(2NO_2\text{-}2MT)_2Cl_2]$	332.69	Bright green	162-164	29.02 (28.88)	3.03 (3.03)	8.36 (8.42)	8.99 (9.64)	73
11C	$[Cu(4NO_2\text{-}2MT)Cl_2]$	332.69	Green	146-148	29.68 (28.88)	2.91 (3.03)	8.50 (8.42)	9.73 (9.64)	73

Table 2.9 Physical and analytical data for Cu(II) complexes of 2–(methylthio)anilines

Entry	Complexes	Mol. wt.	Colour	M. Pt (°C)	%Found (Calculated)				Yield %
					C	H	N	S	
12C	$[Cu(2MA)Cl_2]$	273.67	Dark green	130-132	31.01 (30.72)	3.52 (3.31)	5.04 (5.12)	11.73 (11.72)	88
13C	$[Cu(2Me–2MA)Cl_2]$	287.70	Black	140-141	36.24 (33.40)	3.76 (3.85)	4.89 (4.87)	10.24 (11.15)	19
14C	$[Cu(4Me–2MA)Cl_2]$	287.70	Bright green	150-152	33.74 (33.40)	3.81 (3.85)	4.90 (4.87)	10.94 (11.15)	92
15C	$[Cu(2MeO–2MA)Cl_2]$	303.70	Deep brown	>200	31.72 (31.64)	4.15 (3.65)	4.50 (4.61)	10.33 (10.56)	32
16C	$[Cu(4MeO–2MA)Cl_2]$	303.70	Dark green	120-122	33.67 (31.64)	3.52 (3.65)	4.93 (4.61)	9.79 (10.56)	94
17C	$[Cu(2Cl–2MA)Cl_2]$	308.11	Deep brown	150-152	29.54 (29.83)	2.87 (3.13)	4.32 (4.35)	9.73 (9.95)	24
18C	$[Cu(4Cl–2MA)Cl_2]$	308.11	Green	160-161	35.97 (35.26)	3.41 (3.38)	5.68 (5.87)	13.00 (13.45)	85
19C	$[Cu(2Br–2MA)_2Cl_2]^a$	570.68	Black	110-111	28.95 (29.46)	2.90 (2.83)	4.78 (4.91)	10.61 (11.24)	22
20C	$[Cu(4Br–2MA)Cl_2]$	352.57	Green	160-162	24.29 (23.85)	2.35 (2.29)	3.92 (3.97)	9.86 (9.09)	81

a octahedral compound formed with 2:1 ligand to metal ratio under similar reaction conditions as other compounds

Table 2.10 Physical and analytical data for Schiff-base Cu(II) complexes

Entry	Complexes	Mol. wt.	M. Pt (^{0}C)	Colour	%Found (Calculated)				Yield %
					C	H	N	S	
21C	[Cu(pMS–2MT)$_2$]	636.28	178-179	Dark grey	59.74 (60.40)	5.25 (5.07)	4.35 (4.40)	9.88 (10.08)	90
22C	[Cu(pMS–4Me2MT)$_2$]	664.34	180-181	Dark grey	61.16 (61.47)	5.67 (5.46)	4.10 (4.22)	9.67 (9.65)	84
23C	[Cu(pMS–4MeO2MT)$_2$]	696.34	154-155	Brown	57.81 (58.64)	5.14 (5.21)	3.96 (4.02)	9.35 (9.21)	68
24C	[Cu(pMS–4Cl2MT)$_2$]	705.17	186-187	Dark grey	53.58 (54.50)	3.56 (4.29)	3.99 (3.97)	9.08 (9.09)	75
25C	[Cu(pMS–4Br2MT)$_2$]	794.08	184-186	Dark grey	48.19 (48.40)	3.85 (3.81)	3.49 (3.53)	7.94 (8.08)	87
26C	[Cu(pMS–4NO$_2$2MT)$_2$]	726.28	>200	Brown	53.05 (52.92)	4.60 (4.16)	7.72 (7.71)	8.46 (8.83)	77
27C	[Cu(pMS–2MA)$_2$]	608.23	>200	Deep green	30.05 (30.62)	3.12 (2.51)	2.45 (2.38)	5.04 (5.45)	40
28C	[Cu(pMS–4Me2MA)$_2$]	636.28	>200	Light brown	59.46 (60.40)	5.21 (5.07)	4.28 (4.40)	9.50 (10.08)	88
29C	[Cu(pMS–4MeO2MA)$_2$]	668.28	>200	Dark brown	57.75 (57.51)	4.91 (4.83)	4.15 (4.19)	9.32 (9.60)	38
30C	[Cu(pMS–4Cl2MA)$_2$]	677.12	>200	Light brown	51.01 (53.21)	4.24 (3.87)	3.99 (4.14)	9.21 (9.47)	86
31C	[Cu(pMS–4Br2MA)$_2$]	766.02	>200	Light brown	47.04 (47.04)	3.31 (3.42)	3.64 (3.66)	8.88 (8.37)	82

2.4.2 ^{1}H and ^{13}C NMR shifts for the ligands

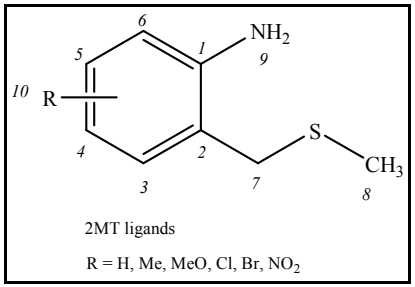

2MT ligands

R = H, Me, MeO, Cl, Br, NO_2

Table 2.11 ^{1}H and ^{13}C chemical shifts (δ) for 2MT ligands in ppm

Ligands	(C)*1*	(C)*2*	H (C)*3*	H (C)*4*	H (C)*5*	H (C)*6*	H (C)*7*	H (C)*8*	H*9*	H (C)*10*
2MT	(144.96)	(121.19)	7.05 *d* (130.49)	6.76 *t* (117.96)	7.14 *t* (128.21)	6.71 *d* (116.15)	3.71 *s* (35.14)	2.01 *s* (14.32)	4.06 *s*	----------
2Me–2MT	(143.23)	(120.49)	6.98 *d* (129.64)	6.68 *t* (117.45)	7.05 *d* (128.67)	-------- (122.69)	3.73 *s* (35.60)	2.02 *s* (14.56)	4.09 *s*	2.22 *s* (17.39)
4Me–2MT	(142.62)	(121.61)	6.85 *s* (131.23)	------- (127.44)	6.93 *d* (128.98)	6.62 *d* (116.52)	3.67 *s* (35.48)	2.02 *s* (14.63)	3.95 *s*	2.25 *s* (35.60)
2MeO–2MT	(147.63)	(121.69)	6.70 *d* (109.44)	6.77 *t* (117.24)	6.69 *d* (122.92)	-------- (134.97)	3.72 *s* (35.30)	2.00 *s* (14.65)	4.28 *s*	3.85 *s* (55.60)
4MeO–2MT	(138.64)	(123.71)	6.70 *d* (116.46)	------- (152.21)	6.64 *s* (113.45)	6.64 *d* (117.41)	3.64 *s* (35.48)	1.99 *s* (14.57)	3.81 *s*	3.73 *s* (55.56)
2Cl–2MT	(141.50)	(120.19)	6.96 *d* (128.28)	6.68 *t* (117.76)	7.27 *d* (128.97)	-------- (122.43)	3.73 *s* (35.54)	2.01 *s* (14.39)	4.60 *s*	----------
4Cl–2MT	(143.85)	(122.84)	6.98 *s* (130.18)	------- (123.14)	7.04 *d* (128.23)	6.58 *d* (117.53)	3.59 *s* (35.20)	1.97 *s* (14.66)	4.07 *s*	----------
2Br–2MT	(142.86)	(122.57)	6.96 *d* (129.83)	6.57 *t* (118.51)	7.37 *d* (131.71)	-------- (110.93)	3.70 *s* (36.04)	1.98 *s* (14.54)	4.59 *s*	----------
4Br–2MT	(144.24)	(109.72)	7.13 *s* (132.83)	------ (123.47)	7.18 *d* (130.99)	6.60 *d* (117.82)	3.60 *s* (35.00)	1.98 *s* (14.57)	4.08 *s*	----------
$2NO_2$–2MT	(143.61)	(124.03)	7.25 *d* (136.55)	6.64 *t* (115.64)	8.07 *d* (125.67)	-------- (133.29)	3.73 *s* (35.20)	1.99 *s* (14.60)	6.62 *s*	----------
$4NO_2$–2MT	(151.60)	(119.95)	7.96 *s* (126.68)	------- (138.42)	8.02 *d* (125.08)	6.67 *d* (114.76)	3.70 *s* (34.94)	2.00 *s* (14.57)	4.76 *s*	----------

s singlet
d doublet
t triplet

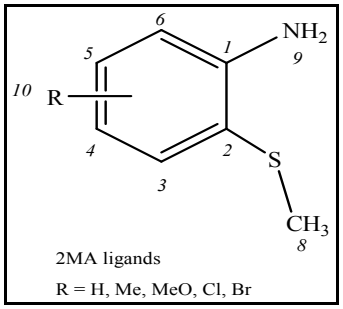

Table 2.12 ^{1}H and ^{13}C chemical shifts (δ) for 2MA ligands in ppm

Ligands	(C)*1*	(C)*2*	H (C)*3*	H (C)*4*	H (C)*5*	H (C)*6*	H (C)*8*	H *9*	H (C)*10*
2MA	(146.78)	(119.86)	7.43 *d* (132.97)	7.16 *t* (118.40)	6.79 t (128.55)	6.76 *d* (114.60)	2.40 *s* (17.35)	4.29 *s*	----------
2Me–2MA	(143.20)	(122.84)	7.11 *d* (128.33)	7.09 *t* (115.25)	6.61 *d* (131.77)	------- (125.12)	2.42 *s* (18.55)	3.57 *s*	2.15 *s* (17.04)
4Me–2MA	(144.39)	(119.97)	7.22 *s* (129.33)	------- (127.78)	6.95 *d* (133.33)	6.67 *d* (114.84)	2.39 *s* (20.15)	4.14 *s*	2.28 *s* (17.51)
2MeO–2MA	(134.90)	(125.46)	6.84 *d* (115.04)	6.83 *t* (122.45)	6.64 *d* (112.29)	------- (147.17)	2.43 *s* (18.80)	3.81 *s*	3.83 *s* (55.36)
4MeO–2MA	(140.32)	(121.49)	6.92 *s* (114.39)	------- (152.29)	6.69 *d* (115.83)	6.66 *d* (117.18)	2.36 *s* (17.15)	3.82 *s*	3.73 *s* (55.59)
2Cl–2MA	(141.32)	(119.41)	7.26 *d* (129.06)	6.68 *t* (116.16)	7.07 *d* (130.05)	------- (126.58)	2.41 *s* (18.42)	3.97 *s*	----------
4Cl–2MA	(145.15)	(115.67)	7.29 *s* (131.64)	------- (122.66)	7.02 *d* (128.26)	6.62 *d* (121.87)	2.36 *s* (17.88)	4.05 *s*	----------
2Br–2MA	(142.55)	(126.91)	7.42 *d* (129.89)	6.66 *t* (115.97)	7.11 *d* (133.18)	------- (109.31)	2.40 *s* (18.57)	4.02 *s*	----------
4Br–2MA	(145.72)	(122.32)	7.41 *s* (131.19)	------- (109.53)	7.14 *d* (134.62)	6.56 *d* (116.09)	2.34 *s* (17.43)	4.16 *s*	----------

s singlet
d doublet
t triplet

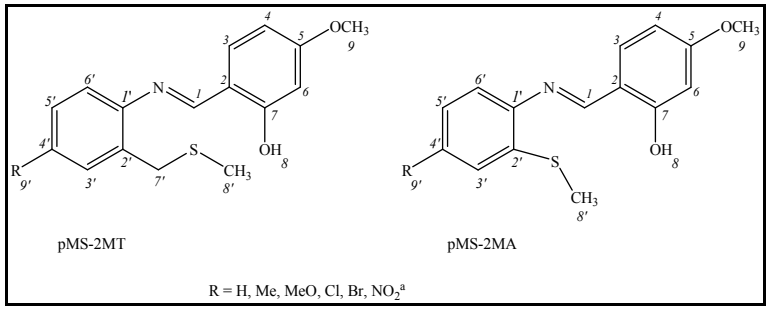

Table 2.13 ^{1}H Chemical shifts (δ) for pMS–2MT and pMS–2MA Schiff base ligands in ppm

Ligands	H*1*	H*3*	H*4*	H*6*	H*8*	H*9*	H3'	H5'	H*6'*	H7'	H*8'*	H *9'*
pMS–2MT	8.50 *s*	7.33 *d*	6.51 *d*	6.54 *s*	13.64 *s*	3.85 *s*	7.30 *s*	7.32 *t*	7.11 *d*	3.81 s	2.06 *s*	7.22 *t*
pMS–4Me2MT	8.48 *s*	7.27 *d*	6.49 *d*	6.53 *s*	13.69 *s*	3.84 *s*	7.15 *s*	7.11 *d*	7.02 *d*	3.78	2.07 *s*	2.35 *s*
pMS–4MeO2MT	8.47 *s*	7.27 *d*	6.49 *d*	6.53 *s*	13.71 *s*	3.84 *s*	6.91 *s*	6.85 *s*	7.10 *d*	3.80 *s*	2.08 *s*	3.83 *s*
pMS–4Cl2MT	8.46 *s*	7.29 *d*	6.51 *d*	6.53 *s*	13.33 *s*	3.85 *s*	7.33 *s*	7.27 *d*	7.04 *d*	3.75 *s*	2.07 *s*	----
pMS–4Br2MT	8.44 *s*	7.41 *d*	6.49 *d*	6.51 *s*	13.35 *s*	3.83 *s*	7.46 *s*	7.27 *d*	6.96 *d*	3.73 *s*	2.05 *s*	----
pMS–4$NO_2$2MT	8.22 *s*	7.34 *d*	6.55 *d*	6.54 *s*	12.94 *s*	3.87 *s*	8.22 *s*	8.20 *d*	7.19 *d*	3.82 *s*	2.08 *s*	----
pMS–2MA	8.54 *s*	7.30 *d*	6.50 *d*	6.54 *s*	13.65 *s*	3.85 *s*	7.24 *s*	7.25 *d*	7.17 *d*	----	2.47 *s*	----
pMS–4Me2MA	8.53 *s*	7.27 *d*	6.49 *d*	6.54 *s*	13.70 *s*	3.84 *s*	7.04 *s*	6.98 *d*	7.07 *d*	----	2.46 *s*	2.38 *s*
pMS–4MeO2MA	8.50 *s*	7.25 *d*	6.48 *d*	6.52 *s*	13.66 *s*	3.85 *s*	6.77 *s*	6.69*d*	7.13 *d*	----	2.45 *s*	3.83 *s*
pMS–4Cl2MA	8.48 *s*	7.25 *d*	6.48 *d*	6.51 *s*	13.34 *s*	3.84 *s*	7.12 *s*	7.04 *d*	7.10 *d*	----	2.45 *s*	----
pMS–4Br2MA	8.48 *s*	7.25 *d*	6.48 *d*	6.51 *s*	13.34 *s*	3.83 *s*	7.26 *s*	7.25 *d*	6.98 *d*	----	2.45 *s*	----

a only substituted in pMS–2MT Schiff-bases
s singlet
d doublet
t triplet

Table 2.14 ^{13}C Chemical shifts (δ) for pMS–2MT and pMS–2MA Schiff-base ligands in ppm

Ligands	C1	C2	C3	C4	C5	C6	C7	C9	C1'	C2'	C3'	C4'	C5'	C6'	C7'	C8'	C9'
pMS–2MT	161.97	113.23	133.6	107.13	164.02	101.02	163.63	55.44	147.42	131.80	130.27	126.91	128.38	118.44	34.59	15.35	----
pMS–4Me2MT	161.17	113.28	133.44	107.03	163.85	101.01	163.63	55.42	144.75	131.70	130.94	136.13	128.96	118.02	34.54	15.43	20.97
pMS–4MeO2MT	160.30	113.38	133.33	107.00	163.79	101.07	163.48	55.89	140.48	133.49	115.53	158.14	113.58	118.92	35.23	15.91	55.96
pMS–4Cl2MT	162.30	113.10	133.79	107.38	164.57	101.08	163.57	55.49	146.08	131.57	130.02	133.71	128.32	119.63	34.34	15.45	----
pMS–4Br2MT	162.22	113.04	132.83	107.30	164.20	100.96	163.45	55.44	146.49	133.98	133.74	119.30	131.23	119.92	34.19	15.39	----
pMS–4$NO_2$2MT	163.83	112.88	133.26	107.98	165.11	101.07	164.08	55.61	153.39	134.39	125.32	145.35	124.04	119.44	34.19	15.39	----
pMS–2MA	160.73	113.19	133.55	107.13	164.03	101.11	163.66	55.54	145.39	134.49	126.92	125.26	124.91	117.03	----	14.78	----
pMS–4Me2MA	159.83	113.29	133.40	107.04	163.93	101.18	163.68	55.44	143.00	134.25	126.10	136.92	125.83	116.67	----	14.94	21.24
pMS–4MeO2MA	158.69	113.36	133.20	106.91	163.68	101.15	163.34	55.50	138.68	136.45	109.89	158.82	111.16	117.31	----	14.80	55.40
pMS–4Cl2MA	160.83	113.05	132.45	107.27	164.23	101.10	163.51	55.43	143.74	133.68	124.99	136.76	124.24	117.76	----	14.64	----
pMS–4Br2MA	160.79	113.01	127.9	107.23	164.21	101.06	163.48	55.40	144.12	137.03	133.68	120.25	126.98	118.06	----	14.63	----

2.4.3 Infrared frequencies and Raman shifts data

The tables below list the infrared frequencies of selected vibrational groups in the ligands and their complexes. The data for each ligand with its metal complexes are shown so that vibrational shifts for each ligand on chelation with metal ions can be easily seen. Separation of thiomethylated compounds into the *ortho* and *para* substituted types is done so as to facilitate the comparative studies of frequency shifts as a result of change in position of substituents on the aromatic ring.

The Raman experiments for the metal complexes of the thiomethylated ligands were unsuccessful as a result of fluorescence which obscured the whole spectra. Since shifts in frequencies on chelation of the ligands to metal ions are to be determined, Raman frequencies of the thiomethylated ligands were not obtained. However the Cu(II) complexes of the Schiff-bases did not undergo fluorescence, hence their Raman shifts and those of the parent ligands were obtained and the corresponding values are recorded in **Table3.19.**

Table 2.15 Selected IR frequencies of *para*–substituted 2–(methylthiomethyl)anilines and complexes (cm^{-1})

Compounds	$\nu_{a(N-H)}$	$\nu_{s(N-H)}$	δ_{NH2}	$\nu_{(C-N)}$	$\nu_{(M-N)}$	$\nu_{(M-Cl)}$	$\nu_{(M-S)}$	$\Delta\nu_{a(N-H)}$
2MT	3424	3352	1618	1272	----	---	----	----
$[Co(2MT)_2Cl_2]$	3281	3218	1610	1251	426	358, 321, 244, 221	284	143
$[Ni(2MT)_2Cl_2]$	3278	3221	1611	1253	428	364, 323, 253, 231	289	146
$[Cu(2MT)Cl_2]$	3294	3217	1609	1251	430	398, 363, 295, 274	327	130
4Me–2MT	3420	3346	1625	1275	----	----	----	----
$[Co(4Me–2MT)_2Cl_2]$	3273	3214	1600	1269	397	327, 248, 224	309	147
$[Ni(4Me–2MT)_2Cl_2]$	3268	3212	1600	1264	400	328, 257, 231	313	152
$[Cu(4Me–2MT)Cl_2]$	3276	3221	1599	1259	405	381, 294, 268	321	144
4MeO–2MT	3409	3341	1626	1293	----	----	----	----
$[Co(4MeO–2MT)_2Cl_2]$	3308	3229	1596	1273	425	335, 261, 231	309	101
$[Ni(4MeO–2MT)_2Cl_2]$	3290	3223	1606	1272	429	341, 261, 231	299	119
$[Cu(4MeO–2MT)Cl_2]$	3256	3202	1617	1272	430	364, 303, 271	338	153
4Cl–2MT	3399	3307	1625	1275	----	----	----	----
$[Co(4Cl–2MT)_2Cl_2]$	3268	3212	1615	1250	390	336, 251, 227	309	128
$[Ni(4Cl–2MT)_2Cl_2]$	3272	3218	1610	1252	394	328, 252, 231	309	127
$[Cu(4Cl–2MT)Cl_2]$	3261	3221	1609	1244	398	297, 272	322	138
4Br–2MT	3398	3317	1624	1275	----	----	----	----
$[Co(4Br–2MT)_2Cl_2]$	3269	3211	1606	1250	381	332, 317, 250, 222	290	129
$[Ni(4Br–2MT)_2Cl_2]$	3269	3215	1607	1251	389	317, 253, 230	293	129
$[Cu(4Br–2MT)Cl_2]$	3259	3219	1607	1244	393	293, 281	322	139
$4NO_2$–2MT	3450	3347	1639	1278	----	----	----	----
$[Co(4NO_2–2MT)_2Cl_2]$	3271	3227	1624	1255	423	356, 337, 251, 231	300	179
$[Ni(4NO_2–2MT)_2Cl_2]$	3256	3198	1624	1255	439	322, 281, 271	296	194
$[Cu(4NO_2–2MT)Cl_2]$	3267	3222	1620	1250	425	380, 365, 294	324	183

Table 2.16 Selected IR frequencies of *ortho*–substituted 2–(methylthiomethyl)anilines and complexes (cm^{-1})

Compounds	$\nu_{a(N-H)}$	$\nu_{s(N-H)}$	δ_{NH2}	$\nu_{(C-N)}$	$\nu_{(M-N)}$	$\nu_{(M-Cl)}$	$\nu_{(M-S)}$	$\Delta\nu_{a(N-H)}$
2MT	3424	3352	1618	1272	----	----	----	----
$[Co(2MT)_2Cl_2]$	3281	3218	1610	1251	426	358, 321, 244, 221	284	143
$[Ni(2MT)_2Cl_2]$	3278	3221	1611	1253	428	364, 323, 253, 231	289	146
$[Cu(2MT)Cl_2]$	3294	3217	1609	1251	430	398, 363, 295, 274	327	130
2Me–2MT	3441	3360	1621	1277	----	----	----	----
$[Co(2Me–2MT)_2Cl_2]$	3286	3252	1603	1267	400	352, 266	327	155
$[Ni(2Me–2MT)_2Cl_2]$	3254	3218	1611	1264	403	347, 244, 228	303	187
$[Cu(2Me–2MT)Cl_2]$	3260	3185	1608	1265	418	351, 284, 274	320	181
2MeO–2MT	3437	3349	1615	1323	----	----	----	----
$[Co(2MeO–2MT)_2Cl_2]$	3340	3250	1589	1270	427	327, 259, 229	303	197
$[Ni(2MeO–2MT)_2Cl_2]$	3337	3246	1589	1271	404, 369	327, 266, 234	308	100
$[Cu(2MeO–2MT)_2Cl_2]$	3329	3201	1592	1273	424	368, 294, 275	334	108
2Cl–2MT	3436	3351	1617	1291	----	----	----	----
$[Co(2Cl–2MT)_2Cl_2]$	3329	3198	1608	1274	399, 381	341, 317, 250, 232	284	107
$[Ni(2Cl–2MT)_2Cl_2]$	3327	3200	1609	1275	428	343, 325, 251, 232	285	109
$[Cu(2Cl–2MT)Cl_2]$	3322	3187	1609	1280	399	334, 286	317	114
2Br–2MT	3428	3345	1614	1288	----	----	----	----
$[Co(2Br–2MT)_2Cl_2]$	3315	3201	1608	1273	425, 381	343, 317, 273, 250	298	113
$[Ni(2Br–2MT)_2Cl_2]$	3313	3201	1607	1274	430, 386	345, 324, 251, 235	302	115
$[Cu(2Br–2MT)Cl_2]$	3303	3189	1602	1274	400	352, 266	327	125
$2NO_2$–2MT	3465	3359	1623	1330	----	----	----	----
$[Cu(2NO_2–2MT)Cl_2]$	3300	3186	1609	1279	426, 394	294, 282	347	165

Table 2.17 Selected IR frequencies of *para*–substituted 2–(methylthio)anilines and complexes (cm^{-1})

Compounds	$\nu_{a(N-H)}$	$\nu_{s(N-H)}$	δ_{NH2}	$\nu_{(C-N)}$	$\nu_{(M-N)}$	$\nu_{(M-Cl)}$	$\nu_{(M-S)}$	$\Delta\nu_{a(N-H)}$
2MA	3446	3345	1603	1298	----	----	----	----
$[Co(2MA)_2Cl_2]$	3219	3173	1597	1282	410	342, 245, 229	306	227
$[Ni(2MA)_2Cl_2]$	3213	3174	1590	1283	413	346, 254, 234	307	233
$[Cu(2MA)Cl_2]$	3242	3193	1586	1282	419, 384	296, 269	350	204
4Me–2MA	3435	3344	1614	1291	----	----	----	----
$[Co(4Me–2MA)_2Cl_2]$	3250	3218	1593	1278	412, 391	337, 227	273	185
$[Ni(4Me–2MA)_2Cl_2]$	3282	3209	1585	1272	416, 387	328, 228	285, 262	153
$[Cu(4Me–2MA)Cl_2]$	----[a]	3175	1596	1274	423, 396	305, 258	324	----
4MeO–2MA	3420	3339	1615	1279	----	----	----	----
$[Co(4MeO–2MA)_2Cl_2]$	3220	3159	1595	1256	432, 402	363, 334, 237, 225	285	200
$[Ni(4MeO–2MA)_2Cl_2]$	3214	3156	1597	1258	435, 408	367, 336, 242, 223	286, 269	206
$[Cu(4MeO–2MA)Cl_2]$	3208	3161	1609	1257	416	302, 275	340	212
4Cl–2MA	3445	3349	1606	1282	----	----	----	----
$[Co(4Cl–2MA)_2Cl_2]$	3208	3163	1599	1264	413, 381	331, 240, 225	273	237
$[Ni(4Cl–2MA)_2Cl_2]$	3203	3165	1601	1267	416, 386	332, 246, 222	274	242
$[Cu(4Cl–2MA)Cl_2]$	3231	3180	1594	1263	422, 391	311, 282	329	214
4Br–2MA	3445	3345	1603	1282	----	----	----	----
$[Co(4Br–2MA)_2Cl_2]$	3204	3161	1598	1267	408, 372	330, 256, 236	304	241
$[Ni(4Br–2MA)_2Cl_2]$	3203	3164	1601	1268	412, 376	331, 257, 228	305	242
$[Cu(4Br–2MA)Cl_2]$	3233	3194	1592	1264	419, 376	298, 274	323	212

a, not observed

Table 2.18 Selected IR frequencies of *ortho*–substituted 2–(methylthio)anilines and complexes (cm^{-1})

Compounds	$\nu_{a(N-H)}$	$\nu_{s(N-H)}$	δ_{NH2}	$\nu_{(C-N)}$	$\nu_{(M-N)}$	$\nu_{(M-Cl)}$	$\nu_{(M-S)}$	$\Delta\nu_{a(N-H)}$
2Me–2MA	3452	3355	1619	1279	----	----	----	----
$[Co(2Me–2MA)_2Cl_2]$	3298	3250	1607	1241	427, 387	325	304	154
$[Ni(2Me–2MA)_2Cl_2]$	3342	3280	1615	1249	401, 392	348, 247	304, 277	110
$[Cu(2Me–2MA)Cl_2]$	3313	3199	1621	1250	406	290, 278	362	139
2MeO–2MA	3383	3293	1620	1269	----	----	----	----
$[Co(2MeO–2MA)_2Cl_2]$	3251	3172	1583	1241	*NA*	*NA*	*NA*	132
$[Ni(2MeO–2MA)_2Cl_2]$	3235	3198	1594	1256	416, 391	360, 250	304	160
$[Cu(2MeO–2MA)Cl_2]$	3251	3171	1585	1245	414	280, 262	314	132
2Cl–2MA	3459	3358	1615	1292	----	----	----	----
$[Cu(2Cl–2MA)Cl_2]$	3340	3199	1581	1271	406	301, 278	----	119
2Br–2MA	3455	3354	1611	1290	----	----	----	----
$[Cu(2Br–2MA)_2Cl_2]$	3276	3183	1583	1273	409	333, 303, 275	----	179

NA not available for far infrared analysis as the yield was too small

Table 2.19 IR frequencies and Raman[a] shifts of Schiff–base ligands and complexes (cm^{-1})

Compound	$\nu_{(C=N)}$	$\nu_{(C-O)}$	$\nu_{(Cu-O)}$	$\nu_{(Cu-N)}$
pMS–2MT	1609 s *(1612 s)*	1291 m *(vw)*		
[Cu(pMS–2MT)$_2$]	1605 s *(1613 s)*	1313 m *(1317 m)*	464 m (*vw*), 449 m *(448 vw)*	405 s *(398 w)*, -------
pMS–4Me2MT	1616 s *(1614 s)*	1280 m *(vw)*		
[Cu(pMS–4Me2MT)$_2$]	1613 s *(1617 s)*	1317 m *(1316 m)*	464 m (*vw*), 449 *(vw)*	425 w (*vw*) , 406 m *(400 w)*
pMS–4MeO2MT	1597s *(1598 s)*	1282 m *(vw)*		
[Cu(pMS–4MeO2MT)$_2$]	1596 s *(1603 s)*	1311 m *(1303 m)*	466 m (*vw*), 444 m *(446 vw)*	421 w (*vw*), 398 s *(391 w)*
pMS–4Cl2MT	1607 s *(1609 s)*	1287 m *(vw)*		
[Cu(pMS–4Cl2MT)$_2$]	1605 s *(1608 s)*	1316 m *(1317 m)*	456 m (*vw*), 437 m *(438 vw)*	406 s*(402 w)*, --------
pMS–4Br2MT	1605 s *(1609 s)*	1286 m *(1287 m)*		
[Cu(pMS–4Br2MT)$_2$]	1603 s *(1611 s)*	1314 m *(1315 m)*	464 m (*463*), 453 m (*vw*)	429 m *(438 vw)*, 402 m *(396 vw)*
pMS–4NO$_2$2MT	1603 s *(1605 s)*	1273 s *(1276 m)*		
[Cu(pMS–4NO$_2$2MT)$_2$]	1599 s *(1604 s)*	1313 s *(1316 w)*	467 m (*vw*), 442 w *(441 vw)*	423 w (*vw*), 399 s *(394 w)*
pMS–2MA	1600 s *(1604 s)*	1289 m *(1273 m)*		
[Cu(pMS–2MA)$_2$]	1607 s *(1615 s)*	1339 m *(1342 s)*	458 m (*vw*), --------	421 m *(425 s)*, 381 m *(394 w)*
pMS–4Me2MA	1600 s *(1606 s)*	1289 m *(1276 m)*		
[Cu(pMS–4Me2MA)$_2$]	1604 s *(1588 s)*	1312 m *(1313 m)*	454 s (*vw*), -------	415 m *(vw)*, 395 m *(403 vw)*
pMS–4MeO2MA	1603 s *(1607 s)*	1285m *(1273 m)*		
[Cu(pMS–4MeO2MA)$_2$]	1582 s *(1596 s)*	1310 m *(1298 w)*	461 m (*462 w*), 431 m (*436 w*)	401 m *(397 w)*, --------
pMS–4Cl2MA	1605 s *(1607 s)*	1291 m *(1286 m)*		
[Cu(pMS–4Cl2MA)$_2$]	1593 s *(1601 s)*	1311 m *(1313 w)*	463 m (*463 w*), 432 m (*vw*)	417 m *(421 w)*, 399 s *(394 w)*
pMS–4Br2MA	1602 s (1604 s)	1291 m (*vw*)		
[Cu(pMS–4Br2MA)$_2$]	1592 s (1600 s)	1311 m (*1314 w*)	465 m *(465 w)*, 452 m (*vw*)	429 m *(430 w)*, 401m *(397 w)*

a values enclosed in brackets are Raman shifts *s*, strong m, medium; *w*, weak vw, very weak

2.4.4 X–ray crystallographic data

Table 2.20 Summary of crystallographic data for $[Cu(4NO_2\text{-}2MT)_2Cl_2]_2$

Compound	$[Cu(4NO_2\text{-}2MT)_2Cl_2]_2$
Empirical formula	$C_{16}H_{20}Cl_4Cu_2N_4O_4S_2$
Formula weight	665.38
Crystal system	Monoclinic
Space group	$P2_1/c$
a (Å)	5.5999(2)
b (Å)	27.2688(9)
c (Ås)	7.6550(2)
α (°)	90.00
β (°)	97.8850(10)
γ (°)	90.00
V (Å^3)	1157.89(6)
Z	4
T (K)	200(2)
D_{calc} (Mg/m^3)	1.908
Crystal size (mm)	0.06 X 0.06 X 0.17
Absorption coefficient (mm^{-1})	2.512
Absorption correction (min., max.)	0.6705, 0.8721
F (000)	668
θ Range for data collection (°)	2.79 – 27.99
Limiting indices	$-4 \le h \le 7$, $-36 \le k \le 35$, $-10 \le l \le 10$
Reflections collected	11213
Unique reflections (R_{int})	3530 (0.0232)
Completeness to θ	27.99 (99.9%)
Refinement method	full-matrix least-squares on F^2
Data/restraints/parameters	2798/0/162
Goodness-of-fit on F^2	1.080
Final R indices [$I > 2\sigma(I)$]	R_1=0.0262, wR_2 = 0.0576
R indices (all data)	R_1=0.0354, wR_2 = 0.0601
Largest difference in peak and hole (e A^{-3})	0.383 and -0.337
CCDC	888074[13]

Table 2.21 Selected bond lengths [Å] and angles [°] for complex $[Cu(4NO_2\text{-}2MT)_2Cl_2]_2$

Cu–N1	2.0750(18)	Cu1–S1	2.3214(6)	
Cu1–Cl1	2.2554(6)	Cu1–Cl2	2.6902(5)	
Cu1–Cl2	2.3184(5)	Cl2–Cu1	2.6902(5)	
S1–C8	1.798(2)	S1–C7	1.817(2)	
N1–C1	1.434(3)	C4–N2	1.464	
N2–O2	1.203(3)	N2–O1	1.212(3)	
N1–Cu1–Cl1	176.82(5)	N1–Cu1–Cl2	85.39(6)	
N1–Cu1–Cl2	88.60(5)	Cl1–Cu1–Cl2	93.19(2)	
Cl1–Cu1–Cl2	94.27(2)	Cl2–Cu1–Cl2	90.625(17)	
N1–Cu1–S1	91.93(5)	S1–Cu1–Cl2	105.455(19)	
Cl1–Cu1–S1	85.69(2)	Cu1–Cl2–Cu1	89.376(17)	
Cl2–Cu1–S1	163.90(2)	C8–S1–C7	102.40(11)	
C8–S1–Cu1	105.25(9)	C7–S1–Cu1	104.90(7)	
C1–N1–Cu1	118.59(13)	O2–N2–O1	122.3(2)	
O2–N2–C4	118.5(2)	O1–N2–C4	119.2(2)	
D–H···A interactions	D–H	H···A	D···A	D–H···A
N1–H11···Cl1	0.826	2.816	3.584	155.32
N1–H12···Cl2	0.878	2.867	3.425	122.97
N1–H12···Cl1	0.878	3.279	3.941	134.09
C2–H2···Cl1	0.949	2.709	3.538	146.28
C3–H3···S1	0.950	2.852	3.651	142.30
C7–H7A···O2	0.990	2.619	3.436	140.00
C7–H7B···C3	0.991	2.699	3.501	138.21
C8– H8A···O2	0.980	2.538	3.079	114.66

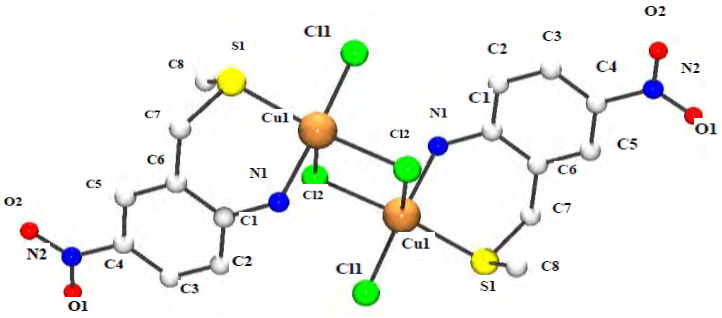

Fig. 2.1 Crystal structure of $[Cu(4NO_2\text{-}2MT)_2Cl_2]_2$

Table 2.22 Summary of crystallographic data for pMS–2MT, pMS–pMe2MT and pMS–2MA

Compound	pMS-2MT	pMS-4Me2MT	pMS-2MA
Chemical formula	$C_{16}H_{17}NO_2S$	$C_{17}H_{19}NO_2S$	$C_{15}H_{15}NO_2S$
Formula weight	287.37	301.39	273.34
Crystal system	Monoclinic	Monoclinic	Orthorhombic
Space group	$P2_1/c$	$P2_1/c$	$P2_12_12_1$
a (Å)	10.7495(3)	11.7158(5)	5.63650(10)
b (Å)	10.5921(2)	13.8428(5)	12.2831(3)
c (Ås)	13.4840(3)	9.5750(4)	19.3196(4)
α (°)	90.00	90.00	90.00
β (°)	105.6620(10)	96.015(2)	90.00
γ (°)	90.00	90.00	90.00
V (Å^3)	1478.28(6)	1544.32(11)	1337.57(5)
Z	4	2	4
T (K)	200(2)	200(2)	200 (2)
D_{calc} (Mg/m^3)	1.291	1.296	1.357
Absorption coefficient (mm^{-1})	0.220	0.213	0.239
F (000)	608	640	576
θ Range for data collection (°)	2.16–28.00	2.60–28.00	1.96–28.00
Limiting indices	$-14 \le h \le 13$, $-13 \le k \le 12$, $-17 \le l \le 17$	$-15 \le h \le 15$, $-18 \le k \le 11$, $-12 \le l \le 12$	$-7 \le h \le 5$, $-16 \le k \le 16$ $-25 \le l \le 25$
Reflections collected	13042	14683	13256
Unique reflections (R_{int})	3530 (0.0139)	3725 (0.0192)	3231(0.0154)
Completeness to θ	28.00 (99.1%)	28.00 (99.9%)	28.00 (99.9%)
Absorption correction	Numerical	Numerical	(Min., max.) 0.8295, 0.9696
Refinement method	full-matrix least-squares on F^2	Full-matrix least-squares on F^2	Full-matrix least-squares on F^2
Data/restraints/parameters	3531/0/249	3725/0/219	3231/0/192
Goodness-of-fit on F^2	1.040	0.976	1.050
Final R indices [$I > 4\sigma(I)$]	R_1= 0.0344, wR_2 = 0.0925	R_1 = 0.0336, wR_2 = 0.0871	R_1 = 0.0268, wR_2 = 0.0718
R indices (all data)	R_1=0.0393, wR_2 = 0.0995	R_1=0.0479, wR_2 = 0.0955	R_1 = 0.0289, wR_2 = 0.0742
Largest difference in peak and hole (e A^{-3})	0.278 and -0.176	0.220 and -0.298	0.201 and -0.204
CCDC	872915[14]	872916[15]	890400[16]

Table 2.23 Selected bond lengths [Å] and angles [°] for Schiff-base ligands

Bonds	pMS–2MT	pMS–4Me2MT	Bonds	pMS–2MA
S1–C16	1.7965(16)	1.7919(17)	S1–C8	1.7945(14)
S1–C15	1.8153(12)	1.8143(14)	S1–C2	1.7617(13)
N1–C8	1.2894(15)	1.2845(17)	N1–C7	1.2801(17)
N1–C9	1.4147(14)	1.4150(17)	N1–C1	1.4146(15)
O1–C2	1.3531(13)	1.3483(16)	C12–O1	1.3438(15)
O1–H1	0.86(2)	0.8400	O1–H1	0.88(2)
C1–C8	1.4433(16)	1.4428(19)	C7–C11	1.4495(16)
C4–07	1.3575(14)	1.3603(16)	O2 –C9	1.4209(18)
O1–C2	1.3531(13)	1.3483(16)	C12–O1	1.3438(15)
C16–S1–C15	100.25(7)	101.00 (8)	C2–S1–C8	103.77(7)
C8–N1–C9	119.67(10)	120.52 (12)	C7–N1–C1	123.50(11)
C2–O1–H1	107.3(14)	109.5	C12–O1–H1	103.2(15)
N1–C8–C1	121.91(10)	122.41 (12)	N1–C7–C11	121.54(12)
N1–C8–H8	121.5(9)	118.8	N1–C7–H7	119.2
C1–C8–H8	116.5(9)	118.8	C11–C7–H7	119.2

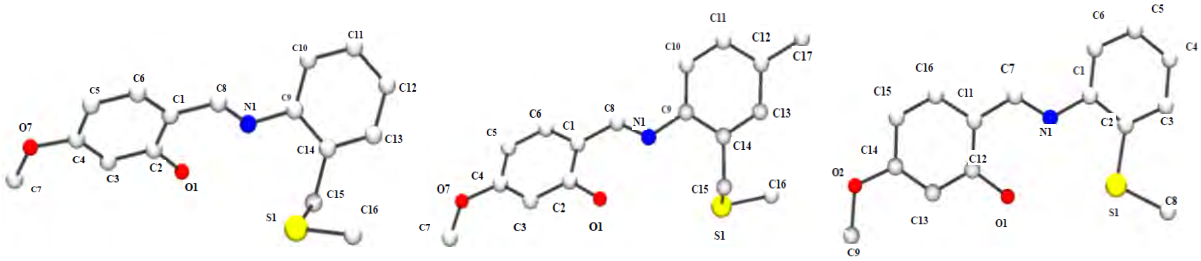

Fig. 2.2 Crystal structures of pMS–2MT, pMS–4Me2MT and pMS–2MA

Table 2.24 Summary of crystallographic data for [Cu(pMS-2MT)$_2$] and [Cu(pMS-4Me2MT)$_2$]

Compound	[Cu(pMS-2MT)$_2$]	[Cu(pMS-4Me2MT)$_2$]
Chemical formula	$C_{32}H_{32}CuN_{24}O_4S_2$	$C_{34}H_{36}N_{24}O_4S_2$
Formula weight	636.26	664.31
Crystal system	Triclinic	Triclinic
Space group	P_1	P_1
Temperature (K)	200(2)	200(2)
a (Å)	7.1941(2)	7.2958(4)
b (Å)	8.4666(3)	8.6889(5)
c (Ås)	12.8106(4)	13.1418(8)
α (^{o})	75.4490(10)	76.031(2)
β (^{o})	82.7680(10)	76.268(2)
γ (^{o})	77.5270(10)	76.380(2)
V (Å^3)	735.31(4)	771.19(8)
Z	1	1
D_{calc} (Mg/m^3)	1.437	1.430
Absorption coefficient (mm $^{-1}$)	0.925	0.885
F (000)	331	347
θ Range for data collection (^{o})	2.53–28.00	2.67–28.00
Limiting indices	$-9 \le h \le 8$, $-11 \le k \le 11$,	$-9 \le h \le 9$, $-11 \le k \le 11$,
	$-16 \le l \le 16$	$-17 \le l \le 16$
Reflections collected	12739	12274
Unique reflections (R_{int})	6517 ()	5938
Completeness to θ	28.00 (99.6%)	28.00(98.3%)
Absorption correction	Numerical	Numerical
Refinement method	full-matrix least-squares on F^2	full-matrix least-squares on F^2
Data/restraints/parameters	6517/3/375	5983/3/395
Goodness-of-fit on F^2	1.077	1.147
Final R indices [$I > 2\sigma(I)$]	R_1=0.0309, wR_2 = 0.0777	R_1=0.0524, wR_2 = 0.1483
R indices (all data)	R_1=0.0343, wR_2 = 0.0802	R_1=0.0533, wR_2 = 0.1488
Largest difference in peak and hole (e A $^{-3}$)	0.368 and -0.296	1.743 and -0.469
CCDC	872913[17]	872914[18]

Table 2.25 Selected bond lengths [Å] and angles [°] for [Cu(pMS-2MT)$_2$] **21C** and [Cu(pMS-4Me2MT)$_2$] **22C**

Compound	**21C**	**22C**	Compound	**21C**	**22C**
Cu1–O101	1.898(5)	1.892(6)	Cu1–N101	1.985(6)	2.002(7)
Cu1–O201	1.930(4)	1.941(6)	Cu1–N201	1.994(5)	1.975(8)
O101–C102	1.310(7)	1.288(10)	N101–C108	1.316(7)	1.275(12)
N101–C109	1.362(8)	1.450(11)	O201–C202	1.289(7)	1.302(10)
N201–C208	1.276(7)	1.322(12)	N201–C209	1.475(6)	1.396(12)
S101–C116	1.808(6)	1.810(9)	S101–C115	1.806(7)	1.784(11)
S201–C216	1.781(7)	1.774(11)	S201–C215	1.842(7)	1.859(11)
O101–Cu1–O201	176.9(3)	177.5(4)	C115–S101–C116	100.4(3)	101.0(5)
O101–Cu1–N201	89.9(2)	91.2(3)	C216–S201–C215	100.1(3)	99.6(5)
O201–Cu1–N201	89.50(18)	89.4(3)	C102–O101–Cu1	121.9(4)	123.6(6)
O101–Cu1–N101	90.3(2)	89.7(3)	C202–O201–Cu1	125.9(4)	122.7(5)
O201–Cu1–N101	90.3(2)	89.6(3)	N101–C108–C101	126.9(5)	123.9(8)
N201–Cu1–N101	179.1(3)	179.1(4)	N101–C108–H108	116.6	118.1
C108–N101–C109	120.8(5)	120.6(8)	N201–C208–C201	124.9(5)	125.7(8)
C108–N101–Cu1	120.8(4)	123.3(6)	N201–C208–H208	117.5	117.2
C109–N101–Cu1	118.2(4)	115.7(6)	C208–N201–Cu1	123.6(4)	121.8(6)
C208–N201–C209	119.0(5)	118.7(8)	C209–N201–Cu1	117.4(4)	119.5(6)

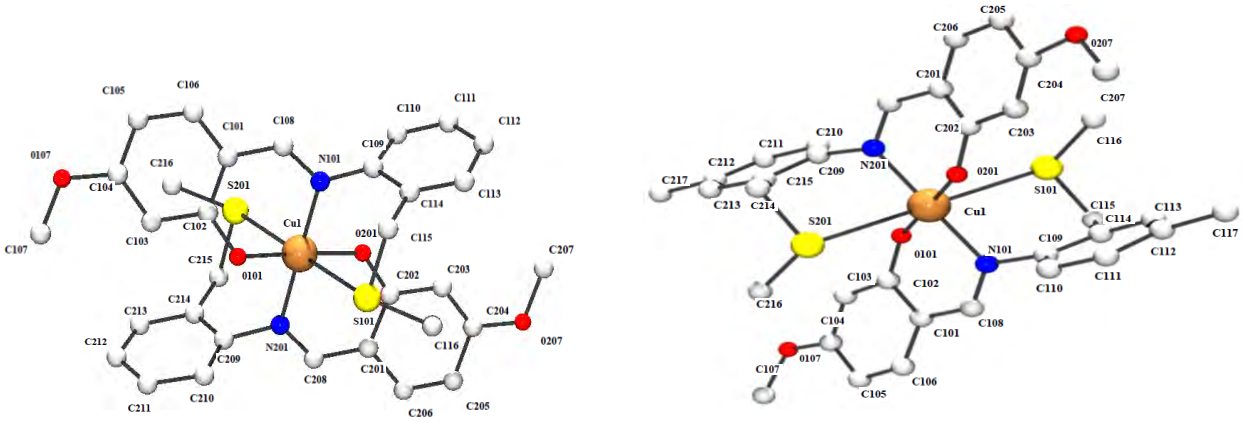

Fig. 2.3 Crystal structures of Cu(pMS–2MT) and Cu(pMS–4Me2MT)

2.4.5 Molar conductivity in DMF

The conductivity of each metal complex was determined in DMF at 10^{-3} M solution at room temperature.

Table 2.26 Molar conductivity of 2MT and 2MA complexes in DMF[19]

Compounds	Λ_m Ω^{-1} cm^2 mol^{-1}	Compounds	Λ_m Ω^{-1} cm^2 mol^{-1}	Compounds	Λ_m Ω^{-1} cm^2 mol^{-1}
$[Co(2MT)_2Cl_2]$	29.9	$[Ni(2MT)_2Cl_2]$	69.2	$[Cu(2MT)Cl_2]$	27.9
$[Co(2Me\text{-}2MT)_2Cl_2]$	36.2	$[Ni(2Me\text{-}2MT)_2Cl_2]$	73.1	$[Cu(2Me\text{-}2MT)Cl_2]$	27.7
$[Co(4Me\text{-}2MT)_2Cl_2]$	35.8	$[Ni(4Me\text{-}2MT)_2Cl_2]$	69.5	$[Cu(4Me\text{-}2MT)Cl_2]$	32.2
$[Co(2MeO\text{-}2MT)_2Cl_2]$	32.4	$[Ni(2MeO\text{-}2MT)_2Cl_2]$	72.1	$[Cu(2MeO\text{-}2MT)Cl_2]$	33.2
$[Co(4MeO\text{-}2MT)_2Cl_2]$	33.2	$[Ni(4MeO\text{-}2MT)_2Cl_2]$	69.4	$[Cu(4MeO\text{-}2MT)Cl_2]$	38.3
$[Co(2Cl–2MT)_2Cl_2]$	32.4	$[Ni(2Cl–2MT)_2Cl_2]$	71.3	$[Cu(2Cl–2MT)Cl_2]$	27.8
$[Co(4Cl–2MT)_2Cl_2]$	28.6	$[Ni(4Cl–2MT)_2Cl_2]$	69.5	$[Cu(4Cl–2MT)Cl_2]$	26.5
$[Co(2Br–2MT)_2Cl_2]$	30.5	$[Ni(2Br–2MT)_2Cl_2]$	71.5	$[Cu(2Br–2MT)Cl_2]$	29.2
$[Co(4Br–2MT)_2Cl_2]$	30.8	$[Ni(4Br–2MT)_2Cl_2]$	74.3	$[Cu(4Br–2MT)Cl_2]$	28.7
$[Co(4NO_2–2MT)_2Cl_2]$	28.8	$[Ni(4NO_2–2MT)_2Cl_2]$	68.1	$[Cu(4NO_2–2MT)Cl_2]$	27.2
$[Co(2MA)_2Cl_2]$	31.7	$[Ni(2MA)_2Cl_2]$	80.7	$[Cu(2MA)Cl_2]$	37.3
$[Co(2Me\text{-}2MA)_2Cl_2]$	32.5	$[Ni(2Me\text{-}2MA)_2Cl_2]$	83.5	$[Cu(2Me\text{-}2MA)Cl_2]$	32.4
$[Co(4Me\text{-}2MA)_2Cl_2]$	37.8	$[Ni(4Me\text{-}2MA)_2Cl_2]$	85.0	$[Cu(4Me\text{-}2MA)Cl_2]$	31.5
$[Co(2MeO\text{-}2MA)_2Cl_2]$	31.5	$[Ni(2MeO\text{-}2MA)_2Cl_2]$	81.4	$[Cu(2MeO\text{-}2MA)Cl_2]$	33.4
$[Co(4MeO\text{-}2MA)_2Cl_2]$	36.8	$[Ni(4MeO\text{-}2MA)_2Cl_2]$	87.4	$[Cu(4MeO\text{-}2MA)Cl_2]$	36.4
----	-----	----	-----	$[Cu(2Cl–2MA)Cl_2]$	29.2
$[Co(4Cl–2MA)_2Cl_2]$	35.2	$[Ni(4Cl–2MA)_2Cl_2]$	83.2	$[Cu(4Cl–2MA)Cl_2]$	28.9
----	-----	----	-----	$[Cu(2Br–2MA)_2Cl_2]$	28.3
$[Co(4Br–2MT)_2Cl_2]$	37.1	$[Ni(4Br–2MA)_2Cl_2]$	79.8	$[Cu(4Br–2MA)Cl_2]$	29.6
$CoCl_2.6H_2O$	38.6	$NiCl_2.6H_2O$	72.7	$CuCl_2.2H_2O$	27.7

2.4.6 Electronic spectra in solution and solid reflectance spectra

As the Cu(II) complexes of 2MT and 2MA ligands are only soluble in DMF and DMSO, both solvents were used as the media for the spectra study in solution. For comparative purposes, the solution spectra of the ligands and other Ni(II and Co(II) complexes were also obtained in same solvents. DMF and DMSO have high donor capacities towards metal ions[7] and their molecules may become coordinated to the metal ion (to form adducts) or could replace the ligand molecule(s) by solvolysis. The solid reflectance spectra of the complexes were therefore obtained in order to study the possible structural changes imposed on the complexes as a result of interaction with these solvents.

The Schiff-bases and their Cu(II) complexes are soluble in solvents such as DCM and $CHCl_3$ but not in polar solvents like EtOH, MeOH, DMSO or DMF, hence their solution spectra were obtained in DCM. It was found unnecessary to obtain their solid reflectance spectra as they retain the same colour when dissolved in DCM – which is a non-coordinating solvent.

2.4.6.1 Electronic spectra of 2MT and 2MA ligands in solution

Table 2.27 Electronic spectra data (nm) of 2MT and 2MA ligands in DMF and DMSO [a]

	π→ π*				ILCT[a]			π→ π*			
Ligand	DMF	DMSO	DMF	DMSO	DMF	DMSO	Ligand	DMF	DMSO	DMF	DMSO
2MT	265	259	297	300	----	----	2MA	273*sh*	261	317	309
2Me–2MT	264	258	298	295	----	----	2Me–2MA	286*sh*	270	309	308*sh*
4Me–2MT	264	259	305	306	----	----	4Me–2MA	272*sh*	262	318	315
2MeO–2MT	265	259	295	297	----	----	2MeO–2MA	284*sh*	270	308	309*sh*
4MeO–2MT	264	259	313	319	----	363	4MeO–2MA	273*sh*	260	324	324
2Cl–2MT	273*sh*	258	304	304	----	349*sh*	2Cl–2MA	285	271	317	317
4Cl–2MT	266	275	311	316	----	----	4Cl–2MA	274	262	322	321
2Br–2MT	274*sh*	258	305	303	----	----	2Br–2MA	285	278*sh*	317	321
4Br–2MT	266	272	313	312	----	----	4Br–2MA	284*sh*	267	325	322
$2NO_2$–2MT	275*sh*	258	295	285	416	412	----	----	----	----	----
$4NO_2$–2MT	273*sh*	258	301	295*sh*	389[b]	392	----	----	----	----	----

a Intraligand charge transfer
b additional ILCT is observed at 381 nm
sh shoulder

2.4.6.2 Electronic spectra of 2MT and 2MA metal(II) complexes in solution and in solid state

Table 2.28 Electronic spectra of Co(II) complexes of 2MT ligands in solution and in solid state

Complexes	Solvent	Wavelength [λ_{max}/(nm)](ε, mol^{-1} dm^3 cm^{-1})							
		$\pi \rightarrow \pi^*$	$\pi \rightarrow \pi^*$	CT	d → d transitions				
$[Co(2MT)_2Cl_2]$	DMF	273*sh*	305 (3250)	324 (498)	375*sh*	487*sh*	532*sh*	607*a* (190)	672*a* (300)
	DMSO	261 (7260)	300 (6850)	322 (1225)	370*sh*	498*sh*	530*sh*	613 (140)	684 (208)
	Solid	----	----	337	486	548	693*sh*	1289*br*	
$[Co(2Me–2MT)_2Cl_2]$	DMF	275*sh*	302 (2990)	325 (425)	370sh	480*sh*	529*sh*	607*a* (210)	672*a* (340)
	DMSO	288*sh*	311 (4529)	319 (458)	384*sh*	489*sh*	534*sh*	612 (96)	684 (132)
	Solid	----	----	341	478	558, 588	677*sh*	1289*br*	
$[Co(4Me–2MT)_2Cl_2]$	DMF	272*sh*	309 (3235)	344 (415)	368*sh*	485*sh*	526*sh*	608 (370)	674*a* (590)
	DMSO	272 (998)	319 (5310)	328 (1080)	370 (40)	482*sh*	533*sh*	623 (76)	677(124)
	Solid	----	----	342	481	547	662*sh*	1292*br*	
$[Co(2MeO–2MT)_2Cl_2]$	DMF	272*sh*	304 (3350)	324 (478)	360*sh*	486*sh*	529*sh*	608 (180)	673 (280)
	DMSO	266*sh*	306 (4270)	319 (473)	354*sh*	479sh	533*sh*	613 (90)	679 (145)
	Solid	----	----	342	481	541	677*sh*	1281*br*	
$[Co(4MeO–2MT)_2Cl_2]$	DMF	264 (8655)	313 (15055)	*m*	*m*	*m*	515 (1165)	594*br*	672*br*
	DMSO	260 (9040)	315 (8420)	353 (1655)	393 (1655)	*m*	525 (965)	597*br*	676 (530)
	Solid	----	----	355	----	531	695*sh*	1317*sh*	
$[Co(2Cl–2MT)_2Cl_2]$	DMF	270*sh*	310 (3840)	323 (464)	350*sh*	479*sh*	522 (16)	608*a* (75)	671*a* (116)
	DMSO	265*sh*	312 (3740)	324 (503)	353*sh*	494sh	530*sh*	612 (124)	678 (207)
	Solid	----	----	344	491	558	678*sh*	1293*br*	
$[Co(4Cl–2MT)_2Cl_2]$	DMF	271 (695)	313 (3075)	322 (420)	385*sh*	480*sh*	527*sh*	607*a* (222)	674*a* (355)
	DMSO	266 (10970)	311 (7310)	332 (1120)	395*sh*	487*sh*	532*sh*	613 (115)	680 (195)
	Solid	----	----	335	495	568	644*sh*	1289*br*	

sh, shoulder *br*, broad *m*, masked

Table 2.28 Electronic spectra of Co(II) complexes of 2MT ligands in solution and in solid state (continued)

Complexes	Solvent	Wavelength [λ_{max}/(nm)](ε, mol^{-1} dm^3 cm^{-1})							
		$\pi \rightarrow \pi^*$	$\pi \rightarrow \pi^*$	CT	d → d transitions				
$[Co(2Br–2MT)_2Cl_2]$	DMF	274^{sh}	311 (3785)	324 (520)	374^{sh}	487^{sh}	533^{sh}	608 (200)	673 (315)
	DMSO	266^{sh}	314 (4320)	325 (530)	368^{sh}	487^{sh}	534^{sh}	613 (113)	683 (170)
	Solid	----	----	344	485	566	661^{sh}	1292^{br}	
$[Co(4Br–2MT)_2Cl_2]$	DMF	275 (980)	314 (3255)	326 (428)	390^{sh}	485^{sh}	526^{sh}	607 (303)	674 (490)
	DMSO	267 (11195)	311 (6180)	333 (1125)	387^{sh}	492sh	537^{sh}	620 (105)	678 (178)
	Solid	----	----	341	493	551	660^{sh}	1280^{br}	
$[Co(4NO_2–2MT)_2Cl_2]$	DMF	272 (2450)	312 (4070)	380 (30800)	433 (1925)	530^{sh}	608 (380)	675 (609)	
	DMSO	274 (2010)	316 (3950)	380 (33405)	430 (1080)	533^{sh}	620 (102)	677 (170)	
	Solid	----	----	369	450^{br}	535	698^{sh}	1288^{br}	

sh, shoulder
br, broad
m, masked

Table 2.29 Electronic spectra of Co(II) complexes of 2MA ligands in solution and in solid state

Complexes	Solvent	Wavelength [λ_{max}/(nm)](ε, mol^{-1} dm^3 cm^{-1})							
		$\pi \rightarrow \pi^*$	$\pi \rightarrow \pi^*$	CT	d → d transitions				
$[Co(2MA)_2Cl_2]$	DMF	273*sh*	312 (5565)	328 (1708)	402sh	486*sh*	520*sh*	607 (285)	668 (390)
	DMSO	271 (1155)	315 (5870)	328 (1790)	----	487*sh*	560 (325)	618 (333)	----
	Solid	----	----	341	471	522, 589	751*sh*	984*sh*	1360*br*
$[Co(2Me\text{-}2MA)_2Cl_2]$	DMF	286 (2655)	308 (3445)	328 (1396)	398*sh*	488*sh*	525*sh*	607 (179)	671 (270)
	DMSO	288*sh*	311 (4529)	328 (1700)	405*sh*	488*sh*	528*sh*	612 (96)	684 (132)
	Solid	--	--	336, 369	589	625	757*sh*	1124	1375
$[Co(4Me\text{-}2MA)_2Cl_2]$	DMF	272 (740)	317 (4930)	332 (1741)	----	491*sh*	527*sh*	608 (180)	672 (286)
	DMSO	272 (998)	319 (5310)	335(1740)	----	487*sh*	535*sh*	613 (76)	677(124)
	Solid	--	--	338	481	521, 567, 593	654*sh*	1016*br*	1327*br*
$[Co(2MeO\text{-}2MA)_2Cl_2]^a$	DMF	274*sh*	314 (6475)	328 (6293)	----	462 (7220)	----	592*sh*	661*sh*
	DMSO	272*sh*	319 (7185)	329 (7605)	----	461 (8620)	----	591*sh*	660*br*
$[Co(4MeO\text{-}2MA)_2Cl_2]$	DMF	272 (773)	324 (8593)	344 (1959)	----	483*sh*	528*sh*	607 (214)	672 (298)
	DMSO	272 (1194)	323 (6518)	346 (2000)	395*sh*	488*sh*	533*sh*	621 (125)	684 (161)
	Solid	--	--	348	481	514, 567, 601	670*sh*	----	1350*br*
$[Co(4Cl\text{-}2MA)_2Cl_2]$	DMF	278 (1400)	323 (6122)	340 (1780)	----	495*sh*	530*sh*	608 (188)	672 (299)
	DMSO	276 (1930)	324 (6460)	340 (1838)	----	492*sh*	534*sh*	614 (82)	673 (129)
	Solid	--	--	337	460	521, 571	655*sh*	931*br*	1330*br*
$[Co(4Br\text{-}2MA)_2Cl_2]$	DMF	283 (2212)	323 (5618)	340 (1874)	----	491*sh*	526*sh*	608 (205)	674 (316)
	DMSO	286 (2815)	323 (7000)	345 (1940)	----	489*sh*	532*sh*	613 (181)	677 (290)
	Solid	--	--	341	460	514, 579	667*sh*	953*br*	1340*br*

a, the solid spectra could not be obtained
sh, shoulder
br, broad
m, masked

Table 2.30 Electronic spectra of Ni(II) complexes of 2MT ligands in solution and in solid state

Complexes	Solvent	Wavelength [λ_{max}/(nm)](ε, mol^{-1} dm^3 cm^{-1})								
		$\pi \rightarrow \pi^*$	$\pi \rightarrow \pi^*$	CT	d → d transitions					
$[Ni(2MT)_2Cl_2]$	DMF	268^{sh}	315 (1950)	322 (410)	424 (12)	584^{sh}	623 (2)	707 (4)	773 (4)	>1100
	DMSO	273^{sh}	300 (523)	327 (374)	425 (12)	----	----	707 (3)	799 (4)	>1100
	Solid	----	----	353	419	660	1145^{br}			
$[Ni(2Me\text{-}2MT)_2Cl_2]$	DMF	276^{sh}	295 (6730)	322 (210)	417 (12)	578^{sh}	622 (3)	696 (4)	776 (3)	> 1100
	DMSO	268^{sh}	312 (1840)	322 (200)	422 (3)	----	----	711(3)	789 (5)	> 1100
	Solid	----	----	353	414	657	1133^{br}			
$[Ni(4Me\text{-}2MT)_2Cl_2]$	DMF	273^{sh}	318 (1990)	330 (516)	417 (19)	585 (7)	618 (9)	689 (9)	766 (6)	>1100
	DMSO	269^{sh}	318 (1985)	332 (503)	429 (11)	----	----	709 (2)	793 (3)	>1100
	Solid	----	----	351	419	665	1155^{br}			
$[Ni(2MeO\text{-}2MT)_2Cl_2]$	DMF	277^{sh}	308 (1720)	322 (221)	418 (17)	580 (7)	618 (9)	689 (9)	771 (5)	>1100
	DMSO	270^{sh}	310 (1870)	322 (213)	428 (14)	----	----	712 (4)	797 (6)	>1100
	Solid	----	----	370	398^{sh}	650	1104^{br}			
$[Ni(4MeO–2MT)_2Cl_2]$	DMF	273^{sh}	324 (2231)	341 (589)	421 (41)	575 (18)	618 (18)	690 (16)	763 (5)	>1100
	DMSO	270^{sh}	324 (2210)	344 (577)	411 (17)	----	-----	708 (6)	771 (7)	> 1100
	Solid	----	----	348	*m*	672	1100^{sh}			

sh, shoulder
br, broad
m, masked

Table 2.30 Electronic spectra of Ni(II) complexes of 2MT ligands in solution and in solid state (continued)

Complexes	Solvent	Wavelength [λ_{max}/(nm)](ε, mol^{-1} dm^3 cm^{-1})								
		$\pi \rightarrow \pi^*$	$\pi \rightarrow \pi^*$	CT	d → d transitions					
[Ni(2Cl–2MT)$_2$Cl$_2$]	DMF	273^{sh}	315 (1915)	328 (360)	418 (18)	584 (7)	621 (10)	690 (10)	778^{sh}	>1100
	DMSO	267^{sh}	317 (1940)	328 (471)	411 (14)	----	----	710 (3)	763 (3)	>1100
	Solid	--	--	353	404	654	1140^{br}			
[Ni(4Cl–2MT)$_2$Cl$_2$]	DMF	272^{sh}	312 (946)	328 (520)	414 (11)	577^{sh}	621(2)	698 (4)	769 (3)	>1100
	DMSO	275^{sh}	324 (2170)	337 (542)	400 (34)	----	----	705 (4)	764 (4)	>1100
	Solid	--	--	364	407^{sh}	654	1137^{br}			
[Ni(2Br–2MT)$_2$Cl$_2$]	DMF	274^{sh}	316 (1948)	328 (360)	418 (18)	586 (7)	621 (8)	689 (10)	771^{sh}	>1100
	DMSO	269^{sh}	316 (1950)	329 (484)	420 (12)	----	----	718^{sh}	790 (2)	>1100
	Solid	--	--	353	406	654	1129^{br}			
[Ni(4Br–2MT)$_2$Cl$_2$]	DMF	278^{sh}	324 (2049)	334 (516)	417 (19)	586^{sh}	621 (8)	689 (8)	769 (4)	>1100
	DMSO	274^{sh}	325 (2160)	337 (520)	411 (12)	----	----	702 (3)	762 (4)	>1100
	Solid	--	--	356	402	653	1147^{br}			
[Ni(4NO$_2$–2MT)$_2$Cl$_2$]	DMF	275^{sh}	315^{sh}	376 (649)	422 (484)	585 (7)	621 (9)	688 (8)	767 (5)	>1100
	DMSO	270^{sh}	315^{sh}	348 (632)	440 (498)	----	----	713 (3)	761 (4)	>1100
	Solid	--	--	363	412, 460	665	1129^{br}			

sh, shoulder
br, broad

Table 2.31 Electronic spectra of Ni(II) complexes of 2MA ligands in solution and in solid state

Complexes	Solvent	Wavelength [λ_{max}/(nm)](ε, mol^{-1} dm^3 cm^{-1})								
		π → π*	π → π*	CT	d → d transitions					
[Ni(2MA)$_2$Cl$_2$]	DMF	272^{sh}	319 (2505)	332 (613)	416 (17)	576^{sh}	626^{sh}	698 (6)	772 (6)	>1100
	DMSO	271 (595)	318 (2515)	330 (640)	432 (12)	----	----	706^{sh}	802 (4)	>1100
	Solid	----	----	338	392^{sh}	602	1014^{br}	1316^{br}		
[Ni(2Me–2MA)$_2$Cl$_2$]	DMF	276^{sh}	315 (2225)	331 (640)	419 (16)	576^{sh}	620 (7)	700 (7)	779^{sh}	>1100
	DMSO	279^{sh}	319 (2325)	334 (646)	422 (12)	----	----	708^{sh}	786 (4)	>1100
	Solid	----	----	370	423^{sh}	----	728	1204^{br}		
[Ni(4Me–2MA)$_2$Cl$_2$]	DMF	273^{sh}	326 (2688)	338 (667)	412 (23)	577^{sh}	622 (4)	701 (6)	793^{sh} (7)	>1100
	DMSO	275 (559)	322 (2637)	341 (687)	410 (18)	----	----	713^{sh}	833 (7)	>1100
	Solid	----	----	332, 365	*m*	592	886	1210^{br}		
[Ni(2MeO–2MA)$_2$Cl$_2$]	DMF	278^{sh}	320 (2530)	332 (637)	412 (19)	573^{sh}	622^{sh}	697 (6)	776 (6)	>1100
	DMSO	278^{sh}	320 (2324)	332 (639)	413 (23)	568^{sh}	628^{sh}	698 (7)	774 (7)	>1100
	Solid	----	----	351, 365	433^{sh}	----	742	1250^{br}		
[Ni(4MeO–2MA)$_2$Cl$_2$]	DMF	272 (136)	324 (955)	350 (788)	423 (22)	579^{sh}	628 (12)	709 (13)	790 (12)	>1100
	DMSO	276 (560)	323 (2680)	357 (748)	423 (18)	----	----	710^{sh}	817 (11)	> 1100
	Solid	----	----	334	395^{sh}	591	888	1237^{br}		
[Ni(4Cl–2MA)$_2$Cl$_2$]	DMF	278 (731)^{sh}	324 (2745)	343 (703)	411 (26)	----	----	704 (8)	781 (10)	>1100
	DMSO	281 (814)	325 (2777)	347 (711)	423 (23)	----	----	707^{sh}	798 (9)	>1100
	Solid	----	----	338	398^{sh}	594	961^{br}	1312^{br}		
[Ni(4Br–2MA)$_2$Cl$_2$]	DMF	279^{sh}	323 (2720)	345 (715)	420 (17)	586^{sh}	619^{sh}	701 (5)	774 (5)	>1100
	DMSO	280^{sh}	323 (2683)	349 (728)	424 (12)	----	----	708^{sh}	804 (6)	>1100
	Solid	----	----	343	405^{sh}	591	957^{br}	1311^{br}		

sh, shoulder
br, broad
m, masked

Table 2.32 Electronic spectra of Cu(II) complexes of 2MT ligands in solution and in solid state

Complexes	Solvent	Wavelength [λ_{max}/(nm)](ε, mol^{-1} dm^3 cm^{-1})			
		$\pi \rightarrow \pi^*$	$\pi \rightarrow \pi^*$	CT	$d \rightarrow d$
$[Cu(2MT)Cl_2]$	DMF	266 (4530)	295 (5750)	327 (2150), 434 (437)	931 (89)
	DMSO	259 (8350)	298 (8250)	322 (2095), 430^{sh}	925 (99)
	Solid	----	----	353, 400	706^{br}
$[Cu(2Me–2MT)Cl_2]$	DMF	275^{sh}	301 (3860)	329 (1705), 433 (390)	930 (85)
	DMSO	275^{sh}	306 (4780)	325 (2223), 430^{sh}	936 (92)
	Solid	----	----	354, 469	713^{br}
$[Cu(4Me–2MT)Cl_2]$	DMF	266 (5010)	300 (5370)	330 (2330), 435 (550)	923 (93)
	DMSO	259 (7700)	303 (6965)	330 (2207), 430^{sh}	916 (125)
	Solid	----	----	356, 450	754^{br}
$[Cu(2MeO–2MT)Cl_2]$	DMF	272^{sh}	301 (4060)	327 (895), 434 (130)	876 (60)
	DMSO	----	305 (4805)	334 (1988), 504^{sh}	912 (88)
	Solid	----	----	371, 402, 479	771^{br}
$[Cu(4MeO–2MT)Cl_2]$	DMF	266 (4900), 287^{sh}	308 (4680)	327 (2334), 439 (778)	582 (628), 821 (81)
	DMSO	259 (6265), 286 (5200)	312 (5565)	336 (2309), 447 (489)	595 (290), 885 (95)
	Solid	----	----	352, 403, 479	786^{br}

sh, shoulder
br, broad
m, masked

Table 2.32 Electronic spectra of Cu(II) complexes of 2MT ligands in solution and in solid state (continued)

Complexes	Solvent	Wavelength [λ_{max}/(nm)](ε, mol^{-1} dm^3 cm^{-1})			
		$\pi \rightarrow \pi^*$	$\pi \rightarrow \pi^*$	CT	$d \rightarrow d$
$[Cu(2Cl–2MT)Cl_2]$	DMF	275^{sh}	305 (3750)	328 (1890), 436 (290)	939 (80)
	DMSO	----	309 (4940)	332 (1865), 431^{sh}	938 (108)
	Solid	----	----	356, 413	773^{br}
$[Cu(4Cl–2MT)Cl_2]$	DMF	266 (8130)	306 (5370)	330 (1905), 435 (329)	942 (85)
	DMSO	261 (11680)	309 (6710)	335 (1969), 430^{sh}	936 (90)
	Solid	----	----	364, 405	782^{br}
$[Cu(2Br–2MT)Cl_2]$	DMF	275^{sh}	305 (3940)	329 (1706), 437 (260)	937 (72)
	DMSO	----	310 (5450)	331 (1870), 431^{sh}	934 (83)
	Solid	----	----	351, 414, 463	778^{br}
$[Cu(4Br–2MT)Cl_2]$	DMF	267 (9120)	306 (5370)	326 (2540), 436 (324)	947 (85)
	DMSO	262 (12640)	308 (6880)	333 (2015), 430^{sh}	920 (83)
	Solid	----	----	348, 425	795^{br}
$[Cu(4NO_2–2MT)Cl_2]$	DMF	267 (8440), 299^{sh}	312^{sh}	377 (1850), 397 (14030), 415 (1515)	946 (30)
	DMSO	263 (7530), 301^{sh}	322^{sh}	381 (1700), 399 (1400), 428 (1640)	925 (87)
	Solid	----	----	367, 450	765^{br}

sh, shoulder
br, broad

Table 2.33 Electronic spectra of Cu(II) complexes of 2MA ligands in solution and in solid state

Complexes	Solvent	Wavelength [λ_{max}/(nm)](ε, mol^{-1} dm^3 cm^{-1})			
		$\pi \rightarrow \pi^*$	$\pi \rightarrow \pi^*$	CT	d → d transitions
$[Cu(2MA)Cl_2]$	DMF	275^{sh}	308 (3957)	328 (2328), 432 (395)	903 (70)
	DMSO	280 (2720)	317 (4535)	328 (2860), 432^{sh}	870 (102)
	Solid	----	----	353	706^{br}
$[Cu(2Me–2MA)Cl_2]$	DMF	273^{sh}	300 (5080)	336 (3360), 428 (2070)	503 (1605)
	DMSO	273^{sh}	306 (6340)	336 (3426), 425^{sh}	548 (1860), 999 (130)
	Solid	----	----	354, 469	713^{br}
$[Cu(4Me–2MA)Cl_2]$	DMF	277^{sh}	312 (4995)	331 (2673), 437 (320)	928 (80)
	DMSO	273^{sh}	315 (6850)	333 (2710), 500^{sh}	896 (86)
	Solid	----	----	356, 450	754^{br}
$[Cu(2MeO–2MA)Cl_2]$	DMF	275^{sh}	315 (5805)	335 (3664), 454 (3400))	*m*
	DMSO	275^{sh}	311 (8230)	384(3986), 460 (3390)	1000 (18)
	Solid	----	----	371	771^{br}
$[Cu(4MeO–2MA)Cl_2]$	DMF	275^{sh}	300 (3895)	333 (2837), 428 (2145)	544 (903), 587 (704)
	DMSO [c]	276^{sh}	315 (5760)	332 (3018), 433 (1510)	539^{sh}, 590^{sh}, 692 (70)
	Solid	----	----	352, 403, 479	786^{br}
$[Cu(2Cl–2MA)Cl_2]$	DMF	275^{sh}	304 (5690)	333 (3280), 364 (5424), 413 (3335)	*m*
	DMSO	276^{sh}	304 (4940)	331 (2590), 368 (2160), 396 (2070)	497^{sh}, 1039^{br} (108)
	Solid	----	----	356, 413	773^{br}
$[Cu(4Cl–2MA)Cl_2]$	DMF	279^{sh}	319 (5288)	336 (2810), 435 (330)	906 (80)
	DMSO	277^{sh}	320 (6630)	336 (2900)	518 (108), 571^{sh}, 615^{sh}, 906(82)
	Solid	----	----	364, 405	782^{br}
$[Cu(2Br–2MA)_2Cl_2]$	DMF	281 (3210)	314 (3622)	332 (2430), 436 (370)	901 (40)
	DMSO	286 (4565)	315 (5620)	332 (2820)	500^{sh}, 886 (54)
	Solid	----	----	351, 414, 463	778^{br}
$[Cu(4Br–2MA)Cl_2]$	DMF	285^{sh}	319 (5132)	333 (2922), 433 (390)	565^{sh}, 625^{sh}, 913 (75)
	DMSO	281^{sh}	320 (7220)	332 (2824)	507 (107), 569^{sh}, 615^{sh}, 896 (105)
	Solid	----	----	348, 425	795^{br}

sh shoulder *br* broad *m* masked

2.4.6.3 Electronic spectra of Schiff-base ligands and complexes in solution

Table 2.34 Electronic spectra of Schiff-base ligands and complexes in DCM

Compound	Wavelength [λ_{max}/(nm)](ε, mol^{-1} dm^3 cm^{-1})				
	π → π*	π → π*	n → π* (C=N)	CT	d → d
pMS–2MT	249 (1170)	299 (4420)	339 (9120)		
[Cu(pMS–2MT)$_2$]	260^{sh}	306 (16300)	364 (19890)	393 (4370)	598^{br} (98)
pMS–4Me2MT	253 (2520)	299 (8970)	343 (23250)		
[Cu(pMS–2Me2MT)$_2$]	265^{sh}	307 (16050)	363 (20140)	396 (4490)	611^{br} (120)
pMS–4MeO2MT	255 (2310)	301 (7580)	350 (21300)		
[Cu(pMS–4MeO2MT)$_2$]	264^{sh}	310 (16530)	364 (22460)	396 (4500)	615^{br} (118)
pMS–4Cl2MT	254 (2520)	303 (11280)	343 (27900)		
[Cu(pMS–4Cl2MT)$_2$]	264^{sh}	306 (15760)	364 (16680)	394 (4400)	598^{br} (90)
pMS–4Br2MT	252 (2220)	303 (10140)	344 (24290)		
[Cu(pMS–4Br2MT)$_2$]	264^{sh}	313 (17100)	354 (20810)	396 (4450)	601^{br} (98)
pMS–4NO$_2$2MT	253 (4570)		370 (40100)		
[Cu(pMS–4NO$_2$2MT)$_2$]	265^{sh}	309 (23830)	376 (24500)	400 (8870)	580 (170)
pMS–2MA	246 (54430)	272, 282 (40500)	359 (41730)		
[Cu(pMS–2MA)$_2$]	261 (16600)	328 (20500)	409 (14850)	-----	660 (152)
pMS–4Me2MA	245 (30030)	275 (24000)	359 (24000)		
[Cu(pMS–2Me2MA)$_2$]	261 (16600)	282, 303 (31000)	392 (22800)	-----	684 (130)
pMS–4MeO2MA	244 (46130)	281 (37070)	368 (39000)		
[Cu(pMS–4MeO2MA)$_2$]	261 (38000)	285, 304 (32500)	392 (22800)	-----	660 (80)
pMS–4Cl2MA	246 (40680)	276 (31080)	362 (35860)		
[Cu(pMS–4Cl2MA)$_2$]	254 (20950)	286, 304 (19100)	390 (12350)	-----	661 (120)
pMS–4Br2MA	244^{sh}	277 (16800)	365 (16000)		
[Cu(pMS–4Br2MA)$_2$]	258 (34920)	286, 303 (32200)	392 (20980)	-----	657 (60)

REFERENCES

1. D. R. Burfield and R. H. Smithers, *Journal of Organic Chemistry*, 1983, **48**, 2420.
2. J. P. Chupp, T. M. Balthazor, M. J. Miller and M. J. Pozzo, *J. Org. Chem*., 1984, **49**, 4711.
3. S. J. Hodson, M. J. Bishop, J. D. Speake, F. Navas III, D. T. Garrison, E. C. Bigham, D. L. Saussy Jr., J. A. Liacos, P. E. Irving, M. J. Gobel and B. W. Sherman, *J. Med. Chem.*, 2002, **45**, 2229.
4. C. G. Stuckwisch, *J. Am. Chem*. Soc., 1949, **71**, 3417.
5. M. Matsui, Y. Marui, M. Kushida, K. Funabiki, H. Muramatsu, K. Shibata, K. Hirota,M. Hosoda and K. Tai, *Dyes and Pigments*, 1998, **38**, 57.
6. G. Trapani, M. Franco, A. Latrofa, A. Reho and G. Liso, *Eur. J. Pharm. Sci.*, 2001, **14**, 209.
7. D. Shashank, T. Vishawanth, Md. Arif Pasha , V. Balasubramaniam, A. Nagendra, P. Perumal and R. Suthakaran, *International Journal of ChemTech Research*, 2009, **1**, 224.
8. J. K. Malik, Dr. F. V. Manvi1, Dr B.K. Nanjwade and S. Singhet, *Drug Invention Today*, 2009, **1**, 32.
9. B. A. Dreikorn, G. P. Jourdan, H. R. Hall, J. B. Deeter, and N. Jones, *J. Agric. Food Chem*., 1990, **38**, 549.
10. G. M. Sheldrick, *Acta Crystallogr., Sect. A: Foundations of Crystallography* 2008, **64**, 112.
11. G. M. Sheldrick, *NATO ASI Series, Series E: Applied Sciences*, 1997, **347**, 219.

13 G. M. Sheldrick, T. R. Schneider, *Methods Enzymol.* 1997, **277**, 319.

14 CCDC-888074 contains the supplementary crystallographic data for this compound. These data can be obtained free of charge from The Cambridge Crystallographic Data Centre via www.ccdc.cam.ac.uk/data_request/cif.

15 CCDC-872915 contains the supplementary crystallographic data for this compound. These data can be obtained free of charge from The Cambridge Crystallographic Data Centre via www.ccdc.cam.ac.uk/data_request/cif.

16 CCDC-872916 contains the supplementary crystallographic data for this compound. These data can be obtained free of charge from The Cambridge Crystallographic Data Centre via www.ccdc.cam.ac.uk/data_request/cif.

17 CCDC-890400 contains the supplementary crystallographic data for this compound. These data can be obtained free of charge from The Cambridge Crystallographic Data Centre via www.ccdc.cam.ac.uk/data_request/cif.

18 CCDC-872913 contains the supplementary crystallographic data for this compound. These data can be obtained free of charge from The Cambridge Crystallographic Data Centre via www.ccdc.cam.ac.uk/data_request/cif.

19 CCDC-872914 contains the supplementary crystallographic data for this compound. These data can be obtained free of charge from The Cambridge Crystallographic Data Centre via www.ccdc.cam.ac.uk/data_request/cif.

20 W. J. Geary, *Coord. Chem. Rev.*, 1971, **7**, 81.

DISCUSSION

This chapter brings out the key issues of the results obtained for all the compounds synthesized and used in this research work, so that decisive conclusions can be reached. In most part of the discourse, 2–(methylthiomethyl)anilines (2MT) and 2–(methylthio)anilines (2MA) with their metal(II) complexes are jointly discussed as they have similar properties such as reaction stoichiometry, colour, electronic spectra *etc*. Where there are variations between the two groups, the differences are noted and discussed.

The electronic effect of substituents on the ring is also discussed in relation to their electron withdrawing/donating property. Where applicable, position of substituent on the ring as *ortho* or *para* to the amine group (**Fig. 3.1**) in relation to subsequent effect on property of compounds is discussed.

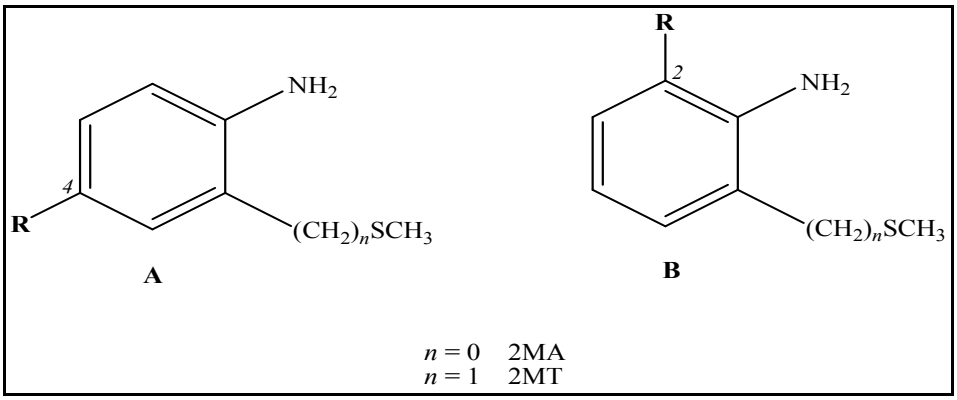

Fig. 3.1 *para* (A) and *ortho* (B) positions of substituents in 2MA and 2MT ligands

3.1 ELEMENTAL ANALYSIS AND YIELDS

The elemental analysis of a compound is a preliminary test carried out to ascertain the composition of elements in it. It is a helpful tool as it shows in which stoichiometry or ratio the ligand possibly binds to a metal ion in a given complex. It is also an indication of the purity of the synthesized compound. The microanalyses were submitted in replicate. The data as contained in **Tables 2.1–2.3**, and **Tables 2.4–2.10** (Chapter 2) for ligands and complexes respectively show that the C, H, N results are generally better than the S values. It is noted that the error is greatest for the sulfur figures, especially for the nickel complexes. This may reflect the formation of metal sulfides during combustion analysis, leading to a decrease in precision. The NMR spectra of these ligands however indicate they are pure.

The elemental analysis results of the Schiff-base ligands are in close agreement with their predicted values. The stoichiometry of the Cu(II) complexes was determined as $[Cu(SB)_2]$ where SB is Schiff-base, by elemental analysis and was confirmed by X-ray crystallographic studies.

Yields of most of the compounds synthesized were above 50%, however low yields were derived for a few compounds. The yields were especially low in the case of the *ortho*-substituted copper complexes of 2MA ligands in comparison with their *para*-substituted analogues and their Co(II) and Ni(II) counterparts. No such discrimination in yields obtained was seen in any other set of metal complexes. Low yields recorded might be as a result of the unsuitability of the reaction conditions to the formation of those *ortho*-substituted products. Cobalt(II) complexes of 2MA ligands such as Co2MA, Co(2Me–2MT), Co(2MeO–2MA) and Co(4Cl–2MA) were also synthesized with low yields and were found to be particularly soluble in the solvents used to purify them.

3.1.1 2–(Methylthiomethyl)anilines, 2–(methylthio)anilines and their Schiff-base ligands

Most of the thiomethylated-aniline ligands used in this work has been previously synthesized (except the bromo-substituted derivatives).[1-7] These ligands were synthesized during this research study so they could be fully characterized and be used in biological studies. The elemental analysis data are generally in good agreement with the expected ligands' formula composition in most cases.

The elemental analysis results obtained for the Schiff-base ligands are in excellent agreement with the expected values, indicating the reaction between the anilines and the aldehyde was by 1:1 stoichiometry of the reactants.

3.1.2 Complexes of 2–methylthiomethyl)anilines and 2–(methylthio)anilines

Tables 3.4–3.9 display the elemental composition of the metal complexes. From the elemental composition results, the Co(II) complexes of both 2MT– and 2MA–based ligands indicate a 2:1 ligand to metal binding ratio including two chlorine atoms.

The Ni(II) complexes of both groups similarly show 2:1 ligand to metal combination stoichiometry with two chlorine atoms.

However, Cu(II) complexes formed in 1:1 ligand to metal combination irrespective of the addition method (metal to ligand or ligand to metal) used. Irrespective of the reaction temperature with the 2MT ligands, the same stoichiometry was derived for the complexes. In order to facilitate comparative studies with Cu(II) complexes with 2MT ligands, the complexes of 2MA ligands were prepared at room temperature to ensure the formation of 1:1 complexes since Dunski[8] has reported a 2:1 formation ratio for copper(II) complex with 2MA under reflux. The exception to this 1:1 stoichiometry formation of the copper complexes is Cu(2Br–2MA) formed in 2:1 ratio even under similar reaction condition as others. The reason for this is not clearly understood as its counterpart Cu(2Cl–2MA) formed in 1:1 ratio.

3.1.3 Cu(II) Complexes of Schiff-bases

The elemental analysis obtained for the copper complexes are also in excellent agreement with the predicted values. Cu(II) complexes of both pMS–2MT and pMS–2MA Schiff-bases were formed in 2:1 ligand to metal stoichiometry.

3.2 NMR SHIFTS OF 2MT AND 2MA LIGANDS

The one– and two–dimensional proton and carbon-13 nuclear magnetic resonance shifts of all the ligands were determined in deuterated chloroform for proper assignments of signals due to resonating protons and carbon nuclei so that comparative studies could be made.

The proton NMR chemical shifts of most of the 2MT ligands have been reported by Hiraki *et al*[9] and Chupp *et al*[2] with the exception of the bromo–substituted ligands. Likewise the proton NMR shift values of some 2MA ligands have been reported[10-13] with the exception of *ortho*-(MeO, Cl, Br) and *para*-Br substituted ligands. The Carbon-13 NMR shifts were not reported and these values have been assigned here with the aid of 1D- as well as 2D-NMR spectroscopy which are recorded in **Tables 2.11-2.12** in Chapter 2.

The ^{1}H spectrum of 4Br–2MT with the other one- and two-dimensional NMR spectra in **Fig. 3.2**–**3.6** is representative and typical of other 2MT ligands. The ^{1}H spectrum shows a *singlet* peak due to the methyl protons close to 2 ppm, another singlet peak of the methylene protons at a higher frequency of 3.6 ppm, with the low intensity *singlet* peak due to amine protons around 4 ppm are observed. The aromatic protons absorb between 6.6 and 7.2 ppm. The spectra of 2MA ligands are similar, differing in the absence of signal due to methylene protons. The NMR shifts of complexes were not measured due to their possession of paramagnetic metal ions.

Of the various resonating groups present in the ligands, the amine protons show the most sensitivity to electronic effect of substituents on the ring as one changes from neutral (H) to electron–donating (Me, OMe) to electron–withdrawing groups (Br, Cl, NO_2). The position of these ring substituents relative to that of amine also influences the shifts of amine protons. The lone pair of electrons on the aniline nitrogen is in conjugation with the π–system of the ring, it is thus expected that variation in the electronic nature of the substituents attached to the aromatic ring should have a direct effect on the nitrogen atom and

consequently on the protons attached to it. It is well known that chemical shift (δ) depends on molecular structure and solvent and ^{1}H nucleus is sensitive to hybridization of atom to which it is attached and electronic effects. These highlights are discussed below.

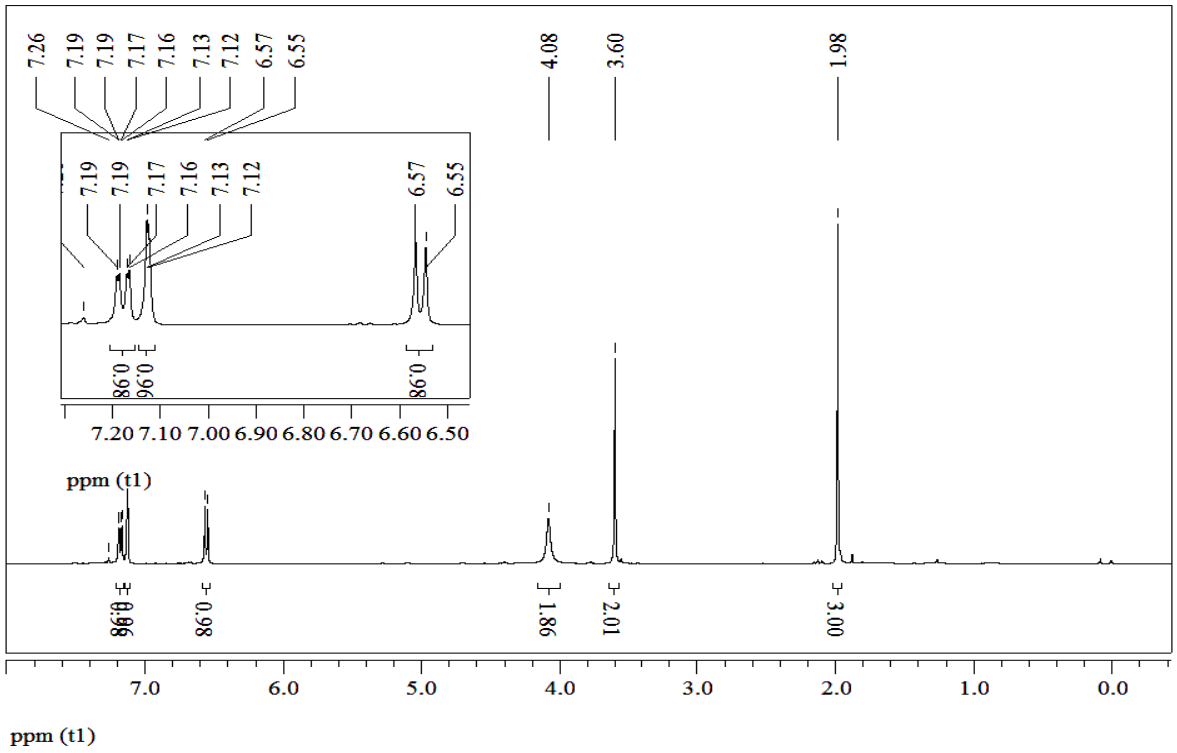

Fig. 3.2 ^{1}H–NMR spectrum (400 MHz) of 4Br–2MT in $CDCl_3$

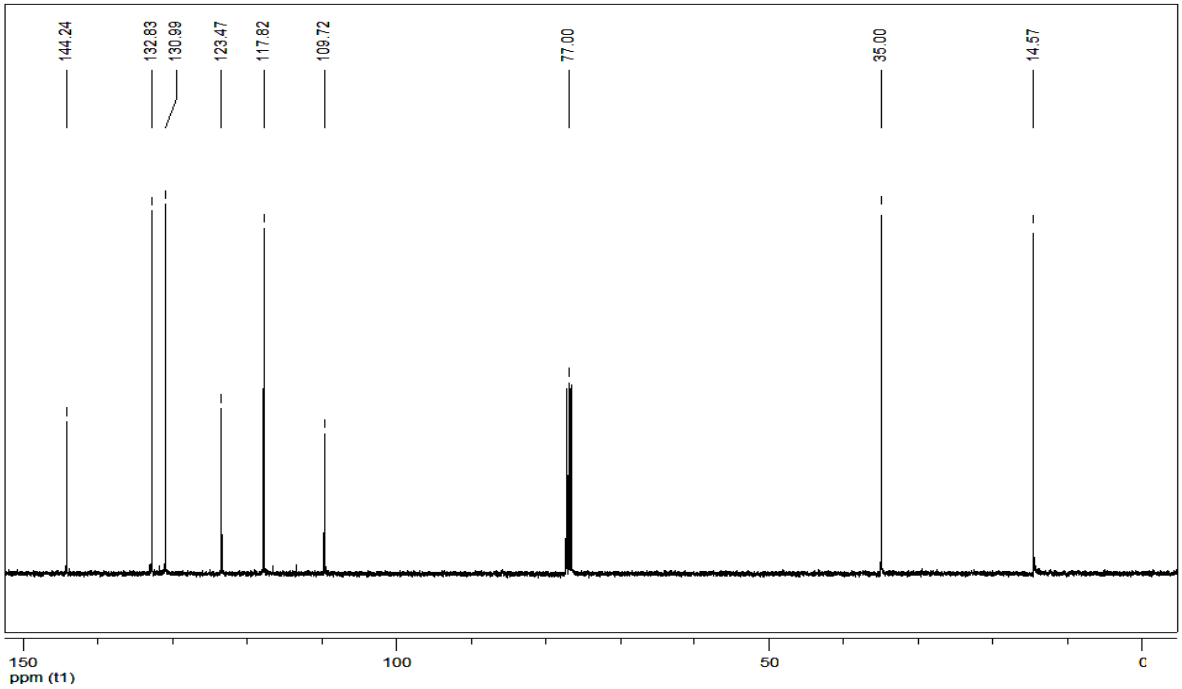

Fig. 3.3 ^{13}C–NMR spectrum (100 MHz) of 4Br–2MT in $CDCl_3$

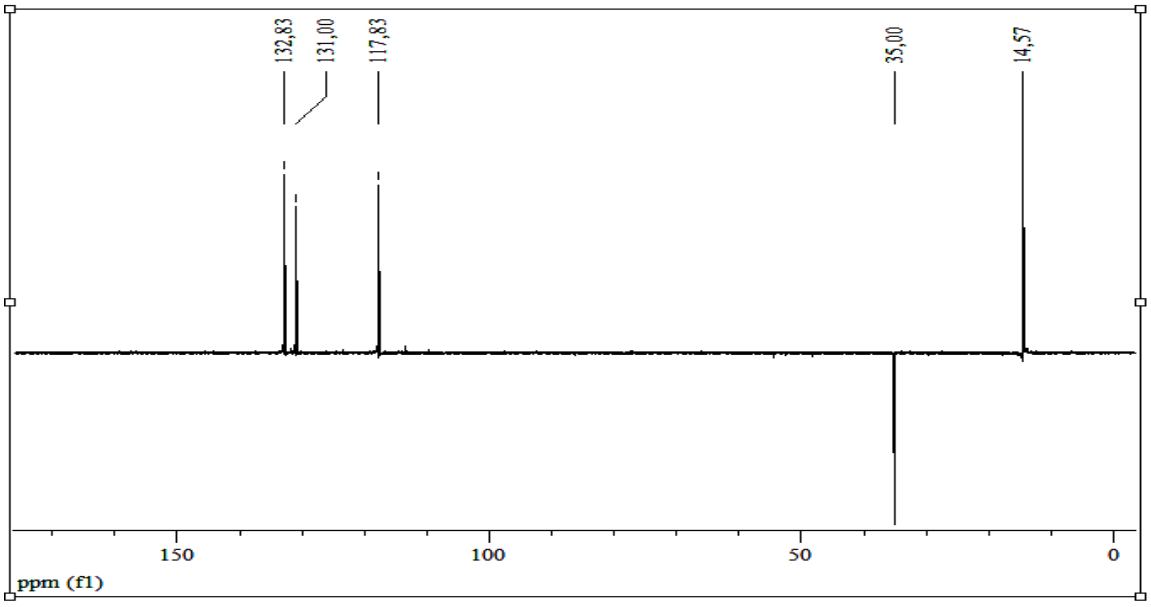

Fig. 3.4 DEPT135 NMR spectrum (100 MHz) of 4Br–2MT in $CDCl_3$

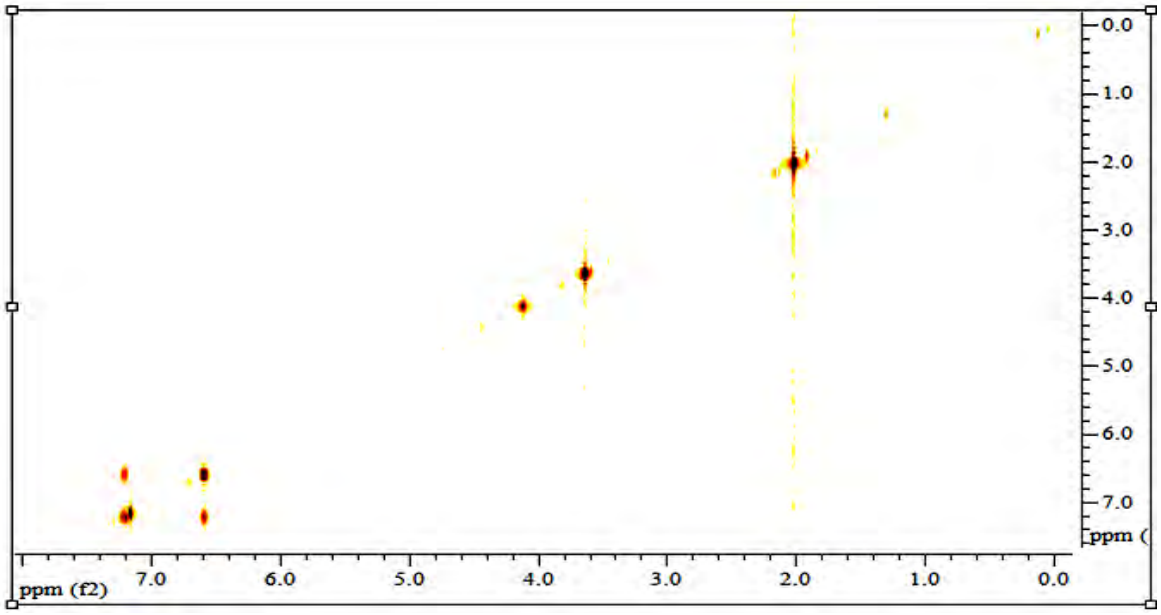

Fig. 3.5 COSY NMR spectrum (400 MHz) of 4Br–2MT in $CDCl_3$

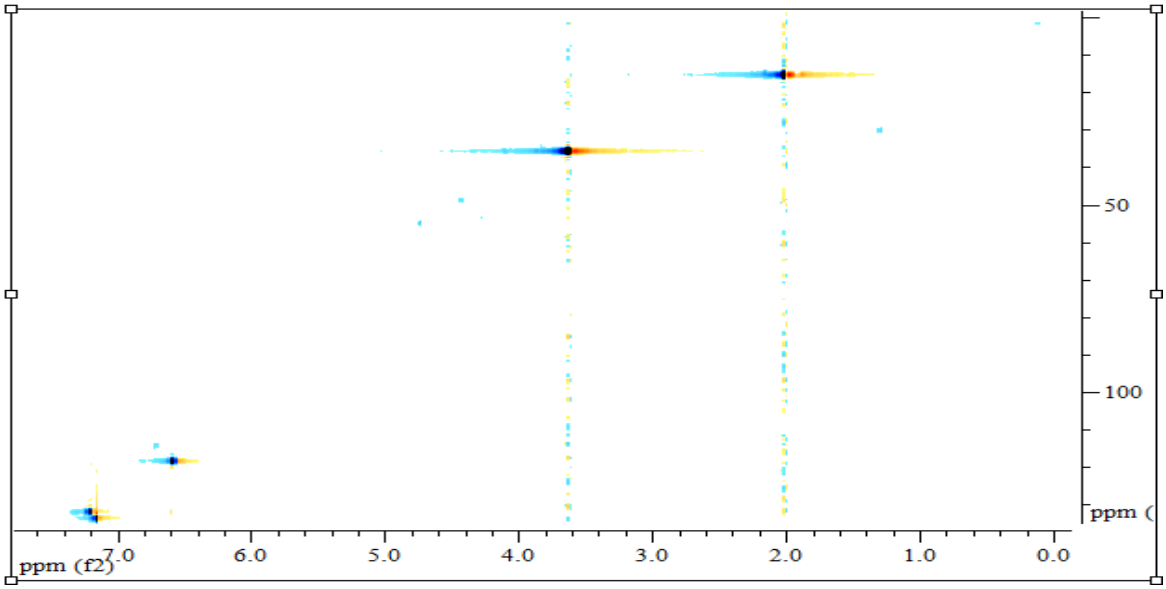

Fig. 3.6 HSQC NMR spectrum (100 MHz) of 4Br–2MT in $CDCl_3$

3.2.1 Trend in NMR shifts of amine protons of 2–(methylthiomethyl)anilines

Position of ring substituent (*para*/*ortho* to aniline nitrogen): Observation made from **Tables 2.11 and 2.12** shows the NMR shift values of the *para*-substituted ligands (**Fig. 3.7A**) are higher than those of their corresponding *ortho* analogues (**Fig. 3.7B**), regardless of electronic nature of substituent. The close proximity of all substituent groups in the *ortho*–substituted irrespective of their electronic nature serves an effect of reducing the electron density on aniline nitrogen atom because of a stronger inductive effect operative at this position compared to *para* position where they are distal to nitrogen. Hence they all deshield amine protons more than 2MT. As expected, the withdrawing groups deshield more strongly than the rest.

Table 3.1 Trend in chemical shifts of NH_2 protons of *para*– and *ortho*–substituted 2MT ligands

Ligands (*para*)	δ	Ligands (*ortho*)	δ
4MeO–2MT	3.81	2MeO–2MT	4.28
4Me–2MT	3.95	2Me–2MT	4.09
2MT	4.06	2MT	4.06
4Br–2MT	4.08	2Br–2MT	4.59
4Cl–2MT	4.07	2Cl–2MT	4.60
$4NO_2$–2MT	4.73	$2NO_2$–2MT	6.62

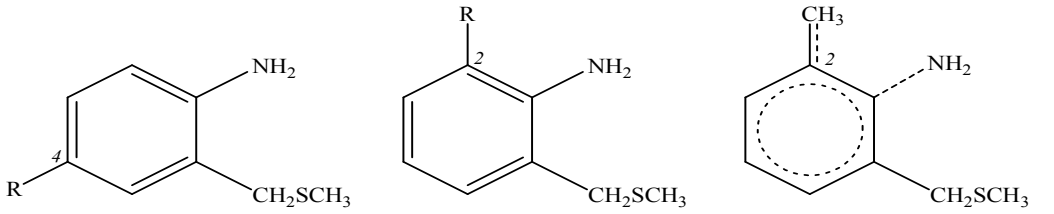

para–substituted 2MT **A** *ortho*–substituted 2MT **B** Hyperconjugation in 2Me–2MT **C**

Fig. 3.7 Substitution in 2MT ligands (**A, B**) and hyperconjugation (**C**)

This explains the very high frequencies observed for the halogens, more especially for NO_2 group at this position. Despite its electron–donating ability as an entity, the strongly negative oxygen atom of MeO group directly attached to the ring at this position withdraws electrons from the ring, consequently from nitrogen. The net effect is to increase the frequencies of amine protons. The methyl group has the same effect on amine protons by hyperconjugation (**Fig. 3.7C**). In the *para* position, these substituents influence the electron density on the nitrogen by mesomerism effect. This is a longer range effect compared to the *ortho* inductive effect whose range is shorter.

Another explanation as to why amine protons absorb at higher frequencies with substituent at *ortho* position could be the reduced probability of hydrogen bonding with NH_2. Hydrogen bonding in amine groups is known to lower their frequencies.[14] In addition, the close proximity of these relatively bulkier groups *ortho* to amine group could induce a structural distortion of NH_2 to pyramidal which reduces the conjugation with aromatic ring, hence a deshielding effect is observed.

Electronic effect of ring substituent: the observed trend in NMR shifts of amine protons as a result of changing the substituent places the neutral 2MT in the middle of those with electron donating and withdrawing nature. Amine protons have higher chemical shift values in ligands with withdrawing groups than those with the donating groups, regardless of the position of the substituent. This is as a result of increase in the electron density on the aniline nitrogen as a result of increase in conjugation with electron donating groups, subsequently reducing the frequencies of the protons attached to this nitrogen as they become more shielded. Hence an upfield shift in frequencies is observed for both methyl and methoxy groups relative to 2MT (neutral, H substitution). Conversely, the electron withdrawers such as the halogen and nitro groups decrease the conjugation of the aromatic system, thereby decreasing the electron density on the nitrogen atom; its protons are deshielded and they resonate at higher frequencies.

3.2.2 Trend in NMR shifts of other protons of 2–(methylthiomethyl)anilines

Aromatic protons: A trend similar to that in amine protons, though less pronounced, is found for protons on the aromatic ring of the *para*–substituted ligands. Protons *3* and *5* were particularly similar in trend as a result of their equidistance to the substituent at position *4*. Those on the *ortho*–substituted rings on the other hand show irregularities and do not display a noticeable trend probably due to the *ortho*–effect.[15]

Nature and position of substituents determine the shape of the NH_2, as either pyramidal or planar. In planar configuration, the NH_2 lone pair is in conjugation with the aromatic ring while in its pyramidal structure, the overlap of its lone pair is hindered due to a decrease in flattening leading to a decrease of charge delocalization via the π bond. As a result, substituents that make the NH_2 planar will shield amine protons.

Methyl and methylene protons: The aliphatic methyl protons attached to sulfur are not affected by substituent change on aromatic ring since they are distal to the aromatic ring to experience any mesomeric effect. On the other hand, the carbon bearing the methylene protons is attached to the ring hence they also share in the π–conjugation of the ring. Generally, they absorb at lower frequencies with any *para* substituent type but at higher frequencies with any *ortho* substituent, similar to the trend observed in amine protons.

3.2.3 Trend in NMR shifts of protons of 2–(methylthio)anilines

The frequencies of all protons (methylene, amine and aromatic) of substituted 2MA ligands are generally lowered compared to that of 2MA (H, light atom substituent) irrespective of the electronic nature or position of substituent (**Table 3.2**). This is suggestive of the presence of stronger hydrogen bonding between the amine protons and sulfur, which is reduced as bulkier groups are attached to the ring. There is also a possibility of change in the planarity of the NH_2 with the aromatic system to a pyramidal configuration with attachment of bulkier groups. The consequence is to reduce the frequencies of the amine protons of substituted ligands relative to 2MA.

The NMR shifts for *para*-substituted 2MA ligands are seen to be lower than those of their *ortho*-analogues. It could be that the substituent at the *ortho* position enhances the pyramidal orientation of the NH_2 group decreasing the probability of hydrogen bonding with the thioether group. Further physical studies may be used to verify this.

Table 3.2 Trend in chemical shifts of the NH_2 protons of *para*– and *ortho*–substituted 2MA ligands

Ligands (*para*)	δ	Ligands (*ortho*)	δ
4MeO–2MA	3.82	2MeO–2MA	3.81
4Me–2MA	4.14	2Me–2MA	3.57
2MA	4.29	2MA	4.29
4Br–2MA	4.16	2Br–2MA	4.02
4Cl–2MA	4.05	2Cl–2MA	3.97

3.2.4 Comparison of amine protons shifts in 2MT and 2MA ligands

In 2MA ligands, the effect of the direct attachment of sulfur to the aromatic ring is not expected to have a bearing on the substituent since S is *meta* to the substituent at both the para and *ortho* positions. Its effect is however directly on the amine group to which it is proximal. In general if the frequency shifts of amine protons in 2MT and 2MA ligands are compared, we can make the following generalizations:

In the unsubstituted ligands 2MT and 2MA, the effect of sulfur attachment to the aromatic ring is to increase the conjugation of the ring and decrease the electron demand on amine nitrogen in the case of the latter; thereby its protons absorb at higher frequencies relative to those of 2MT ligands. This trend is likewise observed in *para*–substituted ligands.

Conversely, the frequencies are lower in *ortho* substituted 2MA ligands in comparison to their 2MT analogues, perhaps due to a change in the orientation of NH_2 group relative to the aromatic ring. Moreover, NH_2 is a comparatively small group, and the atomic groups in the *ortho*-position of the aromatic ring do not significantly change the orientation of the lone electron pair of the amine nitrogen atom, favoring conjugation with the π-system of the ring.[16]

3.3 NMR SHIFTS OF SCHIFF-BASE LIGANDS

The NMR shifts of the Schiff-bases are recorded in **Table 2.13** and the spectra are shown below in **Fig. 3.8–3.15**. For the pMS–2MT ligands, the upfield region consist of singlet peaks for the methyl protons of the thioether group in the range 2.05–2.08 ppm and methylene protons in the range 3.73–3.81 ppm. The methyl protons in pMS–2MA ligands absorb at higher frequencies between 2.45 and 2.47 ppm, indicating the protons are more deshielded here. Another singlet peak due to the methoxy protons appears between 3.83–3.87 ppm in the spectra of all the ligands. Additional singlet signals are observed for those Schiff-bases substituted with methyl and methoxy groups on their phenyl rings at 2.35–2.38 ppm and 3.83 ppm respectively.

The aromatic protons of the two phenyl rings appear as multiplets in the range 6.48–8.22 ppm. The downfield region shows two separate singlet peaks due to azomethine proton (8.44–8.54 ppm) and the phenolic proton (12.94–13.71 ppm) in all the ligand. The signal due to phenolic proton was confirmed as it was exchangeable on shaking with deuterium oxide. The high frequency of its absorption is an indication of hydrogen bonding between this proton and imine nitrogen. This phenomenon is usually observed in resonance signals of alcoholic protons and much more the aromatic phenolic protons and has been reported in Schiff-bases derived from 2-hydroxybenzaldehyde and aniline.[17] The signal due to phenolic proton also shows sensitivity to change in electronic nature of substituents on aromatic ring; its frequency increases with electron donating power of substituents. The effect of substituent type is carried through resonance across the aromatic rings to the absorption of phenolic proton. The ligand with the methoxy substituent gives the highest frequency absorption at 13.71 ppm. The more donating substituents increase the electron density on the proton and consequently increase its availability for hydrogen bonding. The converse can be said of the electron withdrawing substituents like NO_2, hence the phenolic proton here absorbs at a lower frequency value of 12.94 ppm.

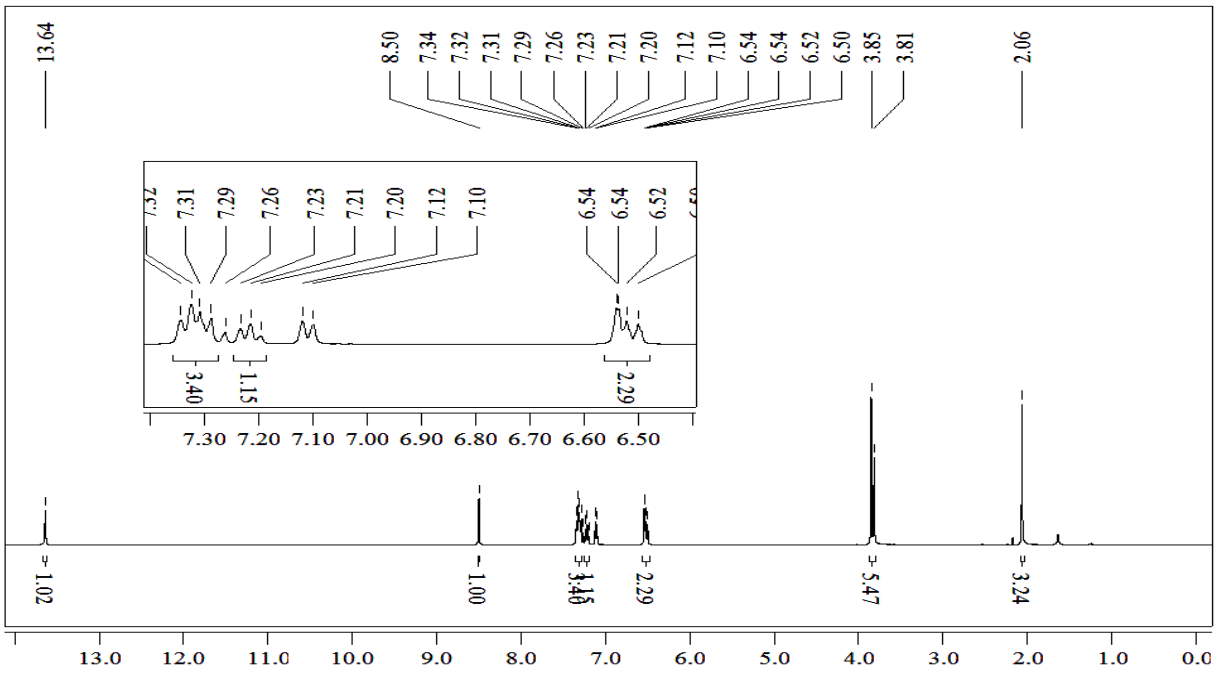

Fig. 3.8 ^{1}H–NMR spectrum (400 MHz) of pMS–2MT in $CDCl_3$

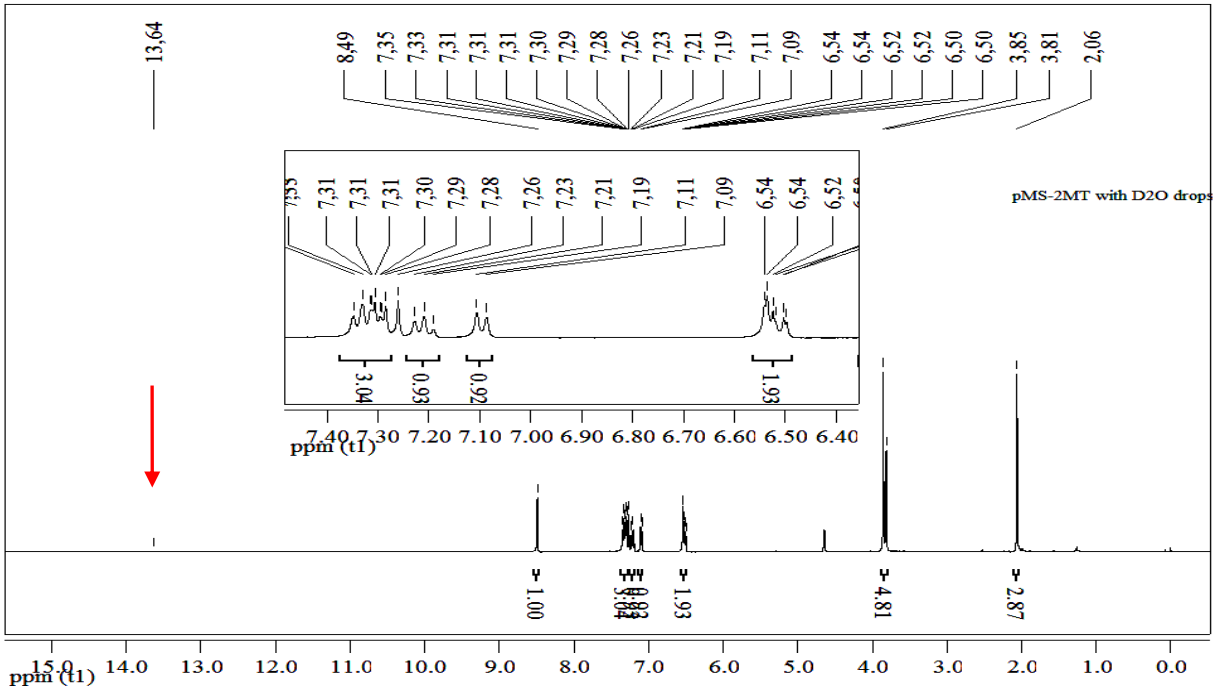

Fig. 3.9 ^{1}H–NMR spectrum (400 MHz) of pMS–2MT in $CDCl_3$ showing the disappearance of signal due to phenolic proton after deuterium shake

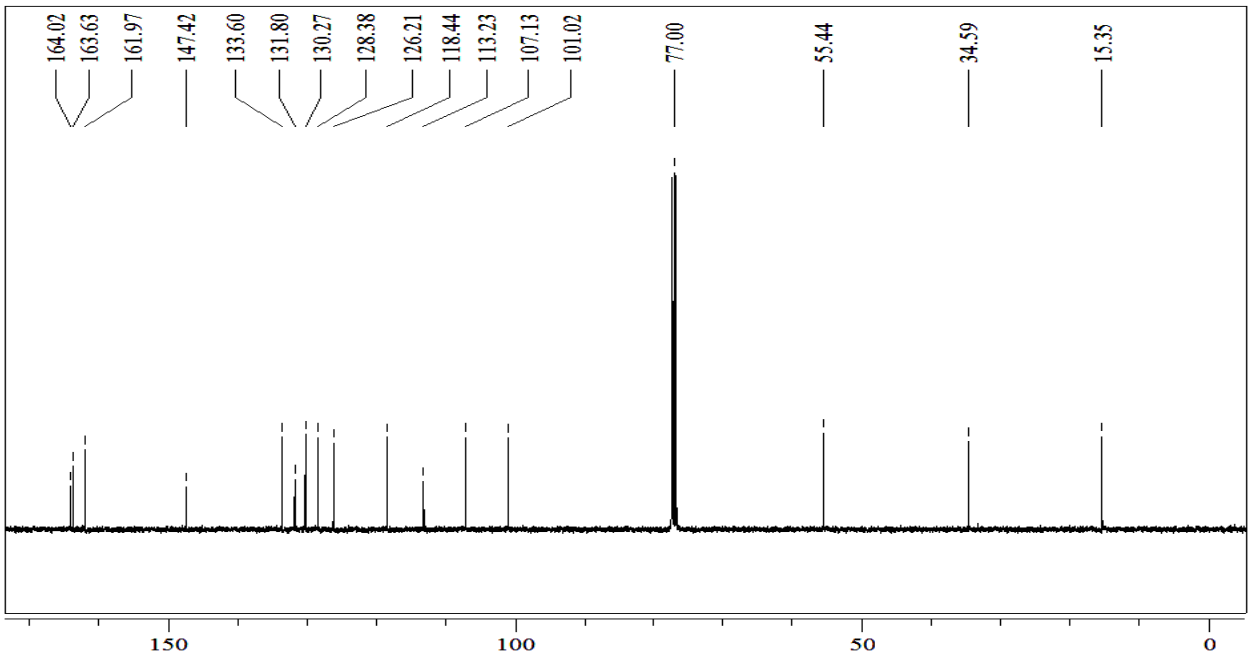

Fig. 3.10 ^{13}C–NMR spectrum (100 MHz) of pMS–2MT in $CDCl_3$

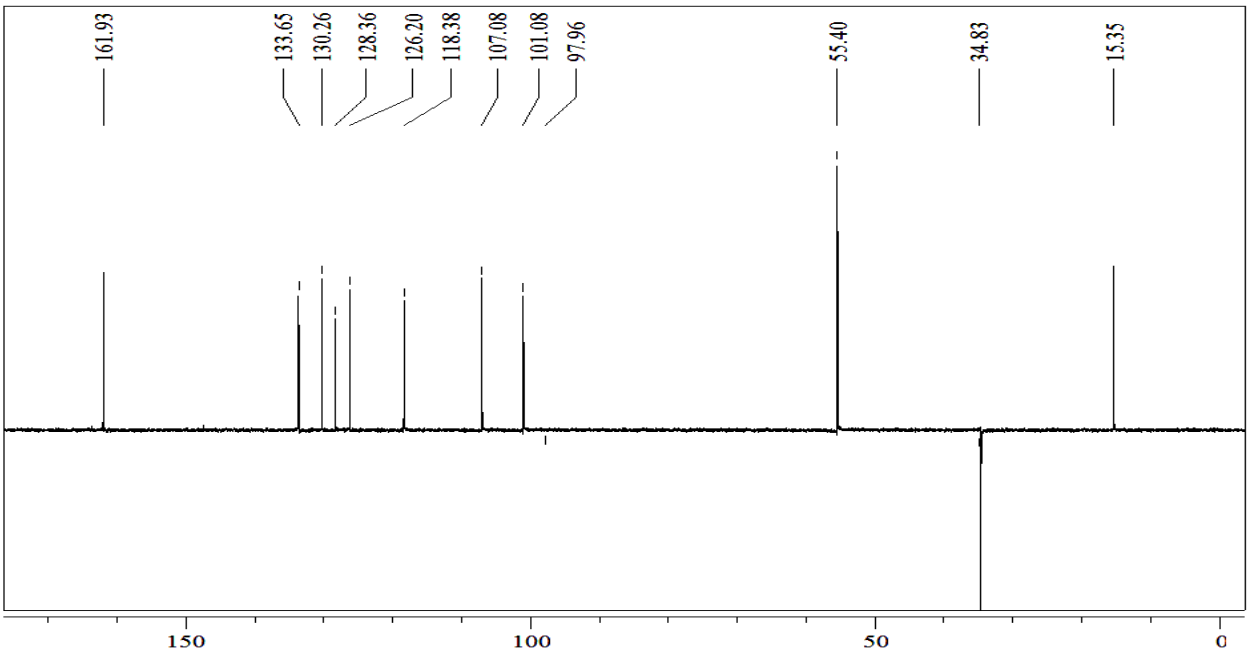

Fig. 3.11 DEPT135 NMR spectrum (100 MHz) of pMS–2MT in $CDCl_3$

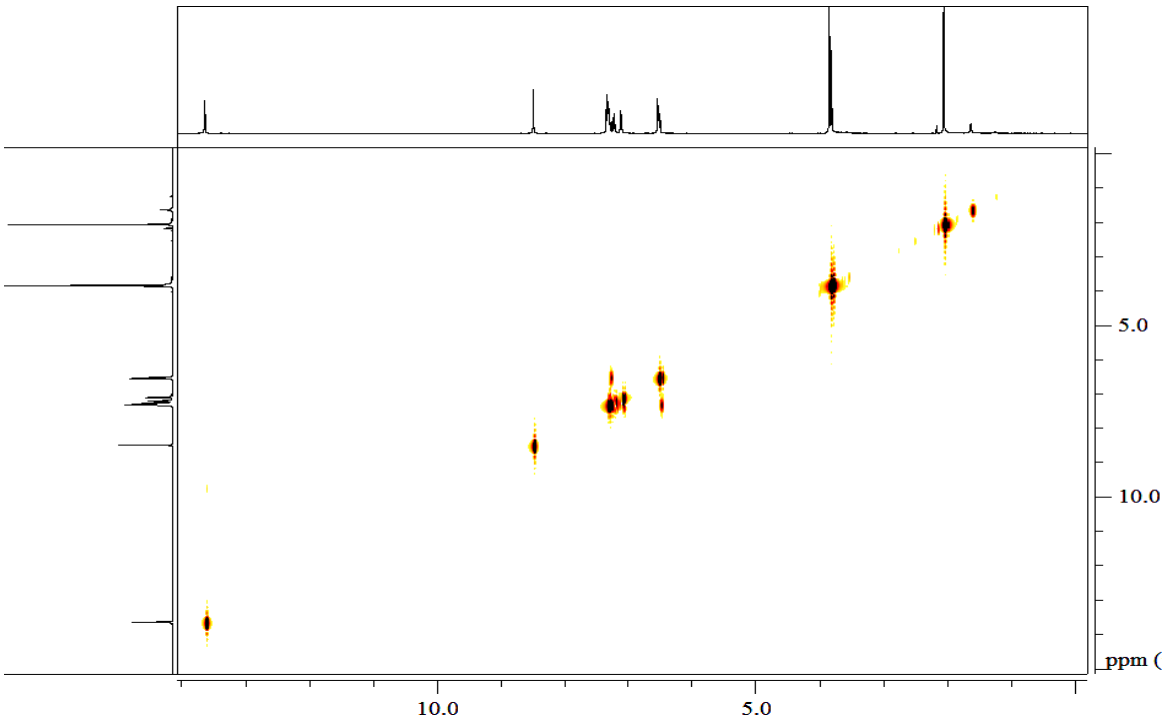

Fig. 3.12 COSY 2D-NMR spectrum (100 MHz) of pMS–2MT in $CDCl_3$

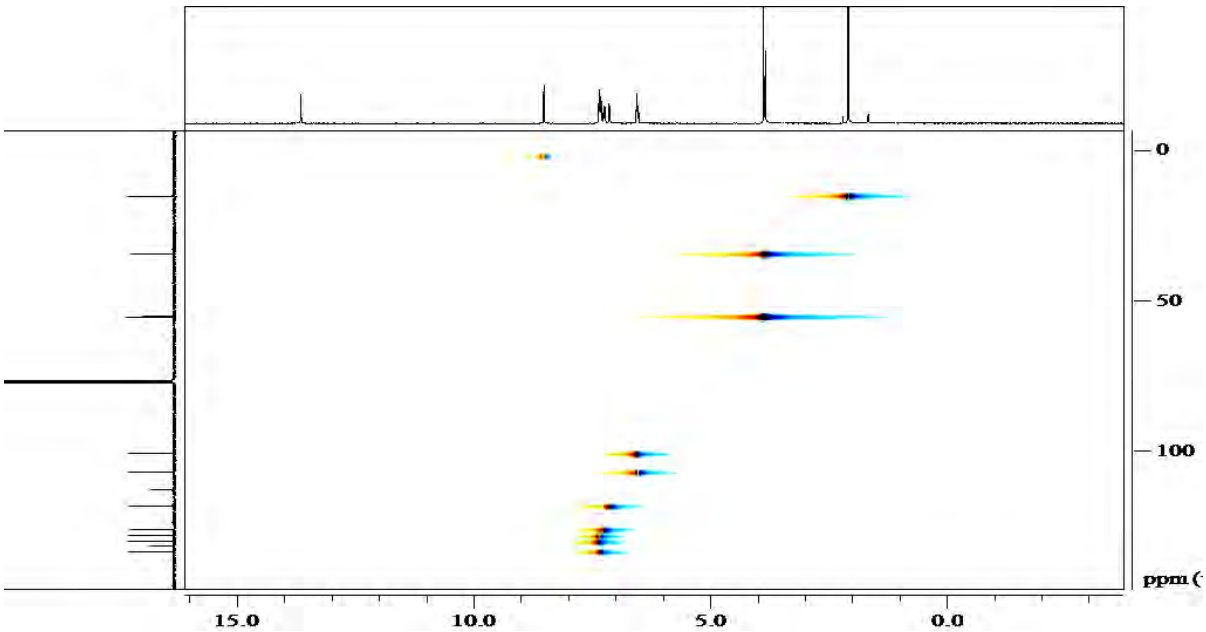

Fig. 3.13 HSQC 2D-NMR spectrum of pMS–2MT in $CDCl_3$

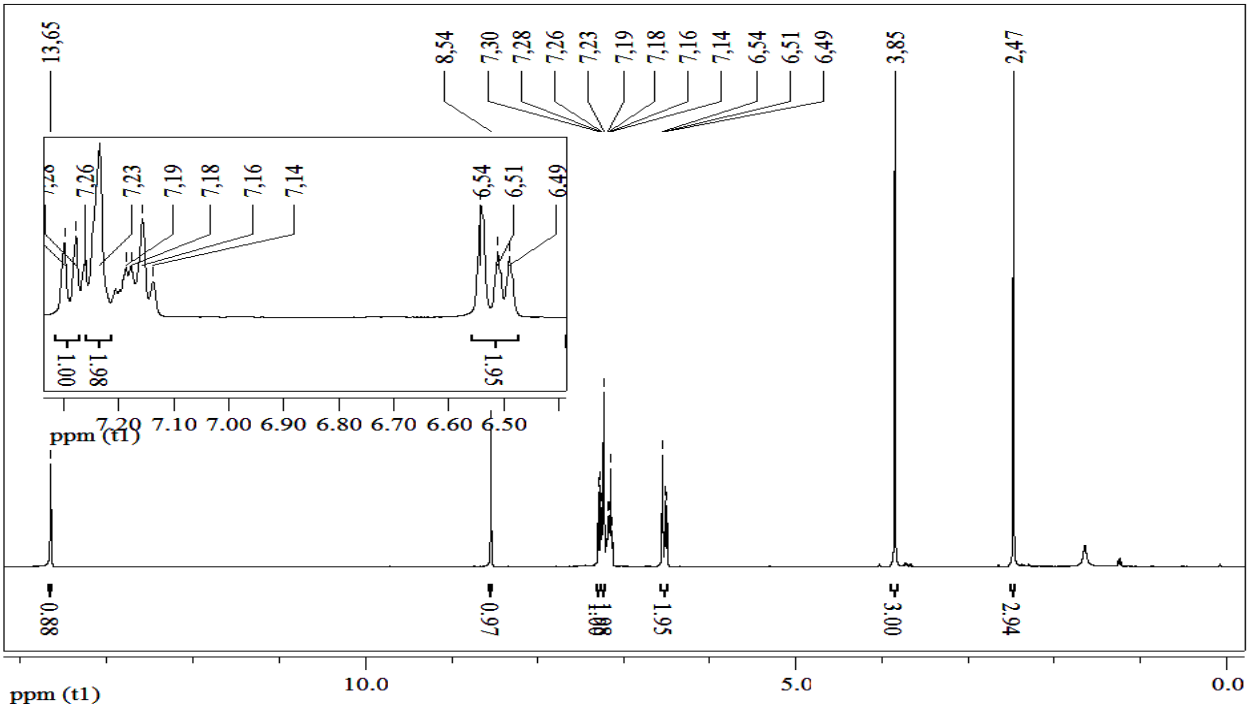

Fig. 3.14 ^{1}H-NMR spectrum (400 MHz) of pMS–2MA in $CDCl_3$

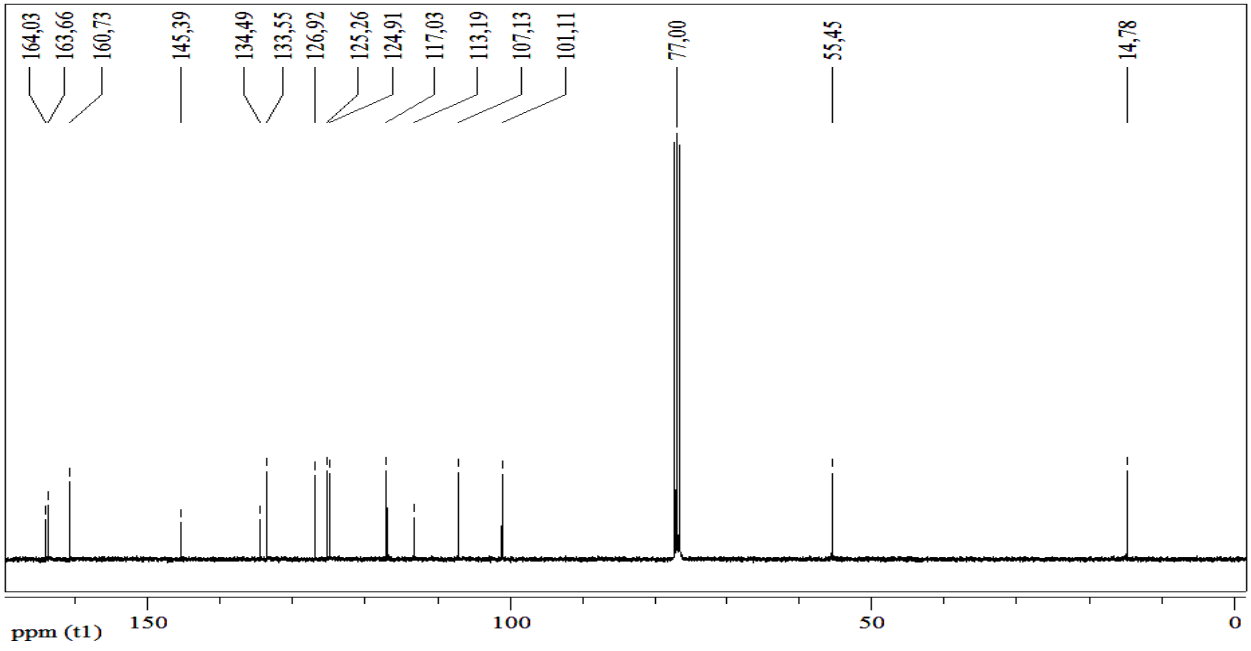

Fig. 3.15 ^{13}C-NMR spectrum (100 MHz) of pMS–2MA in $CDCl_3$

3.4 MID INFRARED SPECTRA OF 2MT AND 2MA LIGANDS

The mid infrared spectra were obtained for the thiomethylated ligands, the Schiff-bases and their metal(II) complexes in the region 4000 – 650 cm^{-1} and their corresponding values are recorded in **Tables 2.15–2.19**. The vibrational frequencies in the 2MT and 2MA ligands found within this range include those characterized by primary amines such as N–H stretches, NH_2 scissor bend, NH rock and C–N stretch. The N–H asymmetric and symmetric stretches are usually found in the region 3500 – 3300 cm^{-1}, NH_2 bend around 1590 – 1600 cm^{-1}, C–N stretch around 1280 cm^{-1} and NH rock near 800 cm^{-1} for aromatic primary amines.[18] The bands expected from the thioether group due to C–S–C bend (around 1100 cm^{-1}) and C–S stretch (650 – 780 cm^{-1}) were not observed as they are weak bands.[19] The discussion will focus on N–H (asymmetric and symmetric) and C–N stretches as these are usually shifted on chelation.

The N–H stretches were assigned using the equation given by Bellamy and Williams[20] for predicting N–H asymmetric and symmetric stretches in primary amines where more than two bands are observed. As some of these ligands were already reported and because they bear similarity with aniline, the frequencies of the vibrating groups were confirmed by comparing with values in literature, those of aniline[21-23] and other related compounds in the literature.[24-28]

3.4.1 N–H asymmetric and symmetric stretches

Two N–H stretches are usually expected in the primary amine group in the thiomethylated anilines, asymmetric stretch being higher in frequency than the symmetric.

2MT ligands

As expected two N–H bands due to asymmetric and symmetric stretches were observed in the regions 3446 – 3398 cm^{-1} and 3346 – 3317 cm^{-1} respectively for these ligands. A third shoulder band described[24] as the overtone of the NH_2 bending mode was observed in the ligands around 3200 – 3100 cm^{-1}. The spectra of these ligands are shown in **Fig. 3.16** and **3.17**.

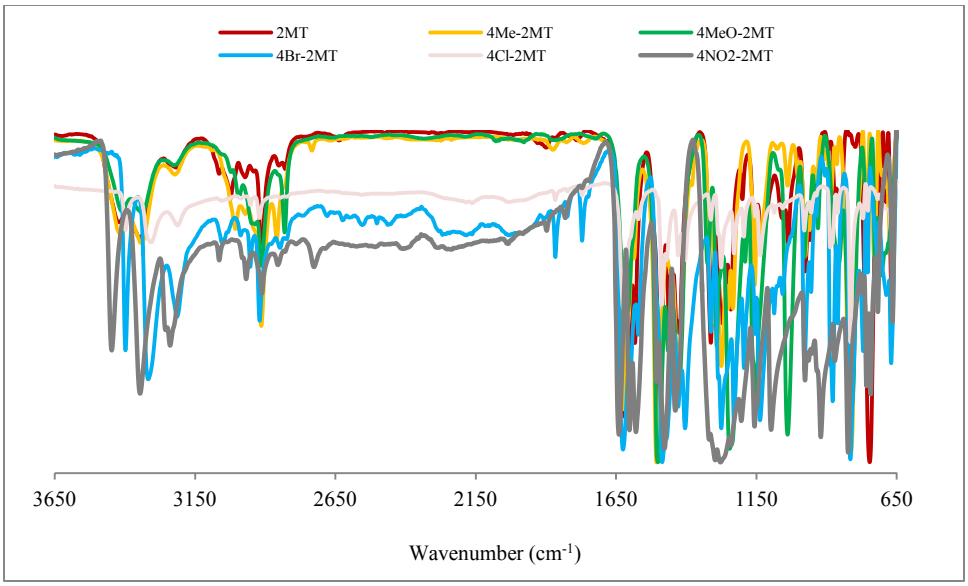

Fig. 3.16 Mid IR of 2MT and *para*-substituted ligands

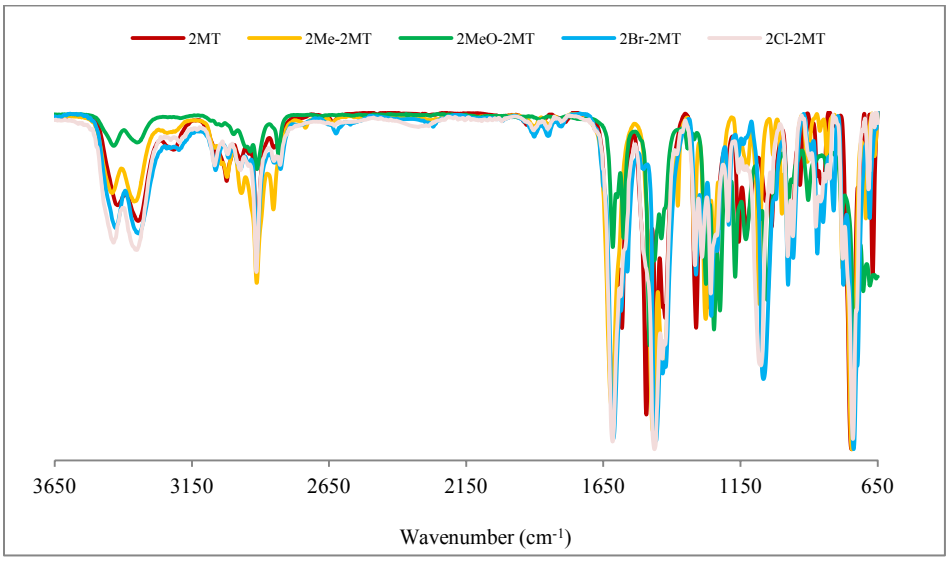

Fig. 3.17 Mid IR of 2MT and *ortho*-substituted ligands

2MA ligands

Both N–H asymmetric and symmetric stretches were likewise observed in the ranges 3459 – 3383 and 3355 – 3293 cm^{-1} respectively and the shoulder band is also observed in the region 3200 – 3150 cm^{-1} (**Fig. 3.18–3.19**). Maji *et al*[29] and other groups[30,31] who previously reported the synthesis of 2MA assigned the infrared frequencies of N–H asymmetric and symmetric stretches, N–H shoulder stretch, NH_2 scissor bend and C–N stretch infrared frequencies in the ranges 3470 – 3424, 3365 – 3325, 3080 – 3050, 1600 – 1610 and 1300 – 1310 cm^{-1} respectively.

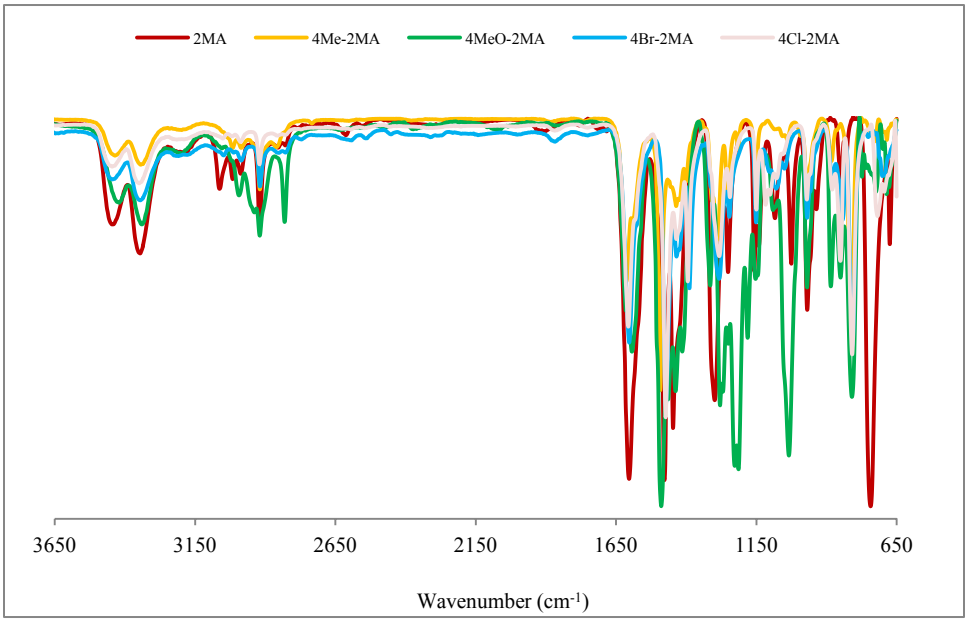

Fig. 3.18 Mid IR of 2MA and *para*-substituted ligands

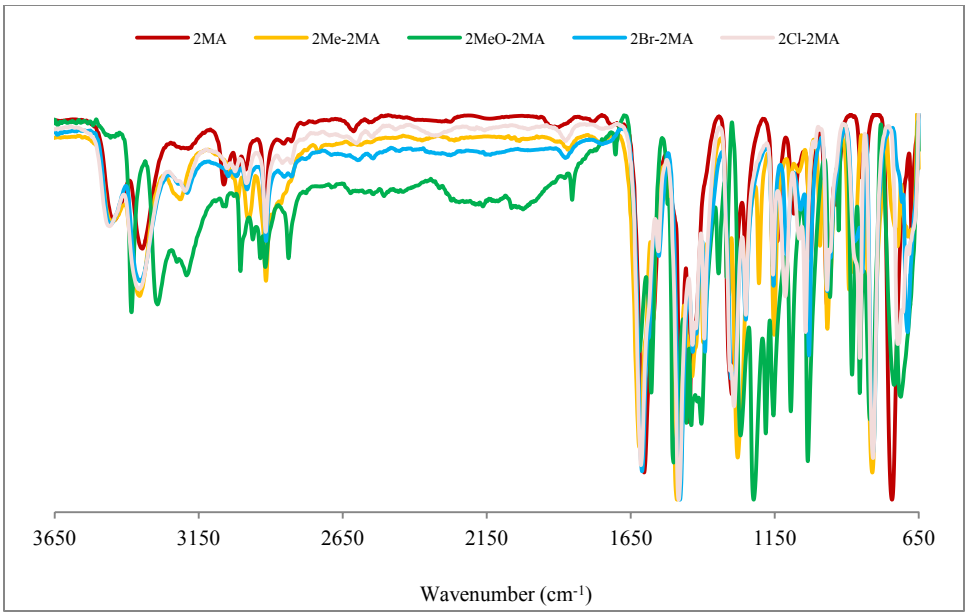

Fig. 3.19 Mid IR of 2MA and *ortho*-substituted ligands

Comparative studies

1. *Ortho*/para substitution effect: Both N–H stretches in *ortho*-substituted ligands absorb at higher frequencies in comparison with those of the *para*-substituted analogues in 2MT ligands. This is in perfect agreement with the observation made with the effect of position of substituent on the NMR frequencies of amine protons. It could be recalled that with *ortho*-substitution, the amine protons absorb at higher frequencies, being shifted downfield in comparison with same substituent at the para position. Similar pattern is observed with 2MA ligands with *ortho*-substituted ligands absorbing at higher frequencies.

2. Electronic effect of substituent: Considering the effect of the nature of ring substituent on N–H stretches, the electron donating groups absorb at higher vibrational frequencies than the withdrawing groups in 2MT ligands, the exception being the nitro–substituted compounds.

An opposite effect is observed with 2MA ligands where the withdrawing groups have higher frequencies than the donating groups. This has a direct relationship with the amine protons chemical shifts where higher frequencies are observed with electron withdrawing substituents.

3. Effect of thioether position: The frequencies of vibrations due to asymmetric stretch of N–H in 2MT ligands are generally lower than those of their corresponding 2MA ligands. The only exception is the *ortho*–methoxy substituted 2MA with a lower frequency. The higher frequencies observed in 2MA ligands could be as a result of electron contribution of the comparatively electronegative sulfur of the thioether to the aromatic ring which reduces the electron density on nitrogen lone pair of electrons. Consequently, the N–H bond of 2MA derivatives has more electron density. In 2MA ligands, the effect of sulfur direct attachment to the aromatic ring is not expected to have a direct bearing on the substituent since S is *meta* to the substituent at both the para and *ortho* positions. Its effect is however directly on the nitrogen to which it is proximal.

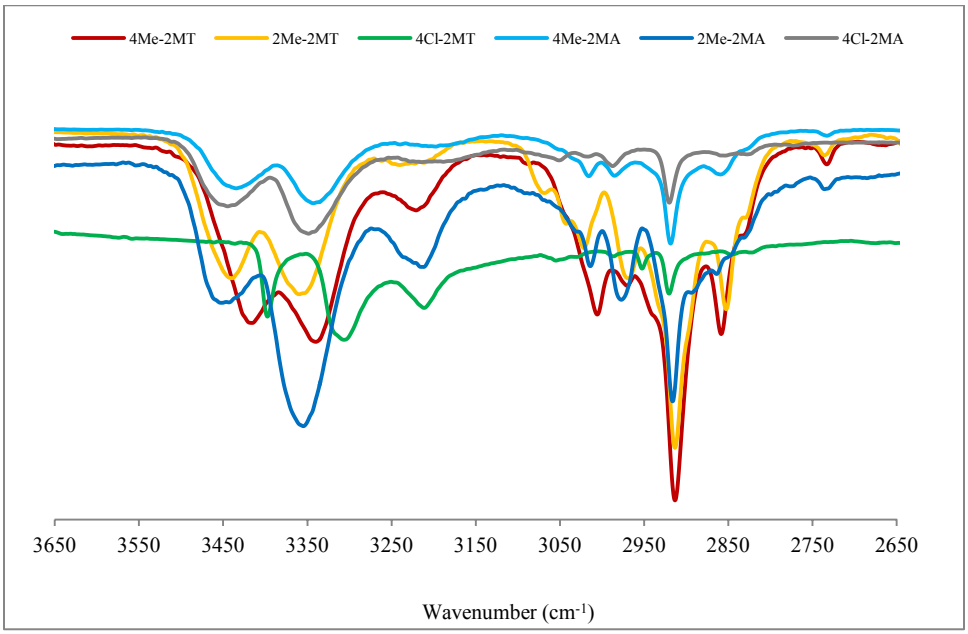

Fig. 3.20 Comparison of N–H frequencies in selected 2MT and 2MA ligands

3.4.2 C–N stretch

The C–N band in aromatic aniline compounds is expected around 1280 cm^{-1}. This was observed in the range 1269 – 1330 cm^{-1} in both ligands; the higher frequencies in 2MA ligands are consistent with what is observed in their N–H frequencies. The only exception is the *para*-methoxy compound (**Fig. 3.21**) which absorbs at a lower frequency.

The effect of position of substituent on the C–N frequency is also consistent with what was observed on the N–H stretch in 2MT ligands, the *ortho*-substituted ligands absorb at higher energies. In contrast, the trend is reversed for 2MA ligands as the electron donating groups in the *ortho*-substituted show lower frequencies compared to their para analogues and *vice versa* for the electron withdrawing groups.

The electronic nature of substituent does not seem to show any significant effect on the C–N stretch in 2MT ligands as there is no consistent linear trend observed. 2MA ligands show similar trend in C–N stretch as with N–H stretch, with electron withdrawing groups absorbing at higher frequencies than the withdrawers. This may reflect the vagrancies associated with the differences in vibrational coupling experienced by substituted benzenes when comparing different substitution patterns.[32]

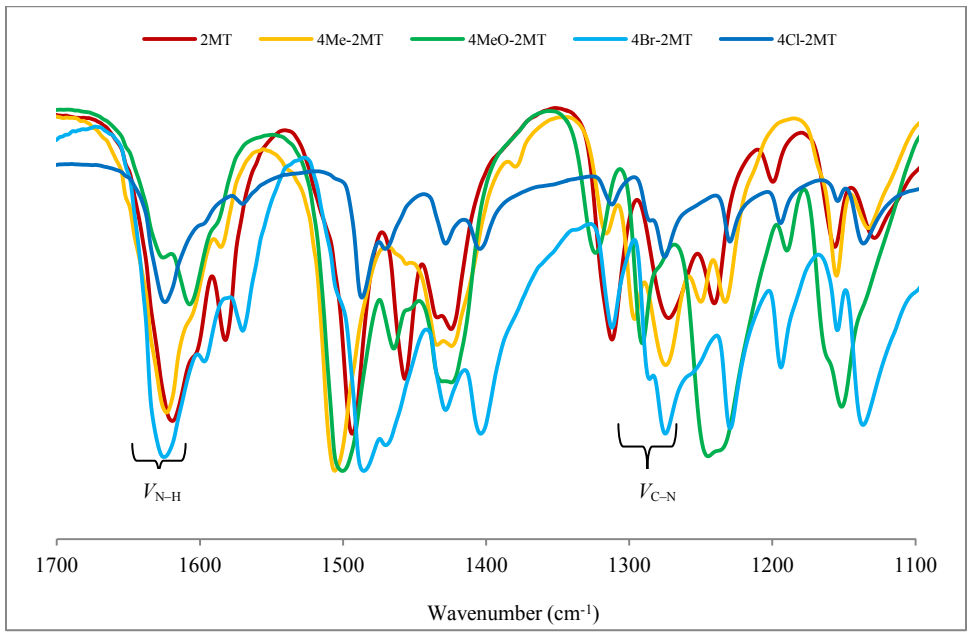

Fig. 3.21 NH_2 bend and C–N stretches in selected 2MT ligands

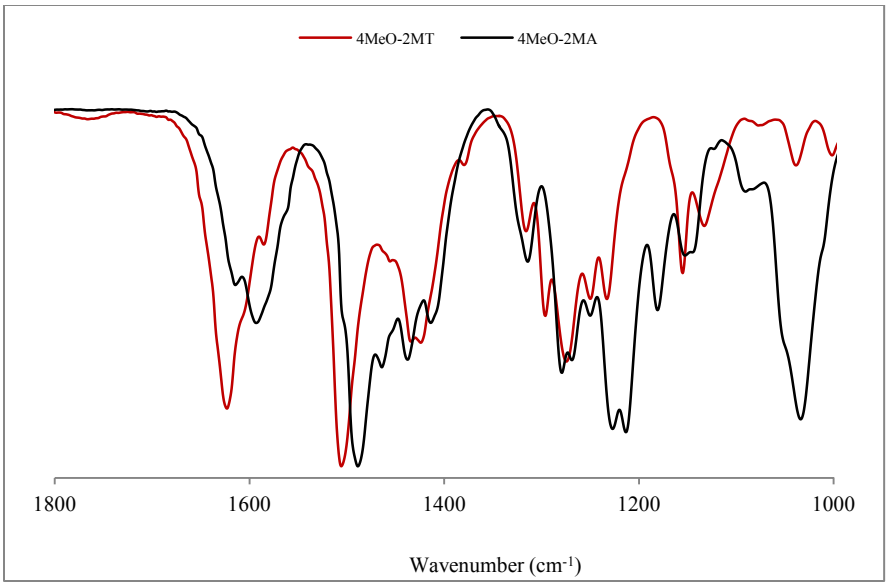

Fig. 3.22 Comparing the NH_2 bend and C–N stretch of *para*–methoxy 2MT and 2MA

3.5 MID AND FAR INFRARED SPECTRA OF 2MT AND 2MA METAL COMPLEXES

In the infrared spectra of these complexes, the bands of interest are those associated with amine group commonly found in the mid infrared region and those attributable to metal–ligand vibrations found in the far infrared region of the spectrum. As the ligands used in this study are of SN donor type and the metal chloride salts were used for complexation, metal to ligand vibrations expected are M–N, M–L and M–S stretches. From the elemental analysis results, there was no deprotonation of the amine protons on complexation and the two N–H stretches are observed in the mid infrared region. The corresponding Raman shifts could not be obtained for the metal complexes of the 2MT and 2MT ligands as they fluoresced under the laser beam and the spectra were obscured.

3.5.1 N–H stretches

It is well known that aniline compounds show intra- and inter-molecular hydrogen bonding and the extent of the bond is determined by the nature of the amine. The tendency to form hydrogen bonds is very strong in ammonia and primary amine complexes, except when the NH_2 group of the amine is sterically hindered. In secondary amine complexes, the tendency is very slight.[16] Hydrogen bonded N–H bands are observed in the spectra of some of the complexes used in this study, especially those of 2MA complexes and the nickel complexes in general. The N–H stretches were assigned using the equation given by Bellamy and Williams[20] for N–H asymmetric and symmetric stretches in primary amines, where more than two possible N–H bands were observed as a result of intra- and inter-molecular hydrogen bonding. The *ortho*-substituted complexes show greater deviation (**Tables 3.16 and 3.18**) from the standard deviation of 4.8 cm^{-1}, indicating the amino hydrogen atoms may not be equivalently hydrogen bonded.

Both N–H asymmetric and symmetric stretches are lowered in the complexes. The shift to lower frequency of these stretches upon chelation has been interpreted to be the result of the electron density of the nitrogen being directed to the metal ion, leaving the amino protons less tightly bound to the nitrogen.[33] N–H frequencies observed in 2MT complexes generally occur at higher frequencies than those in 2MA complexes, hence the magnitude of the N–H frequency shift, $\Delta\nu_{N-H}$ ($\Delta\nu_{N-H} = \nu_{N-H(ligand)} - \nu_{N-H(complex)}$) for the former is smaller relative to the analogous 2MA complexes. The complexes of 2MA ligands are abundantly hydrogen bonded as could be seen from their N–H stretches (**Fig. 4.14**). Hence they display far lower frequencies in comparison to their analogous 2MT complexes. The magnitude of the N–H frequency shift should reflect the strength of the bonding interaction between the metal ion and the ligand nitrogen. A large $\Delta\nu_{N-H}$ indicates strong metal–ligand vibration.

Apart from the bathochromic shift experienced by N–H bands on coordination, another effect is the hyperchromic shift of the bands to higher absorptions. The formation of M–N bonds by a coordinating group having one or more N–H bonds increases the electron demand of the nitrogen and therefore increases the polarity of the N–H bonds. This induces an increase in change in the N–H dipole moment during vibration, resulting in an increase in total absorption.[34] Most of the metal complexes show both bathochromic and hyperchromic shift of their N–H bands, as seen from **Fig. 3.23 and 3.24** that the N–H of metal complexes show stronger absorptions and are shifted to lower energies on chelation. No consistent trend was shown among the three series of complexes that could be used to judge the coordinating ability of Co(II), Ni(II) or Cu(II) ions in these complexes.

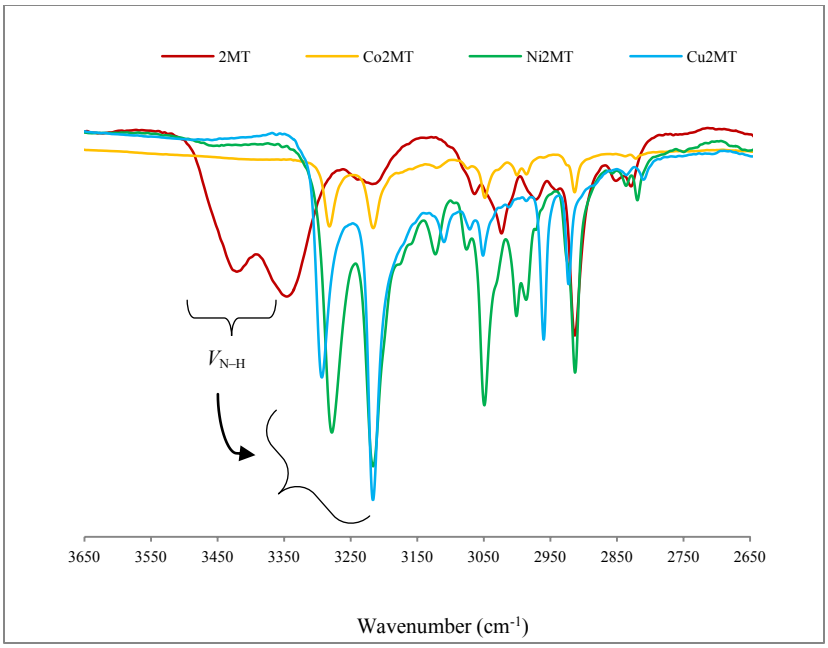

Fig. 3.23 Effect of coordination on N─H bands of 2MT and complexes

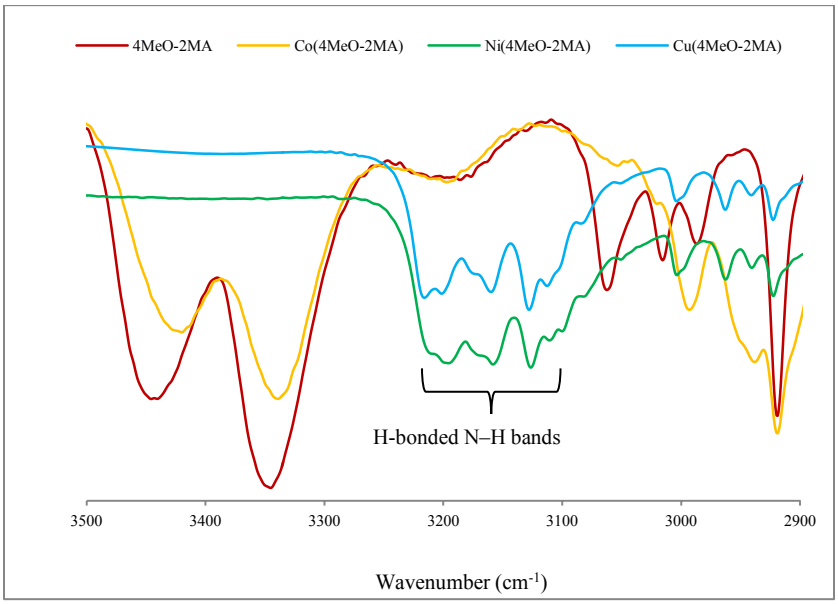

Fig. 3.24 Hydrogen bonding and effect of coordination on NH bands in 2MA ligands

3.5.2 C–N stretch

C-N shifts to lower frequencies on complexation as expected as a result of decrease in the C=N double bond character. Similar trend was also observed in the shift of this band in the complexes of both series of ligands (**Fig. 3.25**). The absorption intensity of the bands also reduces on complexation.

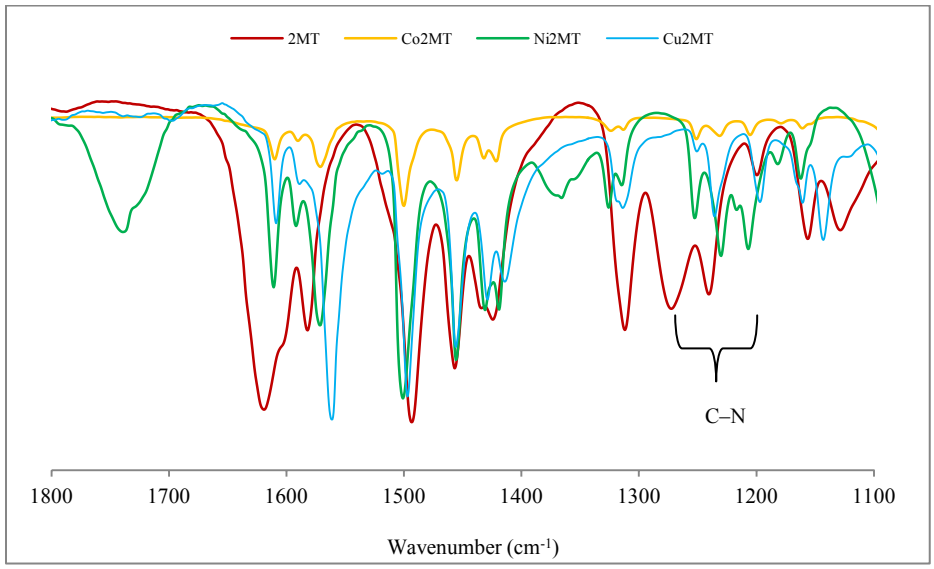

Fig. 3.25 Shift of ν_{C-N} on coordination in 2MT ligands

3.5.3 Metal to ligand vibrations

The assignments here will be complicated by the appearance of metal sensitive torsional ring vibrations on chelation, which appear in this region. The greater vibrational coupling experienced within the far infrared could also complicate the spectra.[35,36] The metal complexes used in this study do not show a consistent trend in metal–ligand vibrations. As a result, no correlation could be made between the coordinating ability of metal ions in terms of the effect the position or the electronic nature of substituents on the aromatic ring has on the metal–ligand frequency. In general, the nickel and cobalt complexes behave similarly as the infrared absorptions of their metal–ligand vibrations occur at same or nearly equivalent frequency. This is expected if they are isostructural in the solid state. The copper complexes are non-isostructural. Hence both nickel and cobalt complexes will be jointly discussed.

3.5.3.1 M–N stretch

In the 2MT complexes, the only band attributed to M–N stretch occurs in the region 380–440cm^{-1} for all the complexes with medium absorption. A large $\Delta\nu_{N-H}$ should indicate strong metal–ligand vibrations. In the complexes, no correlation could be seen between the change in shift of either the asymmetric or symmetric N–H stretch on chelation and M–N stretch. **Fig. 3.26** gives an overview of these M–L stretches.

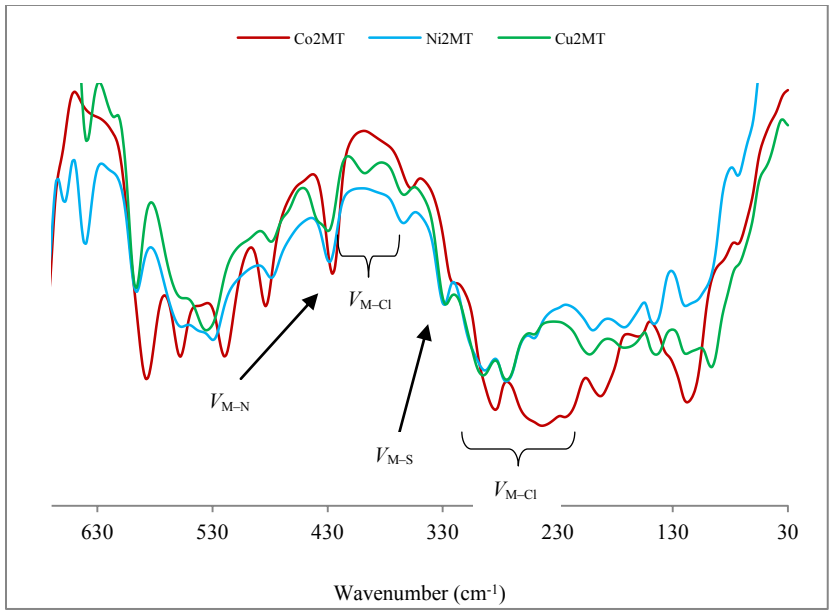

Fig. 3.26 Metal to ligand vibrations in metal complexes

Most 2MA complexes show two bands in the region 370 – 435 cm^{-1} and these have been assigned to M–N stretches. That one band is observed in a few cases like in the *ortho*-substituted 2MA copper complexes could be that the octahedral structure is more perfect here and the two M–N bonds being in a perfect trans position absorb at same or almost equal frequency. The methoxy group has the highest frequency for the M–N stretch, confirming it stabilizes the complex and subsequently the metal–ligand vibration with its electron donating property. Conversely, the electron withdrawing halogens are seen with lowest M–N values. The methoxy group seems to be able to perturb the structure of the molecule effectively by strongly influencing the electronic distribution of participating atoms.

Considering the trend in M–N frequency from Co(II) to Cu(II), no noticeable trend exists. Since the nature of M–N bond in coordination compounds has been shown to depend on the charge of the metal ion, the type of available bonding orbitals, the hybrid state of the nitrogen, and the tendency of the metal to form covalent bonds; the change of substituents on the aromatic ring and the oxidation state of the metals being the same may not be sufficient to cause a noticeable change in M–N bond. It has been shown in a series of amine complexes, where the charge on the metal ions increased from +l to +3, that there was a corresponding decrease in the absorption frequency of the coordinated N–H bands.[19]

3.5.3.2 M–Cl stretch

The vibrations due to M–Cl stretches consist of a mixture of medium and intense band in all the complexes. For copper complexes of 2MT ligands, the first set of bands is found in the range 335–400 cm^{-1} and the second set absorbs in the region 266 – 303cm^{-1}. The higher M–Cl vibrations are assigned as terminal chlorine bonding to Cu^{2+} while the lower frequency vibrations are due to those vibrations in which the chlorine is bridging. This is confirmed by the crystal structure of $[Cu(4NO_2\text{-}2MT)Cl_2]_2$ which shows a planar arrangement of the atoms around the Cu^{2+} center whereby the 2 chloride ions are *cis* to each other and one of them is involved in an axial bridging bonding with the Cu^{2+} of the adjacent molecule. This gives rise to different M–Cl vibrations in which the terminally bound Cl^- absorb at a higher frequency than the bridging Cl^-. In addition, two bands are usually expected from interactions of 2 chloride ions in a *cis* arrangement with same metal ion in a planar structure.

M–Cl vibrations in nickel and cobalt complexes occur at lower frequencies than those of copper complexes. This is as a result of change in geometry from the five–coordinate copper(II) to (distorted) octahedral Ni(II) and Co(II), decrease in M-Cl bond frequency is expected as the coordination number of a particular metal ion increases.[37]

The two sets of M–Cl absorptions are found in the ranges 317–347 cm^{-1} and 220–261 cm^{-1}. The first set of bands is assigned to M–Cl bands in a distorted pseudo–octahedral trans configuration in both complexes where only one or two such bands is (are) expected depending on how symmetrical the 2 chlorine trans bonds are to each other. The lower frequency vibrations have been attributed to other low symmetry components arising from M–Cl vibrations.[37]

Only one set of M–Cl bands is observed in Cu(II) complexes of 2MA ligands in the range 258–311 cm^{-1}. This indicates another type of arrangement around the copper center where all the chloride ions are bridging two metal centers to form an octahedral geometry round each metal ion, as suggested by the lower frequencies of these M–Cl bands. In 2MT copper complexes, only one chloride ion is bridging two metal centers.

One M–Cl band is observed around 325–347 cm^{-1} in nickel and cobalt complexes, indicating the 2 chlorine ions are in trans configuration in the structures. An additional band of higher frequency (364 cm^{-1}) is seen in the methoxy substituted complexes perhaps as a result of different spatial orientation of the compound with the presence of the strongly donating methoxy group.

Two more bands associated with M–Cl bands are observed for 2MA complexes in the region 200–260 cm^{-1}. Such bands have been similarly reported by Ikram.[37]

3.5.3.3 M–S stretch

The vibrations due to M–S stretch are found to be of weak, medium or strong intensity depending on the coordination environment. As it is in the case of the other metal–ligand stretches, M–S vibrations absorb at higher energies in copper complexes (between 315 and 350 cm^{-1}) than in the nickel and cobalt complexes (260 – 310 cm^{-1}) of 2MT ligands. Following similar trend, those of 2MA complexes absorb in the ranges 320 – 360 cm^{-1} and 270 – 307 cm^{-1} for the copper complexes and other two complexes respectively.

The only indication of a higher geometry obtainable in Ni and Co complexes compared to Cu complexes is the lower frequencies of the M–Cl and M–S bands observed in the former. Metal–ligand vibrations are lowered as the coordination number of metal ion increases.

The shift to lower energies of the M–S bands in complexes of 2MA ligands could be as a result of the conjugation of the lone pairs of the thioether sulfur with the aromatic ring which reduces their availability for binding with the metal ions whereas those of the 2MT complexes are more available and strengthens the bonding to attached metal ions.

As mentioned earlier, no trend with respect to effect of electronic nature or position of substituent is seen on these vibrations as was observed in N–H stretch. However a trend can be seen when the metal–ligand

vibrations of 2MT and 2MT complexes are compared; in general those of the former absorb at higher frequencies than those of their analogous 2MA complexes.

In the metal(II) complexes studied by Kratzl[23], the trend observed for $\Delta\nu_{(N-H)}$ was of the order Zn (210 cm^{-1}), Cu (240 cm^{-1}), Co (255 cm^{-1}), Ni (270 cm^{-1}), Pd (300 cm^{-1}), which is an indication of the bond strength between the metal ion and nitrogen. Similar trend is observed for complexes of unsubstituted ligands but no longer holds as substituents are added to the ring, which could imply that the electronic nature of some of the substituents are not defined in certain positions on the ring. For example, the methoxy group also has a negative inductive effect from its electronegative oxygen atom, especially at the *ortho* position aside its electron donating tendency as a group. This can be confirmed by its deviations in certain observations made above.

The following summary can be made for the observations in the infrared spectra of 2MT and 2MA ligands and complexes:

There seems to be a correlation between the NMR shifts of amine protons and N–H IR asymmetric stretch frequencies from the consideration of *ortho*/para position of substituents in 2MT ligands but not with electronic nature of substituent. This implies the electronic nature of the substituents used here does not significantly affect the property of 2MT ligands. For 2MA ligands, the position as well the electronic nature of substituents as reflected in the NMR shifts of amine protons have a linear relationship with the N–H infrared asymmetric stretch frequency.

In the study, 2MA ligands are consistent in the effect of electronic nature on NMR shifts and IR stretches observed, the electron withdrawing groups deshielding more effectively the amine protons and decreasing the amine conjugation, consequently increasing the N–H frequency. The 2MT ligands however show consistency in the effect of the position of substituent, the *ortho*-substituted compounds deshielding the amine protons more effectively and decreasing the amine conjugation, consequently increasing the N–H frequency.

This difference in behavior of these two series of ligands could be due to inequality of hydrogen bonding of the amine protons, as the N–H stretches of the *ortho*-substituted ligands do not obey closely the relationship proposed by Bellamy[17] for NH symmetric and asymmetric stretches, the standard deviation being much higher than 4.8 cm^{-1}.

3.6 INFRARED SPECTRA AND RAMAN SHIFTS OF SCHIFF-BASE LIGANDS AND COMPLEXES

The N–H stretches observed in the spectra of the reacting 2MT/2MA amine ligands are absent in the IR spectra of these Schiff-bases. Strong bands characteristic of the azomethine C=N stretches[38] are seen in the region 1600-1610cm^{-1}. The infrared spectra of imines shows that the C=N stretching frequency absorb in the region between 1680 and 1603 cm^{-1} when H, alkyl or phenyl are bonded to carbon and nitrogen atoms.[38] The broad band due to the phenolic O–H vibration in the ligands is not observed as a result of involvement of its hydrogen in intramolecular bonding with the azomethine nitrogen.[16] The phenolic O–H was deprotonated on complexation and this was confirmed by the crystal structures of the complexes (**Figures 3.48** and **3.49**). The frequencies of C=N stretches are lowered by 5-20 cm^{-1} while those of C–O stretches (1328-1342 cm-1) are shifted to higher frequencies by 20-40 cm^{-1} as a result of coordination of azomethine nitrogen and phenolic oxygen respectively to the metal centre.[39]

New bands of medium intensity appear in the far infrared region of the complexes in the range 430 – 467 cm^{-1} and are assigned as Cu–O stretches in an octahedral field. Another set of bands of medium intensity are seen between 380 and 429 cm^{-1}; these are due to Cu–N stretching modes.

The Raman shifts for each of the groups that are Raman-active were found close to the IR values (allowing for instrumental calibration issues) confirming their assignments. The Raman and IR spectra for the ligands and their complexes are shown by **Fig. 3.27**–**3.41**.

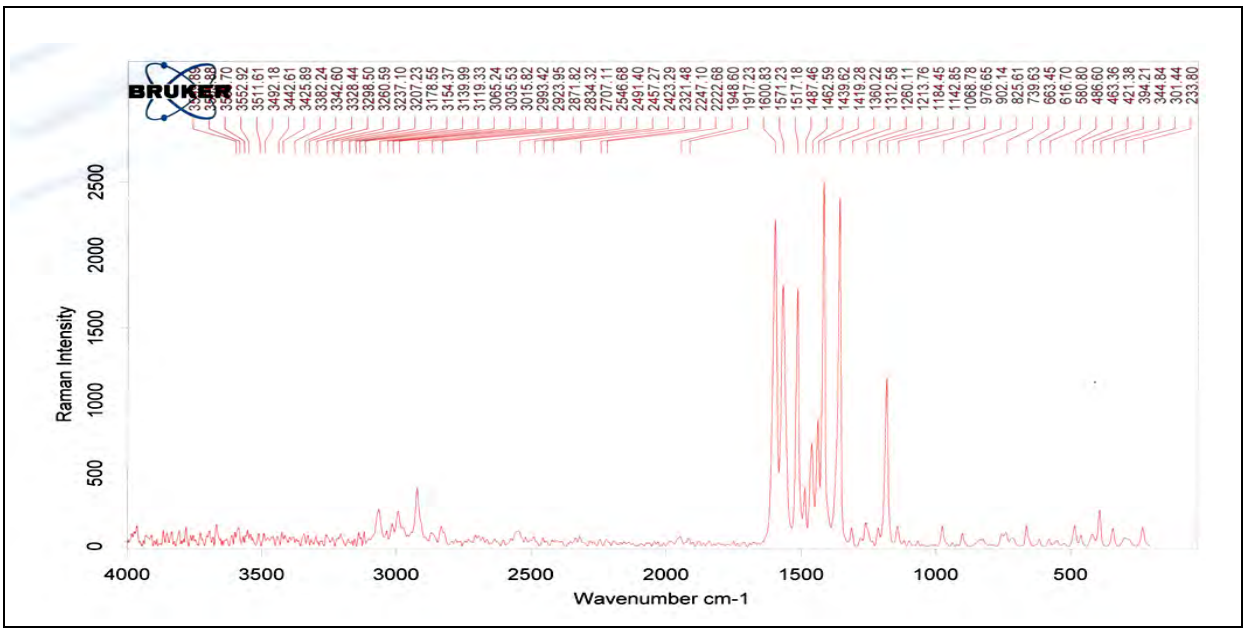

Fig. 3.27 Raman spectrum of [Cu(pMS–4Cl2MA)$_2$]

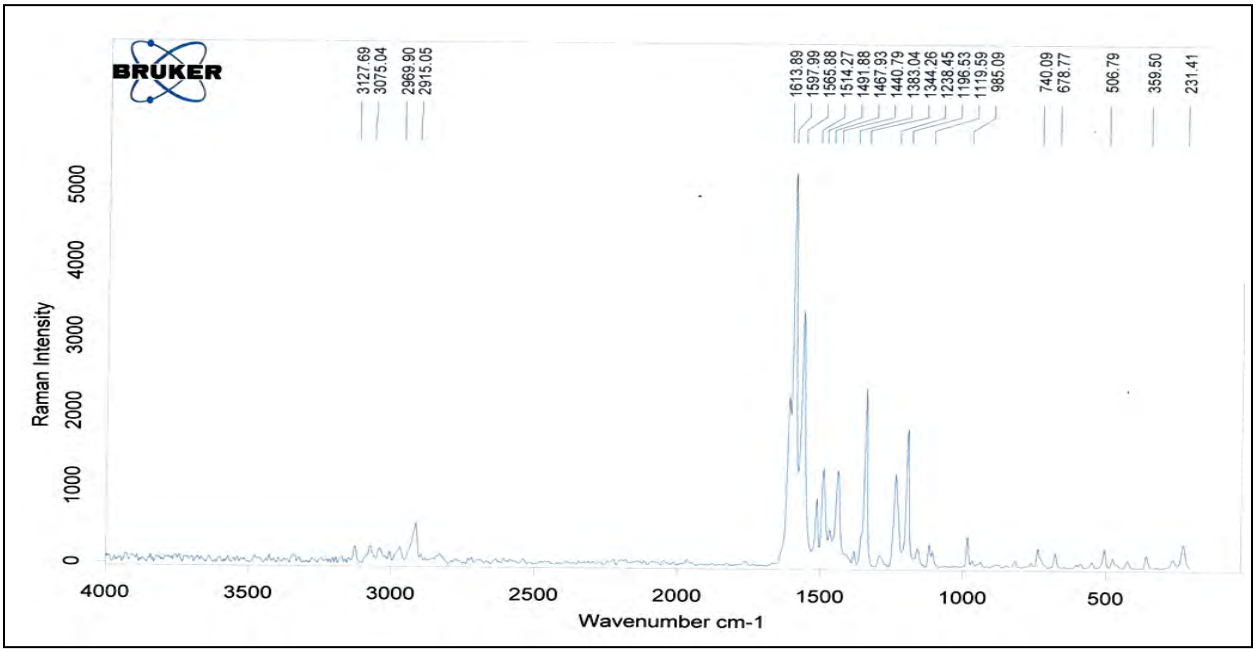

Fig. 3.28 Raman spectrum of pMS–4Me2MT

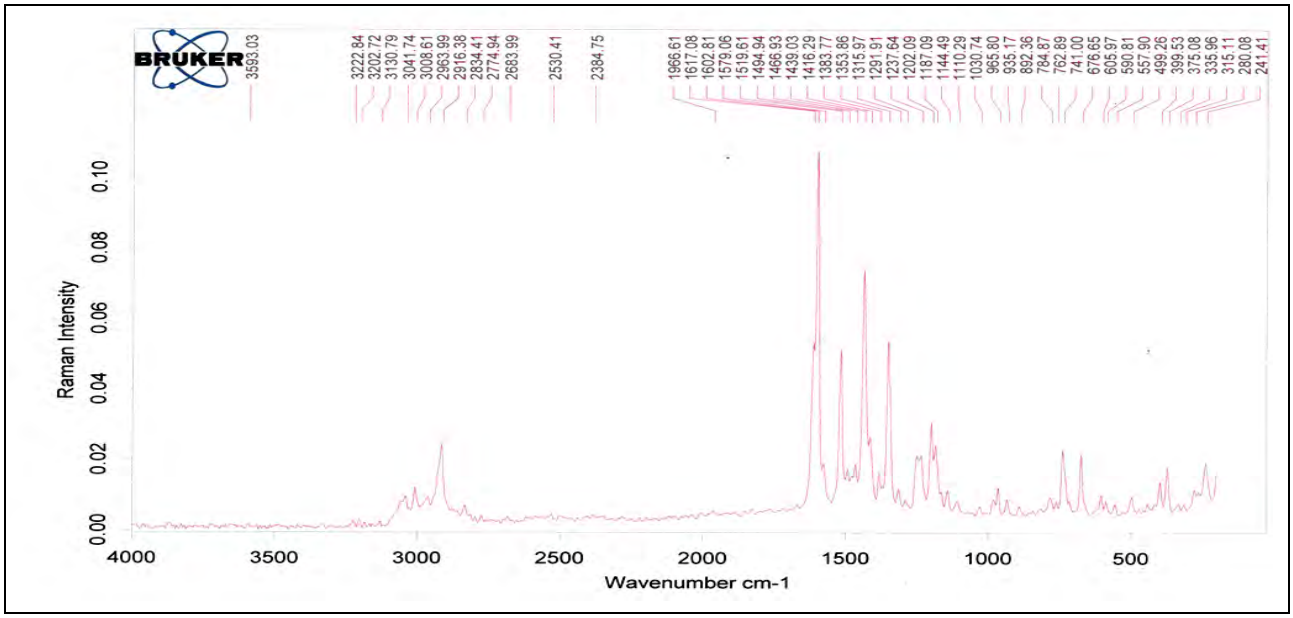

Fig. 3.29 Raman spectrum of [Cu(pMS–4Me2MT)$_2$]

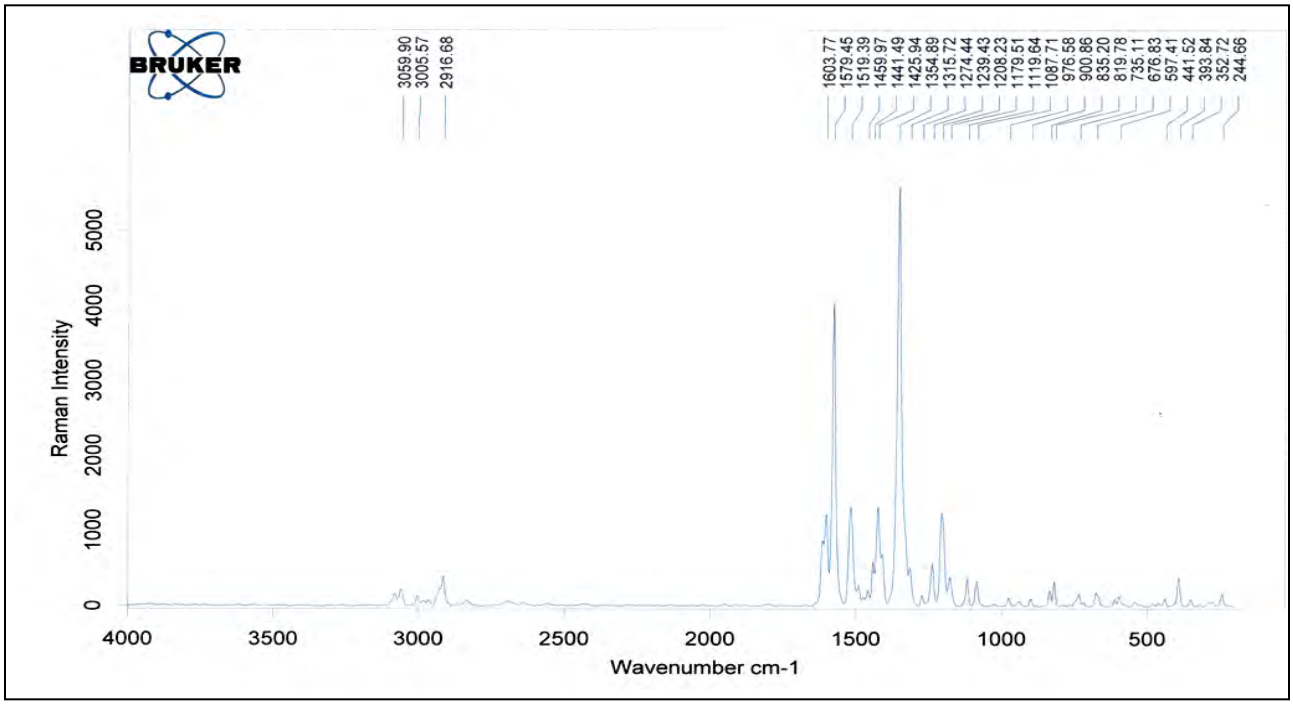

Fig. 3.30 Raman spectrum of [Cu(pMS–4MeO2MT)$_2$]

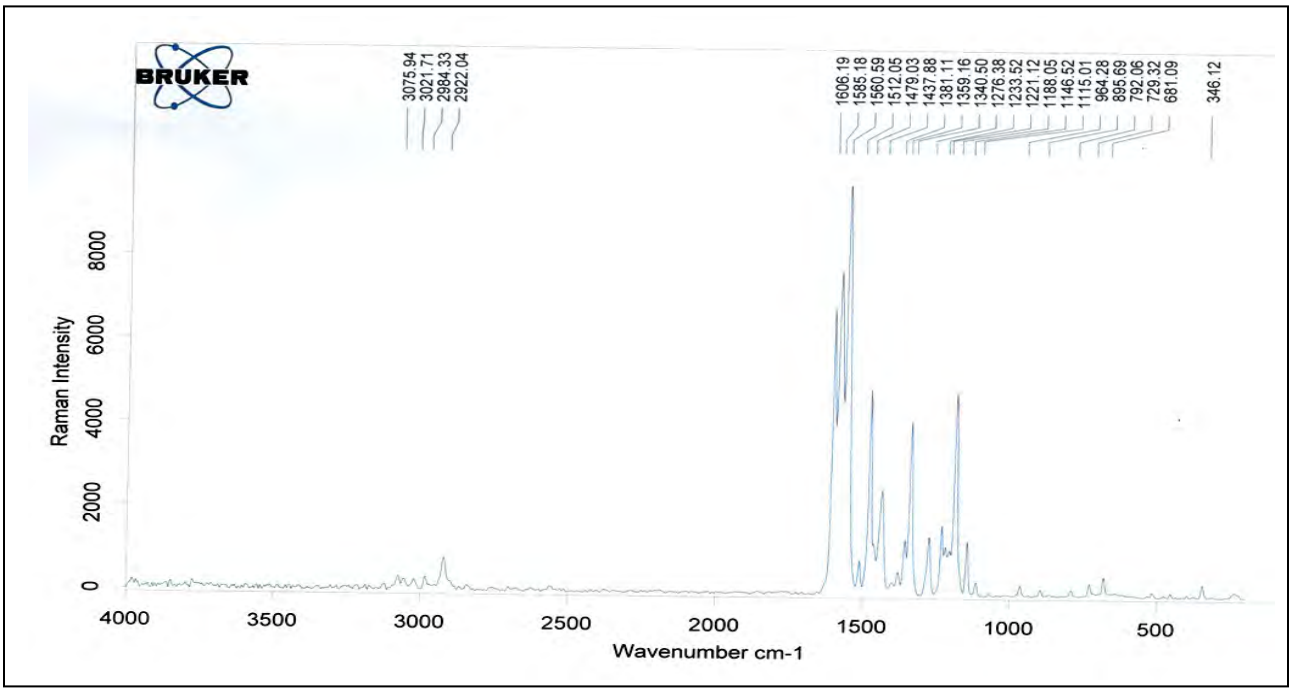

Fig. 3.31 Raman spectrum of pMS–4Me2MA

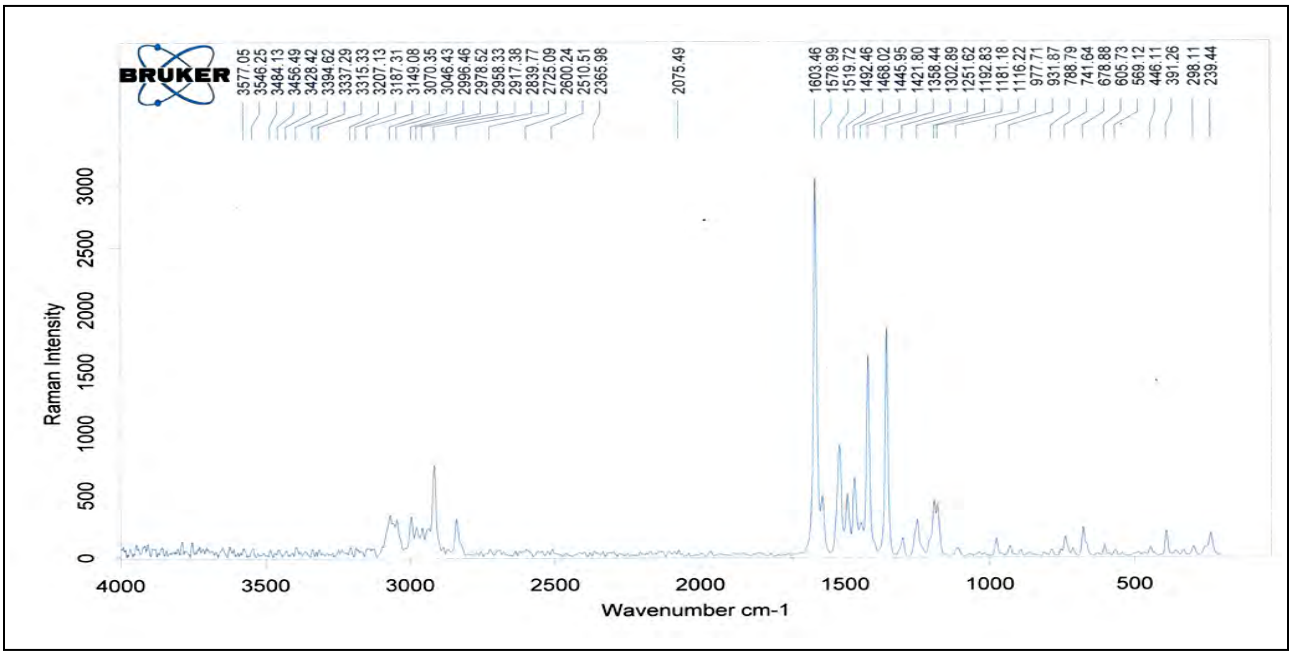

Fig. 3.32 Raman spectrum of [Cu(pMS–4Me2MA)$_2$]

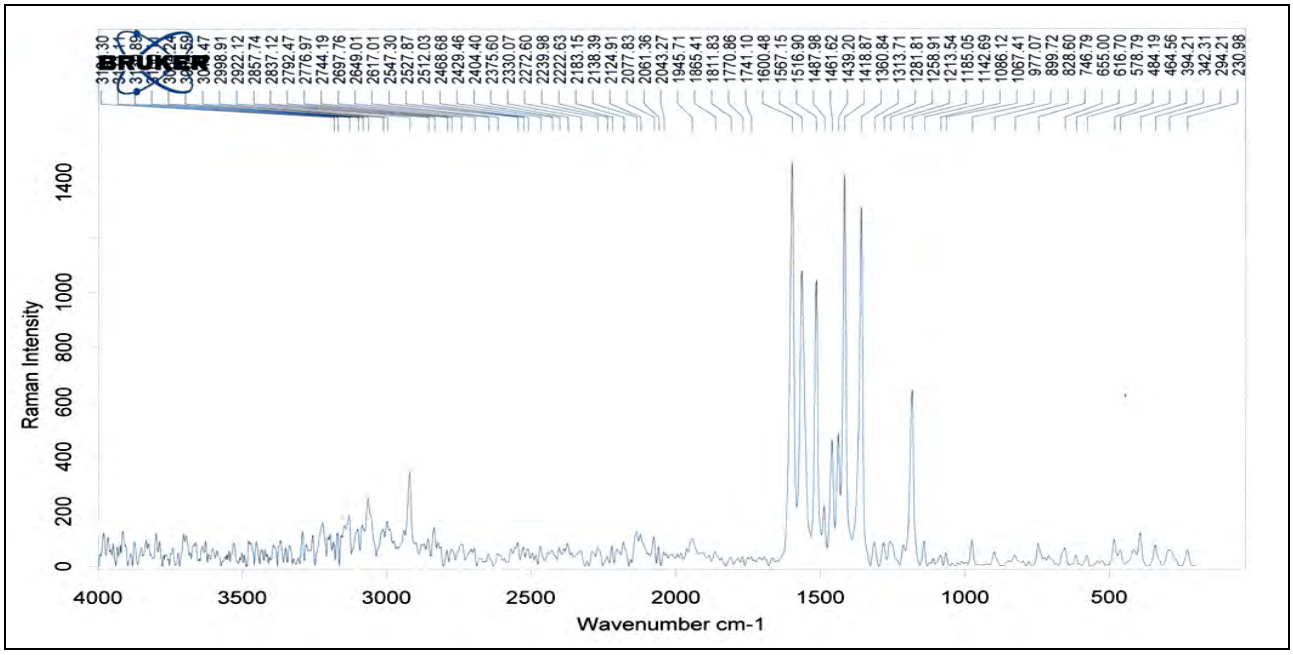

Fig. 3.33 Raman spectrum of [Cu(pMS–4Br2MA)$_2$]

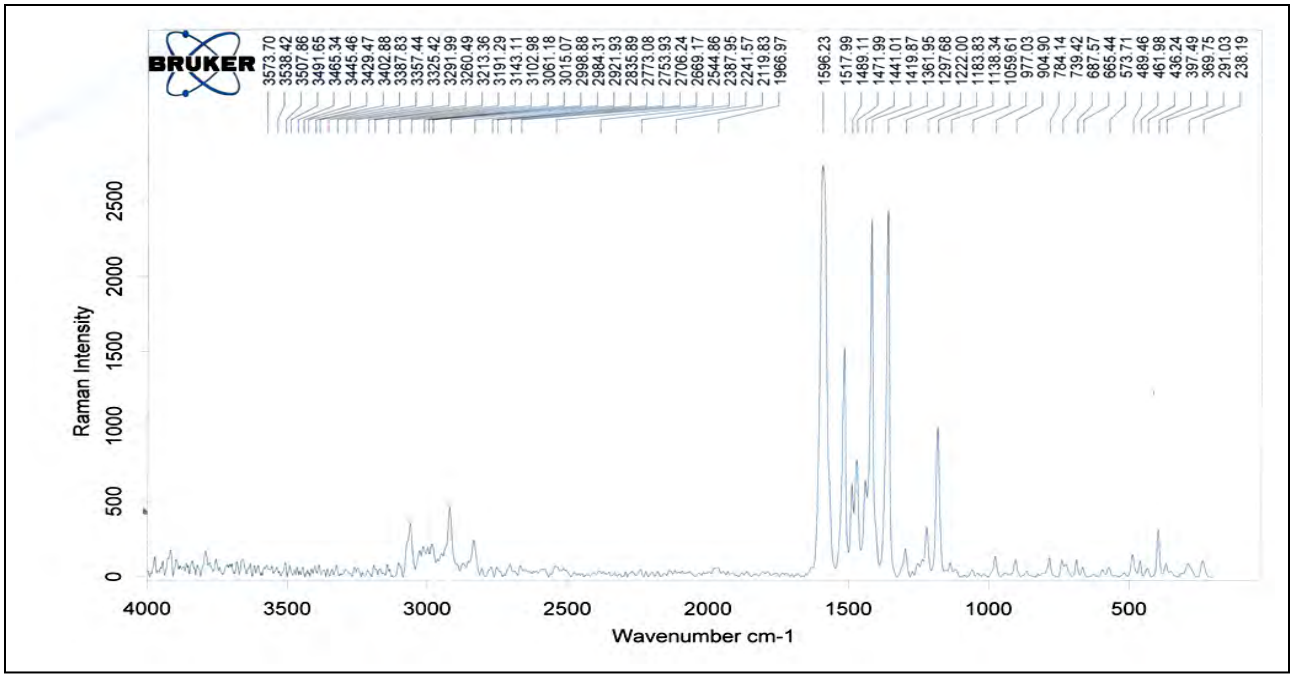

Fig. 3.34 Raman spectrum of [Cu(pMS–4MeO2MA)$_2$]

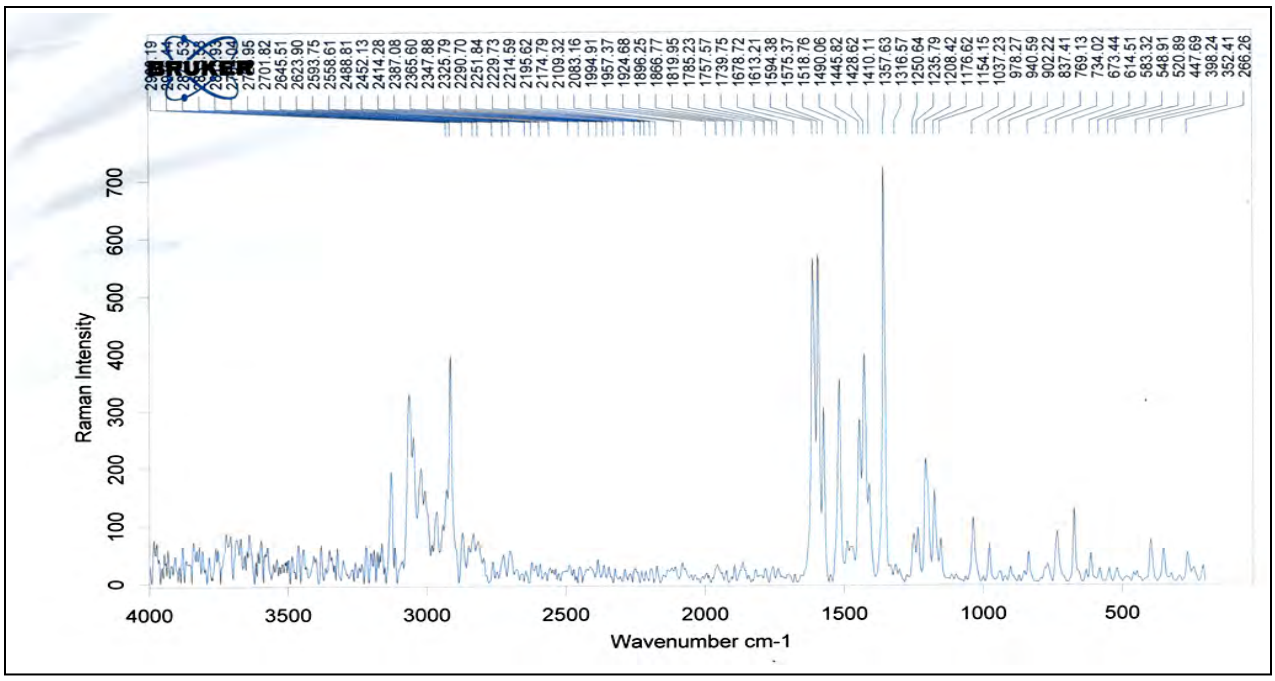

Fig. 3.35 Raman spectrum of $[Cu(pMS–2MT)_2]$

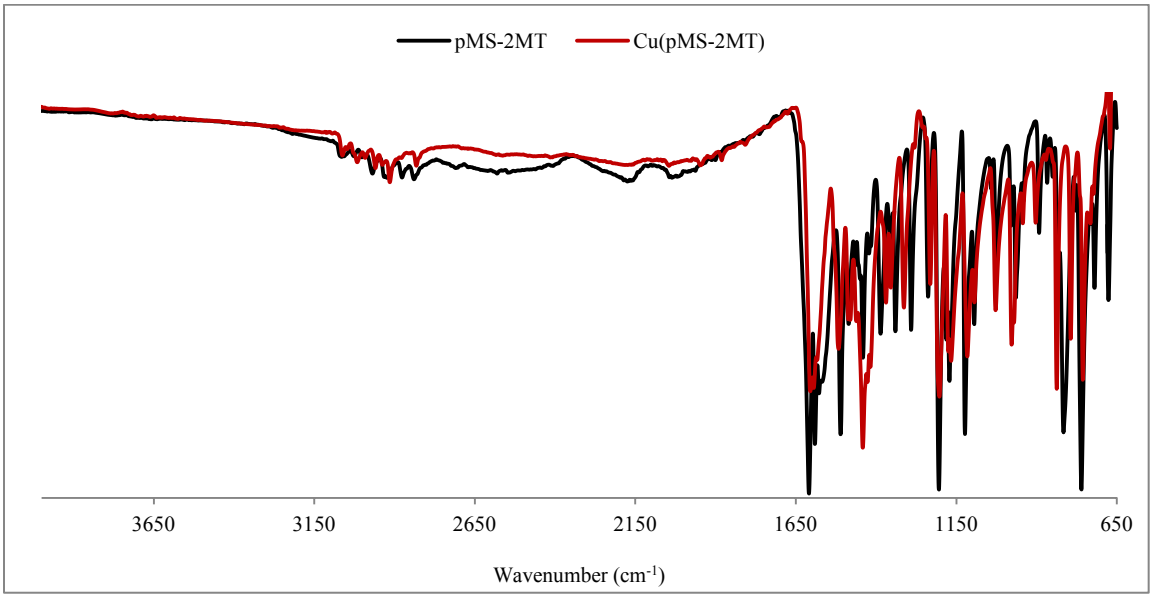

Fig. 3.36 Mid–IR spectra of pMS–2MT and $[Cu(pMS–2MT)_2]$

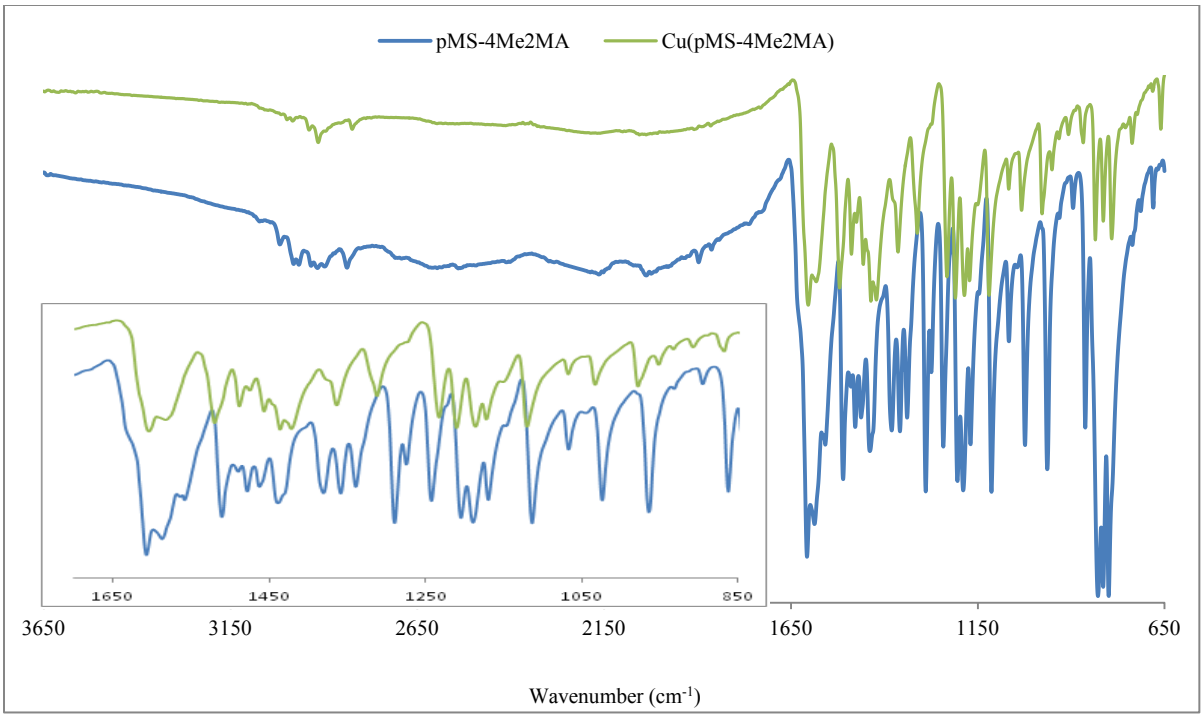

Fig. 3.37 Mid–IR spectra of pMS–4Me2MA and [Cu(pMS–4Me2MA)$_2$]

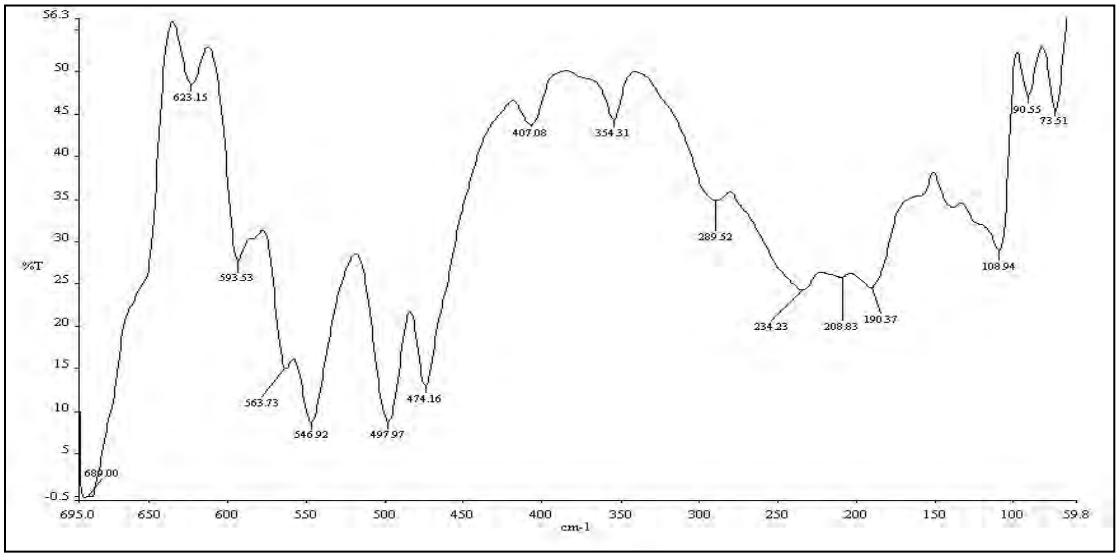

Fig. 3.38 Far–IR spectrum of pMS–4MeO2MT

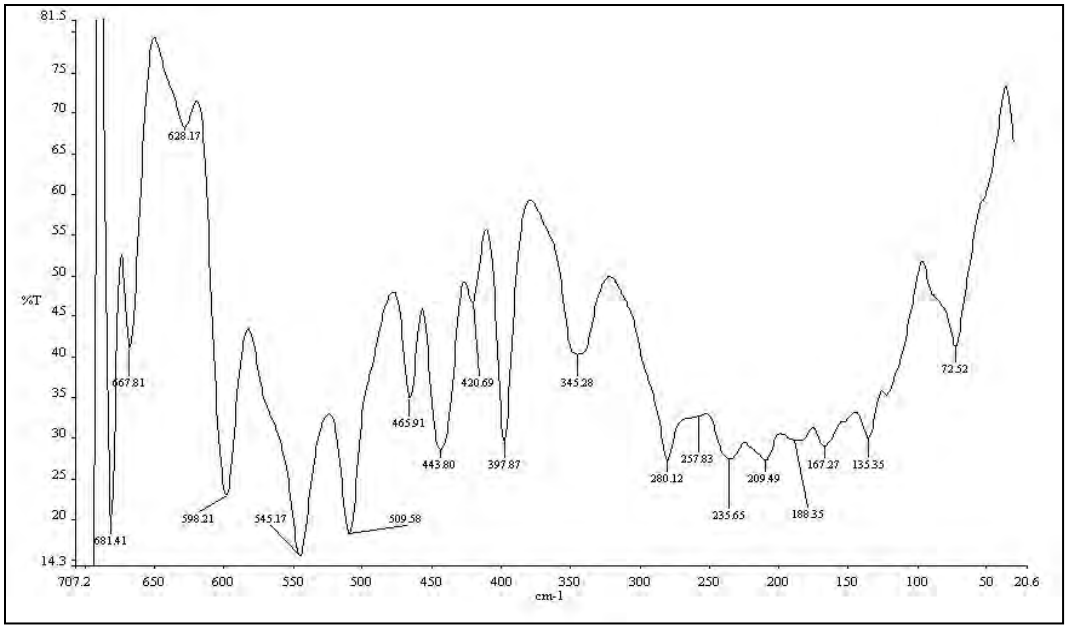

Fig. 3.39 Far–IR spectrum of [Cu(pMS–4MeO2MT)$_2$]

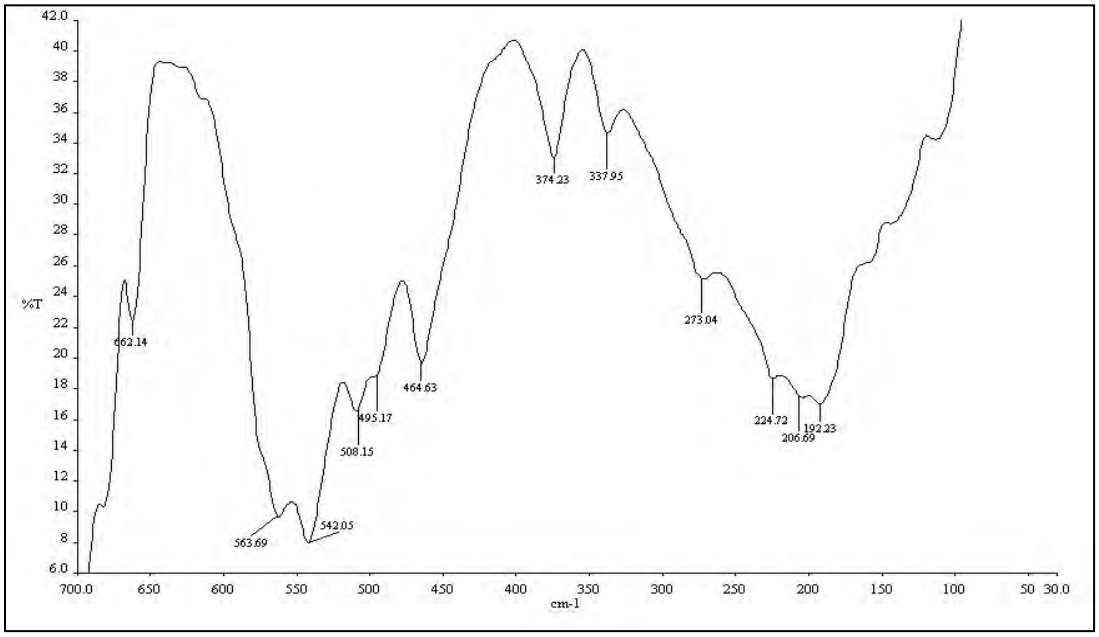

Fig. 3.40 Far–IR spectrum of pMS–4NO$_2$2MT

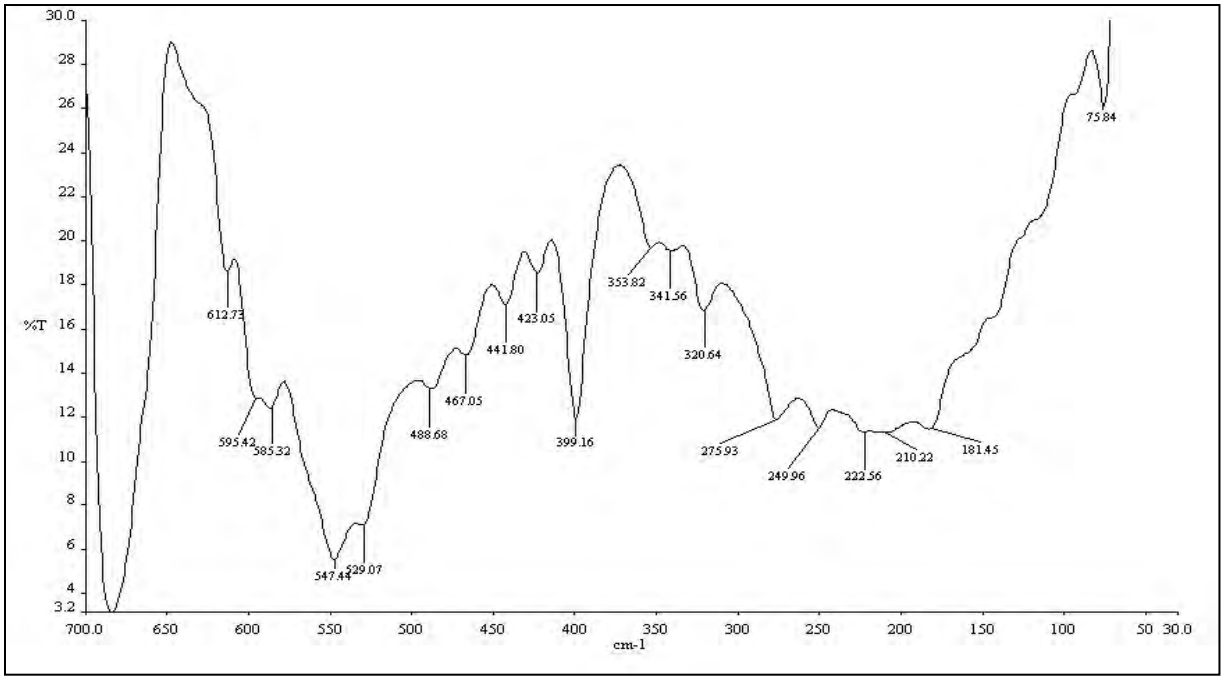

Fig. 3.41 Far–IR spectrum of $[Cu(pMS–4NO_2 2MT)_2]$

3.7 CRYSTALLOGRAPHIC DATA

3.7.1 Crystallographic data of $[Cu(4NO_2–2MT)_2Cl_2]_2$ (**11C**)

A single crystal of **11C** was grown by the slow evaporation of a mixture of DMSO/EtOH (2:1) solution. The molecular structure of **11C** is shown in **Fig. 3.42** together with the atom numbering scheme. The crystal data and structure refinement for **11C** are recorded in **Table 2.20.** The complex molecule crystallizes in the monoclinic space group $P2_1/c$.

The four corners of the square plane are occupied by the aniline nitrogen (N1), thioether sulfur (S1) and two chloride ions (Cl1, Cl2) in a *cis* arrangement to each other. One of the Cl (Cl2) is involved in axial bonding with the Cu(II) of the adjacent molecule while Cl1 is terminally bonded to only one Cu(II). There are one or two sets of possible axial coordination seen in this complex depending on the acceptable bond distance for $Cu–Cl_{apical}$. Each axial coordination is made by one of the chloride ions (Cl2) bonding with the Cu(II) ion of the adjacent cell layer and the $Cu–Cl_{apical}$ distance (Cu1–Cl2 and Cl2–Cu1) for one set is 2.690 Å which is within the range for $Cu–Cl_{apical}$ distance of many Cu(II) octahedral compounds[40-42] and the other set of $Cu–Cl_{apical}$ distance is longer at 2.932 Å.

When one considers that the 2.932 Å distance is longer than would enable effective interaction between the Cu and Cl2, the axial coordination is reduced to one and a dimeric square pyramidal structure results (**Fig. 3.42**) with $NSCl_3$ coordination per each Cu(II). The coordination geometry around Cu(II) will then be described as trigonal bipyramidal distorted square based pyramidal,[43] as revealed by the magnitude of the trigonality index[44] τ of 0.22 [$\tau = (\beta - \alpha)/60$, where α =N1–Cu1–Cl1=176.82(54)^o and β = Cl2–Cu1–S1 = 163.90(2) ^{o}; for perfect square pyramidal and trigonal bipyramidal geometries the τ values are zero and unity, respectively.

On the other hand, considering that similar and longer bond lengths have been reported for $Cu–Cl_{apical}$ in tolbachite,[45] the first Cu(II) octahedral mineral compound, the arrangement around Cu(II) in **11C** comprises of $NSCl_4$ giving rise to polymeric octahedral structure of the molecule. Each $CuNSCl_2$ shares one equatorial Cl^- with the adjacent Cu(II) in an apical bond and the sixth bond is formed by the equatorial Cl^- of the adjacent Cu(II) also binding to it apically. This linkage results in ladder-like octahedral sheets (**Fig. 3.43)**. A distorted octahedral or tetragonal structures were earlier suggested for the copper(II) complexes of 2MT, 2Me–2MT, 2Cl–2MT and 4Cl–2MT.[23] From the above crystal structures, the possibility of this suggestion is seen.

Bond distances for Cu–N (2.075 Å) and Cu–S (2.321 Å) fall within the ranges expected.[46,47] The Cu–S(thioether) distance is typical of equatorially bound thioether sulfur.[48-50] The Cu–Cu distances observed are of different lengths; 3.532 Å, 3.808 Å, 5.600 Å, 8.554 Å. As dimeric copper complexes can range from normal paramagnetic to the other extreme of strongly antiferromagnetic as a result of Cu–Cu interactions, further studies need to be carried out to investigate the nature of paramagnetism obtainable in these complexes.

Extensive hydrogen bonding operates within the molecule and most of these distances measured are within the range for such bondings.[51] **Table 3.21** contains the data for possible intra- and intermolecular interactions within the lattice of **11C**.

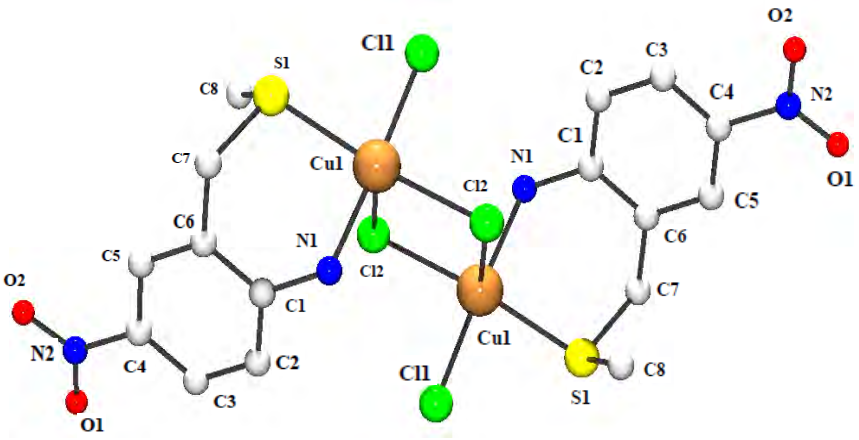

Fig. 3.42 Dimeric square pyramidal structure of Cu(4NO_2–2MT) **11C**. Ellipsoids drawn at 50% probability and hydrogen atoms are omitted for clarity

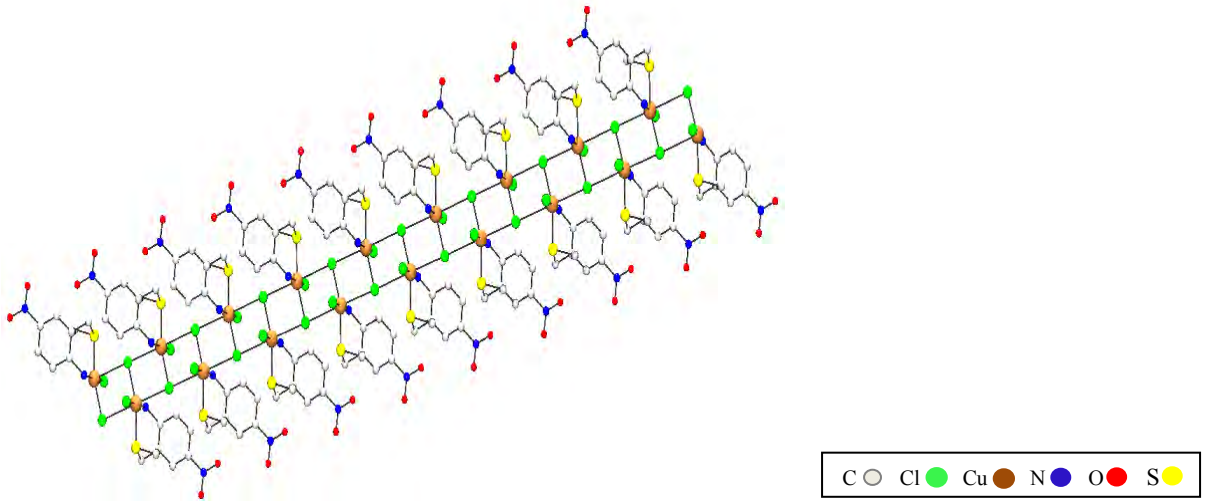

Fig. 3.43 Ladder-like polymeric octahedral structure of Cu(4NO_2–2MT) **11C**. Ellipsoids drawn at 50% probability and hydrogen atoms omitted for clarity

3.7.2 Crystallographic data of Schiff-base ligands

The molecular structures of Schiff-bases pMS–2MT (**21**), pMS–4Me2MT **(22**) and pMS–2MA (**27**) were determined by single crystal X–ray diffraction and are shown in **Fig. 3.44-3.46**. The Schiff-bases were grown by slow evaporation from DCM/EtOH mixture. Compounds **21** and **22** crystallized out in the monoclinic $P2_1/n$ space group and **27** in the *ortho*rhombic P_{212121} space group.

The C=N bond distances are nearly equal in **21** (1.289 Å) and **22** (1.285 Å), but slightly shorter in **27** (1.280 Å) as a result of conjugation of sulfur lone pairs with the ring while C–N bond length is similar in the three compounds. The C–S distance of the thioether group is almost the same in **21** and **27**, and the conjugation of the S lone pairs in **27** is further shown by the shorter bond length of S1–C2 (1.762 Å) compared to S1–C15 (1.815 Å and 1.814 Å in **21** and **22** respectively). The C–O bond is in order of decreasing distance **21** (1.353 Å) > **22** (1.348 Å) > **27** (1.344 Å) and this reflects a slightly more extensive conjugation in a similar order. The presence of the –methyl group in **22** contributes more electrons to the system by resonance. There is no effect of conjugation or substitution on C–N bond as it has same length (1.415 Å) in the three compounds. The O1–H1 bond distance is seen to be the larger in **27** than the other two compounds, indicating the its phenolic proton is more acidic. The hydrogen bond distances between the phenolic oxygen and the nitrogen are 1.840 Å, 1.860 Å and 1.790 Å respectively and the distance

separating the separating the two non hydrogen atoms C2…N1 (2.870 Å in **21** and **22**), C12...N1 (2.860 Å in **27**) fall within the expected range (2.6–3.5 Å).[52]

The angles are as expected around the imine nitrogen (C8–N1–C9, C7–N1–C1) and are close to 120° in the ligands, indicating the nitrogen lone pairs are planar and overlap effectively with the pie electron system of the aromatic ring.

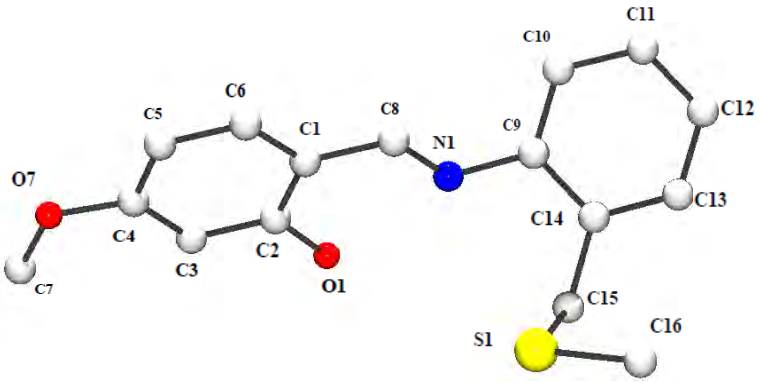

Fig. 3.44 Labelled ORTEP drawing of pMS–2MT **21** with ellipsoid at 50% probability. Hydrogen atoms are omitted for clarity

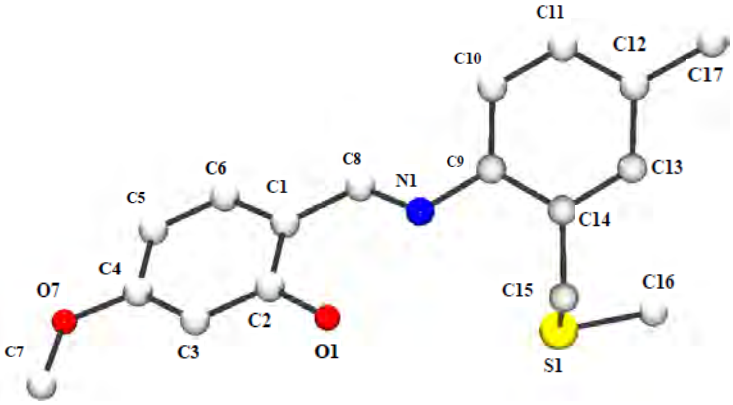

Fig. 3.45 Labelled ORTEP drawing of pMS–4Me2MT **22** with ellipsoid at 50% probability. Hydrogen atoms are omitted for clarity

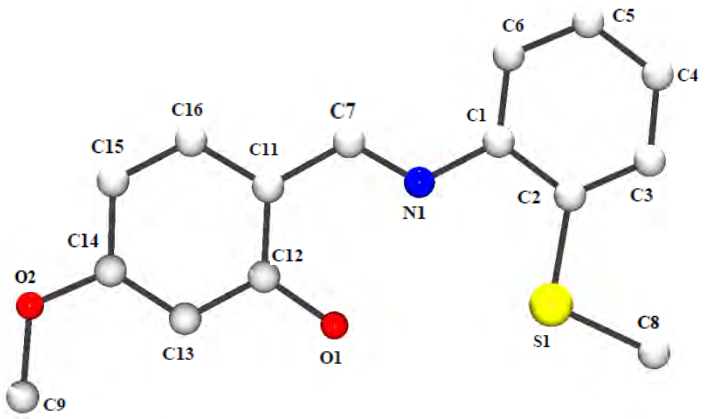

Fig. 3.46 Labelled ORTEP drawing of pMS–2MA **27A** with ellipsoid at 50% probability. Hydrogen atoms are omitted for clarity

3.7.3 Crystallographic data of Schiff-base complexes

The molecular structures of Schiff-base copper complexes [Cu(pMS-2MT)$_2$] **21C** and [Cu(pMS-pMe2MT)$_2$] **22C** were determined by single crystal X–ray crystallography and are shown in **Fig. 3.47** and **3.48.** The complexes were grown by slow evaporation from chloroform/EtOH mixture and crystallized out in the triclinic P_1 space group.

The crystal structures of **21C** and **22C** comprise of Cu(II) ion surrounded by 2N and 2O in the basal plane and 2S axially bonded in a slightly distorted octahedral arrangement. Two molecules of each ligand, acting as a tridentate ligand bind to the copper ion in a trans arrangement of the N, S and O donor atoms. The two Cu–S bond lengths are long and equal for both Cu–S bonds in each complex, 2.960 Å and 2.973 Å respectively. Longer bond distances usually observed in Cu–L, (where L is Cl^-, Br^-, I^- or S) arise as a result of the large size of the donor atom and do not imply weaker binding.[53] Such bond distances have been observed in Cu–S of some Schiff-base complexes.[54] The bond distances between the phenolic oxygen and the aromatic carbons (C202–O201, C102–O101) decrease on chelation by 0.043 – 0.06 Å as a result of extensive conjugation through the whole molecule, this is further confirmed by the bond lengths involving atoms used in bonding with the Cu(II). There is an alternate decrease and increase in the bond lengths of C=N, C–S and that of C–N indicating their participation in metal chelation and in conjugation.

All the in–plane angles are close to the expected 90^o and 180^o in both complexes typical of octahedral complexes viz (O101–Cu1–N201 89.9^o and 91.2^o, O101–Cu1–N201 89.9^o and 91.2^o, O201–Cu1–N201

89.5° and 89.4°, O101–Cu1–N101 90.3° and 89.7°, O201–u1–N101 90.3° and 89.6°, O101–Cu1–O201 176.9° and 177.5°, N201–Cu1–N101 179.1° and 179.1°); the distortion in the octahedral structure is mostly found around sulfur atoms. This is as a result of the strain imposed by two molecules of a tridentate ligand in an octahedral arrangement around the metal centre, hence notable distortions are seen in the angles connected to sulfur atoms in the range 83.0–96.0° (S201–Cu1–N101, S201–Cu1–O101, *etc*) and the planar angle of 177.69° is seen at S201–Cu1–S10. The distortion is slight however and the complexes can be said to possess tetragonally distorted octahedral structures.

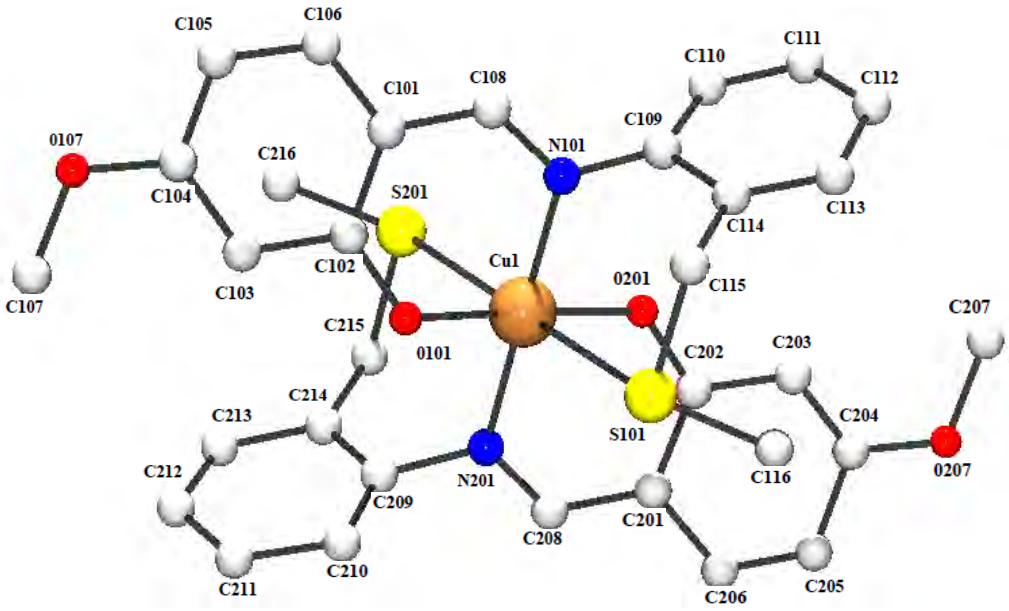

Fig. 3.47 Labelled ORTEP drawing of **21C** with ellipsoid at 50% probability. Hydrogen atoms are omitted for clarity

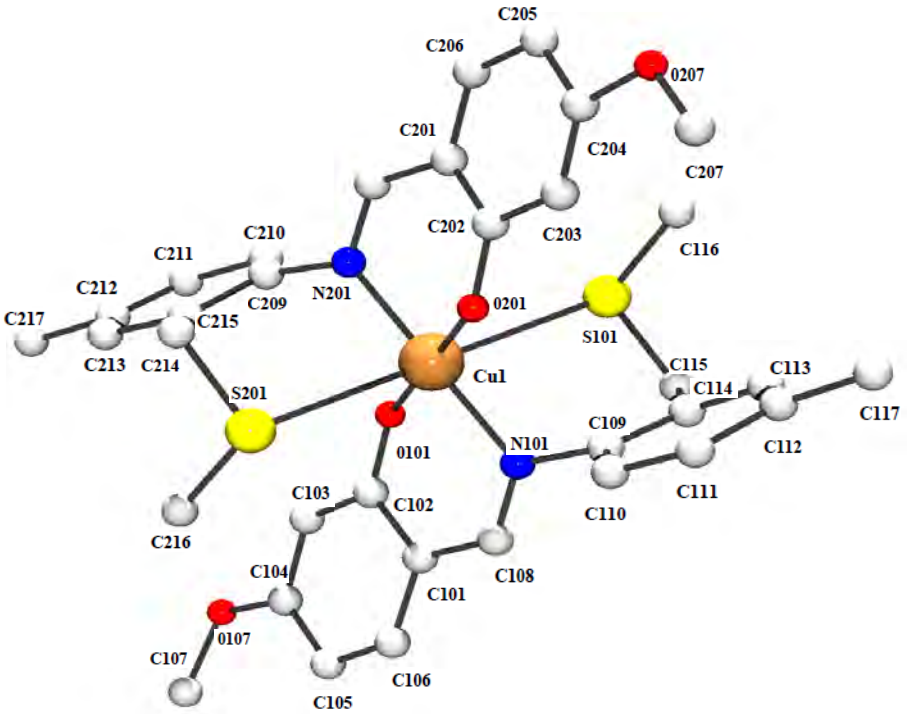

Fig. 3.48 Labelled ORTEP drawing of **22C** with ellipsoid at 50% probability. Hydrogen atoms are omitted for clarity

3.8 COLOUR VARIATION AND SOLID REFLECTANCE SPECTRA OF 2MT AND 2MA METAL COMPLEXES

Colour of transition metal complexes with metal ions in variable oxidation states could indicate the geometry of the complexes. Limitation to this generalization occurs in instances of unexpected colour in complexes whose geometries should indicate otherwise, for example, in manganese d^0 complexes (purple $KMnO_4$), d^{10} (brick red HgI_2), d^{10} s^2 (orange red BiI_3, yellow PbI_2) and blue octahedral cobalt(II) complexes. Charge transfer transitions in most of these complexes have been ascribed as being responsible for the intense colours seen.

In the complexes used in this research, colours of the solid complexes cannot be a sole indicator of their geometries as some anomalies were observed in colour of complexes in relation to their geometries especially in the solid state. This discussion attempts to relate the colour of complexes with their UV absorptions in the solid state since the latter has a direct bearing on the colour absorbed.

Complexes of 2–(methylthiomethyl)anilines and 2–(methylthio)anilines with same metal ion gave similarly coloured compounds in most cases and a few instances of variation is discussed, with the major difference occurring with the Co(II) complexes. An overview of the colour of the complexes is given in **Fig. 3.49**.

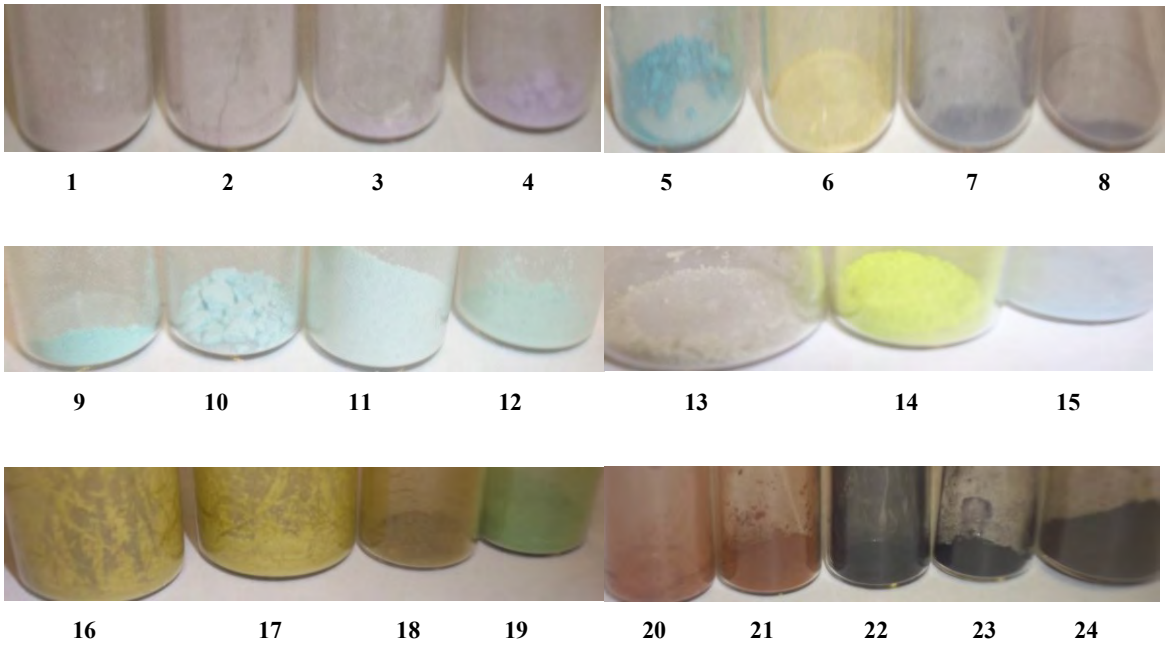

1 $[Co(2MeO–2MT)_2Cl_2]$	**2** $[Co(4Cl–2MA)_2Cl_2]$	**3** $[Co(4Cl–2MT)_2Cl_2]$	**4** $[Co(2Cl–2MT)_2Cl_2]$
5 $[Co(2Me–2MA)_2Cl_2]$	**6** $[Co(4NO_2–2MT)_2Cl_2]$	**7** $[Co(4Br–2MA)_2Cl_2]$	**8** $[Co(4MeO–2MA)_2Cl_2]$
9 $[Ni(2Me–2MT)_2Cl_2]$	**10** $[Ni(2MeO–2MT)_2Cl_2]$	**11** $[Ni(4Cl–2MT)_2Cl_2]$	**12** $[Ni(2Cl–2MT)_2Cl_2]$
13 $[Ni(2MeO–2MA)_2Cl_2]$	**14** $[Ni(4NO_2–2MT)_2Cl_2]$	**15** $[Ni(4Br–2MA)_2Cl_2]$	**16** $[Cu(2MT)Cl_2]$
17 $[Cu(4Cl–2MT)Cl_2]$	**18** $[Cu(2Cl–2MT)Cl_2]$	**19** $[Cu(4Me–2MA)Cl_2]$	**20** $[Cu(2Br–2MT)Cl_2]$
21 $[Cu(2Me–2MT)Cl_2]$	**22** $[Cu(2Me–2MA)Cl_2]$	**23** $[Cu(4MeO–2MA)Cl_2]$	**24** $[Cu(2Br–2MA)_2Cl_2]$

Fig. 3.49 An overview of colour in metal complexes of 2MT and 2MA

Each set of the metal complexes of Co(II), Ni(II) and Cu(II) studied has similar elemental composition in most cases except in the case of $[Cu(2Br–2MA)_2Cl_2]$ (see **Tables 2.4–2.9** in Chapter 2). The only modification to their structures is the variation in electronic nature of substituent group on the aromatic

ring and change in position of those substituents on the ring. There was no consistent trend observed in colour of complexes as a result of these variations.

Based on their elemental compositions and from the commonly observed geometries for each metal ion with ligands of this type, Co(II) complexes could be tetrahedral with 2 ligands acting as monodentate donors with only N atoms and 2 Cl^- ions or octahedral with 2 S also participating in which case the ligands chelate bidentately. Co(II) tetrahedral complexes are generally blue while the pink colouration is common with the octahedrally coordinated ones. Among the 2MT and 2MA Co(II) complexes, the pink colour is more common, the few deviants are the methoxy (dark purple, purple black), nitro (yellow) and the *ortho*-methyl (blue) complexes.

The solid reflectance spectra of Co(II) complexes are seen in **Fig. 3.50–3.52**. The complexes of 2MT have similar spectra except $[Co(4MeO–2MT)_2Cl_2]$ whose ligand field transitions seen to be masked by the charge transfer band. In the solid spectra of the 2MA complexes, the glaring exception is $[Co(2Me–2MA)_2Cl_2]$ whose transitions are obviously those of tetrahedral milieu, its blue colour bearing a strong evidence to this as well. Apart from these two, the deviation from pink colour will be attributed to their intense charge transfer transitions, as seen in blue purple $[Co(2Me–2MT)_2Cl_2]$ and yellow $[Co(4NO_2–2MT)_2Cl_2]$. The other complexes show pink colour commonly associated with octahedral Co(II) complexes.

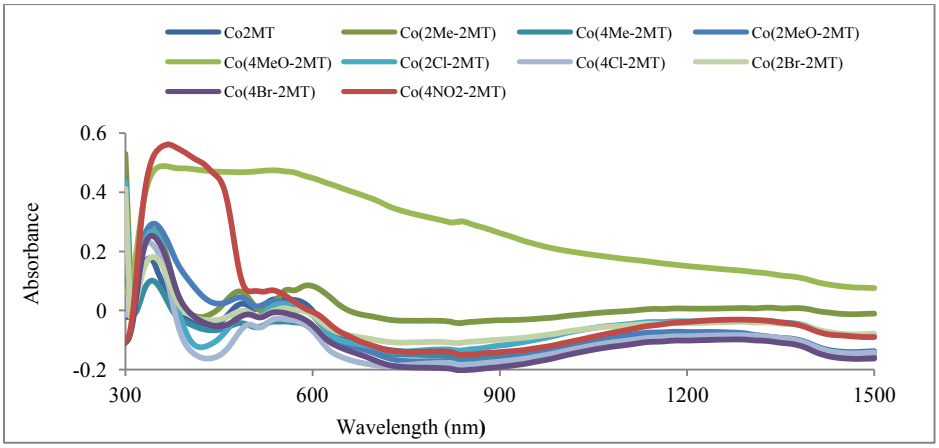

Fig. 3.50 Solid reflectance spectra of Co(II) complexes of 2MT

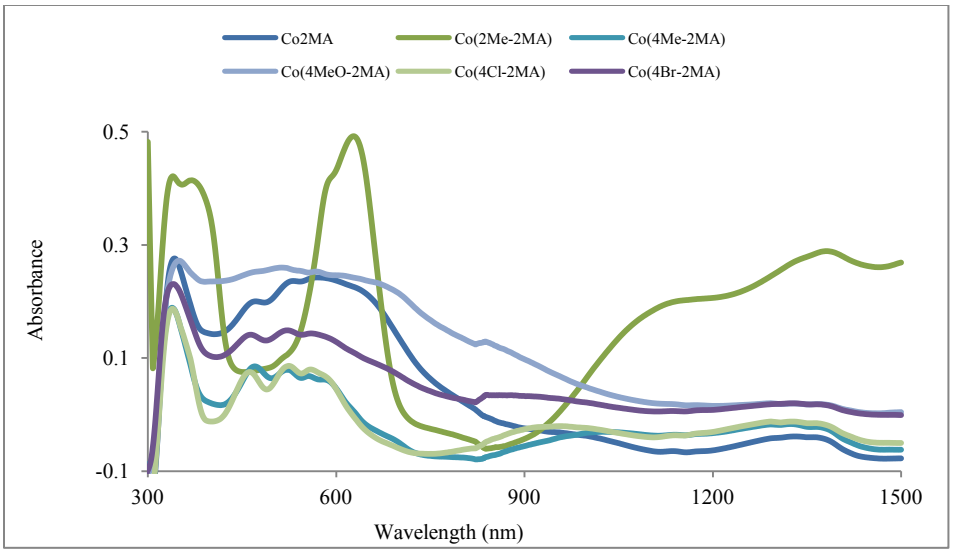

Fig. 3.51 Solid reflectance spectra of Co(II) complexes of 2MA

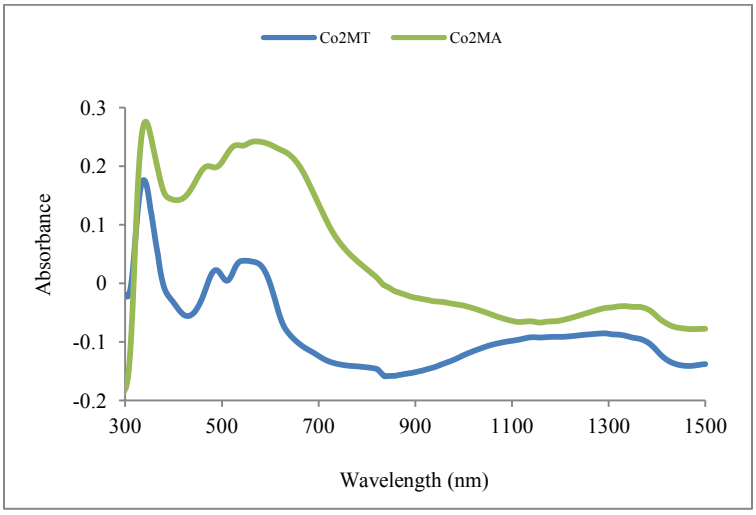

Fig. 3.52 Solid reflectance spectra of Co2MT and Co2MA

Similar proposition can be applied to the Nickel(II) complexes of both 2MT and 2MA ligands. The commonest colour is green, the few deviations are found with the nitro (yellow) and *para*–methoxy–2MA complexes which are yellow and pale blue respectively. The solid reflectance spectra of nickel(II) complexes (**Fig. 3.53**) likewise indicate they are all of similar geometry in 2MT complexes. The spectrum of the green Ni(2MeO-2MA) is shifted to higher wavelengths relative to others probably as a result of the

ortho-position of the methoxy substituent, this may not indicate any change in geometry compared to others since it shares the same green colour with others. As most octahedral Ni(II) complexes are green, the solid Ni(II) complexes of 2MT and 2MA are assigned the (pseudo) octahedral structure.

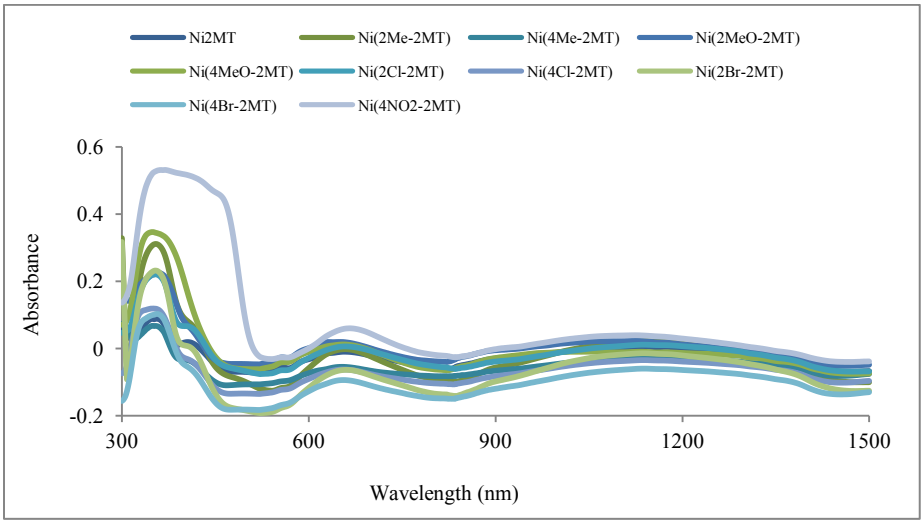

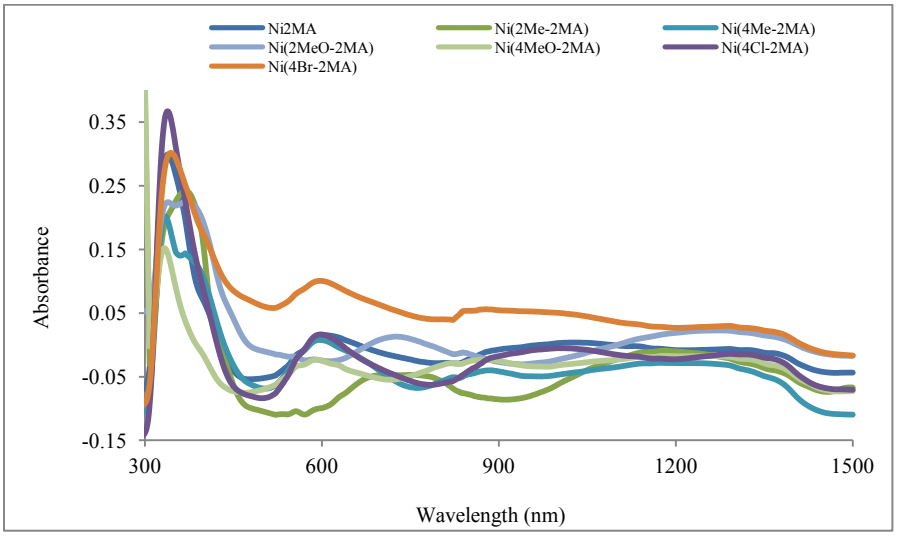

Fig. 3.53 Solid reflectance spectra of Ni(II) complexes of 2MT (top) and 2MA (bottom) ligands

Copper(II) complexes are known with diverse colours in different geometries. The complexes of 2MT ligands display two major types of colour, green and varying shades of brown; the green colour is shown by complexes with electron withdrawing substituents with the exception of the *ortho*-bromo substituted which shares same colouration of brown with those complexes with electron donating group. The intense colour shown by the latter group is due to ligand charge transfer transitions and not a change in geometry as suggested by the similarity in the shapes of their spectra (**Fig. 3.54** *top*). Hence the solid Cu(II) complexes of 2MT have similar square-pyramidal geometry as seen from the X-ray crystal data of Cu(4NO_2–2MT).

All the *ortho*-substituted Cu(II) complexes of 2MA are either dark coloured or brown while all the *para*-substituted are green regardless of their substituted nature. As suggested in the case of 2MT complexes, the geometry of these complexes could be similar despite the difference in their colour. The solid reflectance of these two groups differ slightly (**Fig. 3.54** *bottom*), those of the *ortho*-substituted have the ligand field transitions masked by their charge transfer bands as in the case of Cu(4MeO–2MA). Single crystal X-ray crystallography or modeling studies of these *ortho*-substituted would be useful to explain if there is a structural difference between them and their analogous *para*-derivatives.

Since the para-substituted complexes share similarity with the spectra of those of 2MT complexes, they are likely to also possess the octahedral geometry.

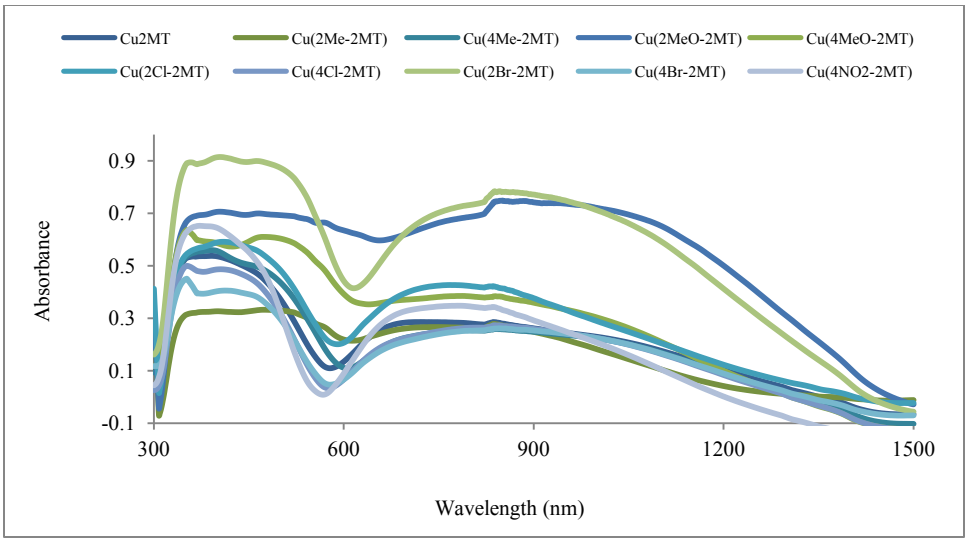

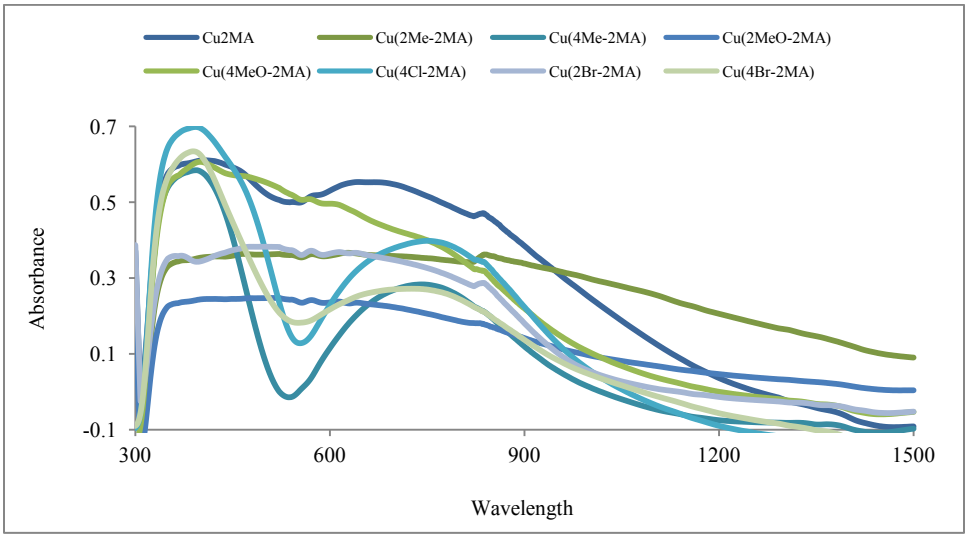

Fig. 3.54 Solid reflectance spectra of Cu(II) complexes of 2MT (*top*) and 2MA (*bottom*) ligands

Comparing the spectra of 2MT and 2MA complexes, similarity can be seen between these two sets of complexes except with the Cu(II) complexes of 2MA in the *ortho*-substituted cases mentioned earlier. The spectra of 2MA complexes show a slight shift to a higher energy in all cases (**Fig. 3.55)**.

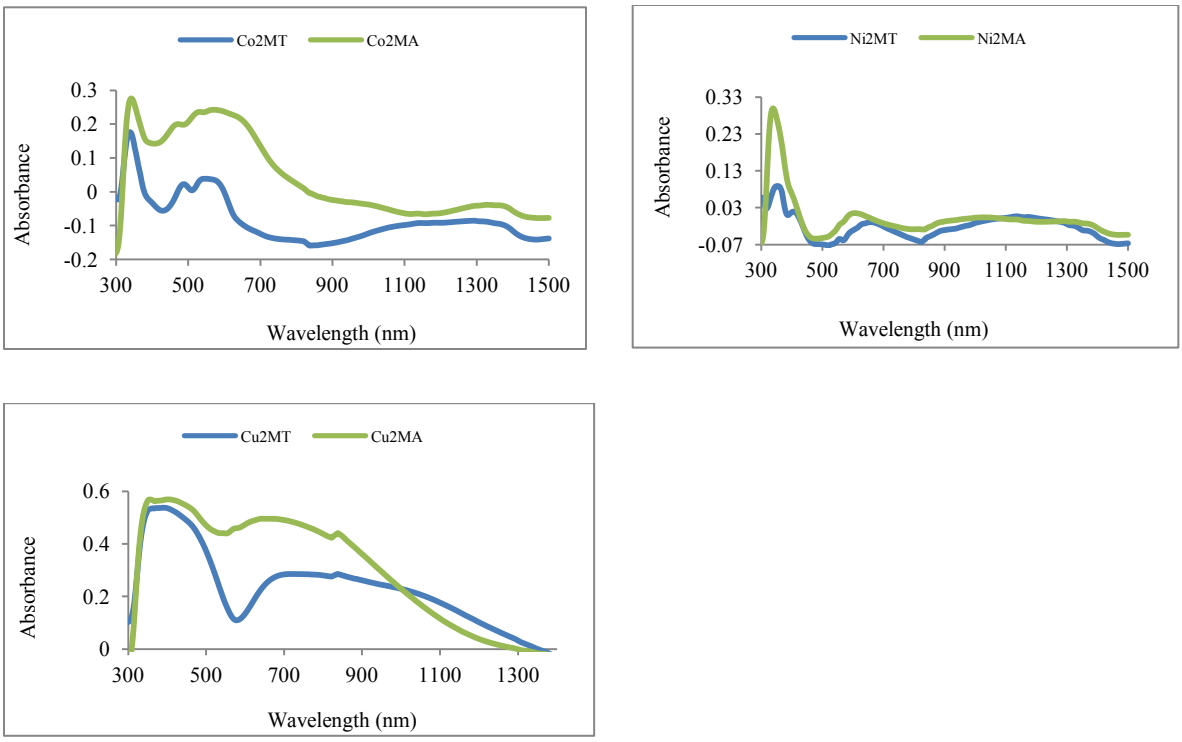

Fig. 3.55 Comparison between solid spectra of 2MT and 2MA complexes

3.9 SOLUBILITY

The metal complexes of both 2MT and 2MA ligands behave similarly in their solubility. The cobalt and nickel complexes show almost similar solubility property. This could also imply their isostructurality. They dissolve in most organic solvents while the copper complexes only dissolve in DMSO and DMF. Solubility could also indicate the type of structure existing in a complex; polymeric structures sometimes show insolubility in common organic solvents as demonstrated by the copper complexes. Crystallographic data of Cu($4NO_2$–2MT) has shown it to have a polymeric structure in which a molecule links with the next one by the formation of chlorine bridges, in addition there are intra– and inter–molecular hydrogen and van der Waals bonding giving rise to a very rigid structure (**Fig. 3.43**). This could explain why copper complexes could only dissolve in strongly polar organic solvents like DMF and DMSO. Hence the solid cobalt and nickel complexes are most probably existing as monomers. All the complexes are not soluble in water, which is an indication that they are non–ionic complexes.

Since comparative studies are also to be made between the 2MT and 2MA ligands as well as between their metal complexes, tests involving the use of solvents were carried out in DMF and DMSO.

The Schiff-base ligands and their copper complexes are only soluble in dichloromethane and chloroform.

3.10 MOLAR CONDUCTIVITY

The electrolytic nature of 2MT and 2MA metal complexes was determined in DMF at 10^{-3} M. DMSO could not be used as values for conductivity tests in DMSO for different electrolyte types are not consistent[55-59] and can lead to ambiguity in results obtained. Values for conductivity in DMF at 10^{-3} M solution have been reported in literature for different electrolyte ranges[60-64] the results obtained were compared with these standard values.[65] The molar conductivity values at room temperature are reported in **Tables 3.26** and **3.27** for metal complexes of 2MT and 2MA where the two series are seen to behave similarly, hence their conductivity will be jointly discussed.

Co(II) complexes have values ranging between 28.6 and 37.8 μS and this shows they behave as non-electrolytes in solution. Cu(II) complexes demonstrate similar behaviour with values in the range 26.5–37.3 μS. This shows no chloride ion is outside the coordination sphere or displaced by the solvent molecule. The values between 68.1 and 87.4 μS for Ni(II) complexes indicate they are 1:1 electrolytes and in this case, one chloride ion is outside the coordination sphere. The possibility exists that due to solvolysis effect of DMF, its molecule displaces the chloride ion from its bonding to Ni(II) and a compound formed is suggested to be of the type $[Ni(L_2Cl(DMF))Cl]$ where L is any 2MT or 2MT ligand. The electrolytic nature of the Schiff-base complexes could not be determined as their solubility was limited to solvents such as DCM and $CHCl_3$.

3.11 ELECTRONIC SPECTRA OF 2MT AND 2MA LIGANDS AND COMPLEXES

The electronic spectra of 2MT and 2MA ligands and their Co(II), Ni(II) and Cu(II) complexes are discussed in this section. The solvents used were determined by the solubility of the metal complexes. Hence the electronic spectra of the compounds were obtained in DMF and DMSO. The solid reflectance spectra of the metal complexes were also obtained so that the effect of these polar solvents on the solid structures on dissolution could be studied and compared. It should be noted that there are grating changes in the instrument used for solution studies at ≈ 330, 680, 900 nm and these are reflected in some of the solution UV spectra. Similar occurrence is observed in the solid reflectance spectra around 830 nm.

3.11.1 2MT and 2MA Ligands

The electronic spectra of the ligands are recorded in **Table 2.2.7** (Chapter 2). They are typical of transitions within the aromatic ring; $\pi \rightarrow \pi^*$ and occurring between 250-310 nm in both 2MT and 2MA ligands. There is no constant trend observed in either the intensity or wavelengths of transitions in ligands as the solvent is changed from DMF to DMSO (see **Fig. 3.56 -3.57**).

In both 2MT and 2MA series a hypsochromic shifting of $n \rightarrow \pi^*$ band to a higher energy takes place when the substituents are changed from the *para* to *ortho* position. This indicates the presence of substituents at the *para* position enhances a decrease in energy of this transition. The polar solvent molecules are able to solvate the nitrogen lone pairs more effectively when the substituents are farther away (at the para position) thereby lowering the energy of the *n* orbital relative to *ortho* substitution.[66]

The $\pi \rightarrow \pi^*$ transitions in 2MA ligands experience a red shift with change in substituent position from *para* to *ortho*. Attractive polarization forces between π, π^* states and the solvent molecules lower the energies of both the non-excited and excited states and often reduces that of the excited state more significantly, as a result, the $\pi \rightarrow \pi^*$ transition may experience a small red shift as observed in 2MA ligands. When the reduction in energy for both states is almost similar, the $\pi \rightarrow \pi^*$ transition does not experience a shift and this is observed in 2MT ligands whose transition does not show sensitivity to change in position of substituents.[66]

Both bands absorb at higher wavelengths in 2MA ligands compared to corresponding 2MT ligands as a result of increased conjugation of the ring by the sulfur lone pairs.

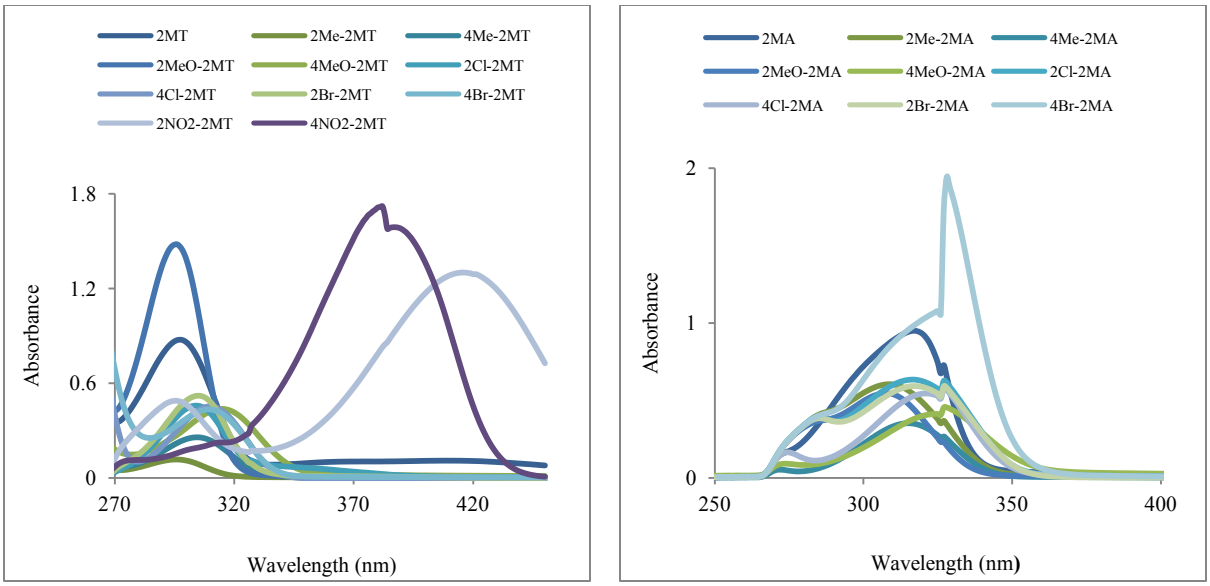

Fig. 3.56 Electronic spectra of 2MT (left) and 2MA (right) ligands in DMF in the near UV region

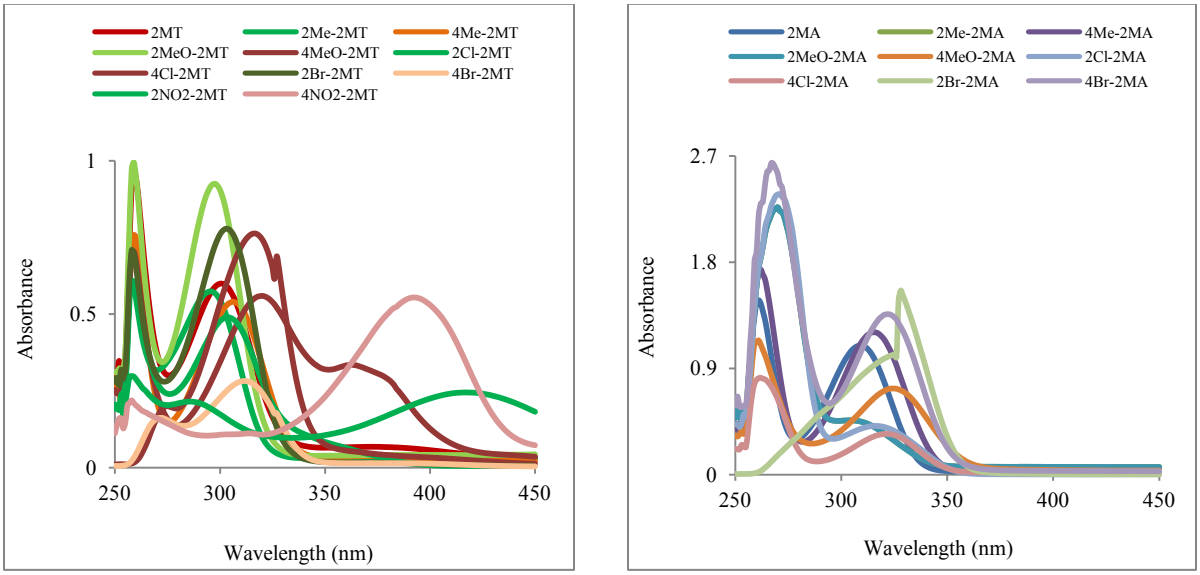

Fig. 3.57 Electronic spectra of 2MT (left) and 2MA (right) ligands in DMSO in the near UV region

3.11.2 Metal(II) complexes

In the solid reflectance spectra of the Co(II), Ni(II) and Cu(II) complexes of 2MT and 2MA, the ligand bands are not observed, probably because their intensities are too low to be observed in the solid state. They are however observed in the spectra of complexes in DMF and DMSO solutions. The two $\pi \rightarrow \pi^*$ ligand bands are bathochromically shifted in most cases. This could be as a result of increase in the conjugation of the ligands on complexation.

3.11.2.1 Co(II) complexes

The diffuse reflectance spectra of Co(II) complexes of 2MT and 2MA are similar in general (see Section 3.8 also), the exception being Co(2Me–2MA) and the *para*–methoxy substituted ones. They generally show a low energy broad band in the region 1250–1360 nm (**Fig. 3.58**). Another set of bands appears as multiplets between 500 and 600 nm, these transitions are more numerous in 2MA complexes than in those of 2MT. Very close to this region, a distinct set of bands occur around 450–495 nm. A very high intensity band in the near UV is seen between 335 and 370 nm. Shoulder bands are seen 640 and 1000 nm in the spectra of the complexes, indicating that even in the solid state, these complexes have many spin forbidden transitions occurring through vibronic coupling.

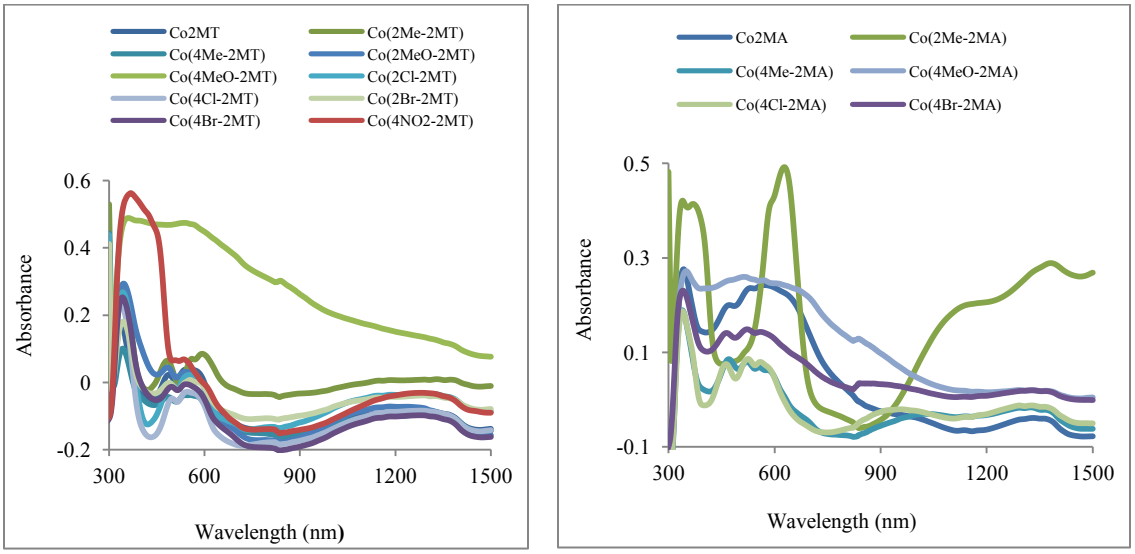

Fig. 3.58 Solid reflectance spectra of Co(II) complexes of 2MT (left) and 2MA (right)

In a tetrahedral or octahedral environment around Co(II), three bands are expected. For octahedral complexes, the lowest energy band is a transition corresponding to $^4T_{1g} \rightarrow {}^4T_{2g}$ absorbing in the range 1110–1520 nm, the second band due to $^4T_{1g} \rightarrow {}^4A_{2g}$ transition (620–750 nm) is not often observed because of its low intensity as the transition involves a two-electron process for strong fields; the highest energy transition occurs in the visible near 500 nm (470 – 590 nm) [67] and has been assigned to $^4T_{1g} \rightarrow {}^4T_{1g}$ (*P*). The visible band frequently has a shoulder or a fine structure to it. Tetrahedral Co(II) complexes show bands at lower energies and of higher intensities than those of octahedral configuration.

From the solid reflectance spectra data obtained, the low energy broad band (1250–1360 nm) can be assigned as transition due to $^4T_{1g} \rightarrow {}^4T_{2g}$, no band due to the second transition between (620–750 nm) was observed and the third band was seen as multiple transitions (450–495 nm, 500–600 nm), this characteristic is associated with it and is said to arise as a result of low symmetry components to the ligand field[68] or transitions to doublet states.[69] The high intensity band in the near UV is due to S → Co charge transfer.

On this basis, the solid cobalt(II) complexes here are assigned to octahedral geometry in the solid state. They could be tetragonally distorted type of structure as up to six spin allowed transition are allowed in this type of structure. For example, in the case of $Co(s\text{-}Et_2en)_2X_2$, all the bands could be observed except for the lowest transition between the split component of the ground state ^4T_1g.[70] Co(2Me–2MA) is assigned the tetrahedral geometry due to transitions at 589 and 625 nm with high intensities and lower ligand field transition at 1100 nm. Solid Co(4MeO–2MT) and Co(4MeO–2MA) give poorly defined spectra as seen in **Fig. 3.59** which source could be ligand-based.

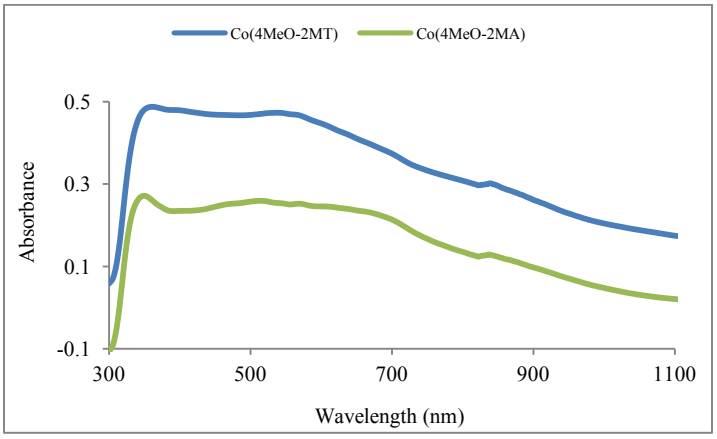

Fig. 3.59 Similarity in solid spectra of *para*-methoxy substituted complexes

In solutions of DMF and DMSO, the electronic spectra of the Co(II) complexes for both sets of ligands in the near UV and visible regions are shown in **Fig. 3.60–3.63** and are observed to show absorptions at the same regions. The spectra are essentially similar in both solvents and the small shift to a higher energy (or lower wavelength) in DMF is because of its higher ligand field strength. The spectra in both solvents will be jointly discussed.

The bands observed occur in the regions close to 600 nm and 670 nm (see **Tables 2.29–2.30** in Section 2.4.6.2), spin forbidden transitions which appear as shoulders between 370 and 530 nm and the very intense band in the region 320–345 nm ascribed as nitrogen to Cu(II) charge transfer. As the range of the UV-Vis spectrophotometer used in the solution studies does not exceed 1100 nm, the low energy bands could not be obtained.

The spectra of the Co(II) complexes (including Co(4MeO–2MA) in solution are reminiscent of tetrahedral bands. In a tetrahedral milieu, the three transitions expected are due to $^4A_2 \rightarrow {}^4T_1(F)$, $^4A_2 \rightarrow {}^4T_1(F)$ and $^4A_2 \rightarrow {}^4T_1(P)$. The lowest energy band due to $^4A_2 \rightarrow {}^4T_1(F)$ transition is usually found in the range 2000–3330 nm and is not often observed as it is weak because the transition is forbidden for electric dipole absorption in pure tetrahedral symmetry and it is frequently overlapped by vibrational bands. The other two bands are of high intensities and lie in the near infrared and visible regions respectively. Their intense absorptions make Co(II) tetrahedral complexes appear blue. Both bands show fine structure with multiple absorption bands. These features have been attributed to spin orbit coupling, low symmetry components of the crystal field and transition to the doublet states. In the spectra studied here, the second and third transitions are not observed. The intense bands around 600 nm with multiple absorptions can be assigned as the highest energy transition, $^4A_2 \rightarrow {}^4T_1(P)$.

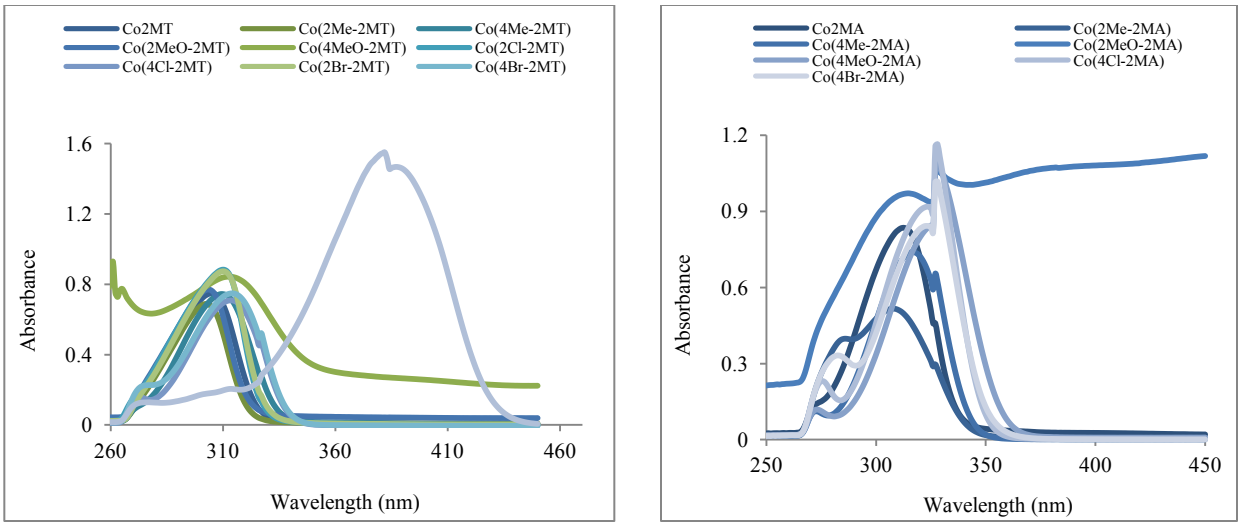

Fig. 3.60 Electronic spectra of Co(II) complexes of 2MT (left) and 2MA (right) ligands in DMF in the near UV region

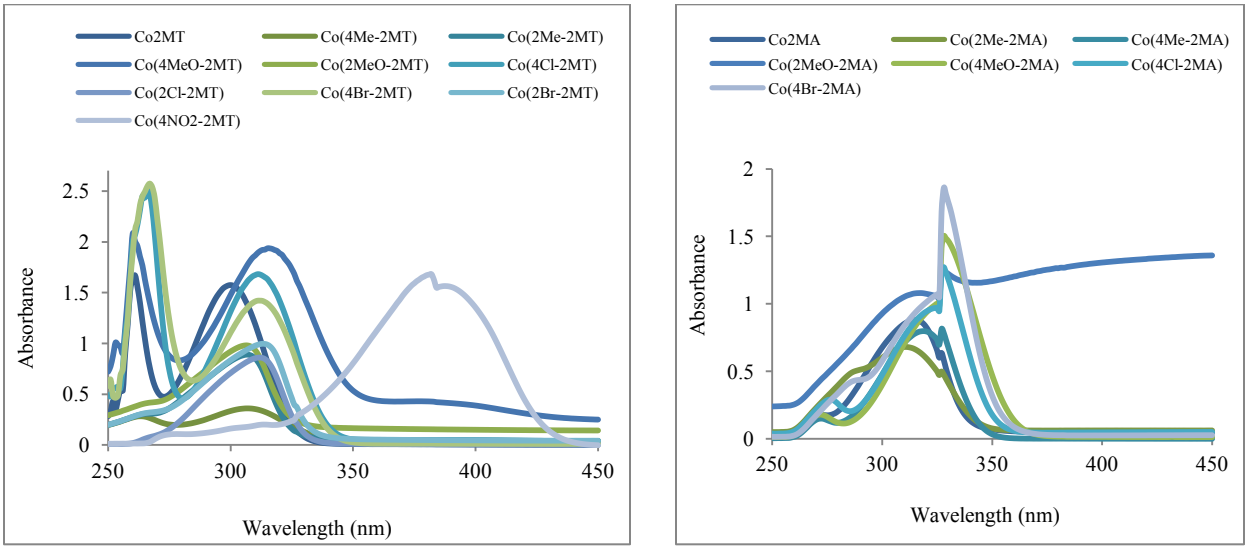

Fig. 3.61 Electronic spectra of Co(II) complexes of 2MT (left) and 2MA (right) ligands in DMSO in the near UV region

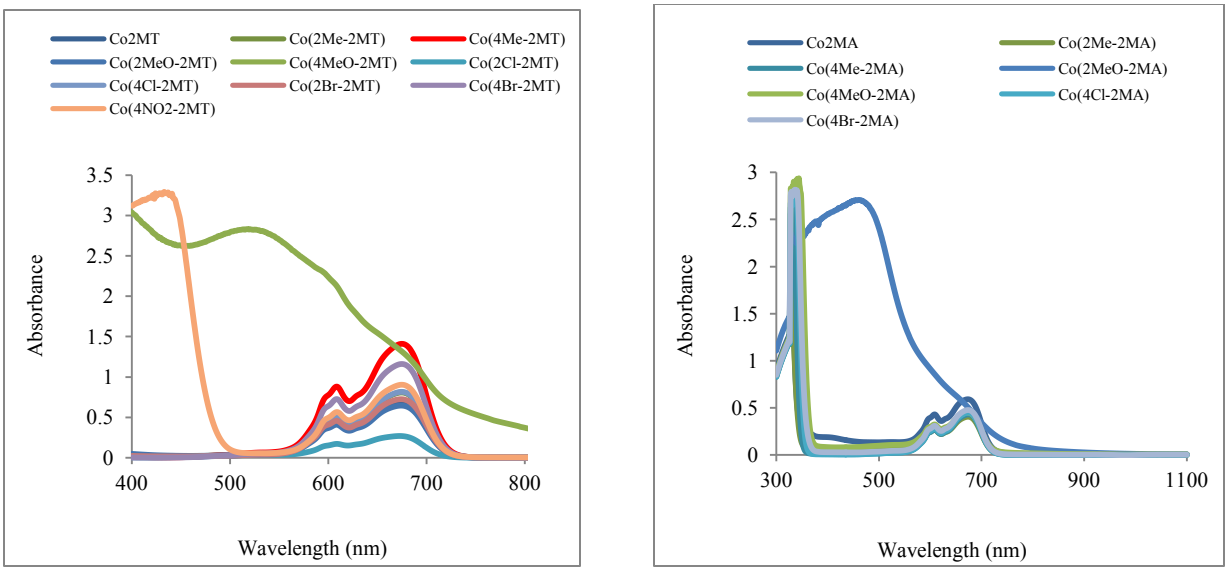

Fig. 3.62 Electronic spectra of Co(II) complexes of 2MT (left) and 2MA (right) ligands in DMF in the visible region

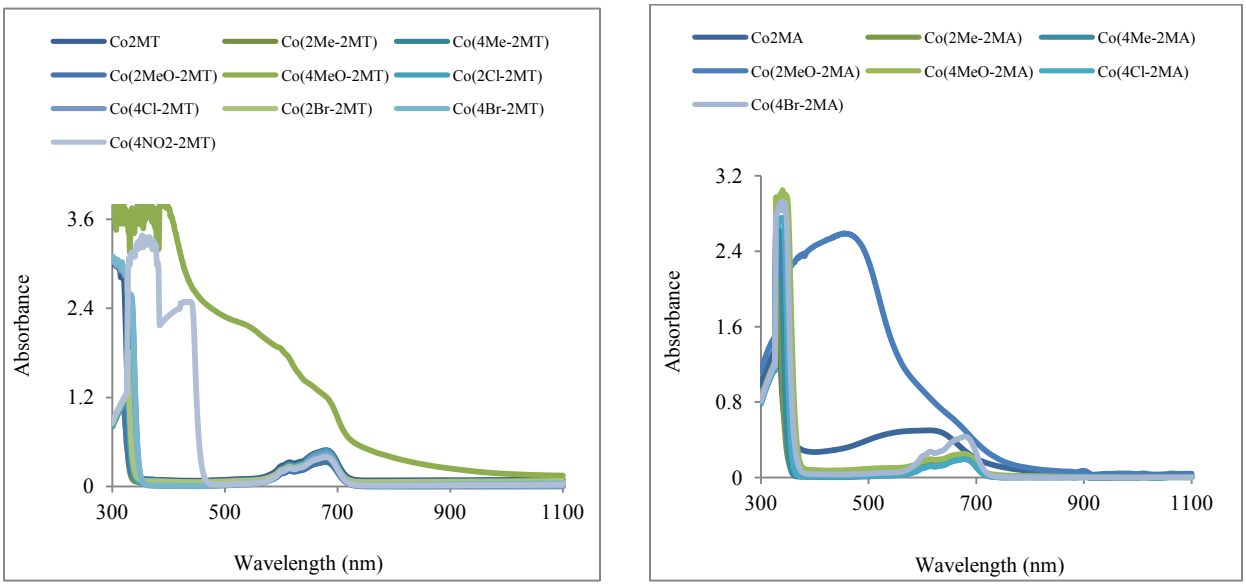

Fig. 3.63 Electronic spectra of Co(II) complexes of 2MT (left) and 2MA (right) ligands in DMSO in the visible region

As earlier explained for the complexes in the different physical states, it could be seen that there is a structural change on going from the solid state to solution. The difference in spectra of typical Co(II) complexes of 2MT and 2MA in the solid state and in solution is shown in **Fig. 3.64**. There is a significant shift to lower energy (about 120 nm) on going from solid to solution (**Tables 2.28 and 2.29**). This shift to

a lower energy indicates a structural change from the solid octahedral geometry to the tetrahedral in the DMF and DMSO solutions. That a structural change or modification has taken place is suspected as the colour changed from pink (or any other observed solid complex colour) to blue when these solvents were added to the solid complexes.

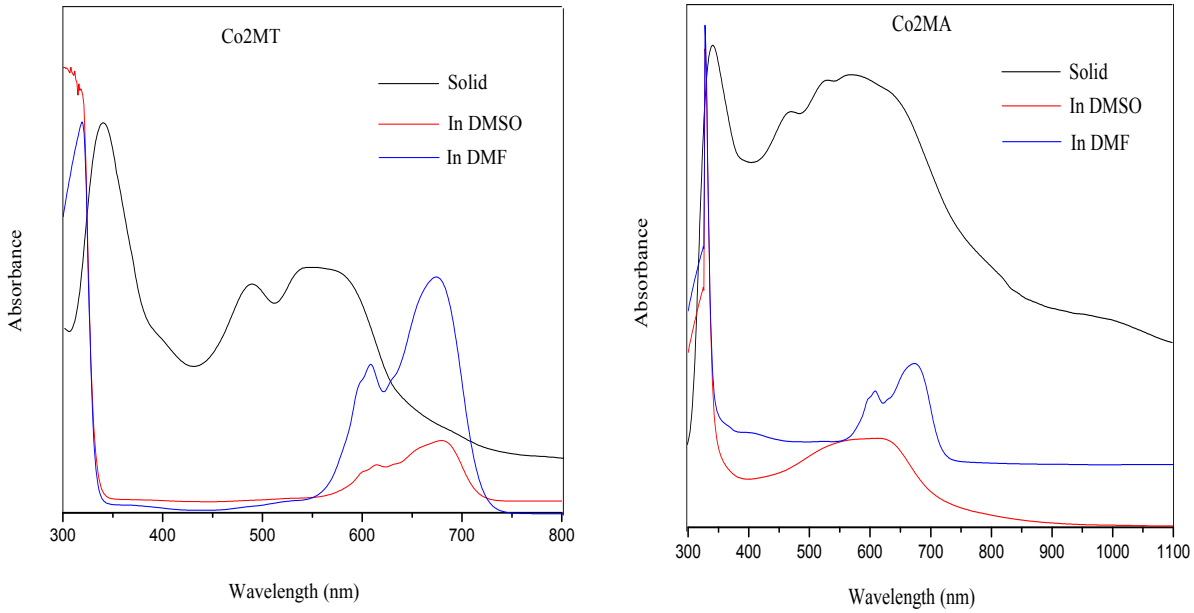

Fig. 3.64 Selected Co(II) complexes in solid state and solution

Taking into consideration that both types of solvent used are strongly coordinating, an interaction between the solid complex and the solvent is capable of modifying the Co(II) centre. This interaction could be in form of coordination of the solvent to the metal ion to form adduct, breaking of the bonds between metal ion and ligand atom(s) and/or subsequent replacement of the ligand atom(s) with the solvent molecules. From the conductivity tests, Co(II) complexes behave as non-electrolytes in DMF, indicating that chloride ions were not displaced. With either DMSO or DMF coordinating to Co(II) by replacing one or more of the ligand atoms, a shift to higher energy is anticipated since either of this solvent has a higher crystal field than the SN and Cl groups present. The other alternative would be breaking of the Co–S bonds by the solvating effect of these solvents, thereby changing the geometry from octahedral to tetrahedral. The latter seems to be the case as the bands in the spectra are seen to move to lower energies on dissolution, indicating that the Co–S bonds are broken without replacement by the solvent molecules.

The spectra of both series of complexes are similar in general as typified by the spectra of methyl substituted complexes of 2MT and 2MA ligands in **Fig. 3.65**.

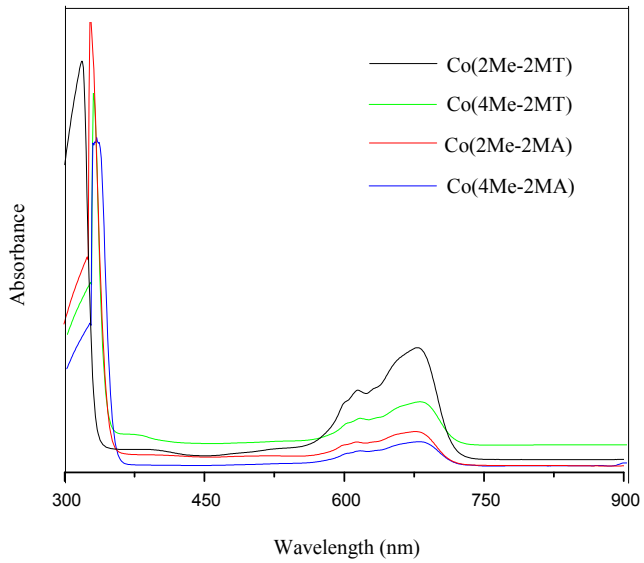

Fig. 3.65 Similarity in 2MT and 2MA Co(II) complexes

The exceptions to the similarity in all the solution spectra are those of Co(4MeO–2MT) and Co2MA. The spectra of Co(4MeO–2MT) in solid state and solution are similar (**Fig. 3.66**), it may be concluded that it retains its structure in solution. It seems to bear some semblance to octahedral geometry but the d → d bands are merged, appearing to be masked by the charge transfer band. Repeated synthesis of this complex has resulted in identical spectra. It is beyond the scope of this work to resolve the spectrum. The spectra of Co2MA in the solid state and in DMSO are similar but very different from that in DMF (**Fig. 3.64**), hence it is suggested that its structure is octahedral in the solid state and in DMSO solution while it is tetrahedral in DMF solution. Co(2Me–2MA) is tetrahedral in solid state and in solution. The solid reflectance spectra of Co(2MeO–2MA) could not be obtained (the yield was too low and was not available for this test) for comparison purposes but it is suggested that it may also be tetrahedral in the solid state as its vibrational frequencies in the mid infrared region are in closer range to those of Co(2Me–2MA) (see **Table 2.18** in Chapter 2).

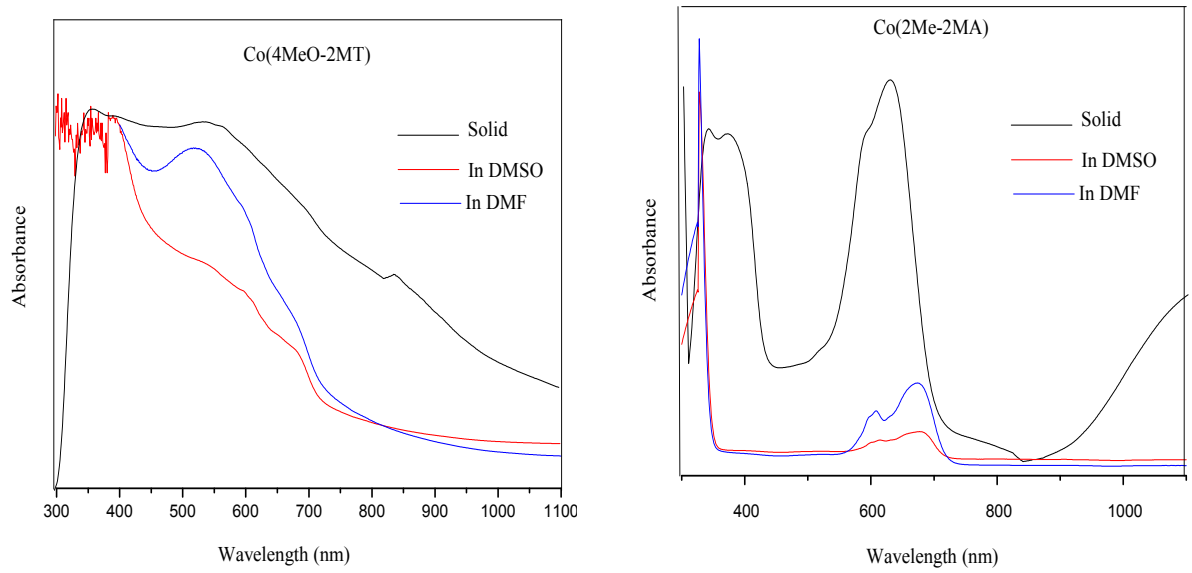

Fig. 3.66 Co4MeO–2MT in solid state and solution

Hence the suggested structures of the other Co(II) complexes in the solid state and in solution are (distorted) octahedral and tetrahedral respectively, with the few exceptions stated earlier. The proposed geometries are drawn below in **Fig. 3.67**.

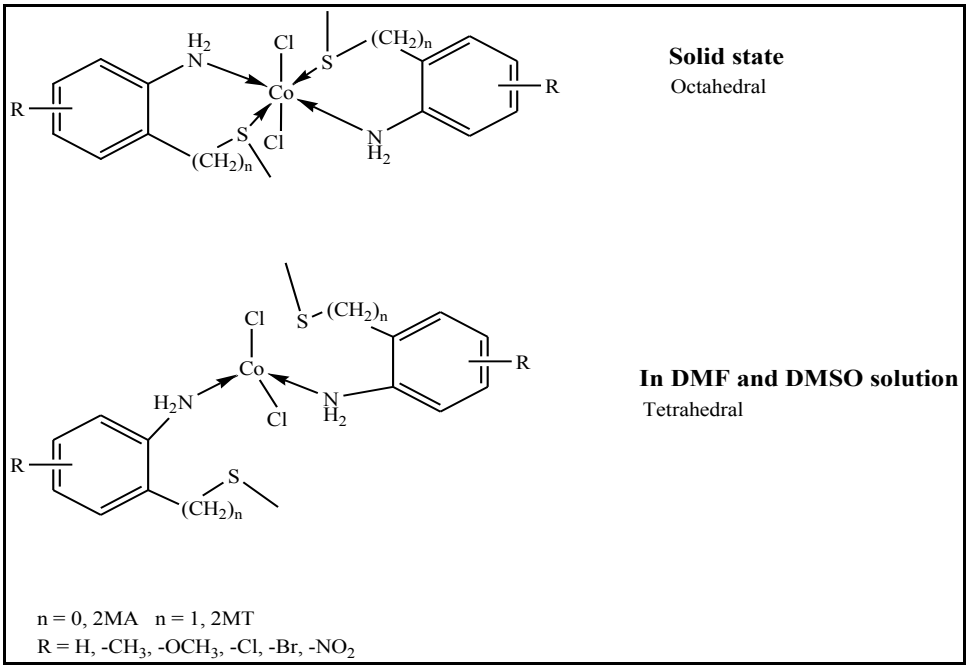

Fig. 3.67 Proposed structures for Co(II) complexes in solid state and solution

3.11.2.2 Ni(II) complexes

The reflectance spectra of Ni(II) complexes of 2MT and 2MA ligands are also similar (**Fig. 3.68**, also see section 3.8). As in the case of Co(II) complexes, three bands are expected for either octahedral or tetrahedral geometry. Four bands are observed in the spectra of Ni(II) complexes, the lowest energy band is broad covering the range 900–1300 nm, the second band occurs in the region 600–660 nm, the third band close to the UV region occurs between 380 and 430 nm and this band is masked in some complexes by the strongly intense charge transfer band around 340 nm, which is the fourth band. These values are in accordance to those predicted for octahedral Ni(II) with the lowest transition corresponding to $^3A_{2g} \rightarrow {}^3T_{2g}$, the second band is due to $^3A_{2g} \rightarrow {}^3T_{1g}$ transition and the third band is assigned to $^3A_{2g} \rightarrow {}^1E_g$. The case of Ni(2MeO–2MA) is already discussed, the shift to longer wavelengths is probably as a result of extended conjugation of the aromatic system by the methoxy chromophore at the *ortho* position.

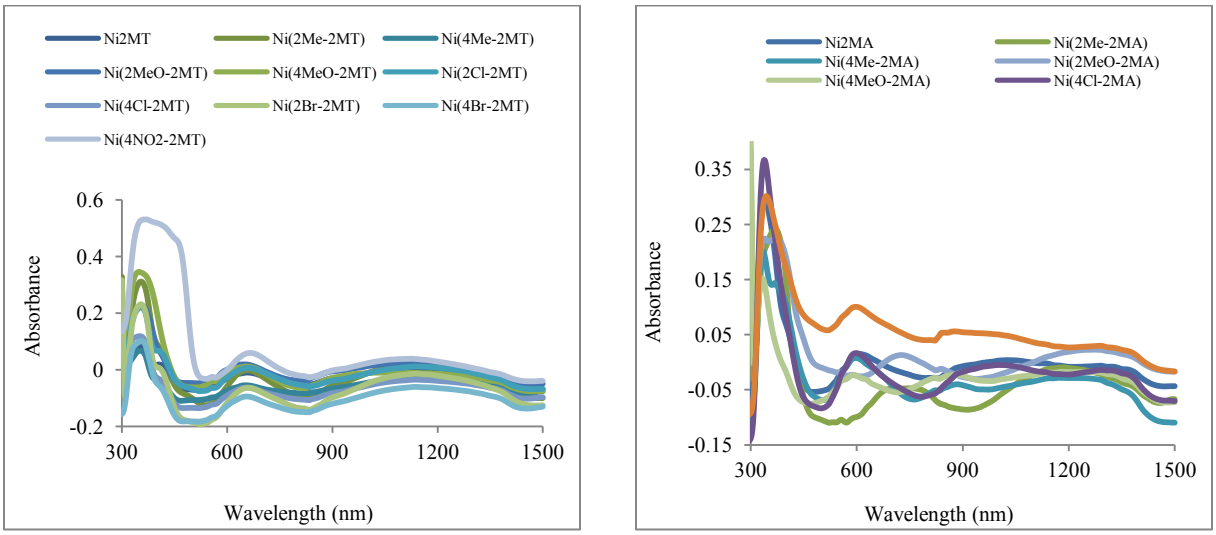

Fig. 3.68 Solid reflectance spectra of Ni(II) complexes of 2MT (left) and 2MA (right) ligands

In solution, the electronic spectra of Ni(II) complexes of both 2MT and 2MA ligands are also similar (**Fig. 3.69-3.72**). Two of the complexes (Ni(2MeO–2MA) and Ni(4Cl–2MA)) have identical spectra while in other complexes, the solvent effect is prominent.

The spectra in DMF solution generally show seven transitions in the UV-visible region; the low energy transition could not be fully observed as the range of the instrument used does not exceed 1100 nm, but it

can be seen to tail into the near IR region from 1100 nm. There are bands of varying intensities at 580, 700 and 770 nm which appear as shoulder bands in some cases. The more prominent bands in the spectra are observed in the ranges 400–435 nm, 610–650 nm and 680–700 nm. The high intensity band between 320 and 380 nm is due to a charge transfer transition from nitrogen to Ni(II).

In DMSO solution, the spectra have fewer transitions comprising of the charge transfer transition between 320 and 380 nm, a shoulder band around 700 nm, the prominent transition in the range 760–840 nm and the low energy band tailing into the near IR around 1100 nm. As can be seen from **Tables 2.30–2.31** (Chapter 2), all the bands in DMSO are replicated in DMF being shifted to higher energies.

The bands in the solution are shifted to higher energy relative to those in the solid spectra (**Fig. 3.73**) and this is in contrast to what obtained in Co(II) complexes. Conductivity of Ni(II) complexes in DMF shows there is a removal of one of the chloride ions from the coordination center hence they were seen to behave as 1:1 electrolytes. A shift to higher energy is expected as a weak coordinating ligand is replaced by a stronger one. One can then surmise that DMF molecule replaces a chloride ion, hence increasing the energy absorptions as reflected in the band shift while retaining the octahedral geometry around the Ni(II).

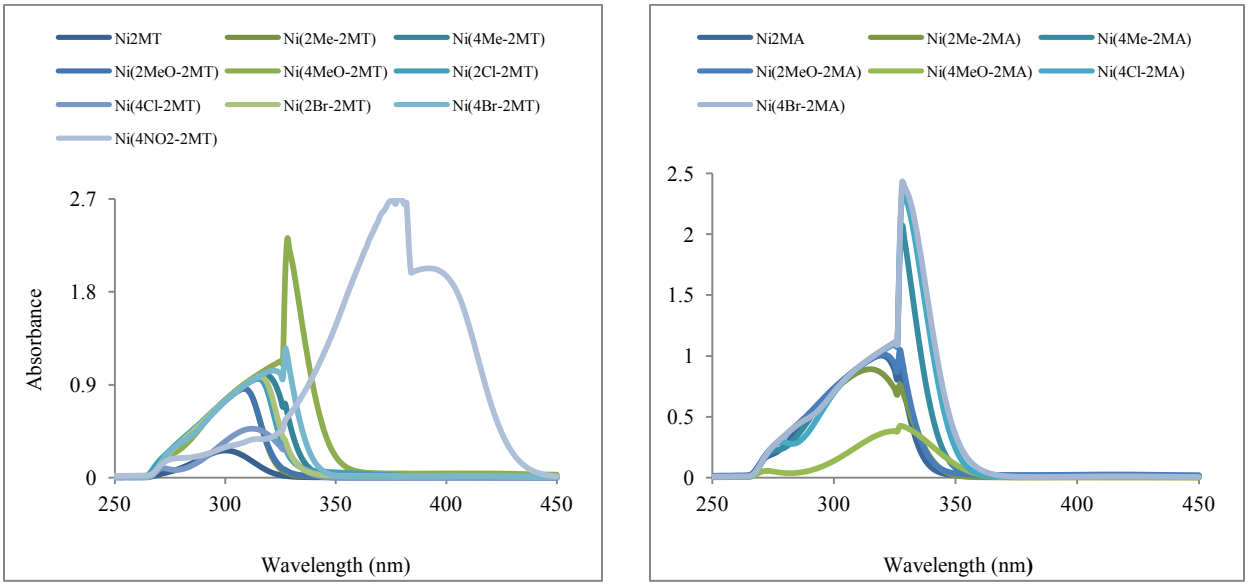

Fig 3.69 Electronic spectra of Ni(II) complexes of 2MT (top) and 2MA (bottom) in DMF in the near UV region

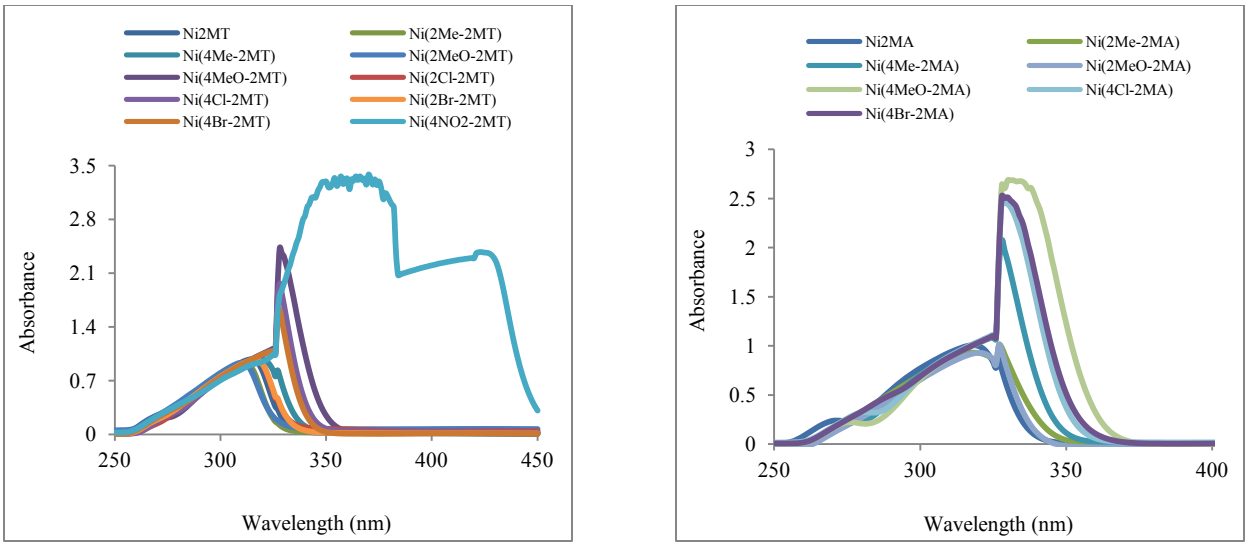

Fig 3.70 Electronic spectra of Ni(II) complexes of 2MT (top) and 2MA (bottom) in DMSO in the near UV region

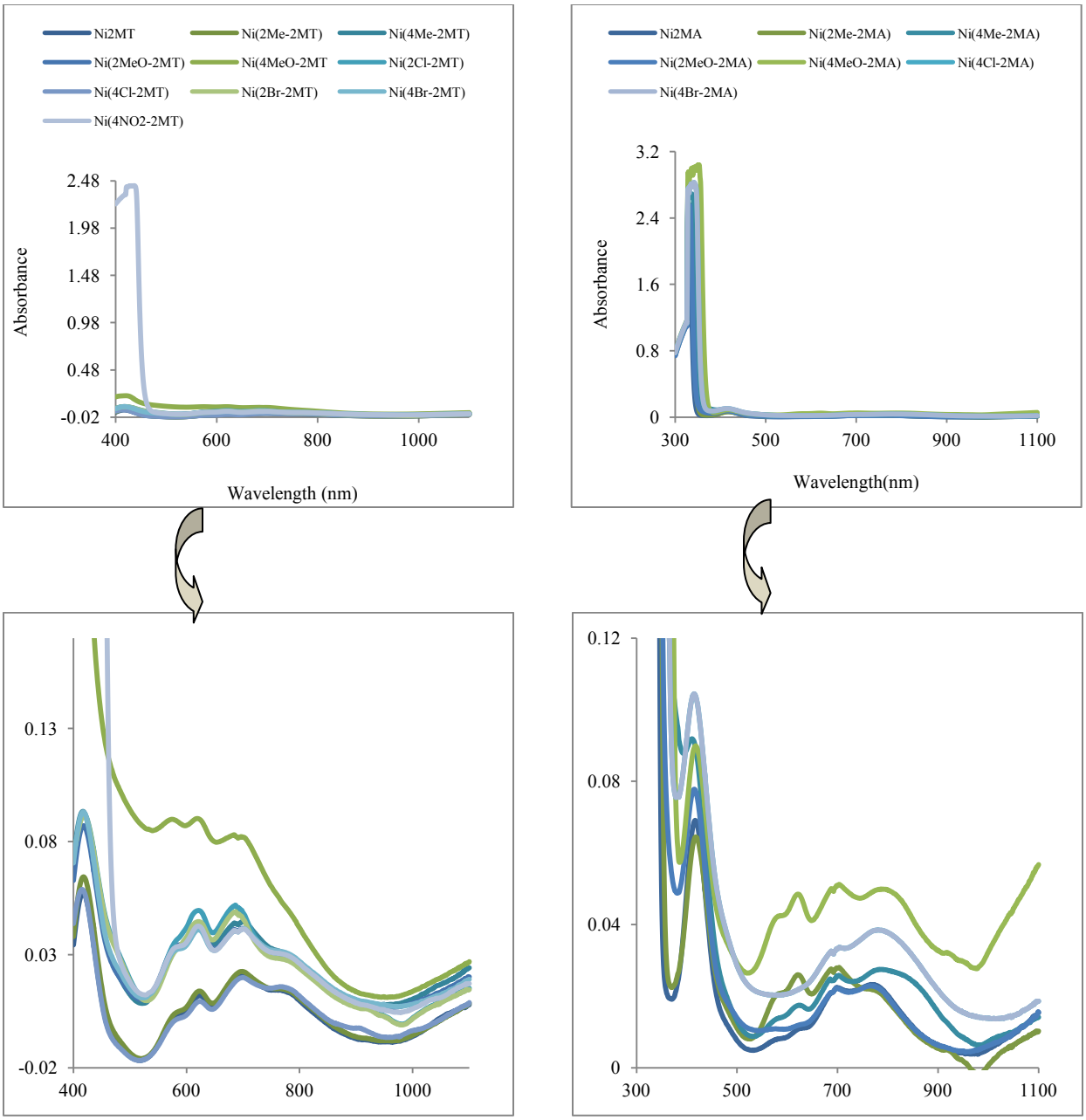

Fig 3.71 Electronic spectra of Ni(II) complexes of 2MT (top left) and 2MA (top right) in DMF in the visible region with expanded views (below)

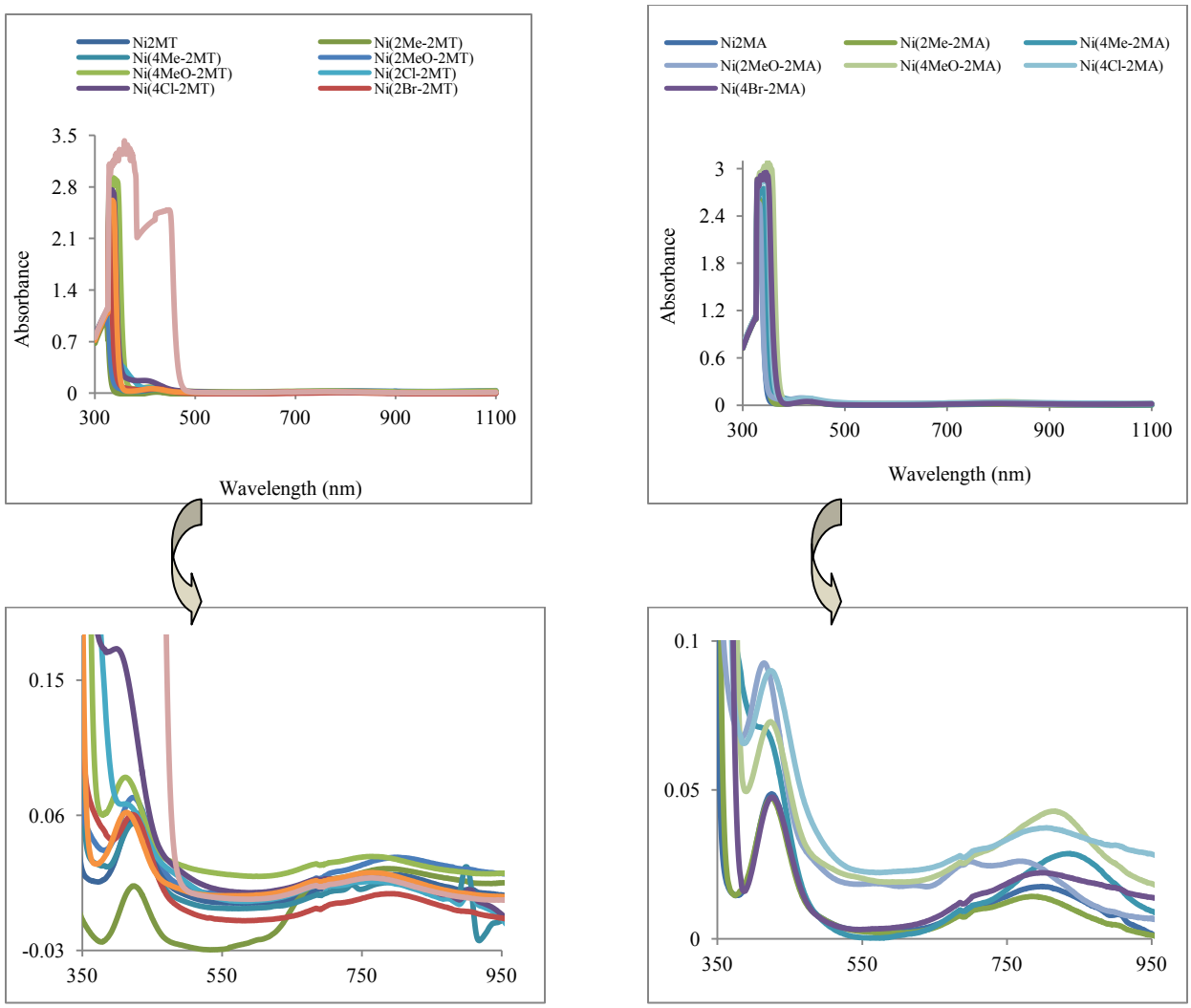

Fig 3.72 Electronic spectra of Ni(II) complexes of 2MT (top left) and 2MA (top right) in DMSO in the visible region with expanded views (below)

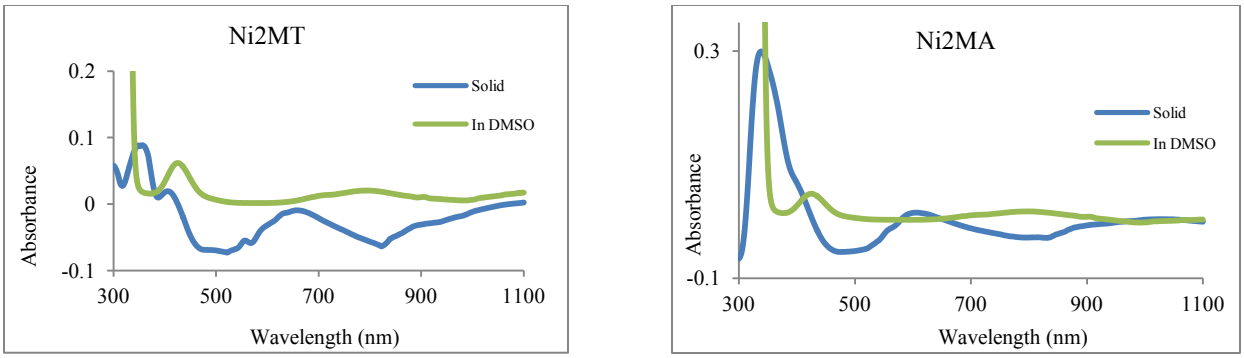

Fig. 3.73 Ni(II) complexes in solid state and solution

One can then suggest that the Ni(II) complexes exist in the (distorted) octahedral geometry in both solid states and in solution. The proposed structures are drawn in **Fig.3.74**.

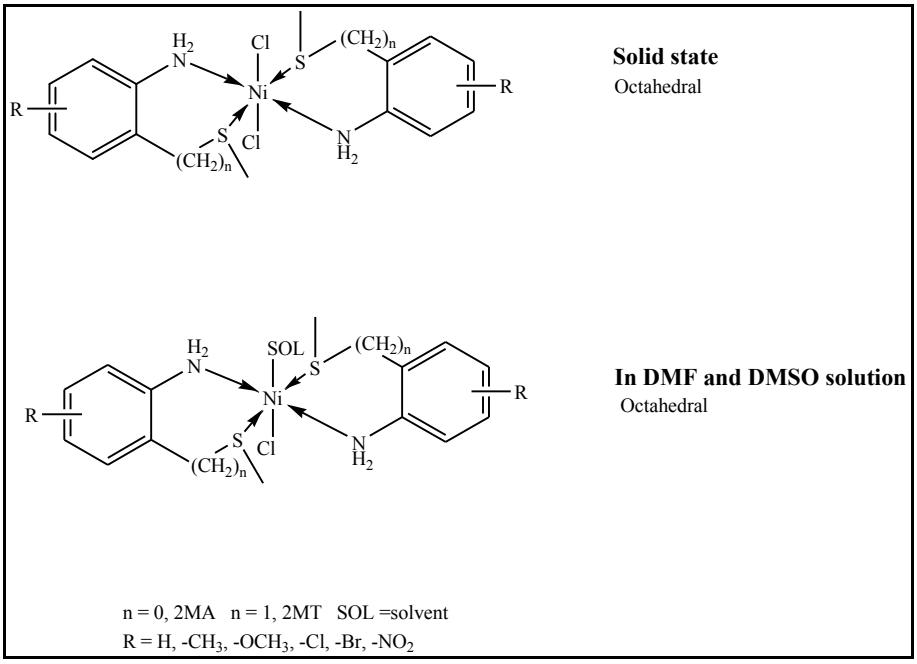

Fig. 3.74 Proposed structures for Ni(II) complexes in solid state and solution

3.11.2.3 Cu(II) complexes

The electronic spectra of Cu(II) complexes of 2MT and 2MA ligands are much similar in DMF and DMSO solvents (**Fig. 3.75–3.78**). They differ only in the noticeable decrease in the intensity of the charge transfer transition which now appears as a shoulder. This charge transfer at 430 nm is associated with sulfur to Cu(II) transition, it could be that DMSO is interacting with the copper ion in such a way that obscures the thioether sulfur overlap with the metal ion, hence the reduced intensity of that band.

From the spectra below, a broad band is seen in the region 700-1100 nm for the 2MT complexes and most of them exhibit similar spectra with the exception of the methoxy-substituted. Those of 2MA can be classified into two main categories; the *para*-substituted complexes have similar spectra with the exception of the para-methoxy and the *ortho*-substituted complexes which also exhibit similar spectra. However, the bands in Cu(2Br–2MA) fall into same category with those of the para-substituted complexes. It could be recalled that this particular compound formed in a 2:1 ligand to metal ratio in contrast to other Cu(II) complexes. This could suggest that the para-substituted complexes have the octahedral geometry in solution. The d→d band is broad between 850 and 1100 nm.

The spectra of the *ortho*-substituted 2MA complexes consist of more spin-forbidden transitions which appear as shoulders, and the 900 nm band seems to be masked by the charge transfer band. An octahedral geometry could still be suggested for them because they display similar electrolyte behaviour in DMF as the para-substituted complexes.

They both show charge transfer transitions from ligand to metal around 330 nm (N→Cu) and around 430 nm attributed to S→Cu. For either an octahedral or tetrahedral copper(II), the electronic spectra usually give one broad band. It is well known that electronic spectra of a Cu(II) complex are not sufficient to decide its geometry.[69]

The d–d band in solid spectra of these Cu(II) complexes differ from that in solution (**Fig. 3.79**) as it is shifted to higher energies in DMF solution as was observed for Ni(II) complexes. Taking into consideration the behaviour of Cu(II) complexes in DMF as non-electrolytes, this shift can be explained. The bond distance of the sixth bond attached to the octahedral Cu(II) is 2.932 Å, between Cu and one of the chloride ions. This bond is long and will be easily displaced by the strongly coordinating DMF and DMSO solvents. This gives rise to a transition of higher energy as the stronger field DMF ligand replaces the weaker Cl^-. This chloride ion is not displaced because it is also equatorially bonded to another Cu(II) in the adjacent layer. The terminal Cl^- was not displaced either because of the stronger equatorial bond it

has with Cu(II). Hence in solution, the octahedral geometry around Cu(II) is maintained but the solvent molecule being the sixth ligand.

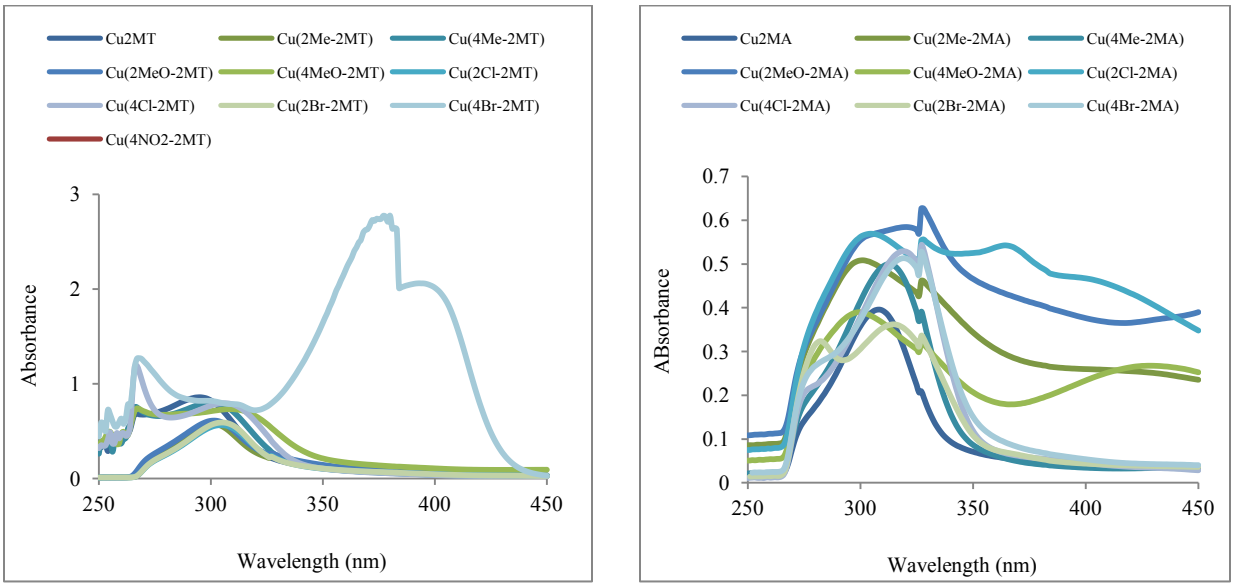

Fig 3.75 Electronic spectra of Cu(II) complexes of 2MT (top) and 2MA (bottom) in DMF in the near UV region

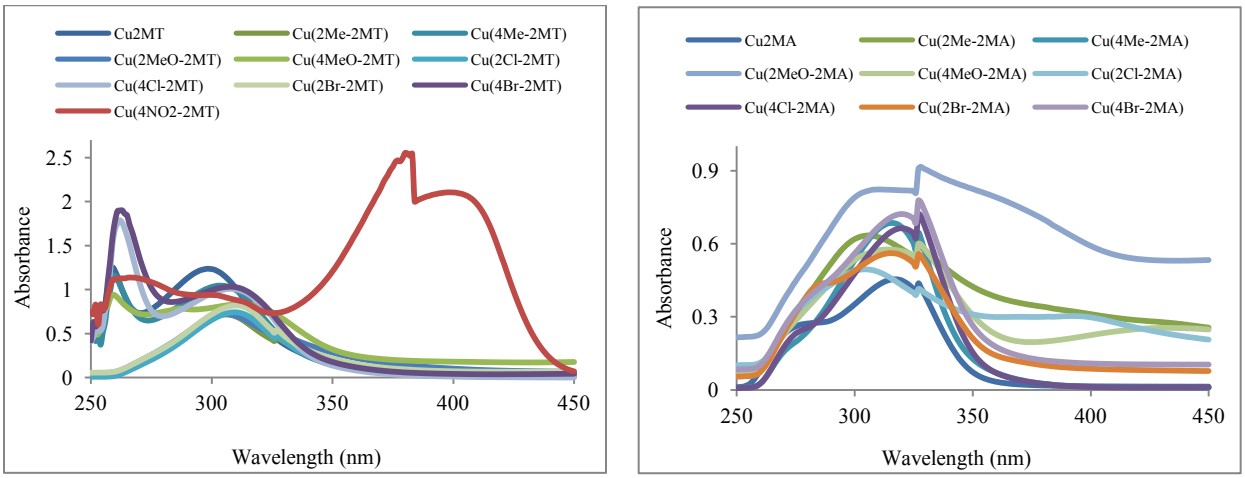

Fig 3.76 Electronic spectra of Cu(II) complexes of 2MT (top) and 2MA (bottom) in DMSO in the near UV region

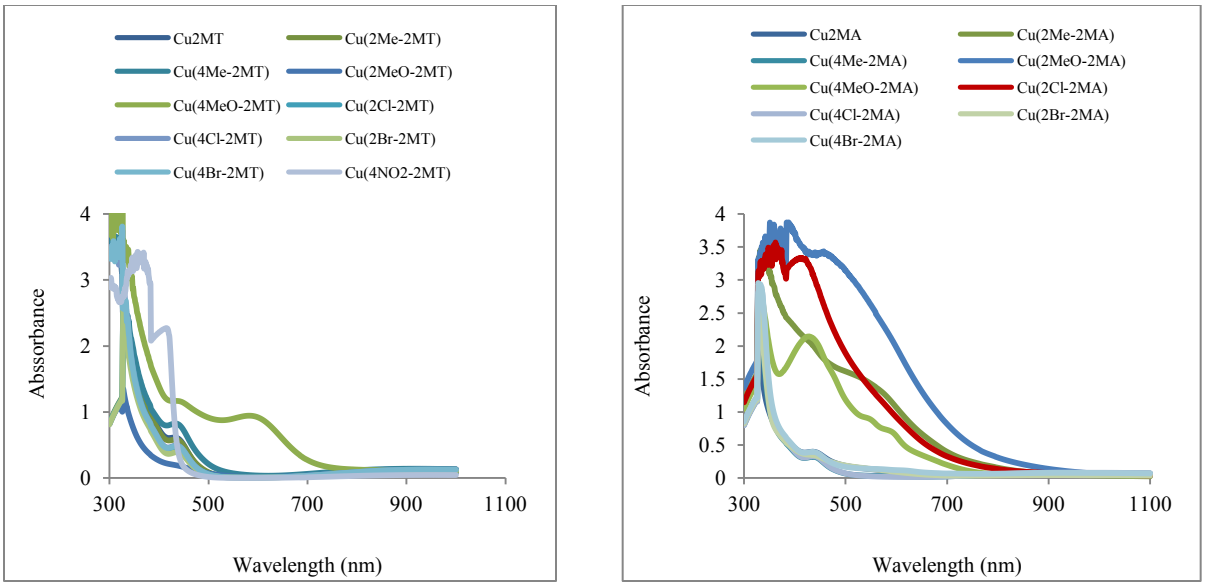

Fig 3.77 Electronic spectra of Cu(II) complexes of 2MT (top) and 2MA (bottom) in DMF in the visible region

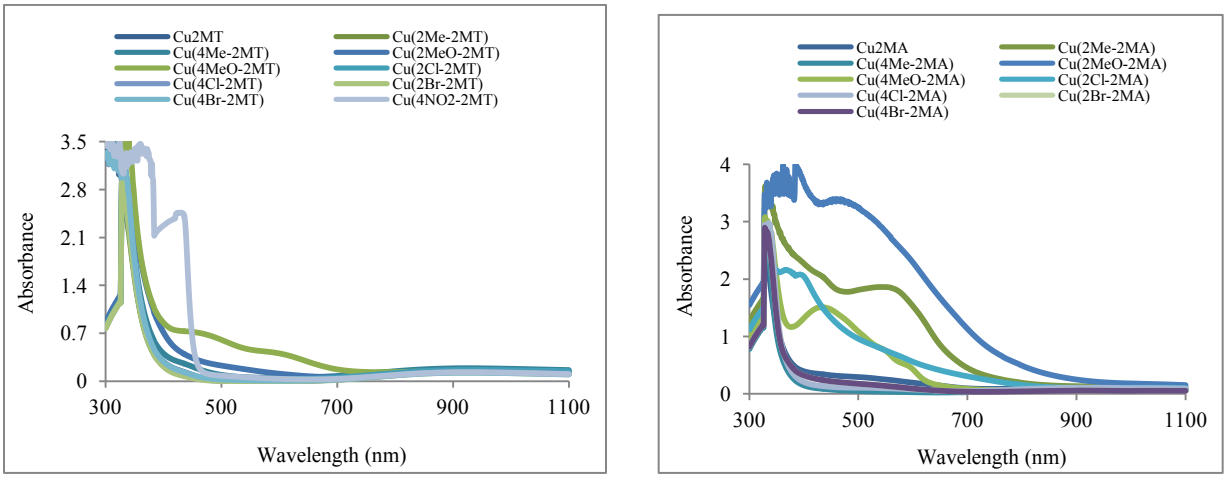

Fig 3.78 Electronic spectra of Cu(II) complexes of 2MT (top) and 2MA (bottom) in DMSO in the visible region

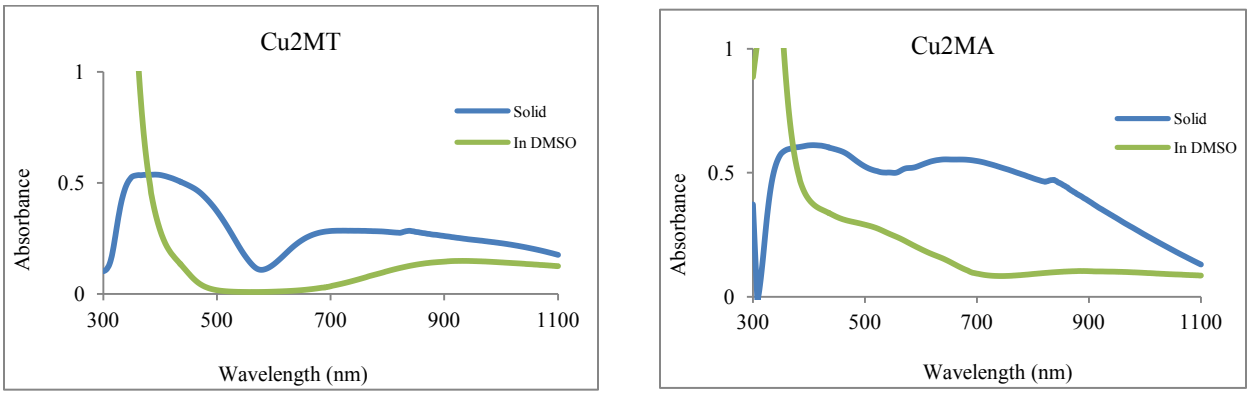

Fig. 3.79 Cu(II) complexes in solid state and solution

On this basis, the structure of Cu(II) complexes in solution is proposed to be octahedral as shown in **Fig. 3.80**.

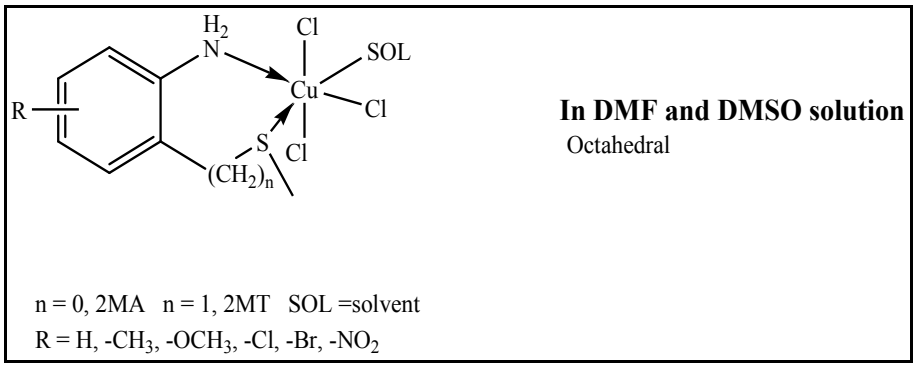

Fig. 3.80 Proposed structures for Cu(II) complexes in solid state and solution

3.11.3 Comparison between the spectra of 2MT and 2MA complexes

The visible bands in the spectra of 2MT and 2MA complexes are generally similar, differing only in small shifts which are not consistent. The spectra in **Fig. 3.81** below indicate similarity in 2MT and 2MA complexes.

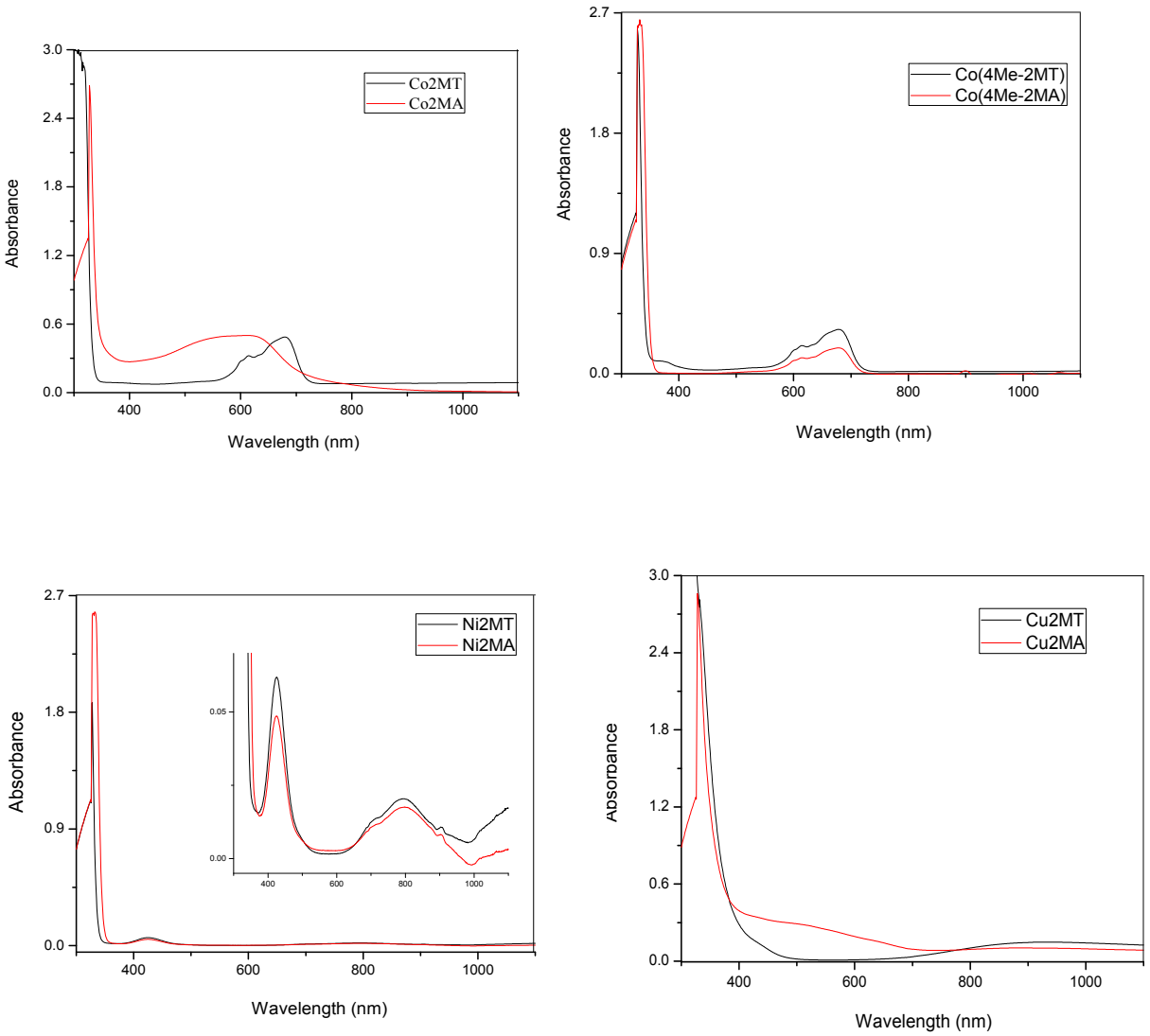

Fig. 3.81 Comparison of bands in 2MT and 2MA complexes

A trend is however noticeable in the energies of the charge transfer band (N → Cu) in the solid Co(II), Ni(II) and Cu(II) complexes as seen in **Fig. 3.82** . The trend Co(II) > Ni(II) > Cu(II) is observed with

2MT complexes and the 2MA complexes follow the trend Co(II) ≈ Ni(II) > Cu(II). The implication of this is that as the metal ions become less readily reducible, the energy involved in transferring electrons from the ligand orbitals to the metal ion increases. The energy of transition to Cu(II) is the lowest, this makes Cu(II) the most reducible of the three ions.

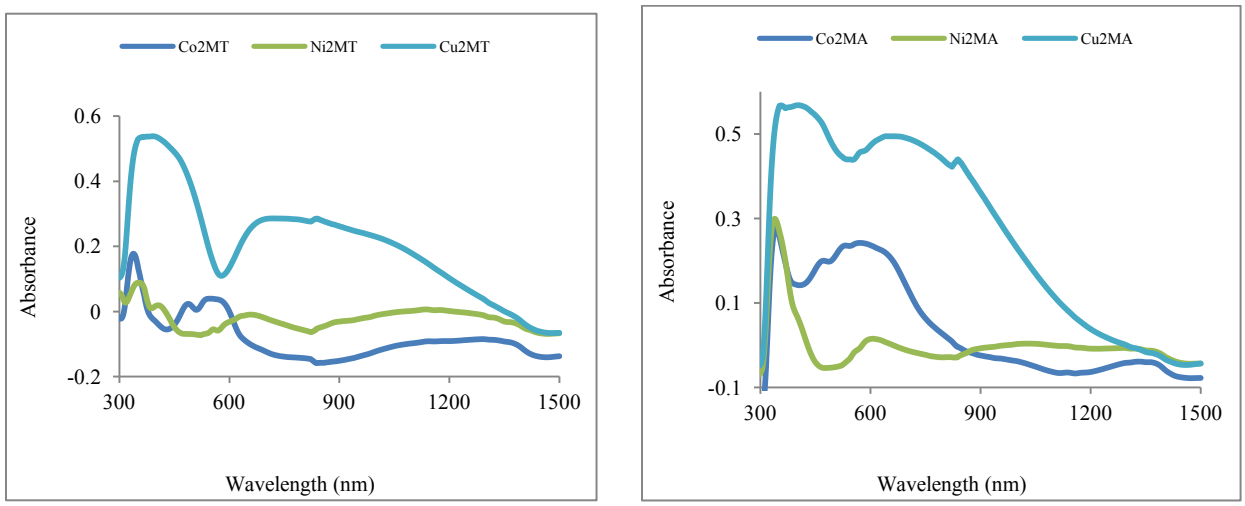

Fig. 3.82 CT and ligand field bands in solid spectra of 2MT (*left*) and 2MA (*right*) complexes

3.12 ELECTRONIC SPECTRA OF SCHIFF-BASE LIGANDS AND COMPLEXES

The spectra of Schiff-base ligands show high energy transition $\pi \rightarrow \pi^*$ of the aromatic ring in the range 244–355 nm (**Fig. 3.83** and **3.84**). The $n \rightarrow \pi^*$ transition of the nitrogen lone pairs of electron to the aromatic ring occurs at a lower energy between 340 and 370 nm. These bands are shifted to longer wavelengths in the spectra of the complexes on complexation (**Fig. 3.85-3.87**) as a result of extensive conjugation of delocalized electrons throughout the compounds. An extra transition around 400 nm attributed to S → M charge transfer is also observed (**Fig. 3.88**), this type of transition is reported in a similar complex.[39] This CT band is not observed in pMS–2MA Schiff-bases, however. The d→d transition spans the region 600 – 615 nm, this is suggestive of a square based geometry around[71] copper(II) in a weak tetragonal field; which is consistent with the observed X-ray crystal structures of **1B** and **2B** in which octahedral structures with long Cu–S axial bonds make the fifth and sixth bonds.

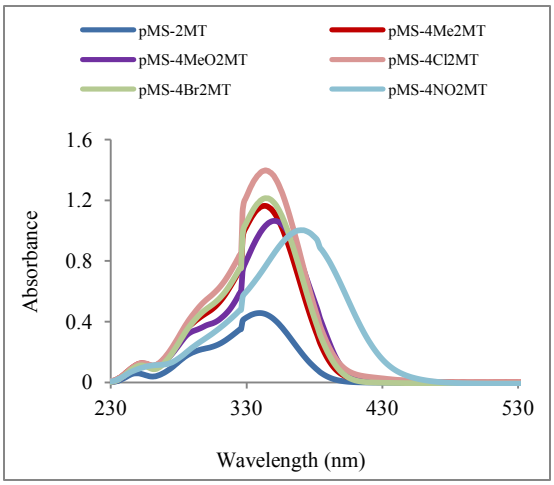

Fig. 3.83 Electronic spectra of pMS–2MT ligands UV region

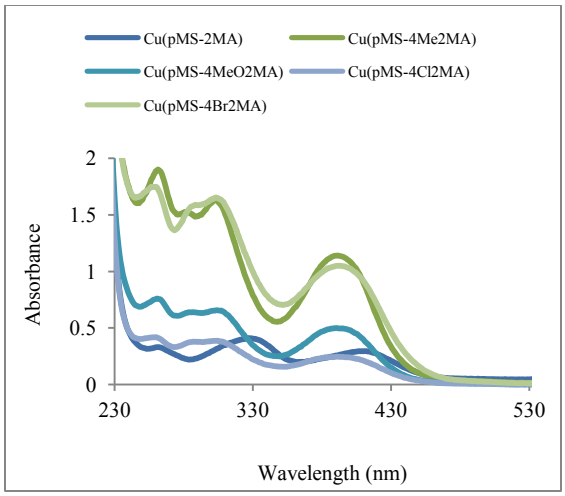

Fig. 3.84 Electronic spectra of pMS–2MA ligands in the in the UV region

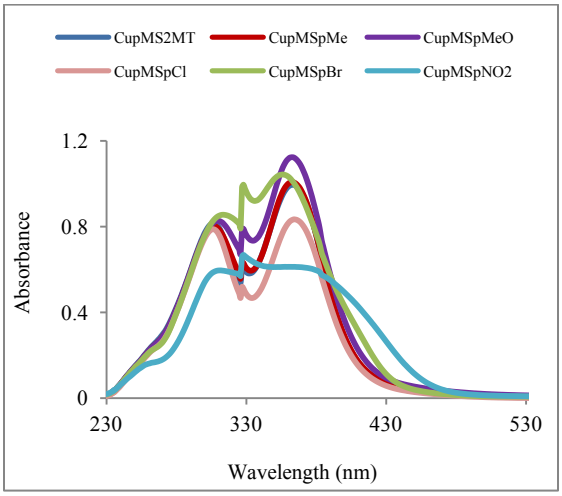

Fig. 3.85 Electronic spectra of Cu(II) complexes of pMS–2MT ligands in the UV region

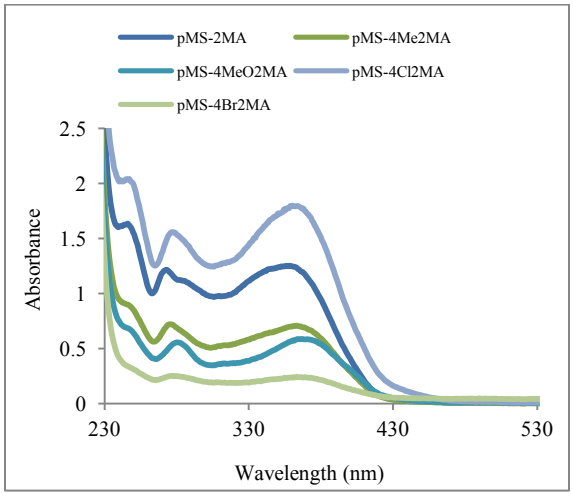

Fig. 3.86 Electronic spectra of Cu(II) complexes of pMS–2MA ligands in the UV region

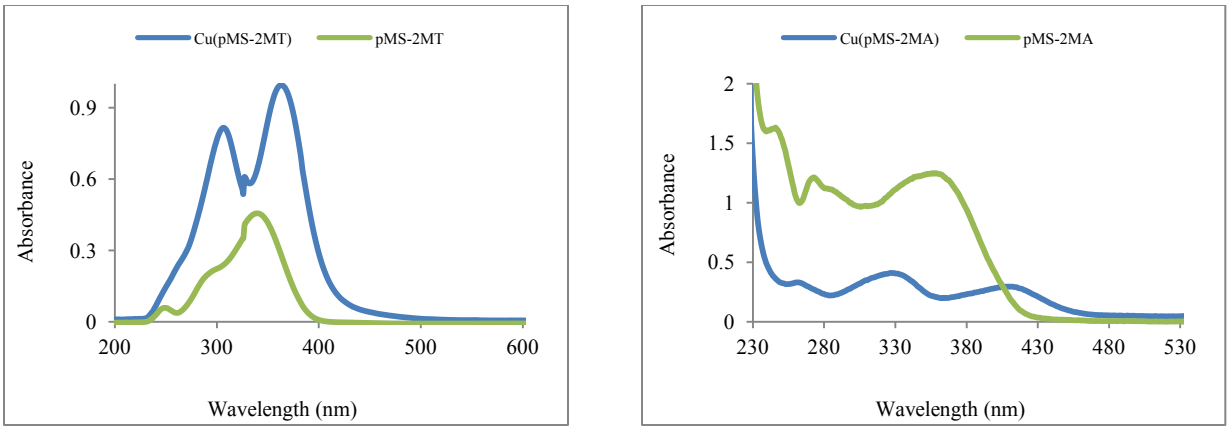

Fig. 3.87 Typical electronic spectra of the Cu(II) complex compared with the Schiff-base ligand

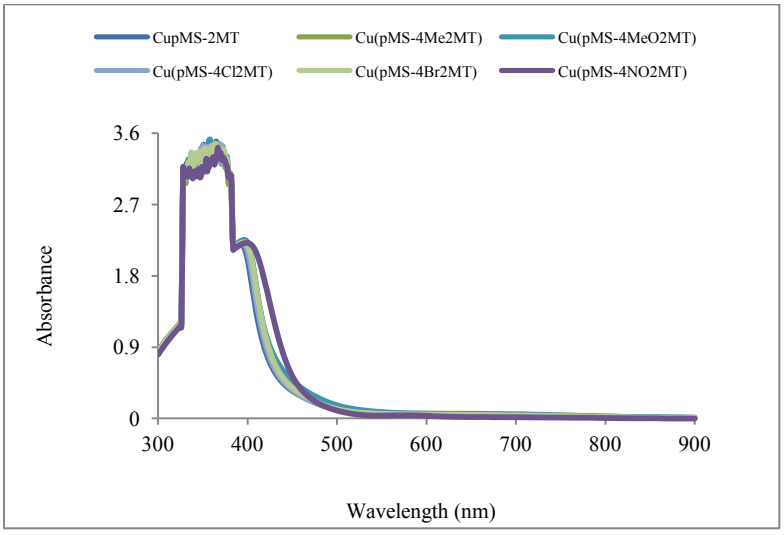

Fig. 3.88 Electronic spectra of Cu(II) complexes of pMS–2MT ligands in the visible region

3.12 REFERENCES

1. P. G. Gassman and G. D. Gruetzmacher, *J. Am. Chem. Soc.*, 1974, **96**, 5487.
2. J. P. Chupp, T. M. Balthazor, M. J. Miller and M. J. Pozzo, *J. Org. Chem.*, 1984, **49**, 4711.
3. P. Claus and W. Vycudilik, *Tetrahedron Letters*, 1968, **9**, 3607.
4. P. G. Gassman and G. Gruetzmacher, *J. Am. Chem. Soc.,* 1973, **95**, 588.
5. P. G. Gassman, T. J. Van Bergen and G. D. Gruetzmacher, *J. Am. Chem. Soc.*, 1973, **95**, 6508.
6. P. G. Gassman, G. D. Gruetzmacher and T. J. Van Bergen, *J. Am. Chem. Soc.*, 1974, **96**, 5512.
7. X. Fang, R. Tang, X. Zhang and J. Li, *Synthesis*, 2011, **7**, 1099.
8. N. Dunski and T. H. Crawford, *J. Inorg. Nucl. Chem*., 1969, **31**, 2073.
9. Y. Hiraki, M. Kamiya, R. Tanikaga, N. Ono and A. Kaji, *Bull. Chem. Soc. Japan*, 1977, **50**, 447.
10. H. Takeuchi, S. Hirayama, M. Mitani and K. Koyama, *J. Chem. Soc. Perkin* Trans. I, 1988, 2277.
11. P. F. Ranken and B. G. McKinnie, *J. Org. Chem.,* 1989, **54**, 2985.
12. B. A. Dreikorn, G. P. Jourdan, H. R. Hall, J. B. Deeter, and N. Jones, *J. Agric. Food Chem.* 1990, **38**, 549.
13. S. Messaoudi, J. Brion and M. Alami, *Adv. Synth. Catal*. 2010, **352,** 1677.
14. http://www.chem.ucalgary.ca/courses/351/Carey5th/Ch13/ch13-nmr-3.html#h-bonding. Date accessed: 31/07/2012
15. L. P. Hammett, *J. Chem. Soc.*, 1937, **59**, 96.
16. P. Sykes, *A Guidebook to Mechanism in Organic Chemistry*, Longman, London, 1975.
17. J. E. Kovacic, *Spectrochim. Acta*, 1967, **23A**(1), 183.
18. P. J. Kruger and D. W. Smith, *Can. J. Chem*., 1967, **45**, 1611.
19. K. Nakamoto, *Infrared and Raman Spectra of Inorganic and Coordination Compounds, Part I: Theory and Applications in Inorganic Chemistry*, New York Wiley, 1984.
20. L. J. Bellamy and R. L. Williams, *Spectrochim. Acta*, 1957, **9**, 341.
21. M. Tsuboi, *Spectrochim. Acta*, 1960, **16**, 505.
22. L. F. Lindoy and S. E. Livingstone, *Inorg. Chem.*, 1968, **7**, 1149.
23. K. Kratzl, H. Fostel and R. Sobczak, *Monatsh. Chemie*, 1972, **9**, 103, 677.
24. J. Whysner, L. Vera and G. M. Williams, *Pharmaco Ther.*, 1996, **71**, 107.
25. P. Hohenberg and W. Kohn, *Phys Rev*. B, 1964, **136**, 864.
26. C. H. Misra, S. S. Parmar and S. N. Shukla, *Canad. J. Chem.*, 1967, **45**, 2459.
27. J. Chatt, L. A. Duncanson and L. M. Venanzi, *J. Chem. Soc.*, 1956, 2712.
28. G. F. Svatos, C. Curran and D J. V. Quagliano, *J. Chem. Soc.*, 1955, **77**, 6159.

29. M. Maji., M. Chatterjee, S. K. Chattopadhyay and S. Ghosh, *Acta Chem. Scand.*, 1999, **53**, 253.

30. H. Takeuchi, S. Hirayama, M. Mitani and K. Koyama, *J. Chem. Soc. Perkin* Trans. *1*, 1986, 2277.

31. M. Matsui, Y. Marui, M. Kushida, K. Funabiki, H. Muramatsu, K. Shibata, K. Hirota, M. Hosoda and K. Tai, *Dyes and Pigments*, 1998, **38**, 57.

32. G. Varsanyi and S. Szoke, *Vibrational Spectra of Benzene Derivatives*, Academic Press, New York and London, 1969.

33. R. J. H. Clark, *Spectrochimica Acta*, 1965, **21**, 955.

34. H. Hubacek, B. Stancic and V. Gutmann, *Monatsh. Chemie*, 1963, **94**, 1118.

35. G. J. Medina, "Ligand isotope vibrational spectroscopic and DFT studies of Pt(II) and Cu(I) complexes". 2005, PhD Thesis, Rhodes University Grahamstown, South Africa.

36. "A spectroscopic study of Cu(I) carbonyl compounds with Schiff bases: Substituted –{*N*-benzylidene-*N*'-{2,2N3(R-$C_6H_4)_2$}]BPH_4". Gerardo Juan Medina and Gareth Mostyn Watkins, *INORG2009, Bloemfontein, South Africa, 13th – 17th Sept 2009.*

37. M. Ikram and D. B. Powell, *Spectrochimica Acta*, 1971, **27A**, 1845.

38. D. J. Curran, S. Siggia, *The chemistry of carbon-nitrogen double bond*, S. Patai (Ed.), Wiley-Interscience, New York, 1970, 162.

39. R. Balamurugan, M. Palaniandavar, H. Stoeckli-Evans and M. Neuburger, *Inorg. Chim. Acta*, 2006, **359**, 1103.

40. B. K. Santra, P.A.N. Reddy, M. Nethaji and A.R. Chakravarty, *Inorg. Chem.*, 2002, **41**, 1328.

41. B. K. Santra, P.A.N. Reddy, M. Nethaji and A.R. Chakravarty, *J. Chem. Soc., Dalton* Trans., 2001, 3553.

42. M. Vaidyanathan, R. Balamurugan, U. Sivagnanam, and M. Palaniandavar, *J. Chem. Soc., Dalton Trans.*, 2001, 3498.

43. G. Murphy, P. Nagle, B. Murphy and B.J. Hathaway, *J. Chem. Soc., Dalton* Trans., 1997, 2645.

44. G. Murphy, C. O. Sullivan, B. Murphy and B.J. Hathaway, *Inorg. Chem*., 1998, **37**, 240.

45. R. D. Willett, G. Pon and C. Nagy, *Inorg. Chem.,* 2001, **40**, 4342.

46. L. Escriche, M. Sanz, J. Casabo, F. Teixidor, E. Molins and C.Miravitlles, *J. Chem. Soc. Dalton* Trans., 1989, 1739.

47. S.B. Sanni, H.J. Behm, P.T. Beurskens, G.A. van Albada, J. Reedijk, A.T.H. Lenstra, A.W. Addison and M. Palaniandavar, *J. Chem. Soc., Dalton* Trans., 1988, 1429.

48. P. C. Burns and F. C. Hawthorne, *American Mineralogist*, 1993, **78**, 187.

49. M. Vaidyanathan, R. Balamurugan, S. Usha and M. Palaniandavar, *J. Chem. Soc., Dalton* Trans., 2001, 3498.

50. J.G. Gilbert, A.W. Addison, A.Y. Nazarenko and R.J. Butcher, Inorg. Chim. Acta, 2001, **324**, 123.
51. http://www.doe-mbi.ucla.edu/CHEM125/bonds.html. Date accessed: 22/07/2011
52. E. Bouwman, W.L. Driessen and J. Reedijk, *Coord. Chem. Rev.*, 1990, **104**, 143.
53. Comprehensive coordination Chemistry, *The synthesis, reactions, properties and applications of coordination compounds*, Ed. Sir George Wilkinson, R. D. Gillard, J. A. Mcleverty. Volume 5 Late Transition Elements, 1st Ed., Pergamon Press, Britain, 1987, 596.
54. Sandipan Sarkar, Pulak K. Dhara, M. Nethaji and Pabitra Chattopadhyay, *Journal of Coord. Chem.*, 2009, **62**, 817.
55. S. K. Ramalingam and S SoundararaJan, *J. Inorg. Nucl. Chem.*, 1967, **29**, 1763.
56. P. G. Sears, G R. Lester and L R Dawson, *J Phys. Chem.,* 1956, **60**, 1433.
57. J. A. Broomhead and L. A. P. Kane-Maguire. *J. Chem. Soc. A.,* 1967, 546.
58. N. N. Greenwood, B P. Straughan and A. E. Wilson, *J. Chem. Soc. A.,* 1968, 2209.
59. A. D. Alien, F. Bottomley, R. 0. Harris, V. P. Reinsalu and C. V. Senoff, *J. Amer. Chem.* Soc., 1967, **89**, 5595.
60. R. V. Bragetti, W. G. Bottler and H. M. Haendler, *Inorg Chem*., 1966, **5**, 379.
61. P. G. Sears, E. D. Wilhoit and L. R. Dawson, *J. Phys. Chem.* 1955, 59, 373.
62. D. P. Ames and P.G. Sears, J. *Phys. Chem.* 1965, *59*, 16.
63. J. H. Enemark and R. H. Holm, *Inorg. Chem.,* 1964, **3**, 1516.
64. T. J. Ouellette and H. M. Haendler, *Inorg. Chem.,* 1969, **8**, 1777.
65. W. J. Geary, *Coord. Chem. Rev.*, 1971, **7**, 81-122.
66. http://teaching.shu.ac.uk/hwb/chemistry/tutorials/molspec/uvvisab1.htm. Date accessed: 05/22/2010.
67. D. Nicholls in *Comprehensive Inorganic Chemistry* 1st ed., Vol. 3 (ed. J. C. Bailar, H. J. Emeleus, Ronald Nyholm and A. F. Trotman-Dickenson), Pergamon Press, 1973, 1080.
68. J. Ferguson, *J. Chem. Phys.* 1963, **39**, 116
69. H. A. Weakliem, *J. Chem. Phys.* 1962, **36,** 2117.
70. L. Sacconi, F. Mani and A. Bencini in *Comprehensive Coordination Chemistry: the synthesis, reactions, properties and applications of coordination compounds*, ed. Geoffrey Wilkinson, R. D. Gillard and J. A. McCleverty, Pergamon, Oxford, 1987, Vol. 5, 2, 45 - Late transition elements.
71. F.J. Richardson and C.N. Payne, *Inorg. Chem*., 1978, **17**, 2111.

BIOLOGICAL ACTIVITY OF COMPOUNDS

The 2MT and 2MA ligands including their metal complexes have the amine functionality alongside with the thioether group in their chemical structures. These two groups are known for conferring biological activity on systems where they are present. Literature is replete with such compounds of biological importance. Hence these compounds were tested in vitro against bacteria and fungus using the antimicrobial susceptibility testing procedure as outlined below. With encouraging results of antimicrobial inhibition from some of the compounds tested, the analogue Schiff–bases derived from their condensation reaction with *para* methoxysalicaldehyde were synthesized. The therapeutic effects of Schiff–bases are well documented in various biological applications and *para* methoxysalicaldehyde is known for its antimicrobial[1-3] and antioxidant[4] properties. Of the three categories of metal complexes tested, Cu(II) complexes have shown the greatest biological activity, the Cu(II) complexes of the Schiff–bases were therefore synthesized. A greater inhibition was expected as a result of combination of these properties. The Schiff-base ligands are soluble in DMF but their Cu(II) complexes were not. As a result, the biological activity of the metal complexes could not be tested. The Schiff–bases tested were not active in the least, no inhibition was observed.

Preliminary investigations to determine the antiplasmodial activity of the thiomethylated ligands and their metal complexes were carried out, their cytotoxicity was also tested in an attempt to assess their selectivity towards the plasmodial or breast carcinoma cell.

4.1 ANTIMICROBIAL SUSCEPTIBILITY TESTING

4.1.1 Materials and measurements

The microorganism strains were purchased from Microbiologics 217 Osseo Avenue North, St. Cloud, MN 56303. The nutrients/growth media were purchased from Merck, Becton Dickinson and Company in South Africa The sterile disks were purchased from Davies Diagnostics South Africa. Ampicillin powder was obtained from Roche Diagnostics GMBH, Mannheim, Germany. Double-distilled Millipore water was collected from the Pharmaceutics Unit of Faculty of Pharmacy, Rhodes University. Sterile saline was prepared by dissolving 0.85 g in double-distilled Millipore water and making up to 100mL. McFarland (0.5) solution was prepared by adding 0.5 ml of 1.175 % $BaCl_2.2H_2O$ to 99.5 mL of 1 % H_2SO_4.[5] The cultivation of *Plasmodium falciparum* and antiplasmodial screening of the test compounds were carried out by Dr van Zyl at the Department of Pharmacy and Pharmacology at University of Witwatersrand. Screening for cytotoxicity assay was conducted by Dr. A. Edkins at the Biomedical and Biotechnology Research Unit at Rhodes University.

The materials used for the antimicrobial susceptibility testing include:

1. *Bacillus subtilis (sub. spizizenii)* ATCC 6633, *Escherichia coli* ATCC 8739, *Staphylococcus aureus* ATCC 6538 and *Candida albicans* ATCC 2091.

2. Mueller Hinton Agar (MHA), Agar bacteriological, Potato Dextrose Agar (PDA) and Nutrient broth

3. Double-distilled Millipore water/sterile water, sterile saline

4. Micropipettes of appropriate volume sizes, pipette tips

5. Test tubes, pipettes, sterile inoculating loop, swab forceps

6. Gloves, masks, safety glasses, 70% ethanol solution

7. 96–well polystyrene tray (round-bottom wells), eppendorf tubes

8. Petri dishes (90 mm), Disks (6 mm diameter)

9. McFarland (0.5) solution, Dimethyl formamide (DMF)

10. Ampicillin (AMP), Ketoconazole (KTZ)

11. Ambient-air Incubator

12. Laminar flow chamber

13. Vortex mixer

14. LEDETECT 96 micro plate reader

15. PerkinElmer Lambda 25 UV/VIS Spectrometer

4.1.2 Procedures and methods[6-8]

The procedures described here were used for both antibacterial and antifungal susceptibility assays. The methods used were agar disk diffusion and micro-broth serial dilution. The procedures were carried out under a sterile aseptic atmosphere in a laminar flow to ensure there was no contamination. These tests were carried out in triplicates.

4.1.2.1 Agar disk diffusion susceptibility testing

This is a combination of Kirby and Bauer (NCCLS /CLSI approved) method.[6] This procedure involves the use of sterile disks impregnated with specific concentration of test agents/antibiotics which are placed on agar plate inoculated with the microorganism and incubated over a period of time. The diameter of zone of inhibition of the microorganism's growth by the antibiotic is measured and interpreted as susceptible (S), resistant (R) or intermediate (I) based on the values established for appropriate recognized reference. Ampicillin (AMP) and Ketoconazole (KTZ) were used as the reference antibiotics for the antibacterial and antifungal assays respectively.

Preparation of culture medium: The medium used to culture the microorganisms used in this research was a combination of MHA and Agar Bacteriological for the antibacterial assay while PDA was used to grow *Candida albicans*. They were prepared by mixing appropriate quantities and making up to the required volume with double-distilled Millipore water in high heat-resistant tightly sealed containers. The mixtures were autoclaved, allowed to cool to 40^{o}C and poured into labelled petri dishes up to 4 mm depth near an open flame. These media were allowed to solidify under a laminar flow. After cooling to

room temperature, these agar plates were turned upside down – to ensure the condensed water droplets at the upper part of the lids do not come in contact with the surface of the medium – and placed in the fridge. A representative sample of the agar plates was incubated overnight in the incubator to serve as negative growth control. No microbial growth was observed and this served to eliminate false results that could otherwise be obtained from an already contaminated medium.

Culture of microorganisms: A microorganism vial containing *Bacillus subtilis (sub. spizizenii)* ATCC 6633 was taken from 4^{o}C storage and allowed to equilibrate to room temperature. A pellet was removed using sterile forceps near an open flame and placed in a micro-centrifuge tube containing 500µL sterile water/saline water. The pellet was crushed using sterile swab until the particles were of uniform size and the suspension appeared homogenous. The swab was saturated with the suspension and transferred to the agar plate. Inoculation of the microorganism over the surface of the agar plate was carried out gently with the swab and inoculating loop to facilitate colony isolation. The plate was incubated at 37^{o}C, growth was observed after 30 h. A fresh culture was prepared from this stock culture by picking one well isolated colony, suspend in 5ml sterile saline, streaking on to a new plate and incubating overnight. Similar procedure was used to culture the other microorganisms, *Candida albicans* was incubated at 35^{o}C and the growth was observed after 48 h.

Preparation of test compounds/antibiotics: The test compounds used were the ligands and their metal(II) complexes synthesized during this research. Each was weighed and dissolved in dimethylformamide to make up to 50mg/L test solution; 5µL of each solution was taken up and applied onto the disks using a micro-pipette. This implies 250µg test compound was impregnated onto each disk. The disks were allowed to dry under the laminar flow.

Ampicillin was used as the primary reference standard for antibacterial testing. Stock solution of Ampicillin was prepared by dissolving 100 mg of it in 1 mL sterile water in a sterile Eppendorf tube and mixing them with the vortex machine. Smaller concentrations of 25 mg/mL and 10 mg/mL were obtained by taking out 0.25 mL and 0.10 mL respectively from the stock solution with a micropipette and diluting to 1 mL with sterile water. 5µL of each of these antibiotic solutions were separately applied to the disks to serve as the reference, that is, 125 and 50µg/disk applications.

The 100 mg/mL stock solution of Ketoconazole used as the reference standard for antifungal testing was similarly prepared by dissolving in DMSO.

Standardization of inoculum: In order to prepare the inoculum, 3 – 5 colonies of similar appearance were picked with a loop and suspended in saline water in a test tube. Standardization of the inoculum solution was achieved by comparing the turbidity of each with that of 0.5 McFarland and adjusting the density by adding more bacteria or more sterile saline. It has been estimated that at this concentration, the inoculum contains 10^8 colony forming units/ml of viable bacterial cells.

Inoculation of microorganisms, application of disks and incubation: The agar plates were inoculated[9] by dipping a sterile swab into the inoculum ensuring that excess inoculum was removed by pressing and rotating the swab firmly against the side of the tube. Each plate was then streaked all over the surface with the swab three times, rotating the plate through an angle of 60^o after each application to ensure uniform. The edge of the agar surface was swabbed last and in the process removing any water droplet condensed there. These surfaces were allowed to dry with the lid closed. This was followed by placement of disks coated with test agents/antibiotics on the inoculated agar surfaces using a pair of sterile forceps, pressing down gently to ensure good contact. Each plate contained 6 disks, evenly spaced on the surface. The plates were placed in the incubator set to 37^oC (or 35^oC in the case of *C. albicans*).

Measurement of zones of inhibition: After overnight incubation (48 h for *C. albicans*), the plates were removed and the diameter of clearance zone surrounding the disk (**Fig. 4.1**–**4.2**), indicating the zone of inhibition, was measured for each disk. Care was taken to ensure the lid was not opened and there was no contact with the bacterial droplets. The diameter of each zone, including that of the disk was measured from the outer surface of the lid using a ruler and recorded in mm **Table 4.1** (Section 4.4.1).

Interpretation of results: For quality control testing, the results are interpreted[10] as sensitive, intermediate or resistant by comparing with that already obtained for a standard drug against similar microorganism being tested. There is a standard interpretive breakpoint established for disk diffusion testing of Ampicillin (AMP) against[10] *Escherichia coli* but none for *Bacillus subtilis (sub. spizizenii)*, and *Staphylococcus aureus* or Ketoconazole (KTZ) against *Candida albicans*, hence no range of values have been designated as sensitive (S), intermediate (I) or resistant (R) for these last three organisms. Consequently, in this study, the results were not interpreted by the S, I, R designations. The results were interpreted by testing the inhibition of AMP and KTZ on the microorganisms at lower concentrations to that used for test compounds (250μg/disk) and comparing the difference in values (**Table 4.1**).

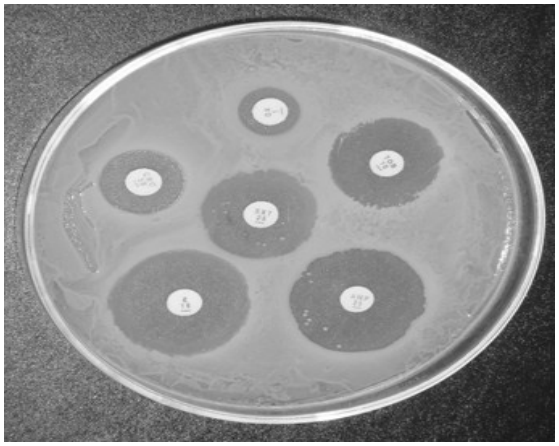

Fig. 4.1 Growth inhibition of microorganisms by compounds

Fig. 4.2 Measurement of inhibition zone of compounds[11]

4.1.2.2 Micro-broth serial dilution

The minimum inhibitory concentration (MIC) was determined for some of the *para* substituted compounds, a majority of which inhibited microbial growth by at least 12 mm (twice the size of the disk diameter). As a result, the microorganisms tested were *Bacillus subtilis (sub. spizizenii)* and *Staphylococcus aureus*. The procedure made use of a 96-well polystyrene tray of which 80 wells were filled with small volumes of a serial two-fold dilution of each test compound. The lowest concentration of antibiotic that inhibits visible growth on surface of broth was taken as MIC.

Preparation of culture medium: Test tubes containing 5mL Nutrient broth each were autoclaved. Four test tubes were used for each bacteria strain. A separate container containing more quantity of Nutrient broth for serial dilution was also autoclaved. These were allowed to cool to room temperature and refrigerated.

Culture of microorganisms: Single colonies of bacterial culture were touched with a loop and grown overnight. A single colony from the fresh bacterial culture was dropped inside the sterilized broth tube using micropipette tip and covered with the tip inside. Three test tubes were inoculated per strain. The test strains were grown to the right A_{625} (absorbance of 0.08 – 0.10) using the spectrophotomer instrument to check the absorbance. At this wavelength/absorbance, the appropriate inoculum size for standard MIC, $10^4 – 10^5$ CFU/mL is achieved.

Preparation of microtitre plates: The test agents/antibiotics were dissolved in DMF to make a concentration of 25 mg/mL in Eppendorf tubes. This implies the starting/highest concentration in well 1 for the test is 12.5 mg/mL. Micropipette of appropriate size was used to dispense 100μL of broth medium into all wells of the microtitre plate. 100 μL of each test compound was dispensed into wells in column 1. Using the micropipettor set at 100 μL, the compounds were mixed into the wells in column 1 by sucking up and down 6 – 8 times without splashing. A two-fold dilution of column 1 was achieved by withdrawing 100 μL from well 1/column 1 and adding to column 2. This made column 2 a two-fold dilution of column 1. It was also thoroughly mixed by sucking up and down 6 – 8 times and 100 μL of this was transferred into column 3. The procedure was repeated down to column 10 only. 100 μL was discarded from column 10 rather than putting it in column 11. Generally, wells 1 – 10 contained the broth, test compounds/antibiotics and the bacterial strain; 11th well contained the blank (broth and bacteria are present but antibiotic is absent) and 12th well contains the control (only broth is present, antibiotic and bacterial strain are absent), **Fig. 4.3**.

Inoculation of microorganisms and incubation: The bacterial solution grown to the right A_{600} was poured into a sterile petri dish. Another micropipette set to 5μL was used to dispense bacteria into wells in columns 11 to 1, in that order. The inoculum was not added to column 12 as it serves as the sterility control and blank for the plate scanner. Different test compounds were placed on different rows of the same plate but a bacterial strain was used per plate to avoid cross-contamination. Proper labelling was done to ensure no misappropriation of the test compounds. The plates were incubated at 37^{o}C and satisfactory growth was obtained within 24 h.

Measurements and interpretation of results: The plates were scanned with the microplate reader using column 12 as the blank. MIC was taken as the plate with lowest concentration of compound that inhibited visible growth on surface of broth.

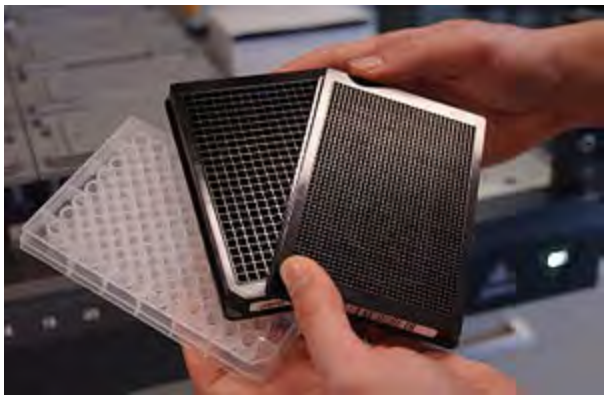

Fig. 4.3 Microtitre plates containing test compounds[12]

4.2 ANTIPLASMODIAL ASSAY PROCEDURE

4.2.1 Parasite cultivation

The chloroquine-resistant Gambian FCR-3 strain of the malaria parasite *Plasmodium falciparum* was cultured *in vitro* in human erythrocytes.[13,14] Parasitized erythrocytes were suspended at a 5% haematocrit in RPMI-1640, supplemented with 10 mM D-glucose, 0.32 mM hypoxanthine, 50 mg/L gentamicin, 10% (v/v) heat inactivated human plasma and was buffered with 25 mM HEPES and 25 mM $NaHCO_3$. Cultures were maintained daily and incubated at 37℃ with a gas mixture of 5% CO_2, 3% O_2 and the balance with N_2. Cultures were synchronized with 5% D-sorbitol when the parasites were in the ring stage for experimental purposes.[15] The percentage parasitaemia and stages were assessed daily by microscopic examination of thin blood smears stained with Giemsa.

4.2.2 Antiplasmodial screening

The antimalarial activity of the various extracts was determined using the tritiated hypoxanthine incorporation assay.[16] The parasite suspension, consisting predominately of the ring stage, was adjusted to a 0.5% parasitaemia and 1% haematocrit and exposed to the various concentrations of the compounds (plated in triplicate) for a single cycle of parasite growth. All assays were carried out using untreated parasites and uninfected red blood cells as controls. Labelled ^{3}H-hypoxanthine (0.5 μCi/ well, Amersham) was added after 24 h and the parasitic DNA was harvested on a Wallac® GFB-filtermat with a Titertek®

cell harvester. The filtermats were dried, transferred to sample bags which were filled with scintillation cocktail and sealed before being counted in the Wallac® beta counter. The counts per minute (cpm) were generated and the parasite survival rate calculated. The concentration that inhibited 50% parasite growth (IC_{50} value) was determined from the log sigmoid dose response curve generated by the Enzfitter® and Prism® software. Chloroquine and quinine were used as the reference antimalarial agents. Each experiment was repeated, at least, in triplicate.

4.3 CYTOTOXICITY SCREENING PROCEDURE

All compounds were tested in triplicate against MDA-MB-231 breast carcinoma cells. The cytotoxicity of the compounds was determined using the WST-1 assay method (Roche). The cells were treated with a range of concentrations of the test compounds or vehicle control. Cells treated with DMSO were considered to represent 100% viability and the viability of cells at each dose was represented relative to this value.

4.4 RESULTS

The available compounds were tested for their antimicrobial inhibition activity using DMF as solvent and 250 µg of each was measured on to the 6 mm disk. The compounds not tested have been used up for other characterisation tests or low-yielding such that, they were not available as at the time of determination of biological activity.

For the cytotoxicity assay, some compounds were not tested as they showed poor or no inhibition against the plasmodial cell.

4.4.1 Antimicrobial susceptibility testing by agar disk diffusion

Table 4.1 Agar disk diffusion test of compounds (250 μg $disc^{-1}$) against chosen strains of microorganisms (disk diameter 6 mm)

Compounds 250 μg/disk	*S. aureus*	*B. subtilis*	*E. coli*	*C. albicans*	Compounds 250 μg/disk	*S. aureus*	*B. subtilis*	*E. coli*	*C. albicans*
2MT	8	7	6	6	2MA	7	8	6	6
Co2MT	11	11	6	6	Co2MA	11	12	6	NT
Ni2MT	8	8	7	NT	Ni2MA	8	8	7	6
Cu2MT	10	14	7	9	Cu-2MA	10	13	7	7
2–Me–2MT	7	6	6	6	2–Me–2MA	7	11	6	6
Co(2–Me–2MT)	NT	NT	NT	6	Co(2–Me–2MA)	NT	NT	NT	6
Ni(2–Me–2MT)	7	8	6	6	Ni(2–Me–2MA)	NT	NT	NT	6
Cu(2–Me–2MT)	9	10	6	8	Cu(2–Me–2MA)	19	20	6	6
4–Me–2MT	8	8	7	6	4–Me–2MA	8	10	6	6
Co(4–Me–2MT)	9	8	6	NT	Co(4–Me–2MA)	12	9	6	6
Ni(4–Me–2MT)	8	10	6	6	Ni(4–Me–2MA)	NT	NT	NT	6
Cu(4–Me–2MT)	10	13	8	9	Cu(4–Me–2MA)	10	12	7	8
2–MeO–2MT	7	6	6	6	2–MeO–2MA	9	11	6	6
Co(2–MeO–2MT)	NT	NT	NT	6	Co(2–MeO–2MA)	NT	NT	NT	6
Ni(2–MeO–2MT)	8	9	6	6	Ni(2–MeO–2MA)	NT	NT	NT	6
Cu(2–MeO–2MT)	18	18	6	10	Cu(2–MeO–2MA)	20	19	6	6
4–MeO–2MT	13	12	7	6	4–MeO–2MA	9	9	6	6
Co(4–MeO–2MT)	14	13	7	6	Co(4–MeO–2MA)	22	17	9	6
Ni(4–MeO–2MT)	9	10	6	6	Ni(4–MeO–2MA)	NT	NT	NT	6
Cu(4–MeO–2MT)	20	18	7	13	Cu(4–MeO–2MA)	15	16	7	6
2–Cl–2MT	8	6	6	6	2–Cl–2MA	7	15	6	6
Ni(2–Cl–2MT)	8	8	6	NT	Cu(2–Cl–2MA)	9	10	6	7
Cu(2–Cl–2MT)	8	8	6	7					
4–Cl–2MT	8	8	7	6	4–Cl–2MA	8	8	7	6
Co(4–Cl–2MT)	10	12	7	9	Co(4–Cl–2MA)	9	9	7	6
Ni(4–Cl–2MT)	8	8	6	NT	Ni(4–Cl–2MA)	NT	NT	NT	6
Cu(4–Cl–2MT)	8	9	7	10	Cu(4–Cl–2MA)	10	9	7	7
2–Br–2MT	7	6	6	6	2–Br–2MA	NT	NT	NT	NT
Ni(2–Br–2MT)	8	8	7	NT	Cu(2–Br–2MA)	9	14	6	7
Cu(2–Br–2MT)	9	7	6	8					
4–Br–2MT	8	9	7	6	4–Br–2MA	9	10	7	6
Co(4–Br–2MT)	10	10	7	9	Co(4–Br–2MA)	11	11	6	6
Ni(4–Br–2MT)	9	8	6	NT	Cu(4–Br–2MA)	13	11	7	6
Cu(4–Br–2MT)	9	9	7	11					
4–NO_2–2MT	7	9	7	6	DMF	6	6	6	6
Ni(4–NO_2–2MT)	8	7	6	NT	AMP 125 μg/disk	40	38	23	NA
Cu(4–NO_2–2MT)	8	10	7	6	AMP 50 μg/disk	26	21	11	NA
					KTZ 125 μg/disk	NA	NA	NA	23
$CoCl_2.6H_2O$	16	13	10	6	$CuCl_2.2H_2O$	8	8	7	8

NT – not tested; NA – not applicable

4.4.2 Antimicrobial susceptibility testing by microbroth serial dilution

Table 4.2 MIC (μg/mL) of *para* substituted compounds by microbroth serial dilution

Compounds	Microorganisms			Compounds	Microorganisms		
	S. aureus	*B. subtilis*	*E. coli*		*S. Aureus*	*B. Subtilis*	*E. Coli*
2MT	1560	1560	1560	2MA	1560	1560	1560
Cu2MT	195	780	780	Cu2MA	780	3120	390
4Me–2MT	1560	1560	780	4Me–2MA	1560	195	780
Cu(4Me–2MT)	195	780	780	Cu(4Me–2MA)	390	24.4	780
4MeO–2MT	3120	3120	1560	4MeO–2MA	1560	780	1560
Cu(4MeO–2MT)	195	195	390	Cu(4MeO–2MA)	195	24.4	390
Co(4MeO–2MT)	195	195	NT	Co(4MeO–2MA)	97.5	195	NT
4Cl–2MT	390	390	390	4Cl–2MA	390	24.4	195
Cu(4Cl–2MT)	195	195	390	Cu(4Cl–2MA)	390	48.8	1560
4Br–2MT	195	780	390	4Br–2MA	195	48.8	195
Cu(4Br–2MT)	195	195	390	Cu(4Br–2MA)	390	780	390
$4NO_2$–2MT	NT	780	NT	$CuCl_2.2H_2O$	780	390	780
Cu($4NO_2$–2MT)	780	97.5	780	$CoCl_2.2H_2O$	195	195	NT

NT – not tested

4.4.3 Antimicrobial susceptibility testing for the Schiff–base ligands

Table 4.3 Agar disk diffusion test of Schiff-base ligands (250 μg $disc^{-1}$) against chosen strains of microorganisms (disk diameter 6 mm)

Compounds 250 μg/disk	*S. Aureus*	*B. subtilis*	*E. coli*	*C. albicans*
pMS–2MT	6	6	6	6
pMS–4MeO2MT	6	6	6	6
pMS–4Br2MT	6	6	6	6
pMS–4Cl2MT	6	6	6	6

4.4.4 Antimicrobial and cytotoxicity assays

Table 4.4 Inhibition of growth of parasite[a] and cancer[b] cell by compounds

Compound	% Parasite growth at 50 μM (SD)	% viability at 50uM (SD)
Cu2MT	5.49 (0.41)	38.0521 (9.71)
Cu(4Me–2MT)	8.21 (0.63)	28.48664 (4.86)
Cup(4MeO–2MT)	0.72 (0.57)	31.64475 (5.66)
Cu(4Cl–2MT)	7.40 (1.31)	37.03055 (4.90)
Cu(4Br–2MT)	6.83 (1.70)	39.04592 (9.34)
Cu(4NO_2–2MT)	8.63 (6.41)	39.74564 (8.09)
Cu(2Me–2MT)	6.93 (0.48)	33.52377 (5.68)
Cu(2Me–2MT)	8.46 (0.94)	29.74039 (6.23)
Cu(2Cl–2MT)	5.91 (0.62)	32.69409 (8.63)
Cu(2Br–2MT)	6.31 (0.61)	36.02779 (6.23)
Cu(4MeO–2MA)	-0.05 (0.26)	31.23485 (6.89)
Cu(2MeO–2MA)	0.03 (0.15)	38.24921 (5.74)
Ni(2MeO–2MT)	55.66 (5.66)	NT
Ni(4MeO–2MT)	93.57 (2.20)	NT
Ni(2MeO–2MA)	84.67 (9.42)	NT
Ni(4MeO–2MA)	119.54 (5.46)	NT
Co(2MeO–2MT)	62.67 (2.46)	NT
Co(2MeO–2MA)	77.43 (1.65)	NT
Co(4MeO–2MT)	104.07 (13.61)	NT

a P. falciparum *b breast cancer cell lines* NT – Not tested

4.5 DISCUSSION

4.5.1 Antimicrobial susceptibility test

From the results displayed in **Table 4.1** for the disk diffusion susceptibility test, it can be observed that the inhibitory activity of each ligand was improved upon chelation with metal ion. This could be because the metal salts also have a measure of biological activity as shown from their inhibitory zones, for example, the hydrated cobalt(II) chloride salt inhibits *S. aureus* more than some its chelated compounds. Of the metal complexes, nickel(II) compounds showed the least inhibitory activity against the microbial growth. The activity of copper complexes on the whole is better than that shown by cobalt complexes.

Comparing the three bacteria and the fungal strains tested, the gram–negative bacterium *E coli* was the most resistant to the compounds used. *C. albicans* was also very resistant as only the methoxy substituted compound could inhibit its growth by a diameter twice the size of the disk. It is well known that the bacterial cell wall is a good target for antimicrobial agents, this resistance by *E. Coli* could be as a result of its thicker peptidoglycan layer of the outer membrane (**Fig. 4.4**) which the test compounds could not interact with sufficiently compared to that of a typical gram-positive bacterium. This fact is widely known and referred to as 'intrinsic resistance' of Gram-negative bacteria. The same explanation may be applicable to the fungal cell wall which consists of polysaccharide materials (**Fig. 4.5**). Both *S. aureus* and *B. subtilis* showed some measure of susceptibility to Co(II) and Cu(II) complexes as could be judged from the sizes of their diameters of inhibition (**Fig. 4.6-4.9**). The electron donating groups seem to be better than the electron withdrawing groups in general.

The minimum inhibitory concentration (Table 5.2) was determined for some of the compounds which showed a measure of inhibitory activity. It was observed that some of the compounds (for example,4Cl–2MA and its copper complex) which did not show a large zone of inhibition are seen to have low MIC values, this could not be accounted for and a further investigation could be made along this direction. The electron withdrawing groups have the least MIC values in general.

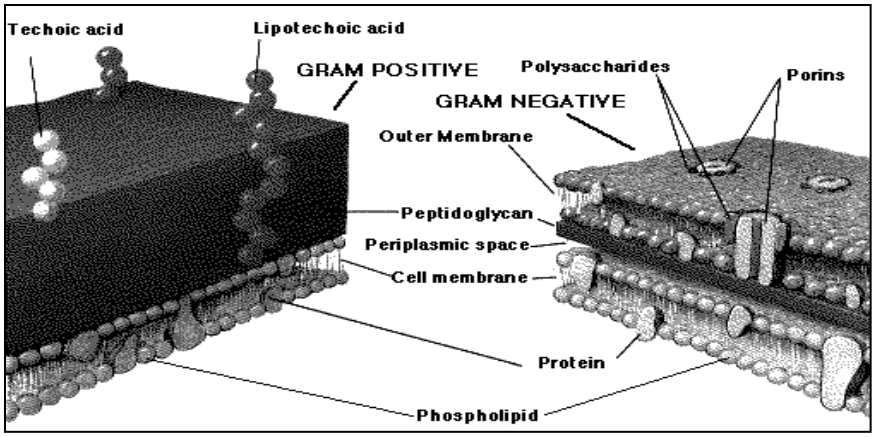

Fig. 4.4 Gram-positive and Gram-negative bacterial cells[17]

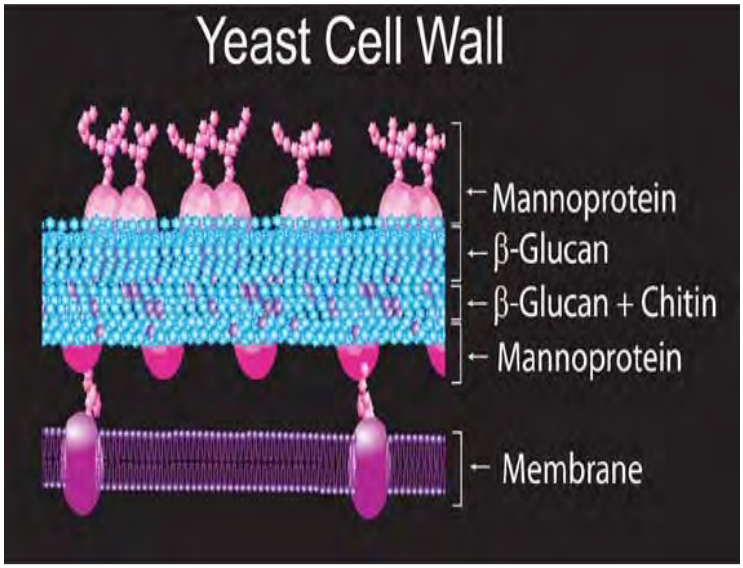

Fig. 4.5 The components of the yeast cell wall[18]

The methoxy substituted compounds showed the most significant activity of all the compounds. Though the methoxy substituted compounds were not as active as the standard Ampicillin; they however have demonstrated very promising inhibitory activity. This could be as a result of the orientation of these compounds in space permitting the amino group to interact more strongly with the microbial cell. It could also be as a result of electron donating effect of methoxy group, pushing more electron density towards the amine group, thereby making it more available for interaction with the microbial cell, than is possible with other groups. This is confirmed by another electron donating group, next to the methoxy, the methyl substituted groups also showed good inhibition of the two gram–positive bacteria.

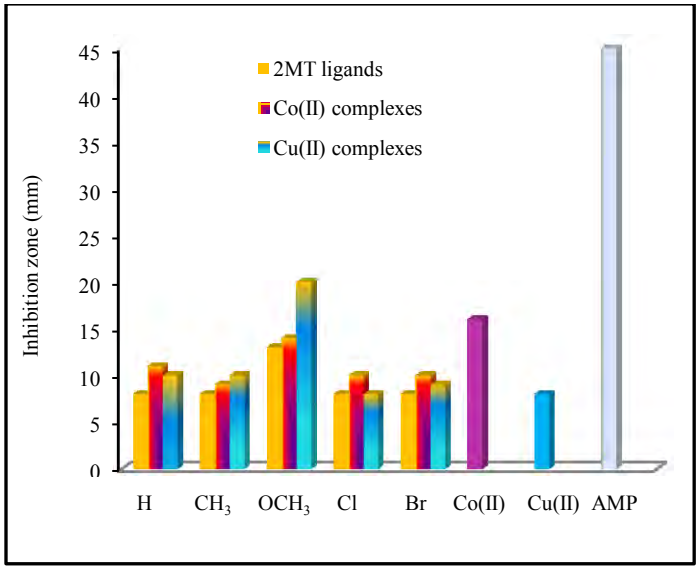

Fig. 4.6 Inhibition of *S. aureus* by *para* substituted 2MT ligands and metal(II) complexes (250 µg/disk)

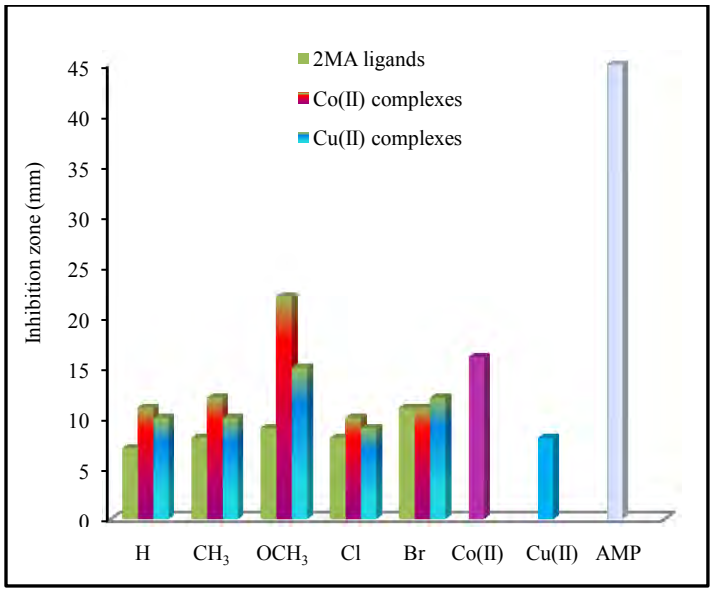

Fig. 4.7 Inhibition of *S. aureus* by *para* substituted 2MA ligands and metal(II) complexes (250 µg/disk)

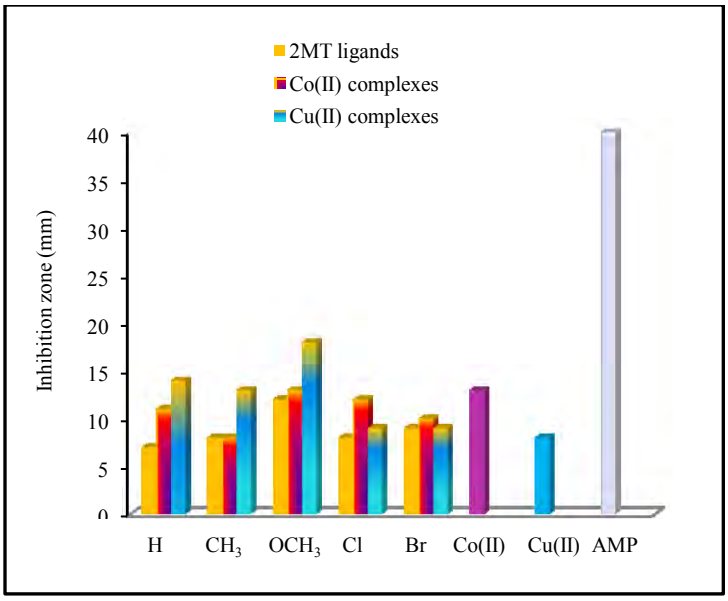

Fig. 4.8 Inhibition of *B. subtilis (spizizenii)* by *para* substituted 2MT ligands and metal(II) complexes (250 µg/disk)

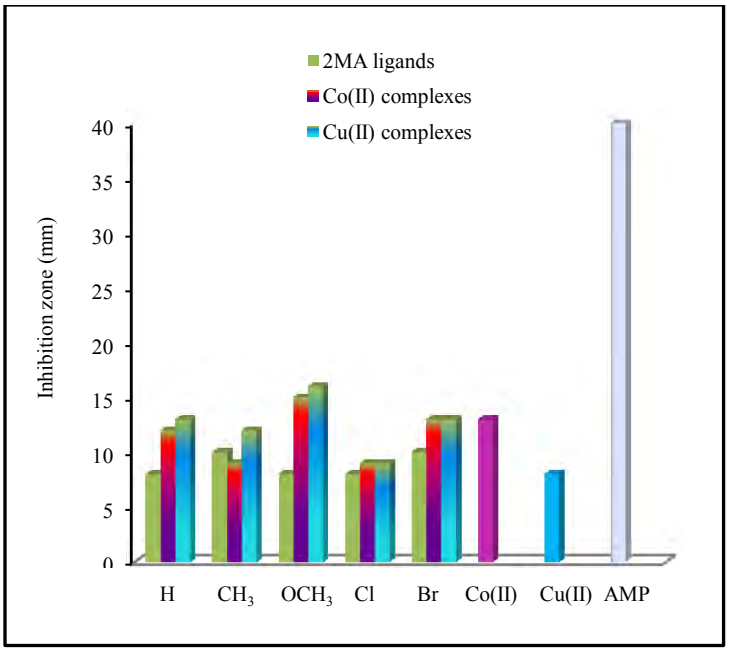

Fig. 4.9 Inhibition of *B. subtilis (spizizenii)* by *para* substituted 2MT ligands and metal(II) complexes (250 µg/disk)

Contrary to antimicrobial/biological activity associated with some Schiff-bases, the Schiff-bases prepared in this research were low in activity as the ligands could not inhibit the growth of any of the strains tested. Many Schiff-bases have shown excellent biological activity. The structural difference between the thiomethylated aniline ligands which showed at least some inhibitory activity and their Schiff-base derivatives is the absence of the amino group. It could imply that the presence of the amino group facilitates the ability of the compounds to interact with the microbial cells. This is an area to look into for further research study as presence of amino groups in many drugs is known to be contributory to their biological property.

Their metal complexes could not be tested as a result of insolubility in either DMF or DMSO.

4.5.2 Antimalarial and cytotoxicity assays

Since the copper complexes showed the highest activity in the antimicrobial inhibitory tests, the copper complexes of 2MT ligands are tested for their antimalaria plasmodial tests. The results as seen in **Table 4.4** are very revealing, with all the complexes tested inhibiting the growth of *P. falciparum* by ≥ 90% at 50 μM. The only compounds tested in the 2MA series, the methoxy substituted, inhibit the parasite growth completely at same concentration, indicating the remaining 2MA copper complexes would also be similar in behavior. Since the methoxy substituted copper complexes have the highest antiplasmodial activity, the analogous Co(II) and Ni(II) are also tested; the results indicate that the *ortho*-methoxy substituted complexes of Ni(II) and Co(II) are able to destroy 15–38% plasmodial cells and the *para*-methoxy complexes show little or no inhibitory activity. The better activity of Cu(II) suggests a difference in mechanism and not just structural, from that obtainable in the other Co(II) and Ni(II). From the UV studies, Cu(II) shows a more reducible property compared to other metal ions, as it relates to the charge transfer, hence a redox potential aspect to activity of the Cu(II) is suggested.

From the above results, it is clear that the chelation to copper(II) ion enhances antiplasmodial activity relative to Ni(II) and Co(II) ions. Furthermore, the presence of methoxy in either the ortho or para position in the copper complexes tested gives rise to almost similar activity while the ortho-positioning of the methoxy could enhance Ni(II) and Co(II) activities. This activity of methoxy compounds in antiplasmodial therapy has been reported[19] and it is suggested its activity could be due to the spatial orientation it imposes on the complexes. The presence of the amino group in these present complexes could also account for their activity as structure-activity studies on some aminoquinolines showed that the

presence of a hydrophobic group (*e.g*. an alkyl spacer) and an amino group for pH trapping are essential for high anti-plasmodial activity.[20]

Cytotoxicity of the most active compounds against cancer cell lines is carried out to ascertain its toxicity effects on human cells. The results in **Table 4.4** indicate the compounds are less toxic to the cell lines, with 28–40% of the cells being viable. From these results, it is to be seen that the compounds are more selective towards inhibiting plasmodial growth than the cancer cells.

The results obtained for these compounds at the 50 μM concentration level show they exhibit excellent antimicrobial activity which is greater than that shown by any antimalarial agent hitherto known to the author. Their preferential selectivity towards the parasite cell rather than the human cell is another good characteristic they have exhibited as potential drug candidates. Three of the compounds in particular show exceptional activity and selectivity hence the compounds are worth further investigating.

In order to identify them as lead antimalarial compounds, they could be tested against resistant strains of parasite and their inhibitory activity determined at much lower concentrations. Since the Cu(II) complexes demonstrated outstanding biological activity in comparison to their Co(II) and Ni(II) counterparts, the mechanism of the interaction of these Cu(II) complexes with the parasite cell needs to be investigated. A mechanism involving the facile reduction of Cu(II) to Cu(II) with subsequent activation of intracellular oxygen has been proposed for the antimalarial activity of some four-coordinate copper(II) complexes.[21] The redox property of ferroquine has been suggested to attribute to its better antimalarial activity than CQ.[22,23] From the solid reflectance of the metal(II) complexes in this study, the charge transfer transition energy for the Cu(II) is n this study, This could help in establishing structure-activity relationship between these agents and the target cells and guide towards the modification of the substituents and ring properties of these chelates.

REFERENCES

1. D. C. Mohana, S. Satish and A. Koteshwara, *Journal of Plant Protection Research*, **4**, 250, 2009.
2. D. C. Mohana and K. A. Raveesha, *Journal of Mycology and Plant Pathology*, **40**, 197, 2010.
3. M. Srikanta Belagihalli, A. Harish Nayaka Mysore and M. Dharmesh Shylaja, *Biochimie*, **93**, 678, 2011.
4. J. Wang, H. Liu, J. Zhao, H. Gao, L. Zhou, Z. Liu, Y. Chen and P. Sui, *Molecules*, **15**, 5807, 2010.
5. J. McFarland, *J. Amer. Med. Assoc.*, **49**, 907, 1176.
6. A. W. Bauer, W. M. M. Kirby, J. C. Sherris and M. Turck, *Am. J. Clin. Pathol*., **36**, 493, 1966.
7. S. M. Finegold and E. J. Baron, *Bailey and Scott's Diagnostic Microbiology*, 7th Ed., C. V. Mosby, St. Louis, 1986.
8. J. H. Jorgensen and J. D. Turnidge, *Susceptibility test methods: dilution and disk diffusion methods*, 1152. In P. R. Murray, E. J. Baron, J. H. Jorgensen, M. L. Landry, and M. A. Pfaller (ed.), *Manual of clinical microbiology*, 9th ed. ASM Press, Washington, D.C., 2007.
9. Blood Safety and Clinical Technology: Guidelines on Standard Operating Procedure, World Health Organization, http://www.searo.who.int/en/Section10/Section17/Section53/Section482_1788.htm. Date accessed: 09/10/2011.
10. Clinical Laboratory Standards Institute, *Performance standards for antimicrobial disk susceptibility tests; Approved standard*—9th ed. CLSI document M2-A9. 26:1, 2006. Clinical Laboratory Standards Institute, Wayne, PA.
11. http://aminj.myweb.uga.edu/ZONE CHART.html. Date accessed: 09/12/2011.
12. http://en.wikipedia.org/wiki/Microtiter_plate. Date accessed: 30/08/2012.
13. J. B. Jensen and W. Trager, *Science*, 1976, **193**, 674.
14. R. L. van Zyl and A. M. Viljoen, *South African Journal of Botany*, 2002, **68**, 106.
15. C. Lambros and J. P. Vanderberg, *Journal of Parasitology*, 1979, **65**, 418.
16. R. E. Desjardins, C. J. Canfield, D. J. Haynes and J. D. Chulay, *Antimicrobial Agents and Chemotherapy*, 1979, **16**, 710.
17. http://filebox.vt.edu. Date accessed: 10/05/2012.
18. Sigmaaldrich.com. Date accessed: 10/05/2012.
19. D. E Goldberg, V. Sharma, A. Oksman, I. Y. Gluzman, Wellems T. E and Piwnica-Worms D. J, *J. Biol. Chem.*, 1997, **272**, 6567.

20. T. J. Egan, *Expert Opin. Ther. Pat.*, 2001, **11**, 185.

21. N. H. Gokhale, K. Shirisha, S. B. Padhye, S. L. Croft, H. D. Kendrick and V. Mckee, *Bioorg. Med. Chem. Lett.*, 2006, **16**, 430.

22. N. Chavain, H. Vezin, D. Dive, N. Touati, J. F. Paul, E. Buisine and C. Biot, *Mol. Pharmaceutics,* 2008, **5**, 710.

23. F. Dubar, S. Bohic, C. Slomianny, J. C. Morin, P. Thomas, H. Kalamou, Y. Guérardel, P. Cloetens, J. Khalife and C. Biot, *Chem. Commun.,* 2012, **48**, 910.

Conclusion

The thiomethylated-aniline ligands 2–(methylthiomethyl)aniline 2MT and 2–(methylthio)aniline 2MA were synthesized with their substituted derivatives (-Me, -MeO, -Cl, -Br, $-NO_2$). Complexes of the ligands with Co(II), Ni(II) and Cu(II) were prepared. The ligands and their metal(II) complexes were characterized by elemental analysis and spectroscopic means. The Co(II) and Ni(II) complexes have the ML_2Cl_2 molecular formula while the Cu(II) complexes (with one exception) formed with $MLCl_2$ stoichiometry. The thiomethylated ligands show bands consistent with primary amine groups and there is no proton loss on coordination. Coordination of these ligands to the metal(II) ions take place through the N and S atoms as evidenced by the decrease in frequency of N–H band and appearance of new bands at the far infrared regions for M–N and M–S bonds respectively.

The solid state configurations for the Co(II) and Ni(II) complexes in general can be suggested to be distorted octahedral from the elemental analysis and the spectroscopic data while the X-ray crystallography data clearly shows the square pyramidal or tetragonally distorted octahedral structure for the Cu(II) complexes.

The electrolytic nature of CoII) and Cu(II) complexes in DMF were found to be similar, they behave as non electrolytes in contrast to Ni(II) complexes which show 1:1 electrolyte nature. The electronic spectra of these metal(II) complexes were found to be different for both their solid forms and in solutions of DMF and DMSO. In solution, the isostructurality of Co(II) and Ni(II) no longer holds. Co(II) complexes have spectra similar to those in tetrahedral geometry, the solvent molecules breaking the Co–S bonds but not binding to the Co(II) center. Ni(II) and Cu(II) complexes became isostructural, being octahedral in solution. In both types of complexes, the solvent molecule becomes attached to the metal center. In Ni(II) complexes, the chloride ion is replaced by the solvent molecule in the process while in the case of Cu(II), the solvent becomes bound to the metal center without displacing the bridging chloride.

In the evaluation of their biological activity, some of the ligands showed some inhibitory activity against the gram–positive bacteria *S. aureus* and *B. subtilis*; the gram-negative bacterium *E. coli* and the fungus *C. albicans* were not susceptible to the compounds at the concentration tested. The activity of each metal complex was higher than that of its corresponding ligand. The methoxy-substituted ligands and their metal complexes however demonstrated promising antimicrobial activity at similar concentration.

In the evaluation of biological activity of some of the Co(II), Ni(II) and Cu(II) complexes of the thiomethylated ligands against *Plasmodium falciparum*, the Cu(II) complexes show outstanding activity in comparison to their analogous metal complexes. At 50 μM concentration level, the Cu(II) complexes show activity equal or better than the prophylactic chloroquine. The Cu(II) complexes with the methoxy-substituted demonstrated exceptional activity but their Co(II) and Ni(II) analogues did not show any activity.

The methoxy-substituted ligands and their Co(II), Ni(II) and Cu(II) complexes were seen to demonstrate exceptional biological activity against the strains of gram-positive bacteria *S. aureus*, *B. subtilis* as well as the *P. falciparum*. This exceptional behaviour of the methoxy-substituted compounds was also observed in the NMR shifts of the ligands, their electronic spectra as well as the frequency shifts of their N–H stretches.

The cytotoxicity of the Cu(II) complexes was determined against the breast cancer cell at 50 μM concentration. 28–40% of the carcinoma cell destroyed shows their preference towards the inhibition of the plasmodial cell rather than the cancer cell. The selectivity demonstrated by these compounds have shown them to be potential antimalarial agents and further investigation can be carried out to identify them as lead drugs.

The structures of these methoxy compounds both in the solid state and in solution could be further investigated as the methoxy group could be changing the orientation of these compounds to enhance activity. Likewise the redox properties of the Cu(II) complexes of the methoxy compounds could be determined in comparison with those of the Co(II) and Ni(II) methoxy complexes.

The Schiff-base ligands and their Cu(II) complexes were prepared and structurally characterized. The ligands showed no biological activity and those of the complexes could not be determined. The inactivity of the ligands might be as a result of their non-polarity. However their catalytic property may be investigated. The long Cu–S bonds could make the S more labile and easier to replace by another group and this property may be useful in catalysis.

The cytotoxicity of the active Cu(II) complexes of the thiomethylated ligands at 50 μM concentration against the breast carcinoma cell was in the range 28–40%, thus showing preference to destroying the parasitic cell instead of the cancer cell. The selectivity demonstrated by these compounds have shown them to be potential antimalarial agents and this could be further investigated.